# SIZE DISTRIBUTIONS, POPULATION DYNAMICS, AND SINGLE-CELL PROPERTIES OF MARINE PLANKTON IN DIVERSE NUTRIENT ENVIRONMENTS

by

Kent Keller Cavender-Bares

B.S. Agricultural and Biological Engineering
Cornell University, 1989

M.S. Environmental Engineering
Stanford University, 1990

Submitted to the Department of Civil and Environmental Engineering in Partial Fulfillment of the Requirements for the Degree of

Doctor of Philosophy
in Civil and Environmental Engineering
at the
Massachusetts Institute of Technology
June 1999



Signature of Author: _____
Department of Civil and Environmental Engineering
May 21, 1999

Certified by: _____
Sallie W. Chisholm
Professor of Civil and Environmental Engineering
Thesis Supervisor

Approved by: _____
Andrew J. Whittle
Chairman, Departmental Committee on Graduate Studies

# SIZE DISTRIBUTIONS, POPULATION DYNAMICS, AND SINGLE-CELL PROPERTIES OF MARINE PLANKTON IN DIVERSE NUTRIENT ENVIRONMENTS

by

Kent Keller Cavender-Bares

Submitted to the Department of Civil and Environmental Engineering on May 25, 1999 in Partial Fulfillment of the Requirements for the Degree of Doctor of Philosophy in Civil and Environmental Engineering

## Abstract

The goal of this thesis is to study the relationship between the community structure of marine microorganisms and nutrient availability. To this end, size spectra of microbes were studied over a range of nutrient regimes, both natural and manipulated. Three transects in the Atlantic provided a natural range of nutrient environments, especially because they captured seasonal variations. The transects encompassed Sargasso Sea, Gulf Stream, and coastal waters, during winter, spring, and summer. Nutrient regimes ranged from surface waters of the Sargasso Sea during stratified periods (low-nutrient), to deeply mixed waters in all three regions of the transects during winter and spring (high-nutrient). Complementing natural variations in nutrients, two experiments were used to study the effects of enrichment on size structure. An *in situ* iron-enrichment experiment conducted in the equatorial Pacific (IronEx II) provided a unique opportunity to monitor changes in community structure following increased nutrient availability. In a second experiment in the Sargasso Sea, enrichments with nitrogen and phosphorus were conducted in bottles, because one or both are commonly thought to be limiting in this region. In order to carry out the goal of this thesis, which depended on the use of flow cytometry to characterize bacterio-, pico-, ultra-, and nanophytoplankton, advancements were made in methods for enumerating a wide range of cell sizes and for estimating cell size from forward angle light scatter. In addition, because ambient concentrations of inorganic nitrogen and phosphorus are exceedingly low (<10nM) in the Atlantic, especially during stratified periods, low-level determinations of these nutrients were made to compliment the analyses of community structure. Size structure varied systematically, although not necessarily as a function of nutrient availability. Two parameters were explored: 1) spectral slope, which indicates the relative contribution of large and small cells to total biomass, and 2) spectral shape, or adherence of the spectra to relationships explained by a power law. The relative ranking of the slopes from specific regions of the transects remained constant throughout different seasons. Shapes ranged from discontinuous to those which adhered to a power law. It is hypothesized that only microbial systems with abundant nutrient inputs and, perhaps, reduced grazing pressure, have smooth spectra whose shapes conform to power laws.

Thesis supervisor: Sallie W. Chisholm
Title: Professor of Civil and Environmental Engineering, and Biology

ACKNOWLEDGEMENTS

My advisor, Penny Chisholm, has played a large role in my life over the last six years, which amounts to nearly one-fifth of my life. Penny has been a role model, an advisor, a confidant, and a friend to me. Six years ago I would never have dreamt that some 16 weeks of my life would be spent at sea by now, and that I would have gained the wonderful experiences that accompany such travels!

I am indebted to my other committee members, Phil Gschwend, Jim McCarthy, and Rob Olson for their patience and devotion to my work over these many years. Through them, I have been able to gain many different insights into the world of oceanography, and science in general.

Over my final year, I have benefited tremendously from involvements with two other scientists. Dave Karl opened his lab to me for what proved to be an extended stay, resulting in a longer-term collaboration. Through this work, I have been able to get a small taste of what it is like to do it first while doing it well. I thank two members of Dave's lab, Terry Houlihan and Karin Björkman, for their tireless assistance. Shortly after my return from Hawaii, Andrea Rinaldo came into my life. Andrea's profound interest in my work, his continual enthusiasm, and his insights—the kind which only someone from another field can offer—were critical to this thesis coming to closure when it did. My friendship with Andrea has made this last year endurable.

Within the Chisholm lab, my thanks go out to many, both past and present. Lisa Moore, Liz Mann, and Gabrielle Rocap have been friends and colleagues, both on land and at sea. I thank Radika Bhaskar and Nianzhi Zhu for laboratory assistance. Sheila Frankel has been an advisor, on many levels, throughout this process, and for her friendship I am very grateful. Perhaps the greatest wisdom Sheila has ever shared was about how smooth a couple weeks on the Sargasso Sea can be...

I thank Peter and Laura for their wonderful friendship throughout the last few years, especially for all the many dinners they provided. I also acknowledge the many other friendships which have made the last several years more enjoyable (Peter & Sarah, Dean & Wendy, Doug & Sabrina, and others).

I wish to acknowledge the unending support of my entire family throughout this seemingly endless process. My dear mother, who has read herself to sleep many a night (and afternoon?) with my writings of phytoplankton, deserves a special thanks! My wife, Jeannine, while last in this list, belongs way at the top. Her friendship and support throughout these past six years has been unyielding. While I may have been able to accomplish this without her, I desire not to imagine it.

I acknowledge financial support from the following sources: a Parsons' Fellowship; MIT/TEPCO funds through the Center for Global Change Science; NSF Grants OCE-9701681 OCE9223793 to S.W. Chisholm; a MIT Global Change Joint Program Fellowship; a MIT Dept. of Civil and Environmental Engineering Teaching Assistantship; and ONR Grant N00014-93-1-1146 to S.W. Chisholm.

TABLE OF CONTENTS

LIST OF FIGURES

Chapter 2



Chapter 3

Chapter 4



Chapter 5

Chapter 6



LIST OF TABLES

Chapter 3

# Chapter 1

# Introduction

# Introduction

Nutrient limitation of aquatic ecosystems has been the focus of many scientific inquiries since the late 1800s, essentially marked by Brandt's (1899) application of Liebig's (1855) Law of the Minimum to marine systems (e.g., Ryther and Dunstan 1971; Eppley *et al.* 1973; Goldman *et al.* 1979; Hecky and Kilham 1988; Howarth 1988; Cullen 1991). The supply of nutrients to the local environment of marine microorganisms can occur by large-scale processes, such as eddy diffusion or upwelling, or by localized processes, such as the flux of regenerated nutrients from a zooplankton grazer. On a micro-scale, Munk and Riley (1952) first proposed that growth rates could be limited by an inadequate diffusive flux of nutrients from the bulk water to the cell surface, a process known as diffusion limitation.

Conventional wisdom indicates that the predominance of large or small phytoplankton cells can be explained by nutrient concentrations. Large cells, such as diatoms, are observed to dominate on a biomass basis in high nutrient areas, while small cells, such as cyanobacteria, dominate in oligotrophic waters of the world ocean. Diffusion limitation can be invoked to explain these distributions based on nutrients, because small cells have higher surface area to volume ratios, which makes them less likely to be diffusion limited at low ambient nutrient concentrations (e.g., Pasciak and Gavis 1974; Morel *et al.* 1991; Hudson and Morel 1990; Chisholm 1992). However, there are alternative explanations which would explain the observed pattens in the abundance of large and small cells. For example, some diatoms exhibit exceptionally high maximum growth rates (Chisholm 1992), which might allow them to take advantage of high-nutrient conditions; the abundance of small cells is often tightly controlled by small, fast-growing grazers (e.g., Landry *et al.* 1997; Caron *et al.* 1999). Thus, a complex series of interactions may lead to the size distributions which are observed for marine microorganisms.

The size structure of microbes impacts organisms on higher trophic levels, even though interactions between trophic levels do not follow the strict model of a linear food chain (Pomeroy 1974). In fact, the microbial community can be thought of more as a web of interactions, in which there is no direct path for energy flow to higher trophic levels. Because of

the circuitous path in which energy flows, microbial communities are often referred to as the microbial loop (Azam *et al.* 1983).

Interest in community structure in the marine environment, and in ways to represent this structure, was traced back to Elton (1927). Sheldon *et al.* (1972) were the first to supply an image of size distributions, or spectra, of plankton across a wide expanse of the world ocean. In spite of methodological limitations which prevented them from characterizing just the living component in their samples, they put forth the Linear Biomass Hypothesis, which states that the amount of biomass in equally-sized logarithmic size classes remains constant—from bacteria to whales. This hypothesis, promoted before the microbial loop was envisioned, provided a provocatively simple image of community structure, and it provided a means for predicting fish stocks, for example, given the biomass of plankton (Sheldon *et al.* 1977). Since then, numerous tests of this hypothesis have been undertaken using increasingly more refined methods. Specifically, microscopy replaced the Coulter Counter, which was used by Sheldon *et al.* (1972), in order to exclude detritus from size spectra (e.g., Rodriguez and Mullin 1986; Sprules *et al.* 1991; Ahrens and Peters 1991; Gaedke 1992; Quiñones-Bergeret 1992; Ruiz *et al.* 1996; Tittel *et al.* 1998). Improved methods for representing spectra have been advanced (Platt and Denman 1977; Blanco *et al.* 1994; Vidondo *et al.* 1997), and flow cytometry, which has the ability to characterize cells more rapidly than microscopy, has been used recently to generate size spectra (Li 1994; Gin 1996; Gin *et al.* in press). The largest obstacle facing the use of flow cytometry, is that these instruments do not measure size directly, and cell size must be estimated based on measurements of light scatter (Ackelson and Spinrad 1988; DuRand 1995; Dusenberry 1995; Gin 1996; Gin *et al.* in press).

The goal of this thesis is to characterize community structure of marine microorganisms over a wide range of nutrient regimes in order to understand the relationship between size structure and nutrient availability. Observations were made across natural gradients in nutrients as well as during experimental manipulations of nutrient regimes. Of the many factors which may influence community structure, nutrients were selected for their universal role in the growth of microorganisms, and because diffusion limitation would be a plausible explanation for changes in community structure along gradients in nutrients. Three transects within the Atlantic

Ocean were designed to provide the maximum variation in ambient nutrients. Two seasonal transects, one each during summer and winter, were used to contrast relatively low- and high-nutrient periods, respectively. A third transect conducted during spring, which featured high spatial resolution, captured both oligotrophic and high-nutrient (i.e., during the spring bloom) periods in the Sargasso Sea on the same cruise.

An iron-enrichment experiment (IronEx II) in the equatorial Pacific (see Chapter 4, Coale *et al.* 1996b)—only the second such experiment to be done *in situ*—provided an unique opportunity to study the effect of elevated nutrient supply on microbial size spectra. Iron has been the focus of investigations in this high nutrient, low chlorophyll (HNLC) region of the world ocean because natural inputs are small, and iron additions to bottle incubations in HNLC regions have resulted in heightened phytoplankton biomass (e.g., Martin and Fitzwater 1988; Coale 1991; Buma *et al.* 1991; Takeda and Obata 1995; Boyd *et al.* 1996; Coale *et al.* 1996a; Zettler *et al.* 1996). In the Sargasso Sea, nitrogen or phosphorus are commonly thought to control microbial growth (e.g., Graziano *et al.* 1996; Cotner *et al.* 1997). Therefore, a bottle enrichment experiment, which had both N and P additions and was conducted during an oligotrophic period, provided a glimpse at the effects of a changing nutrient environment on microbial size structure in this region.

In order to facilitate the study of community structure using size spectra, improved protocols for characterizing small and large cells (Chapter 2) and for estimating cell size (Chapter 3) were developed. The lack of nutrient data for much of the euphotic zone in the Sargasso Sea has prevented the correlation between parameters of size spectra and nutrient concentrations for this region (e.g., Gin *et al.* in press). Thus, inorganic nitrogen and phosphorus were determined at levels below 10 nM (Chapter 5) in order to enable a more complete analysis of changes in community structure as a function of nutrient regime (Chapter 6).

## REFERENCES


Ackelson, S. G. and R. W. Spinrad 1988. Size and refractive index of individual marine particulates: a flow cytometric approach. Applied Optics 27: 1270-1277.

Ahrens, M. A. and R. H. Peters 1991. Patterns and limitations in limnoplankton size spectra. Canadian Bulletin of Fisheries and Aquatic Sciences 48: 1967-1978.

Azam, F., F. T., J. G. Field, J. S. Gray, L. A. Meyer-Reil and F. Thingstad 1983. The ecological role of water-column microbes in the sea. Marine Ecology Progress Series 10: 257-263.

Blanco, J. M., F. Echevarría and C. M. García 1994. Dealing with size-spectra: some conceptual and mathematical problems. Scientia Marina 58: 17-29.

Boyd, P. W., D. L. Muggli, D. E. Varela, R. H. Goldblatt, R. Chretien, K. J. Orians and P. J. Harrison 1996. In vitro iron enrichment experiments in the NE subarctic Pacific. Marine Ecology Progress Series 136: 179-193.

Brandt, K. 1899. Über den Soffwechsel im Meere (Rektoratsrede). Wissenschaftliche Meeresuntersuchungen, Abteilung Kiel, Neue Folge 4: 185-492.

Buma, A. G. J., H. J. W. de Baar, R. F. Nolting and A. J. van Bennekom 1991. Metal enrichment experiments in the Weddell-Scotia Seas: Effects of iron and manganese on various plankton communities. Limnology and Oceanography 36: 1865-1878.

Caron, D. A., E. R. Peele, E. L. Lim and M. R. Dennet 1999. Picoplankton and nanoplankton and their trophic coupling in surface waters of the Sargasso Sea south of Bermuda. Limnology and Oceanography 44: 259-272.

Chisholm, S. W. (1992). Phytoplankton size. Primary Productivity and Biogeochemical Cycles in the Sea. P. G. Falkowski and A. D. Woodhead, Eds. New York, Plenum Press.

Coale, K. H. 1991. Effects of iron, manganese, copper, and zinc enrichments on productivity and biomass in the subarctic Pacific. Limnology and Oceanography 36: 1851-1864.

Coale, K. H., S. E. Fitzwater, R. M. Gordon, K. S. Johnson and R. T. Barber 1996a. Control of community growth and export production by upwelled iron in the equatorial Pacific Ocean. Nature 379: 621-624.

Coale, K. H., et al. 1996b. A massive phytoplankton bloom induced by an ecosystem-scale iron fertilization experiment in the equatorial Pacific Ocean. Nature 383: 495-501.

Cotner, J. B., J. W. Ammerman, E. R. Peele and E. Bentzen 1997. Phosphorus-limited bacterioplankton growth in the Sargasso Sea. Aquatic Microbial Ecology 13: 141-149.

Cullen, J. J. 1991. Hypotheses to explain high-nutrient conditions in the open sea. Limnology and Oceanography 36: 1578-1599.

DuRand, M. D. Phytoplankton growth and diel variations in beam attenuation through individual cell analysis. Ph.D. Thesis, M.I.T. and W.H.O.I., 1995. pp. 263.

Dusenberry, J. A. Picophytoplankton photoacclimation and mixing in the surface oceans. Ph.D. Thesis, M.I.T. and W.H.O.I., 1995. pp. 301.

Elton, C. (1927). Animal ecology Macmillan.

Eppley, R. W., E. H. Renger, E. L. Venrick and M. M. Mullin 1973. A study of plankton dynamics and nutrient cycling in the central gyre of the North Pacific Ocean. Limnology and Oceanography 18: 534-551.

Gaedke, U. 1992. The size distribution of plankton biomass in a large lake and its seasonal variability. Limnology and Oceanography 37: 1202-1220.

Gin, K. Microbial size spectra from diverse marine ecosystems. Ph.D. Thesis, M.I.T./W.H.O.I. Joint Program, 1996. pp. 359.

Gin, K. Y. H., S. W. Chisholm and R. J. Olson in press. Seasonal and depth variation in microbial size spectra at the Bermuda Atlantic Time Series Station. Deep-Sea Research.

Goldman, J. C., J. J. McCarthy and D. G. Peavy 1979. Growth rate influence on the chemical composition of phytoplankton in oceanic waters. Nature 279: 210-215.

Graziano, L. M., R. J. Geider, W. W. W. Li and M. Olaizola 1996. Nitrogen limitation of North Atlantic phytoplankton: analysis of physiological condition in nutrient enrichment experiments. Aquatic Microbial Ecology 11: 53-64.

Hecky, R. E. and P. Kilham 1988. Nutrient limitation of phytoplankton in freshwater and marine environments: A review of recent evidence on the effects of enrichment. Limnology and Oceanography 33: 796-822.

Howarth, R. W. 1988. Nutrient limitation of net primary production in marine ecosystems. Annual Review of Ecology 19: 89-110.

Hudson, R. J. M. and F. M. M. Morel 1990. Iron Transport in marine phytoplankton: Kinetics of cellular and medium coordination reactions. Limnology and Oceanography 35: 1002-1020.

Landry, M. R., et al. 1997. Iron and grazing constraints on primary production in the central equatorial Pacific: an EqPac synthesis. Limnology and Oceanography 42: 405-418.

Li, W. K. W. 1994. Phytoplankton biomass and chlorophyll concentration across the North Atlantic. Scientia Marina 58: 67-79.

Liebig, J. v., Ed. 1855. Principles of agricultural chemistry with special reference to the late researches made in England. Cycles of essential elements: Benchmark papers in Ecology (1974). Dowden, Hutchinson & Ross, Inc.

Martin, J. H. and S. E. Fitzwater 1988. Iron deficiency limits phytoplankton growth in the north-east Pacific subarctic. Nature 331: 341-343.

Morel, F. M. M., R. J. Hudson and N. M. Price 1991. Limitation of productivity by trace metals in the sea. Limnology and Oceanography 36: 1742-1755.

Munk, W. H. and G. A. Riley 1952. Absorption of nutrients by aquatic plants. Journal of Marine Research 11: 215-240.

Pasciak, W. J. and J. Gavis 1974. Transport limitation of nutrient uptake in phytoplankton. Limnology and Oceanography 19: 881-888.

Platt, T. and K. L. Denman 1977. Organisation in the pelagic ecosystem. Helgolaender wiss. Meeresunters 30: 575-581.

Pomeroy, L. R. 1974. The ocean's food web, a changing paradigm. BioScience 24: 499-504.

Quiñones-Bergeret, R. A. Size-distribution of planktonic biomass and metabolic activity in the pelagic system. Ph.D. Thesis, Dalhousie University, 1992. pp. 225.

Rodriguez, J. and M. M. Mullin 1986. Relation between biomass and body weight of plankton in a steady-state oceanic ecosystem. Limnology and Oceanography 31: 316-370.

Ruiz, J., C. M. García and J. Rodríguez 1996. Vertical patterns of phytoplankton size distribution in the Cantabric and Balearic Seas. Journal of Marine Systems 9: 269-282.

Ryther, J. H. and W. M. Dunstan 1971. Nitrogen, phosphorous, and eutrophication in the coastal marine environment. Science 171: 1008-1013.

Sheldon, R. W., A. Prakash and W. H. Sutcliffe 1972. The size distribution of particles in the ocean. Limnology and Oceanography 17: 327-340.

Sheldon, R. W., W. H. Sutcliffe Jr. and M. A. Paranjae 1977. Structure of pelagic food chain and relationship between plankton and fish production. Journal of the Fisheries Research Board Canada 34: 2344-2353.

Sprules, W. G., S. B. Brandt, D. J. Stewart, M. Munawar, E. H. Jin and J. Love 1991. Biomass Size Spectrum of the Lake-Michigan Pelagic Food Web. Canadian Journal of Fisheries and Aquatic Sciences 48: 105.

Takeda, S. and H. Obata 1995. Response of equatorial Pacific phytoplankton to subnanomolar Fe enrichment. Marine Chemistry 50: 219-227.

Tittel, J., B. Zippel, W. Geller and J. Seeger 1998. Relationships between plankton community structure and plankton size distribution in lakes of northern Germany. Limnology and Oceanography 43: 1119.

Vidondo, B., Y. T. Prairie, J. M. Blanco and C. M. Duarte 1997. Some aspects of the analysis of size spectra in aquatic ecology. Limnology and Oceanography 42: 184-192.

Zettler, E. R., R. J. Olson, B. J. Binder, S. W. Chisholm, S. E. Fitzwater and M. R. Gordon 1996. Iron-enrichment bottle experiments in the equatorial Pacific: responses of individual phytoplankton cells. Deep-Sea Research 43: 1017-1029.

Chapter 2

# A dual sheath flow cytometer for shipboard analyses of phytoplankton communities from the oligotrophic oceans

Reprinted with permission from *Limnology and Oceanography*.

Cavender-Bares, K. K., S. L. Frankel and S. W. Chisholm 1998. A dual sheath flow cytometer for shipboard analyses of phytoplankton communities from the oligotrophic oceans. *Limnology and Oceanography* **43**: 1383-1388.

*Limnol. Oceanogr.*, 43(6), 1998, 1383–1388


# A dual sheath flow cytometer for shipboard analyses of phytoplankton communities from the oligotrophic oceans

*Abstract*—Flow cytometry has been used to study phytoplankton since the early 1980s. Because of the wide range of cell sizes and concentrations that occur in natural samples, multiple instrument configurations have been required to characterize pico-, ultra-, and nanophytoplankton. Lengthy changeover times between configurations have made synoptic analyses of phytoplankton communities extremely cumbersome and therefore rare. To overcome this problem, we have added dual-sheath capability and adjustable optics to a commercially available flow cytometer. These additions expand the instrument's capabilities during routine operation. The dual-sheath cytometer can characterize both the submicron picoplankter *Prochlorococcus* at sample flow rates of 10 $\mu$l min$^{-1}$ and, after a 1-min changeover, ultraphytoplankton and nanophytoplankton at sample flow rates >1 ml min$^{-1}$. These capabilities make possible real-time analysis of phytoplankton size spectra at sea.

Flow cytometers can be used to characterize single phytoplankton cells in terms of forward-angle light scatter (FALS) and autofluorescence parameters, which are related to cell size (Van de Hulst 1957; Ackelson and Spinrad 1988)

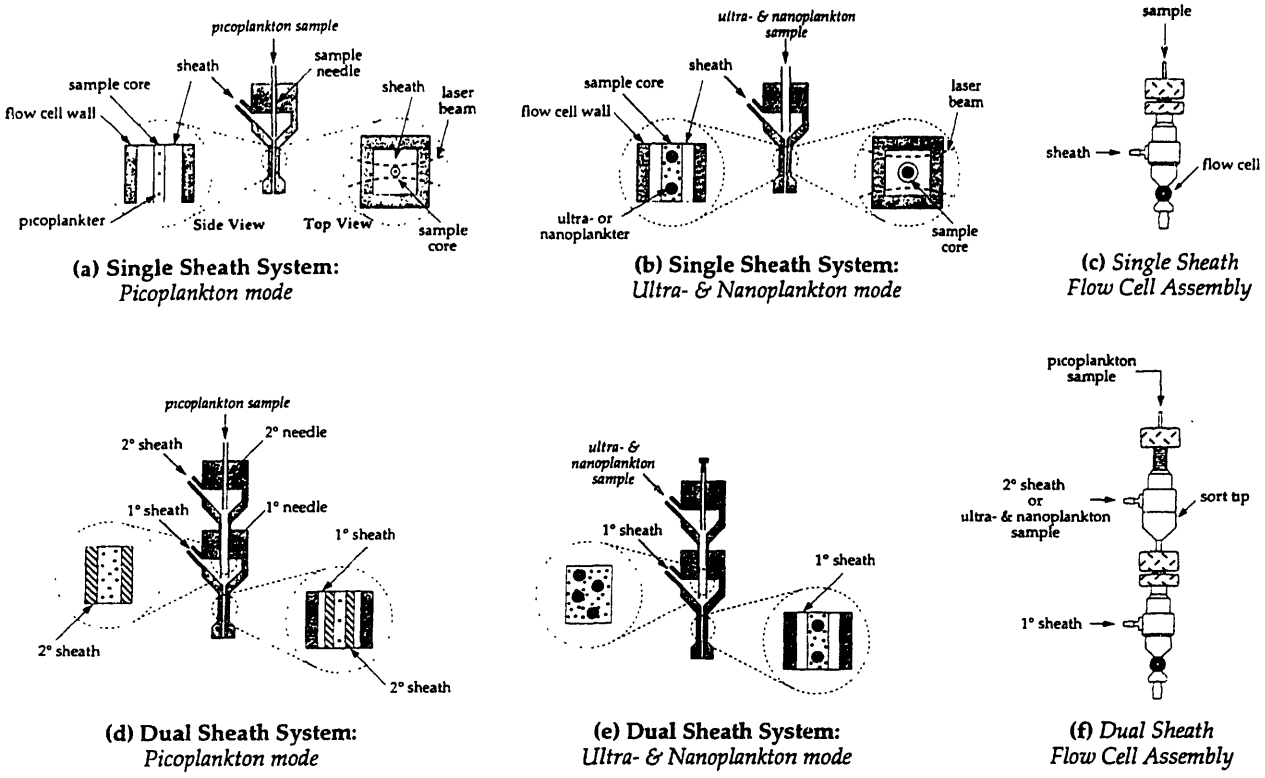


Fig. 1. Schematic representation of single- and dual-sheath flow systems. (a) Typical single-sheath flow system for picophytoplankton analyses. Samples are introduced via the sample needle and hydrodynamically focused by the sheath fluid stream after entering the square flow cell and before passing the excitation beam. (b) For analyses of larger ultraplankton and nanoplankton, the small-diameter sample needle is replaced with a larger one to achieve high sample flow rates. Heavy dashed lines in the top views of (a) and (b) denote the width of the laser beam as it is focused on the sample core—*see* text for dimensions. (c) Sketch of the standard single-sheath flow system. (d) The dual-sheath flow system in picoplankton mode using primary (1°) and secondary (2°) sheaths to produce a stable sample core for picoplankton analyses. (e) Dual-sheath flow system in ultraplankton and nanoplankton mode with the sample introduced via the 2° sheath inlet, while the 1° needle is blocked off. The laser beam is omitted from (d) and (e) for clarity; however, it is identical to that shown in (a) and (b), respectively. (f) Sketch of actual dual-sheath flow system with a Biosense flow cell (Coulter) attached. Note: the picoplankton and ultra- and nanoplankton samples are derived from the same seawater sample and differ only in their introduction rates. The scale in schematics is exaggerated for clarity.

and pigment concentration (Sosik et al. 1989; Li et al. 1993; Jonker et al. 1995), respectively. This technology has been used for a variety of applications in oceanography (e.g., Olson et al. 1985; Ackelson and Spinrad 1988; Chisholm et al. 1988; Neale et al. 1989; Perry and Porter 1989; Robertson and Button 1989; Sosik et al. 1989; Olson et al. 1990*a*,*b*; Orellana and Perry 1992; Li 1994*b*; Li 1995; Vaulot et al. 1995; Binder et al. 1996; Graziano et al. 1996) since its introduction to the field 15 yr ago (Olson et al. 1983; Yentsch et al. 1983). Confronted with heterogeneous mixtures of plankton cells, oceanographers continually strive to push the limits of commercial instruments, which are designed for biomedical research involving homogeneous cell suspensions. However, much of the research to date has been dictated by what the instruments can analyze rather than what the investigator wants to analyze.

In a flow cytometer, cell suspensions are hydrodynamically focused by a particle-free sheath fluid, which creates an annulus of sheath surrounding a circular sample core (Fig. 1a). The light collection optics are in line with the axis of the excitation light for FALS and orthogonal to that axis for autofluorescence. The excitation light and light collection optics are focused to the same point. Light pulses from individual cells are amplified and converted to digital signals for further processing via computer. For peak performance, the flow system, light source, optics, and electronics must be optimized to match the properties of the cells being studied—clearly a challenge when one is analyzing a heterogeneous mixture of phytoplankton.

One of the major analytical challenges for oceanographers using flow cytometry is the wide range of cell sizes and abundances that occur in natural phytoplankton communities. The small end of the spectrum is defined by the submicron picoplankter *Prochlorococcus*, which can reach concentrations $>10^5$ cells $ml^{-1}$ (Olson et al. 1990*a*; Binder et al. 1996). These cells are typically just below the limit of

detection of commercially available flow cytometers in terms of both FALS and autofluorescence. The upper end of the size spectrum cannot be defined in terms of a particular type of cell but instead is set by the rarest species in the sample collected. Because phytoplankton abundances are typically inversely related to cell size (Chisholm 1992; Kiørboe 1993), the rarest species is also usually the largest. In a 50-ml sample, cells can be enumerated down to concentrations of about 25 cells $ml^{-1}$ by flow cytometry (Olson et al. 1993). For comparison, this is roughly the concentration at which diatoms, 5–20 $\mu$m in their longest dimension, are found in the tropical Pacific (Chavez et al. 1996).

The analysis of any cell type requires a careful balance between sensitivity and particle count rate, which are interrelated and dependent on cell size and concentration; therefore, tradeoffs are necessary when setting up a flow cytometer for phytoplankton analyses. In order to detect autofluorescence and FALS signals under all conditions from the smallest picoplankter, *Prochlorococcus*, the sensitivity of commercially available instruments must be improved by reducing both sheath velocity ($<10$ m $s^{-1}$) and sample flow rates ($\sim 10$ $\mu$l $min^{-1}$) and increasing excitation intensity (e.g., Frankel et al. 1990; Olson et al. 1990*a*; Dusenberry and Frankel 1994). As a result, count rates are typically in the range of 20–100 counts $s^{-1}$. In order to achieve a representative sample size of the generally less numerous picoplankter, *Synechococcus*, samples must be run for 10–15 min.

Using these modified, high-sensitivity systems to enumerate large, rarer nanoplankton is not possible because of optical and count rate limitations. An elliptical spot is typically used to analyze larger cells, since the spot should be at least six times the width of the largest cell for even illumination (Shapiro 1995). High-sensitivity systems use a circular laser beam spot of about 20 $\mu$m, which is unsuitable for larger nanoplankton because they are about the same size. An adjustable laser-focusing system (as described by Dubelaar et al. 1989) would alleviate this particular conflict, but low count rates of the rarer cells would cause unrealistically long sample run times. Count rates can be increased somewhat by increasing the sheath flow rate, which controls the sample velocity. However, an increase on the order of 100- to 1,000-fold would be necessary for cells with a concentration of 25 cells $ml^{-1}$. Acceptable count rates of these rare cells can only be achieved by increasing the sample flow rate itself, which increases the diameter of the sample core (*compare Figs. 1a and b*). To this end, Olson et al. (1993) used a wide sample inlet needle on an EPICS V cytometer (Coulter) so that large-volume samples (e.g., 50 ml) could be rapidly processed at sample flow rates $>1$ ml $min^{-1}$. However, the narrow sample core necessary for picoplankton analyses cannot be established using such a wide sample needle, and changing to a smaller needle is very cumbersome.

The European Optical Plankton Analyzer (EurOPA) and its predecessor, the Optical Plankton Analyzer (OPA), were designed to address some of these challenges (Dubelaar et al. 1989; Jonker et al. 1995). They are capable of sample flow rates spanning at least four orders of magnitude, but their flow cell design and optics are optimized for detecting large chain-forming cells. They can analyze 1–2 $\mu$m *Synechococcus* cells (Jonker et al. 1995), but not the smaller picoplankter *Prochlorococcus*, which is a dominant feature of the oligotrophic oceans (Chisholm et al. 1988; Olson et al. 1990*a*; Shimada et al. 1993; Campbell and Nolla 1994; Li 1995; Binder et al. 1996).

To date, the two modifications that optimize commercial flow cytometers for analyzing either small, abundant picoplankton (small laser spot with low sample flow rate) or large, rarer cells (wide laser spot with high sample flow rate) have been incompatible on a single instrument setup. In order to analyze the entire phytoplankton community in a single sample, a lengthy changeover of the flow system and optics is required. Thus, the need to minimize the time between collection and analysis has precluded real-time pico-, ultra-, and nanophytoplankton analyses at sea using a single flow cytometer. To overcome this limitation, we have modified an EPICS V flow cytometer to include a dual-sheath flow system capable of sample flow rates spanning five orders of magnitude and with optics suited for detecting both large and small cells. Only 1 min is required to switch between low and high flow settings, enabling us to collect data on picophytoplankton through nanophytoplankton at sea (Cavender-Bares et al. in press). Here we describe the design and compare its performance to a standard high-sensitivity picophytoplankton configuration (Olson et al. 1990*a*). Because the new design preserves the modifications made by Olson et al. (1993) for analyses of large sample volumes, we do not evaluate that aspect of the instrument's performance here.

A second sheath (e.g., Eisert et al. 1975) was employed to create a flow system flexible enough to produce stable sample flow rates from as low as 1 $\mu$l $min^{-1}$ to $>5$ ml $min^{-1}$. In the typical single-sheath system, sample inlet needles of different sizes must be used to provide low (10 $\mu$l $min^{-1}$; Fig. 1a) and high ($>1$ ml $min^{-1}$; Fig. 1b) sample flow rates, a changeover that cannot be done routinely. The addition of a second sheath (Fig. 1d) allows a low sample flow rate through a secondary (2°) needle; picoplankton samples are hydrodynamically focused first upon entering the primary (1°) needle and then again upon entering the flow cell. The end result is a sample core surrounded by two concentric annuli of sheath fluid. This setup maintains the capability for high sample flow rates via the 1° needle directly. That is, ultraphytoplankton and nanophytoplankton samples can be introduced through the 2° sheath inlet (Fig. 1e), thereby creating an analog to the single-sheath configuration shown in Fig. 1b. As shown in Fig. 1e, the abundant picophytoplankton are present in large-volume samples; however, they cannot be accurately enumerated because the wide sample core prevents them from passing single file through the flow cell. Because of their weak FALS and autofluorescence signals at the lower excitation intensities used in this mode, the picophytoplankton do not confound signals from the larger cells.

The modified flow cell assembly (*see Fig. 1f*) was constructed from two flow chamber bodies and an extra sort tip (parts associated with the original EPICS V), the standard EPICS sample needle for the 2° needle, a large diameter 1° sample needle (1.2 mm internal diameter), and a Biosense quartz flow cell (Coulter). Separate 1° and 2° sheath tanks and the necessary valves and controls were added to the

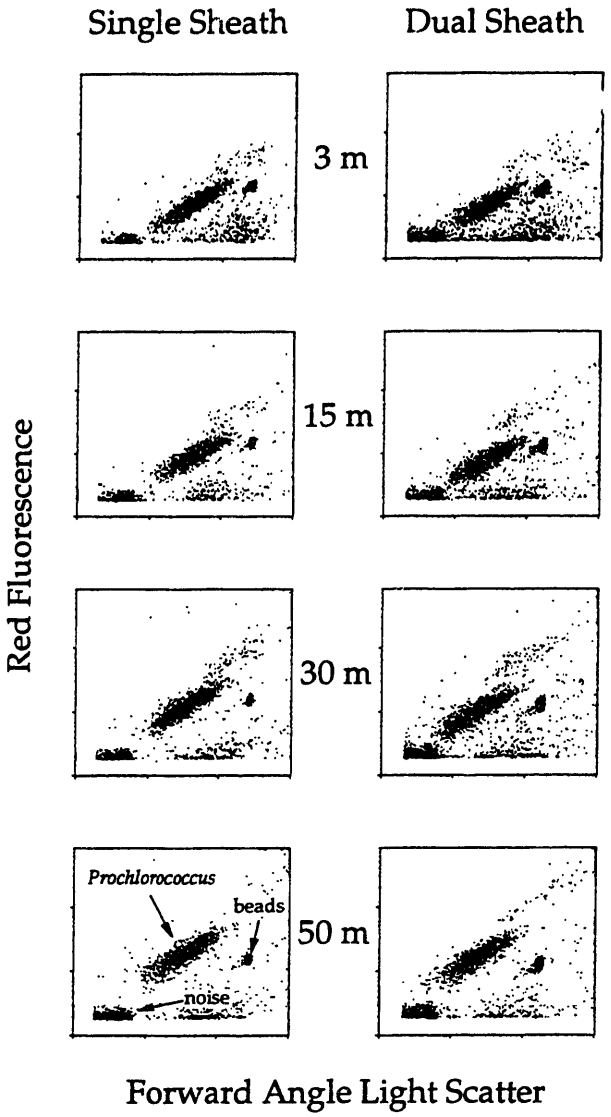


Fig. 2. A comparison of two parameter scatterplots for *Prochlorococcus* at different depths for single- and dual-sheath flow cytometer configurations. Samples (50 ml) were collected at local noon on 28 May 1995 at 4°14'S, 104°57'W in the equatorial Pacific and preserved in 1% gluteraldehyde (Vaulot et al. 1989). Each sample was later thawed, divided into six aliquots, and refrozen in liquid nitrogen. Three aliquots were analyzed on each instrument configuration with calibration microspheres (denoted as "beads") added (0.47 $\mu$m; Polysciences).

EPICS V in order to allow low sample flow (dual-sheath operation) or standard high flow (single-sheath operation) for the analysis of picophytoplankton and larger ultraphytoplankton and nanophytoplankton, respectively. A positive-pressure differential of <13.8 kPa (2 psi) was used to inject the 2° sheath into the 1° sheath operating at 82.7 kPa (12 psi); a syringe pump (Model HA 22, Harvard Apparatus) was used for sample introduction.

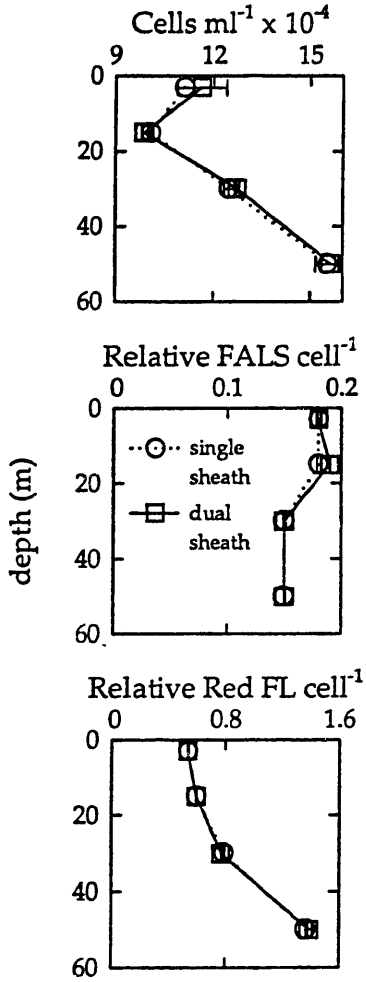


Fig. 3. Quantitative comparison of raw data shown in Fig. 2 for *Prochlorococcus* in terms of cell concentration, FALS, and red fluorescence. Each symbol represents the average (±SD) of three aliquots derived from the same 50-ml sample.

Two focusing configurations of the excitation beam are used to detect both small and large cells. As introduced by Dubelaar et al. (1989), we combined a spherical achromatic lens with a moveable, long focal length, cylindrical lens to produce two different spot sizes. For picophytoplankton analyses, the 488-nm beam produced by the Innova 90 laser (1.5 mm diameter; Coherent) is focused by a 40.5-mm spherical achromatic lens (Melles Griot) to produce a 17-$\mu$m-diameter spot size (*as in Fig. 1a*). For nanophytoplankton analyses, a 150-mm cylindrical lens (Newport) is moved via a precise sliding stage into the path of the beam at a position of 150 mm from the back focal plane of the 40.5-mm achromat. This arrangement produces an elliptical spot 400 $\mu$m wide and 17 $\mu$m high for the analysis of these larger cells (*see Fig. 1b* and Dubelaar et al. 1989).

To test the performance of the dual-sheath system for *Prochlorococcus* analyses, we compared replicate samples

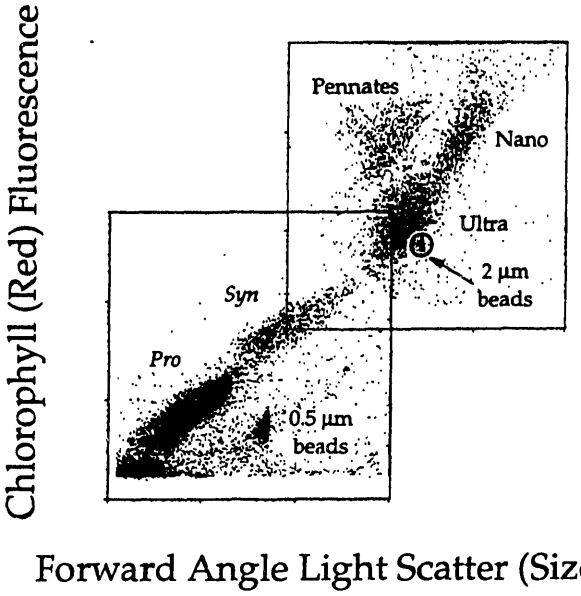


Fig. 4. Typical output from dual-sheath flow system. Lower scatterplot was measured in picoplankton mode (*see Fig. 1d*), and the upper scatterplot includes the populations measured in ultra- and nanoplankton mode (*see Fig. 1e*). Populations of *Prochlorococcus* (Pro) and *Synechococcus* (Syn) are distinct in the lower frame. The phytoplankton in the ultraplankton and nanoplankton groups ("Ultra" and "Nano") are completely visible in the upper panel. This sample contained significant numbers of pennate diatoms that, due to their shape, have a unique signature (Olson et al. 1989). Frames were merged together for this illustration by superimposing *Synechococcus* populations from each instrument mode. Different sample volumes for each mode are represented (2 ml and 0.1 ml for upper and lower panels, respectively) so that the less abundant cells in the upper panel would be clearly visible. *See* Gin (1996), for example, for a discussion of a more accurate merging protocol. Two populations of fluorescent microspheres ("beads") added to samples for intersample comparisons are denoted (0.47 and 2.02 μm; Polysciences). Data were collected at sea in the equatorial Pacific (depth, 10 m; 5 June 1996 at 5°34'S, 106°51'W) inside an iron-enriched patch of surface water (Coale et al. 1996). Note that red fluorescence values for *Synechococcus* are qualitative because of possible spillover of orange fluorescence (from phycoerythrin) into the red fluorescence signal.

using the standard high-sensitivity configuration that uses a single sheath (as described by Olson et al. [1990*a*] with a 40.5-mm spherical lens and a 488-nm laser operating at 800 mW; *see Fig. 1a*) and the dual-sheath system (Fig. 1d). The raw data from a station in the equatorial Pacific are shown in Fig. 2, in the form of two-dimensional scatterplots. The separation of *Prochlorococcus* from the noise—in terms of both FALS and red fluorescence—is adequate for both configurations, which allows accurate characterization at each depth. Indeed, replicate samples analyzed on both instrument configurations show excellent agreement in terms of cell number, mean red fluorescence per cell, and mean FALS per cell (Fig. 3).

This dual-sheath system has enabled us to collect data rapidly over a wider range of size classes—including the picophytoplankton—than previously possible using a single instrument at sea. Figure 4 depicts typical data collected with the dual-sheath system, highlighting its ability to span the pico-, ultra-, and nano-size classes. Moreover, because these size classes can be analyzed rapidly back to back on unpreserved samples, the dual-sheath flow cytometer has facilitated the shipboard collection of data necessary for constructing phytoplankton size spectra (Yentsch and Phinney 1989; Chisholm 1992; Li 1994*a*). Such spectra are enhanced by the inclusion of heterotrophic bacteria (e.g., Quiñones-Bergeret 1992; Gin 1996), now a straightforward process with the recent introduction of DNA stains that are excited at 488 nm (e.g., SYBER Green I; Molecular Probes) and are suitable for enumerating these cells (Marie et al. 1997). Such analyses eliminate the need for complicated dual-beam excitation, which is necessary with ultraviolet-excited DNA stains (Monger and Landry 1993; Binder et al. 1996). Finally, the extremely low sample flow rates (5 $\mu$l min$^{-1}$) necessary for these analyses because of high cell concentrations ($>10^5$ cells ml$^{-1}$) are possible on this dual-sheath system with no further modifications.

*Kent K. Cavender-Bares*
*Sheila L. Frankel*
*Sallie W. Chisholm*[1]

Ralph M. Parsons Laboratory
48-425 Massachusetts Institute of Technology
Cambridge, Massachusetts 02139
E-mail: chisholm@mit.edu.

## References

ACKELSON, S. G., AND R. W. SPINRAD. 1988. Size and refractive index of individual marine particulates: A flow cytometric approach. Appl. Opt. **27:** 1270–1277.

BINDER, B. J., S. W. CHISHOLM, R. J. OLSON, S. L. FRANKEL, AND A. Z. WORDEN. 1996. Dynamics of picophytoplankton, ultraphytoplankton, and bacteria in the Central Equatorial Pacific. Deep-Sea Res. **43:** 907–931.

CAMPBELL, L., AND H. A. NOLLA. 1994. The importance of *Prochlorococcus* to community structure in the central North Pacific Ocean. Limnol. Oceanogr. **39:** 954–961.

CAVENDER-BARES, K. K., E. MANN, S. W. CHISHOLM, M. E. ONDRUSEK, AND R. R. BIDIGARE. Differential response of phytoplankton populations to iron fertilization. Limnol. Oceanogr. In press.

CHAVEZ, F. P., K. R. BUCK, S. K. SERVICE, J. NEWTON, AND R. T. BARBER. 1996. Phytoplankton variability in the central and eastern tropical Pacific. Deep-Sea Res. **43:** 835–870.

CHISHOLM, S. W. 1992. Phytoplankton size, p. 213–237. *In* P. G. Falkowski and A. D. Woodhead [eds.], Primary productivity and biogeochemical cycles in the sea. Plenum.

———, R. J. OLSON, E. R. ZETTLER, R. GOERICKE, J. WATERBURY, AND N. WELSCHMEYER. 1988. A novel free-living prochlorophyte abundant in the oceanic euphotic zone. Nature **334:** 340–343.

COALE, K. H., AND OTHERS. 1996. A massive phytoplankton bloom induced by an ecosystem-scale iron fertilization experiment in the equatorial Pacific Ocean. Nature **383:** 495–501.

[1] To whom correspondence should be addressed.

DUBELAAR, G. B. J., A. C. GOENEWEGEN, W. STOKDIJK, G. J. VAN DEN ENGH, AND J. W. M. VISSER. 1989. Optical plankton analyser: A flow cytometer for plankton analysis, II: Specifications. Cytometry **10:** 529–539.

DUSENBERRY, J. A., AND S. L. FRANKEL. 1994. Increasing the sensitivity of a FACScan flow cytometer to study oceanic picoplankton. Limnol. Oceanogr. **39:** 206–209.

EISERT, W. G., R. OSTERTAG, AND E.-G. NIEMANN. 1975. Simple flow microphotometer for rapid cell population analysis. Rev. Sci. Inst. **46:** 1021–1024.

FRANKEL, S. L., B. J. BINDER, H. M. SHAPIRO, AND S. W. CHISHOLM. 1990. A high-sensitivity flow cytometer for studying picoplankton. Limnol. Oceanogr. **35:** 1164–1169.

GIN, K. 1996. Microbial size spectra from diverse marine ecosystems, p. 359. Ph.D. thesis, Massachusetts Institute of Technology/Woods Hole Oceanographic Institution Joint Program.

GRAZIANO, L. K., R. J. GEIDER, W. K. W. LI, AND M. OLAIZOLA. 1996. Nitrogen limitation of North Atlantic phytoplankton: Analysis of physiological condition in nutrient enrichment experiments. Aquat. Microb. Ecol. **11:** 53–64.

JONKER, R. R., J. T. MEULEMANS, G. B. J. DUBELAAR, M. F. WILKINS, AND J. RINGELBERG. 1995. Flow cytometry: A powerful tool in analysis of biomass distributions in phytoplankton. Water Sci. Technol. **32:** 177–182.

KIØRBOE, T. 1993. Turbulence, phytoplankton cell size, and the structure of pelagic food webs, p. 1–72. *In* J. H. S. Blaxter and A. J. Southward [eds.], Advances in marine biology. Academic Press.

LI, W. K. W. 1994*a*. Phytoplankton biomass and chlorophyll concentration across the North Atlantic. Sci. Mar. **58:** 67–79.

———. 1994*b*. Primary production of prochlorophytes, cyanobacteria, and eucaryotic ultraphytoplankton: Measurements from flow cytometric sorting. Limnol. Oceanogr. **39:** 169–175.

———. 1995. Composition of ultraphytoplankton in the central North Atlantic. Mar. Ecol. Prog. Ser. **122:** 1–8.

———, T. ZOHARY, Y. Z. YACOBI, AND A. M. WOOD. 1993. Ultraphytoplankton in the eastern Mediterranean Sea: Towards deriving phytoplankton biomass from flow cytometric measurements of abundance, fluorescence and light scatter. Mar. Ecol. Prog. Ser. **102:** 79–87.

MARIE, D., F. PARTENSKY, S. JACQUET, AND D. VAULOT. 1997. Enumeration and cell cycle analysis of natural populations of marine picoplankton by flow cytometry using the nucleic acid stain SYBER Green I. Appl. Environ. Microbiol. **63:** 186–193.

MONGER, B., AND M. R. LANDRY. 1993. Flow cytometric analysis of marine bacteria using Hoechst 33342. Appl. Environ. Microbiol. **59:** 905–911.

NEALE, P. J., J. J. CULLEN, AND C. M. YENTSCH. 1989. Bio-optical inferences from chlorophyll *a* fluorescence: What kind of fluorescence is measured by flow cytometry? Limnol. Oceanogr. **34:** 1739–1748.

OLSON, R. J., S. W. CHISHOLM, S. L. FRANKEL, AND H. M. SHAPIRO. 1983. An inexpensive flow cytometer for the analysis of fluorescence signals in phytoplankton: Chlorophyll and DNA distributions. J. Exp. Mar. Biol. Ecol. **68:** 129–144.

———, ———, E. R. ZETTLER, M. A. ALTABET, AND J. A. DUSENBERRY. 1990*a*. Spatial and temporal distributions of prochlorophyte picoplankton in the North Atlantic Ocean. Deep-Sea Res. **37:** 1033–1051.

———, ———, ———, and E. V. ARMBRUST. 1990*b*. Pigments, size, and distribution of *Synechococcus* in the North Atlantic and Pacific Oceans. Limnol. Oceanogr. **35:** 45–58.

———, D. VAULOT, AND S. W. CHISHOLM. 1985. Marine phytoplankton distributions measured using shipboard flow cytometry. Deep-Sea Res. **32:** 1273–1280.

———, E. R. ZETTLER, AND K. O. ANDERSON. 1989. Discrimination of eukaryotic phytoplankton cell types from light scatter and autofluorescence properties measured by flow cytometry. Cytometry **10:** 636–643.

———, ———, and M. D. DURAND. 1993. Phytoplankton analysis using flow cytometry, p. 175–186. *In* P. F. Kemp, B. F. Sherr, E. B. Sherr, and J. J. Cole [eds.], Handbook of methods in aquatic microbial ecology. Lewis.

ORELLANA, M. V., AND M. J. PERRY. 1992. An immunoprobe to measure Rubisco concentrations and maximal photosynthetic rates of individual phytoplankton cells. Limnol. Oceanogr. **37:** 478–490.

PERRY, M. J., AND S. M. PORTER. 1989. Determination of the cross-section absorption coefficient of individual phytoplankton cells by analytical flow cytometry. Limnol. Oceanogr. **34:** 1727–1738.

QUIÑONES-BERGERET, R. A. 1992. Size-distribution of planktonic biomass and metabolic activity in the pelagic system, p. 225. Ph.D. thesis, Dalhousie Univ.

ROBERTSON, B. R., AND D. K. BUTTON. 1989. Characterizing aquatic bacteria according to population, cell size, and apparent DNA content by flow cytometry. Cytometry **10:** 70–76.

SHAPIRO, H. M. 1995. Practical flow cytometry, 3rd ed. Wiley-Liss.

SHIMADA, A., T. HASEGAWA, I. UMEDA, N. KADOYA, AND T. MARUYAMA. 1993. Spatial mesoscale patterns of West Pacific picophytoplankton as analyzed by flow cytometry: Their contribution to subsurface chlorophyll maxima. Mar. Biol. **115:** 209–215.

SOSIK, H. M., S. W. CHISHOLM, AND R. J. OLSON. 1989. Chlorophyll fluorescence from single cells: Interpretation of flow cytometric signals. Limnol. Oceanogr. **34:** 1749–1761.

VAN DE HULST, H. C. 1957. Light scattering by small particles. Wiley.

VAULOT, D., C. COURTIEST, AND F. PARTENSKY. 1989. A simple method to preserve oceanic phytoplankton for flow cytometric analyses. Cytometry **10:** 629–635.

———, MARIE, D., R. J. OLSON, AND S. W. CHISHOLM. 1995. Growth of *Prochlorococcus*, a photosynthetic prokaryote, in the equatorial Pacific Ocean. Science **268:** 1480–1482.

YENTSCH, C. M., AND OTHERS. 1983. Flow cytometry and sorting: A technique for analysis and sorting of aquatic particles. Limnol. Oceanogr. **28:** 1275–1280.

YENTSCH, C. S., AND D. A. PHINNEY. 1989. A bridge between ocean optics and microbial ecology. Limnol. Oceanogr. **34:** 1694–1705.

*Received: 6 January 1998*
*Accepted: 18 May 1998*
*Amended: 2 June 1998*

Chapter 3

# Estimating phytoplankton cell size using flow cytometry

Kent K. Cavender-Bares

Sallie W. Chisholm

ABSTRACT

Size spectra provide a means for representing the distribution of microbial plankton in a synoptic manner, which is taxon-independent. In order to use flow cytometry to construct size spectra, it is necessary to convert light scatter signals to cell volume. In the past, methods to do this have relied on experimental calibrations using laboratory cultures. In an effort to use field samples for the calibration process, we have developed a protocol for creating an instrument calibration. It is based on the sorting capability of flow cytometers and cell sizing using the Coulter Counter. Using this method, a calibration curve has been constructed using a range of field populations from *Prochlorococcus* up to cells having a diameter of about 5 μm. We have compared the calibration data to previous methods and find good agreement.

## INTRODUCTION

Flow cytometry provides a means for enumerating and characterizing hundreds of phytoplankton cells per second and has, for this reason, gained appeal over more time-intensive analyses of microorganisms such as epifluorescent microscopy. Its introduction to oceanography (Yentsch *et al.* 1983; Olson *et al.* 1983) led to the characterization of the picoplankter *Prochlorococcus* (Chisholm *et al.* 1988), has deepened our understanding of the distribution and ecology of several different phytoplankton groups (Vaulot *et al.* 1990; Olson *et al.* 1990b; Olson *et al.* 1990a; Li *et al.* 1993; Campbell *et al.* 1994; Li 1994; Li 1995; Vaulot *et al.* 1995; Binder *et al.* 1996; Reckermann and Veldhuis 1997), and has been a valuable tool for following the response of specific phytoplankton groups during enrichment experiments (e.g., Price *et al.* 1994; Zettler *et al.* 1996; Graziano *et al.* 1996; Timmermans *et al.* 1998; Cavender-Bares *et al.* 1999).

Light scatter and pigment autofluorescence are regularly used qualitatively in order to separate phytoplankton groups from each other. For example, *Synechococcus* displays orange fluorescence, which results from autofluorescence of phycoerythrin; the orange fluorescence signal is used to distinguish this picoplankter from *Prochlorococcus*, which lacks orange fluorescence. Similarly, *Synechococcus* is distinguished from the typically larger ultraphytoplankton because these cells also lack orange fluorescence. Light scatter is a necessary parameter to distinguish groups within the ultra- and nanoplankton size range (e.g., Zettler *et al.* 1996). Pennate diatoms, because of their elongated shape, have a characteristic forward angle light scatter (FALS) signal which is much lower than more spherical cells of similar volume, and they can be distinguished due to their low ratio of FALS to red fluorescence (Olson *et al.* 1989). The utilization of both fluorescence and light scatter signals allows the distinction between dual populations of *Prochlorococcus* (e.g., Moore *et al.* 1998). Beyond the use of these signals to make qualitative distinctions, quantitative characterization of phytoplankton cells is not straightforward (Ackelson and Spinrad 1988; Neale *et al.* 1989; Sosik *et al.* 1989; Perry and Porter 1989; Robertson and Button 1989; Olson *et al.* 1995; Robertson *et al.* 1998).

The use of FALS as a proxy for phytoplankton cell size is widespread within the community of biological oceanographers who utilize flow cytometers, yet the interpretation of this signal in terms of size is problematic. To date, investigators have relied on empirical calibrations relating mean FALS of marine algal cultures with their mean Coulter volume (Olson *et al.* 1989; DuRand 1995; Gin 1996). These studies have yielded an image of FALS increasing as a power function of volume (e.g., FALS = $\alpha Vol^{\beta}$). However, at least two power functions or a polynomial relationship have been required to fit empirical data spanning several orders of magnitude in volume. Light scattering by particles of varying size and refractive index is explained by Mie theory (Van de Hulst 1957; Bohren and Huffman 1983), and it has been shown that the simplified Raleigh-Gans approximation of the light scattering equations can be used to explain light scatter of small cells such as marine bacteria (e.g., < 0.1 $\mu m^3$) which have refractive indices close to that of the medium (Koch *et al.* 1996; Robertson *et al.* 1998). Mie theory has been used in flow cytometry to estimate the refractive index of several marine phytoplankton via measurements of FALS and light scatter perpendicular to the axis of the laser beam (Ackelson and Spinrad 1988).

Flow cytometry has been used previously (Yentsch and Phinney 1989; Chisholm 1992; Li 1994; Gin 1996) as a means for collecting data to construct size spectra of microbial plankton (e.g., Sheldon *et al.* 1967; Platt and Denman 1978; Ahrens and Peters 1991; Quiñones-Bergeret 1992; Rodriguez and Mullin 1986; Ruiz *et al.* 1992). These methods, however, have depended almost exclusively on calibrations of FALS using laboratory cell cultures. These calibrations have a limitation because the species represented in culture collections may not be representative of field populations, and culturing conditions may not accurately simulate the *in situ* environment. To improve the accuracy of constructed size spectra, we have sought to calibrate FALS in terms of cell volume using field populations of phytoplankton rather than laboratory cultures. Due to the fact that the slopes and shapes of size spectra are significant (e.g., Vidondo *et al.* 1997; Tittel *et al.* 1998), our overall goal was to eliminate as many uncertainties as possible in the process of converting FALS to cell volume, and thus, increase the reliability of interpreting spectral shapes. We chose two new field approaches, one based on filter fractionation and the other based on cell sorting via flow cytometry, to alleviate potential shortcomings of FALS calibrations which rely on laboratory cultures.

The first calibration approach was similar to that previously employed to explore the performance of various filters (Sheldon and Sutcliffe 1969; Sheldon 1972). Using a Coulter Counter, Sheldon (1972) compared the material passing through a filter to the unfiltered water as a function of equivalent spherical diameter (ESD). By plotting percent cell retention against ESD, he found that the ESD associated with *50%* retention of material on the filters closely matched the nominal pore size of membrane filters. Our first method assumes that membrane filters retain *50%* of cells which have an ESD equal to the filter's pore size. Following this assumption, the FALS value associated with *50%* retention was correlated to the nominal pore size of the filters for a variety of stations in the Atlantic Ocean. In a second approach, we sorted cells via flow cytometry to produce subsets of field samples which contained only those cells having FALS signals within a pre-defined, narrow range. The Coulter volumes of these sub-samples were measured and correlated to their FALS value for a wide range of samples originating from stations in the Atlantic and Pacific Oceans.

Results suggest that the approach based on sorting has a greater potential for precise conversions between FALS and cell volume. We found the strongest relationship between these two parameters for pico- and ultraphytoplankton ($\leq 30\ \mu m^3$). For larger cells ($\leq 300\ \mu m^3$), a well defined, but different relationship existed between FALS and cell volume. We believe that preservation effects were more significant for the large cells and were the main reason for the observed differences in the FALS-volume relationship between small and large cells.

## METHODS

*Filtered sample collection and processing*—Samples for the calibration process based on size-fractionating sea water samples were collected on two oceanographic cruises from coastal waters off New England into the Sargasso Sea (Table 1). All samples were prepared at sea with water collected using conventional Niskin bottles or using a bucket from the side of the ship. Water samples of about 100 ml were gravity filtered through polycarbonate membrane filters (Osmonics) with pore sizes ranging from 0.6 to 10 µm. These filtrates were analyzed flow

Table 1: Description of sampling stations for FALS calibration method based on filter fractionation

| Cruise | Date | Station | Cast | Latitude (°N) | Longitude (°W) | Description |
|---|---|---|---|---|---|---|
| OC 279 | June 1996 | n/a | bucket | 34° 44 | 69° 53 | Sargasso Sea |
| | | 1 | 3 | 39°22 | 70°31 | shelf waters |
| | | 4 | 5 | 36° 21 | 69° 54 | Sargasso Sea |
| | | 8 | 43 | 36° 26 | 69° 45 | Sargasso Sea |
| | | 9 | 77 | 37°30 | 69°55 | Gulf Stream |
| | | 10 | 78 | 38°37 | 70°37 | slope waters |
| | | 12 | 80 | 40°0 | 70°43 | shelf waters |
| | | 13 | 81 | 40°33 | 70°51 | shelf waters |
| OC 297 | Feb. 1997 | 3 | 4 | 35°14 | 63°48 | Sargasso Sea |
| | | 5 | 31 | 35°50 | 61°57 | Sargasso Sea |
| | | 7 | 35 | 36°30 | 65°50 | Sargasso Sea |
| | | 8 | 38 | 38°05 | 67°40 | Gulf Stream |
| | | 10 | 40 | 39°50 | 70°40 | slope waters |
| | | 11 | 45 | 40°36 | 71°0 | shelf waters |

cytometrically and were compared to unfiltered aliquots of the same sample. FALS distributions of the filtrate, which were divided into 128 log bins, were divided by the distribution of the unfiltered water sample. The FALS value at which *50%* of the cells were retained on the filter ($FALS_{50\%}$) was associated with a spherical cell having a diameter equal to the nominal pore size of the filter ($D_{pore}$) and an equivalent spherical volume of $V_{pore}$. This operational definition relating FALS and $V_{pore}$ minimized the subjectivity during data analysis and was supported by the findings of Sheldon (1972). Samples prepared with 1 μm or smaller pore size filters were preserved in 0.1% glutaraldehyde (Vaulot *et al.* 1989), and analyzed using a modified EPICS V flow cytometer (Coulter Beckman; Cavender-Bares *et al.* 1998) configured to allow high-sensitivity measurements of picoplankton on land (Setting #1). Samples prepared using filters with pore size of 1 μm or greater were analyzed for ultra- and nanoplankton at sea using the system set up for large sample volume analyses (Setting #2; see also below). An assortment of calibration microspheres (Polysciences) ranging from 0.47 to 10 μm were analyzed on the instrument regularly to ensure that their relative FALS signals did not change day-to-day, thereby confirming that the geometry of FALS collection had not changed significantly.

*Calibration by flow cytometric sorting and Coulter volume sizing*—Samples were collected on several cruises in both the equatorial Pacific and Atlantic oceans (Table 2). In addition to sampling *in situ* planktonic communities using conventional Niskin or Go-Flo bottles or via the ship's flow-through sampling system, samples were also collected from nutrient enrichment studies. Samples were preserved in 0.1% gluteraldehyde (Vaulot *et al.* 1989), frozen in liquid nitrogen initially, and then moved to –80°C storage after several months. Samples were thawed in a 37°C water bath no more than 30 minutes prior to analysis. Samples were introduced via a syringe pump (Model HA 22; Harvard Apparatus) into an EPICS V (Beckman Coulter) flow cytometer. Low sample flow rates (10 μl $min^{-1}$) were achieved using the standard EPICS sample injection tube, while high sample flow rates (1 ml $min^{-1}$) were possible using a large diameter sample injection tube (1.2 mm I.D.; Cavender-Bares *et al.* 1998).

The flow cytometer was configured in sorting mode with a quartz sort tip, and a 5 W argon-ion laser (Innova-90; Coherent) providing 800 mW of 488 nm light. FALS signals were scattered light which passed beyond a wide horizontal obscuration bar, were focused by the

Figure 1:

Representative two-parameter scattergrams of flow cytometry data under sorting conditions. (A) Red fluorescence (Red FL) v. forward angle light scatter (FALS) for the high-sensitivity sorting protocol. A partial population of *Prochlorococcus* and an entire populations of Synechococcus and the ultraplankton were visible, and are shown relative to 2.02 μm beads. (B) Typical sort regions for *Prochlorococcus* and *Synechococcus* populations; cells falling within these regions would be sorted into separate tubes. (C) Scattergram for the lower-sensitivity sorting setup, with ultra and nanoplankton as well as pennate diatoms visible, again shown relative to beads. (D) Typical sort regions for ultra- and nanoplankton populations.

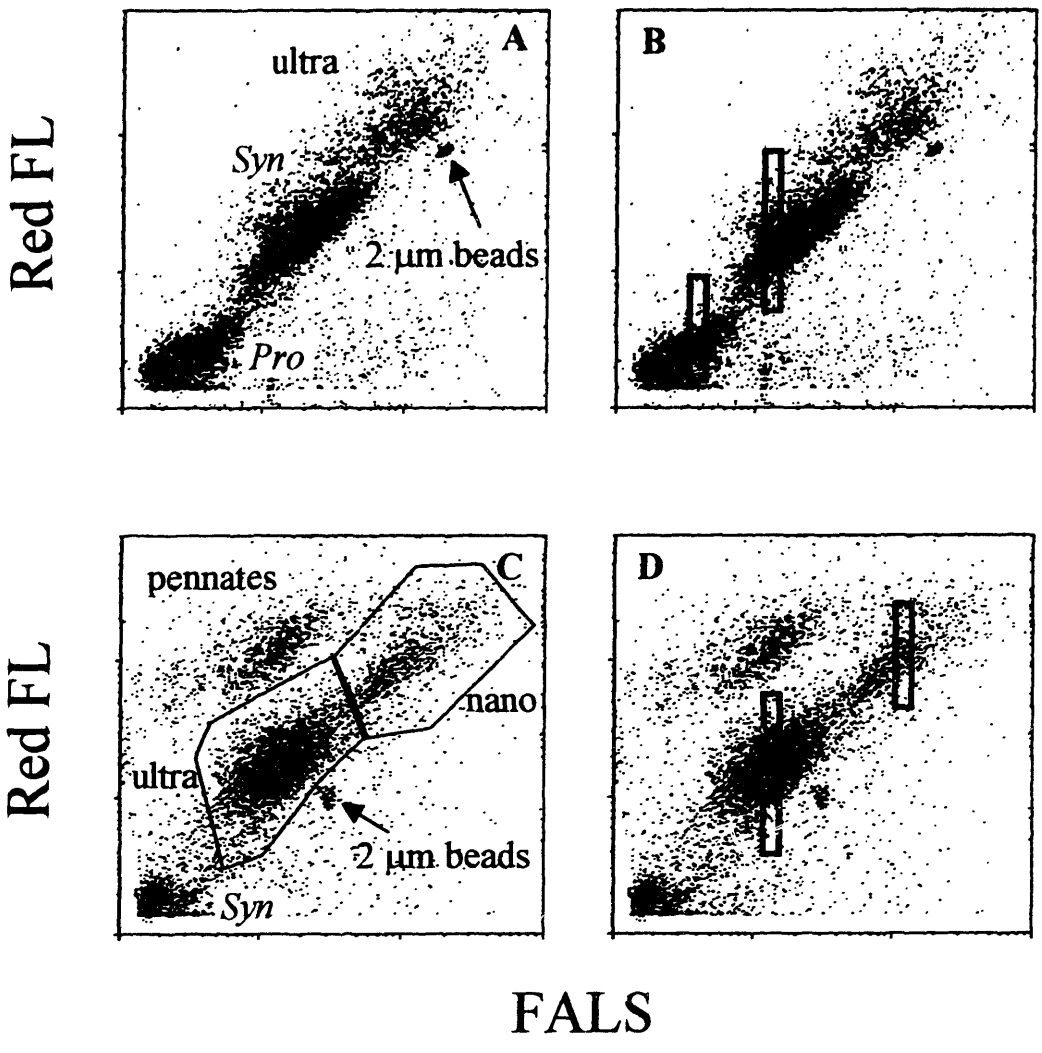
A
ultra
Syn
2 µm beads
Pro
B
C
pennates
nano
ultra
2 µm beads
Syn
D
Red FL
Red FL
FALS

Table 2: Sampling stations for the calibration method based on sorting via flow cytometry. For each sample, columns to the right indicate the number of sub-samples which were sorted and sized for each flow cytometric group.

| Cruise | Date | Station | Cast | Depth (m) | Latitude °N | Longitude (°W) | Description | number of sub-samples sorted per group | | | | | | |
|---|---|---|---|---|---|---|---|---|---|---|---|---|---|---|
| | | | | | | | | *Pro* | *Syn* | ultra | sm. nano | lg. nano | sm. pennate | lg. pennate |
| IronEx II | June 1995 | | 114 | 15 | -5°05 | 106°27 | in, day 4 | | 3 | | | | | |
| (equatorial Pacific) | | | 128 | 15 | -5°12 | 106°32 | in, day 4 | | | 4 | 2 | | | |
| | | | 128 | 10 | -5°12 | 106°32 | in, day 4 | | | | 2 | | | |
| | | | 129 | 20 | -5°12 | 106°51 | out, day 4 | | | | 2 | | | |
| | | | 173 | 15 | -5°44 | 107°05 | in, day 6 | | | | 3 | | | |
| | | | 180 | 15 | -5°44 | 107°05 | in, day 6 | | | 3 | 4 | | | |
| | | | 182 | 15 | -5°44 | 107°05 | in, day 6 | | | 8 | 2 | | | |
| | | | 184 | 15 | -5°44 | 107°05 | in, day 6 | | | 6 | 3 | | | |
| | | | 196 | 15 | -5°44 | 107°05 | in, day 6 | | | 7 | 1 | | | |
| | | | 227 | 3,10,15 | -6°11 | 107°53 | in, day 8 | | 4 | | | | | |
| | | | 231 | 10 | -6°14 | 107°57 | in, day 6 | | | | | | 4 | |
| | | | 253 | 15 | -6°26 | 108°18 | out, day 9 | | | | | | 2 | |
| | | | 255 | 15 | -6°23 | 108°16 | out, day 9 | | | | | | 1 | |
| | | | 288 | 10 | -6°43 | 109°10 | in, 0.4 nM-Fe patch, day 1 | | | | | | 2 | |
| | | | 278 | 15 | -6°51 | 109°5 | out, day 11 | | | | | | 7 | |
| | enrichment experiment | | n/a | | | | +Fe, Si, Zn | | | | | | 4 | 3 |
| | | | n/a | | | | +Fe | | | 2 | 1 | | 1 | |
| | | | n/a | | | | +Fe, Zn | | | | 2 | | 2 | 2 |

Table 2 (con't): Sampling stations for the calibration method based on sorting via flow cytometry. For each sample, columns to the right indicate the number of sub-samples which were sorted and sized for each flow cytometric group.

| Cruise | Date | Station | Cast | Depth (m) | Latitude °N | Longitude (°W) | Description | number of sub-samples sorted per group | | | | | | |
|---|---|---|---|---|---|---|---|---|---|---|---|---|---|---|
| | | | | | | | | *Pro* | *Syn* | ultra | sm. nano | lg. nano | sm. pennate | lg. pennate |
| OC 279 | June 1996 | 5 | n/a | 5 | 34°44 | 69°53 | Sargasso Sea | | | | 5 | | | |
| OC 297 | Feb. 1997 | 5 | 31 | 50 | 35°50 | 61°57 | Sargasso Sea | 3 | 4 | 4 | 1 | | | |
| | | 7 | 35 | 40 | 36°30 | 65°50 | Sargasso Sea | | 4 | 4 | 2 | | | |
| | | 8 | 38 | 3 | 38°05 | 67°40 | Gulf Stream | 3 | 2 | 4 | 2 | | | |
| | | 9 | 40 | 40 | 35°43 | 61°34 | slope waters | | | 3 | 2 | | | |
| | | 10 | 42 | 0 | 39°50 | 70°40 | slope waters | | | 4 | 1 | | | |
| enrichment experiments | | | n/a | | | | day 4, +N&P | | 6 | 5 | | | | |
| | | | n/a | | | | day 4, control | | | 9 | 1 | | | |
| | | | n/a | | | | day 7, +NP&Si | | | | 4 | 8 | | 6 |
| | | | n/a | | | | day 7, +N&P | | | 4 | 7 | | | |
| OC 318 | March 1998 | 3 | n/a | 3 | 31°33 | 64°08 | Sargasso Sea | 4 | 4 | | | | | |

standard EPICS optics, then passed through a filter which permitted only vertically-polarized light to pass (which was the polarization of the laser beam), and were detected by a photo multiplier tube. A Cicero system (Cytomation) was used for signal processing and control of sorting. Three-droplet sorting was used under purify mode which reduced the number of cells sorted yet increased the purity of the sorted sample. Two-dimensional regions from which the sort logic was controlled were constructed such that they delineated narrow ranges in FALS and wide ranges in cellular fluorescence (Fig. 1).

Typically, sort regions were confined to a single population (e.g., *Synechococcus*) as defined flow cytometrically in order to provide a means for discerning any inter-population differences (Fig. 1b,D). We use the terms ultra- and nanoplankton to classify the two subgroups that typically are discernable within the larger phytoplankton (Fig. 1C), but stress that these classifications are operational and confer only relative sizes to the groups (Zettler *et al.* 1996; Cavender-Bares *et al.* 1999). We were unable to resolve the entire *Prochlorococcus* population (Fig. 1A) due to the lower fluorescence sensitivity of the sort tip used here compared to that of the flow cell with an integrated lens for fluorescence detection typically used for picoplankton analyses (Cavender-Bares *et al.* 1998). Approximately 10,000 cells were sorted into filtered sea water and sized within 15 minutes (see below). In some cases—especially for sorting of *Prochlorococcus* and *Synechococcus*—pre-concentration was required prior to sorting since very low sample flow rates (10 $\mu l\ min^{-1}$) necessary for accurate measurements of FALS prevented 10,000 cells to be sorted in a reasonable amount of time. In these cases, cells from three 50-ml samples were collected on a 0.4 micron membrane filter (Poretics) using gentle vacuum (5 inches Hg) to the point where the filter remained moist; the material retained on the filter was then re-suspended in 1 ml of filtered seawater and subjected to the sorting protocol as described above.

Sub-samples which had been sorted flow cytometrically, were sized using a Coulter Counter (Model ZM with Channelizer 128; Beckman Coulter). The instrument was calibrated using calibration microspheres (Polysciences) of similar size to the cells of interest. The mode of data collection termed "edit mode" was used which eliminates signals resulting from cells which do not pass through the center of the aperture orifice. Since smaller aperture sizes permit higher

sensitivity sizing, but have reduced sample flow rates, apertures of 14, 30, and 50 μm were selected to balance sensitivity and flow rate. In order to count and size a similar number of cells for each aperture tube, cell concentration needed to be increased as aperture size was reduced. This was achieved in part by utilizing smaller sample cuvettes for the smaller aperture sizes. The cut-off end of a test tube with a slightly larger diameter than that of the aperture tube worked well to minimize sample volume required for the smaller aperture diameters. Size distributions of cells were collected on the Channelizer and transferred to a PC for statistical calculations.

Studies designed to verify the sorting capability of our system indicted that, when re-run through the flow cytometer, cells did not fall exclusively within the original sort region (*see* Appendix B), but rather displayed some dispersion around a mean centered close to the mode FALS of the cells in the original sort region. For this reason, the mode FALS and the mean Coulter volume of sorted populations are reported here.

## RESULTS

*Calibration based on filter fractionation*—Samples used for this calibration were drawn from a variety of oceanographic regimes (Table 1) because we intended to analyze size spectra from all of these regions. While a clear relationship between $FALS_{50\%}$ and $V_{pore}$ exists (Fig.2), the high variability limits the confidence one would have in predicting volume from a given FALS signal. For example, a FALS signal of 3 units (relative to 2.02 μm beads) could correspond to cells ranging over more than an order of magnitude in volume. For a given water sample, however, repeatability of this method was very good (Fig. 2A, inset) and cannot be used to explain the variation in this combined data set. A second problem is that a clear discontinuity exists in the relationship between $FALS_{50\%}$ and $V_{pore}$ at the juncture between the two instrument settings. This has been seen previously (Gin 1996) and may be an artifact of merging data from two different instrument settings.

*Flow cytometric sorting and cell sizing*—A range of community types was used for the calibration based on sorting and sizing (Table 2), including the Sargasso Sea, the Gulf Stream,

coastal waters, the equatorial Pacific, and samples derived from enrichment studies. Calibration data spanned from mid-way through a typical population of *Prochlorococcus* (0.1 $\mu m^3$) up through nanoplankton having a volume of about 300 $\mu m^3$ (Fig. 3A). A striking feature of the data is the interface between the ultra- and nanoplankton, where cells from both populations have similar FALS, yet differ by a factor of two in volume. This discontinuity falls at a different point in the FALS-volume relationship than does the one from the calibration method based on filter fractionation (Fig. 2B).

The data in Fig. 3 for *Prochlorococcus*, *Synechococcus*, the ultraplankton, and the smaller nanoplankton covers a size range occupied by the vast majority of phytoplankton distinguishable in a 50-ml sample from most of the stations listed in Table 2. There were also special cases, primarily the various enrichment studies, in which larger cells were present in significant numbers. From these samples we were able to sort from three additional groups: small and large pennate diatoms; and a population of large spherical cells, which we have classified as large nanoplankton. As has been shown previously (Olson *et al.* 1989), both small and large pennate diatoms form distinct clusters with FALS signals less than would be expected from volume alone (Fig. 3B). Within the small pennate diatom group, a clear relationship between FALS and volume is lacking, perhaps because the range of cell volumes measured was small. Due to the anomalous light scatter values of these irregularly shaped cells, we did not include the pennate diatoms in the overall calibration derived in this study.

## DISCUSSION AND ANALYSIS

The discontinuity in the relationship between cell volume and FALS at the juncture between the ultraplankton (Fig. 3A) and smaller nanoplankton is problematic. The data suggest that there is a narrow range of FALS, centered around the value of 1.5 bead units, in which the relationship between FALS and cell volume breaks down. A similar discontinuity is also apparent in the FALS to volume relationship of polystyrene microspheres (Fig. 4), which can be reproduced using Mie theory (Ackelson and Spinrad 1988). This suggests that the discontinuity seen in our calibration data may be real and explainable by Mie theory. In order to investigate

this further, we used a program (provided by M. DuRand and R. Greene) which calculates FALS as a function of particle size and refractive index ($m$) after the equations of Bohren and Huffman (1983). The refractive index of polystyrene is typically assumed to be 1.19 (relative to seawater, or 1.59 relative to air; Ackelson and Spinrad 1988; Robertson *et al.* 1998). A small change in $m$ has a large effect on the relationship between volume and FALS (Fig. 4C,D), and we found that a value of 1.21 provided the best fit to the empirical data (Fig. 4D). While it is not critical to our overall analysis, it is worth noting that the value of 1.19 for $m$ was measured at a wavelength of 589 nm (Lide 1992), and that $m$ typically increases as the wavelength of light decreases. Thus, it is possible that an $m$ of 1.21 may be reasonable given the excitation wavelength was 488 nm in our studies. More importantly, we used the microsphere data to estimate the geometry of the optics used for collecting FALS, because this parameter was a necessary input to the program. A range of 3-19° for FALS, in combination with an $m$ of 1.21, provided the best fit to the microsphere data (Fig. 4D). For our instrument, the manufacturer lists a 2-19° range for the wide obscuration bar used, however we have widened the original bar slightly, which is consistent with a decreased angular range of FALS collection. A scattering angle of 3-19° was used for all further computations based on Mie theory.

We then attempted to replicate the discontinuity seen in the calibration data (Fig. 3A) using Mie theory. A range of $m$ values typical for marine phytoplankton (1.04 to 1.07; Stramski and Mobley 1997), nearly accounts for the discontinuity, assuming that the larger cells had an $m$ of 1.04, while the smaller cells had higher $m$ values (Fig. 5A). If we let $m$ increase beyond the relevant range for cultured phytoplankton (Fig. 5B), we see that a higher $m$ can also explain the FALS-volume relationship for the larger cells (e.g., $m = 1.19$). Hence, the relationship seen in the calibration data (Fig. 3A) could be explained by differences in $m$ between the ultra- and nanoplankton groups. We have no measures of $m$ for our samples and cannot rule out differences between groups. Nevertheless, because measurements were made on preserved samples, and because calibration data will be applied to samples run live at sea, we should consider whether the discontinuity might be an artifact of preservation.

Evidence in the literature suggests that flow cytometric characteristics of larger cells, such as those classified here as nanoplankton, may be poorly retained through the preservation

Figure 2:

Calibration data from filter fractionation method. (A) Forward angle light scatter values associated with 50% retention of material on membrane filters ($FALS_{50\%}$) as a function of the equivalent spherical volume of membrane filter pores ($V_{pore}$). Data collected on two different instrument settings: high-sensitivity for picoplankton analyses (#1); and the lower-sensitivity setting for ultra- and nanoplankton analyses (#2). Inset in A shows good repeatability of method for two replicate fractionations (duplicates: circles and inverted triangles) which used the same seawater sample. (B) Data in A with axes switched to aid in comparison to calibration data from sorting-based method shown in Fig. 3. See Table 1 for locations of sampling stations.

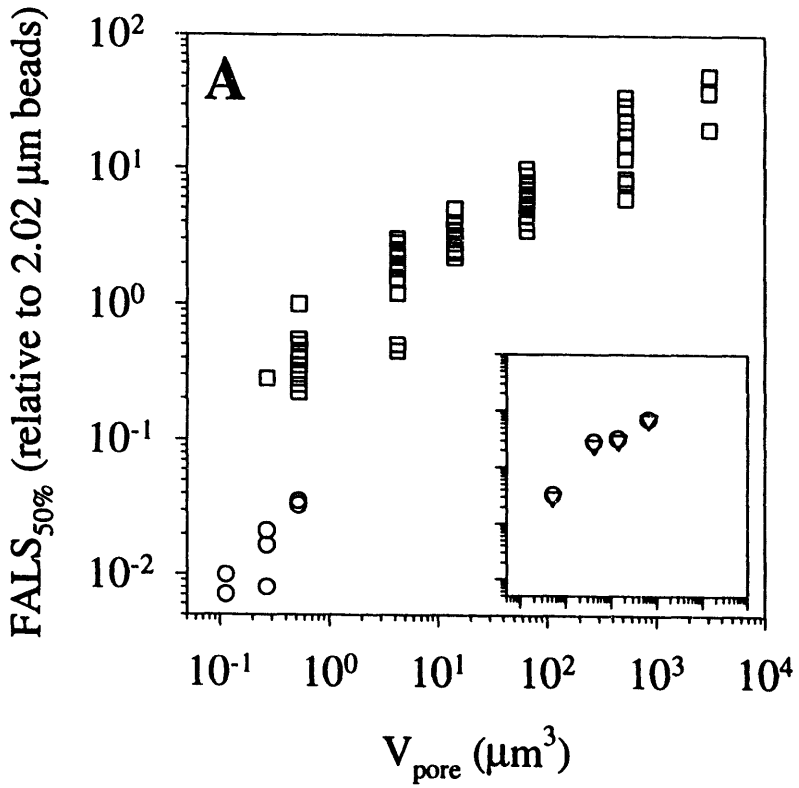
A
$10^2$
$10^1$
$10^0$
$10^{-1}$
$10^{-2}$
$FALS_{50\%}$ (relative to 2.02 µm beads)
$10^{-1}$ $10^0$ $10^1$ $10^2$ $10^3$ $10^4$
$V_{pore}$ (µm$^3$)

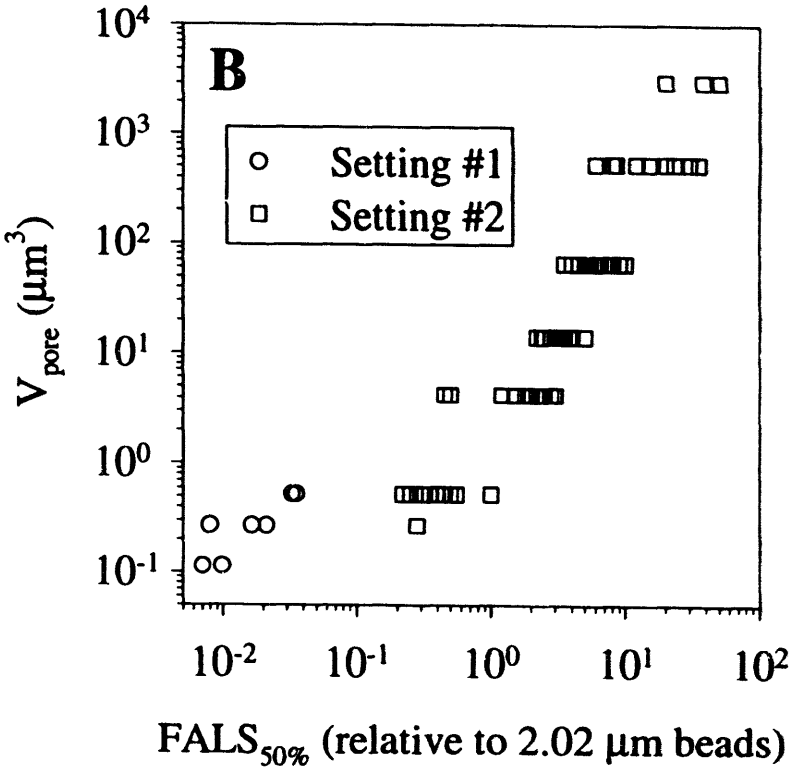
B
Setting #1
Setting #2
$10^4$
$10^3$
$10^2$
$10^1$
$10^0$
$10^{-1}$
$V_{pore}$ (µm$^3$)
$10^{-2}$ $10^{-1}$ $10^0$ $10^1$ $10^2$
$FALS_{50\%}$ (relative to 2.02 µm beads)

Figure 3:

Calibration data from sorting-based method. Cell size as a function of forward angle light scatter (FALS) for subsamples sorted from preserved field samples (*see* Table 2). The mean Coulter volume was plotted against the mode FALS of cells within a sort regions (e.g., Fig. 1B,D). (A) Data for *Prochlorococcus* through the nanoplankton. (B) Data from pennate diatoms (large and small) compared with the data from A, which are plotted as small filled circles.

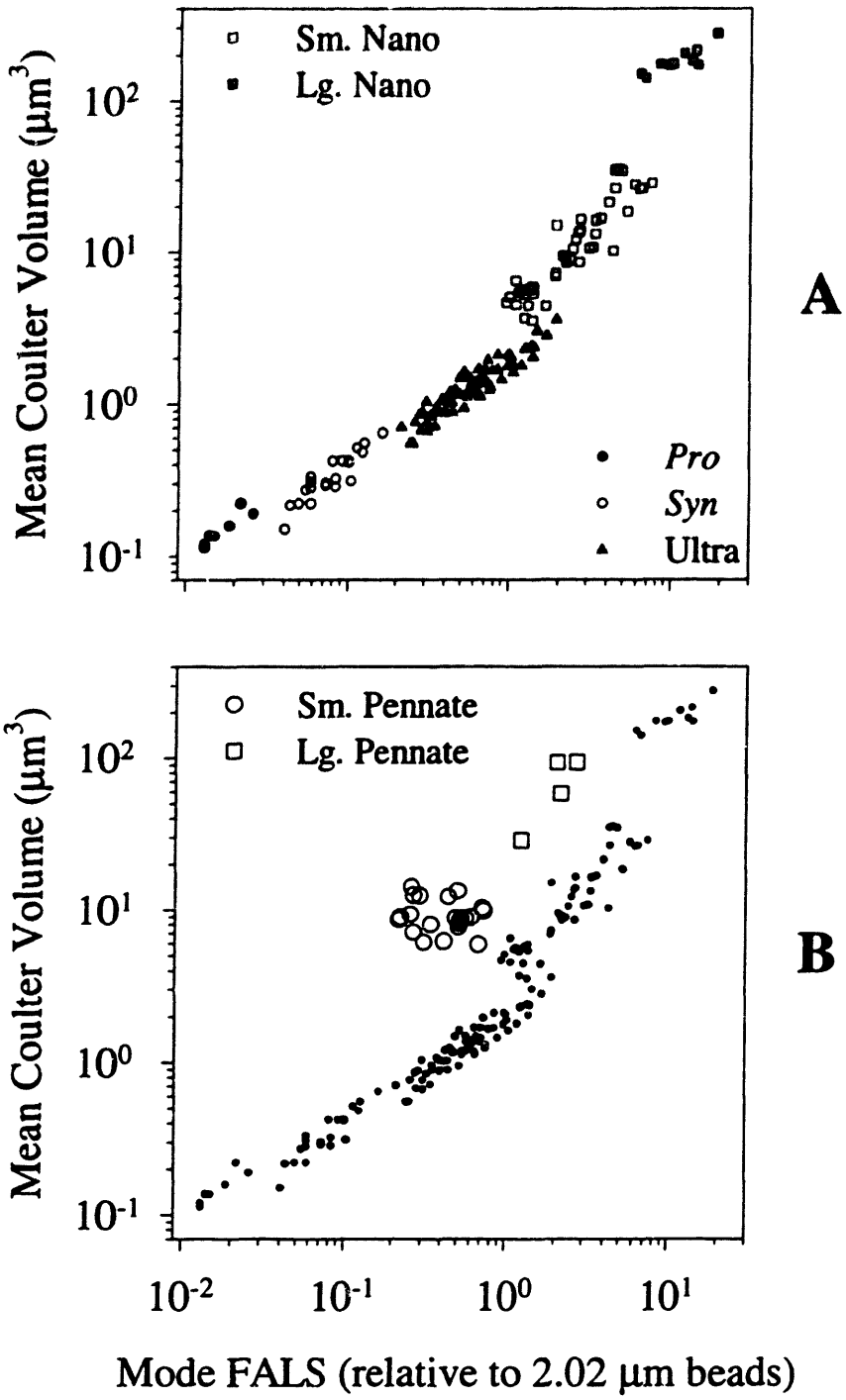
Sm. Nano
Lg. Nano
Pro
Syn
Ultra
Mean Coulter Volume (µm³)
10²
10¹
10⁰
10⁻¹
A
Sm. Pennate
Lg. Pennate
B
10⁻²
10⁻¹
10⁰
10¹
Mode FALS (relative to 2.02 µm beads)

Figure 4:

Comparison of Mie theory of light scattering with light scatter measurements by flow cytometry of polystyrene microspheres, which ranged from 0.47 to 10 μm in diameter (filled circles). (A-C) Microsphere data with line computed from Mie theory using a refractive index ($m$) of 1.19 relative to seawater (1.59 relative to air). Angles of collection for forward angle light scatter (FALS) were (A) 1-19°, (B) 2-19°, and (C) 3-19°. (D) Microsphere data with line computed from Mie theory using $m$ = 1.21 relative to seawater (1.62 relative to air). The absorption of beads was set at 0.035 $\mu m^{-1}$ (changes in this had little effect on the shape of the curves), and $m$ of seawater was set at 1.34 relative to air.

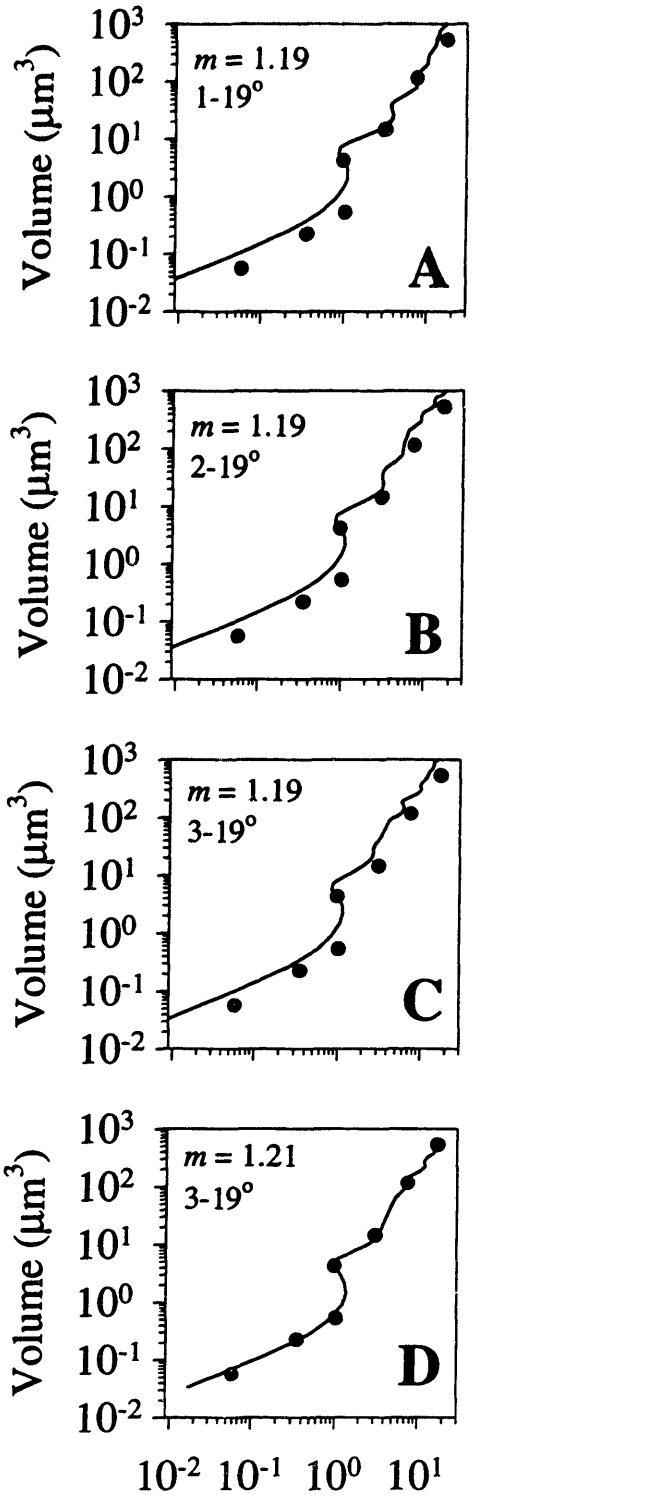
Volume (μm³)
10³
10²
10¹
10⁰
10⁻¹
10⁻²
m = 1.19
1-19°
A
m = 1.19
2-19°
B
m = 1.19
3-19°
C
m = 1.21
3-19°
D
10⁻² 10⁻¹ 10⁰ 10¹
Mean FALS (relative to 2.02 μm beads)

Figure 5:

Comparison of Mie theory of light scattering with calibration data based on the sorting method. (A) Experimental data (filled circles) with lines computed from Mie theory using three different refractive indicies: 1.04, 1.06, and 1.07 relative to seawater (1.39, 1.42, and 1.43 relative to air, respectively). (B) Experimental data with lines computed from Mie theory using four different refractive indicies: 1.06, 1.10, 1.14, and 1.19 relative to seawater (1.42, 1.47, 1.53, and 1.59 relative to air, respectively). In both cases, a scattering angle for FALS of 3-19° was used for Mie theory calculations.

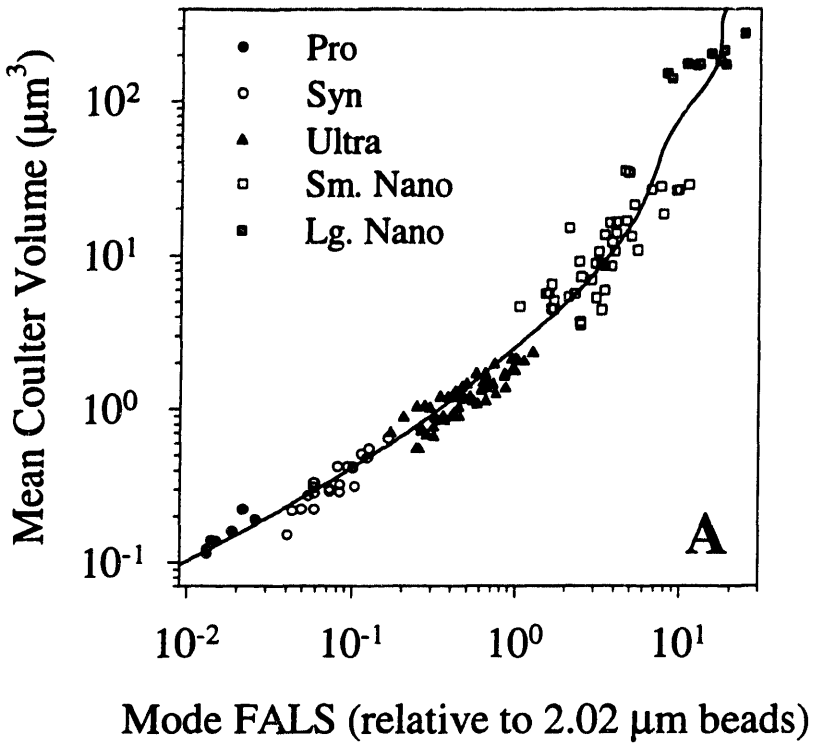
Pro
Syn
Ultra
Sm. Nano
Lg. Nano
A
Mean Coulter Volume (μm³)
10²
10¹
10⁰
10⁻¹
10⁻²
10⁻¹
10⁰
10¹
Mode FALS (relative to 2.02 μm beads)

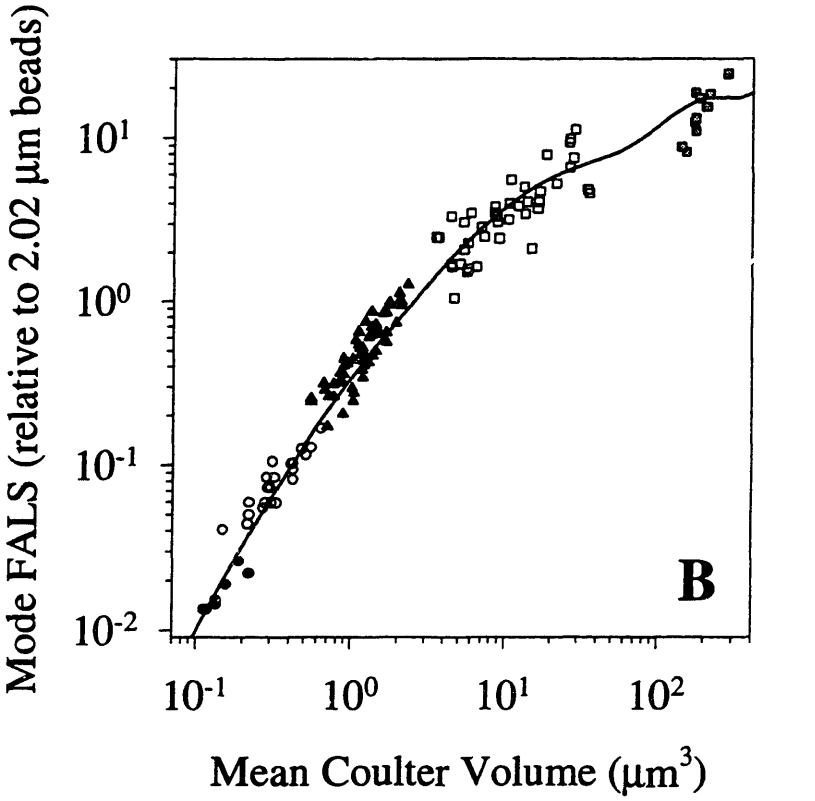
B
Mode FALS (relative to 2.02 μm beads)
10¹
10⁰
10⁻¹
10⁻²
10⁻¹
10⁰
10¹
10²
Mean Coulter Volume (μm³)

Figure 6:

Two-parameter scattergrams of flow cytometry data showing a preservation effect. Red fluorescence (Red FL) v. forward angle light scatter (FALS) for the lower-sensitivity sorting protocol showing the ultra- and nanoplankton populations. A clear shift in the FALS of the nanoplankton relative to the ultraplankton is visible in the preserved sample. Compared to the calibration microspheres (2.02 μm) added to both samples, FALS of the ultraplankton changed little, while that of the nanoplankton population changed by about a factor of 1.4. The sample came from the IronEx II experiment, cast 288 10m (*see* Table 2).

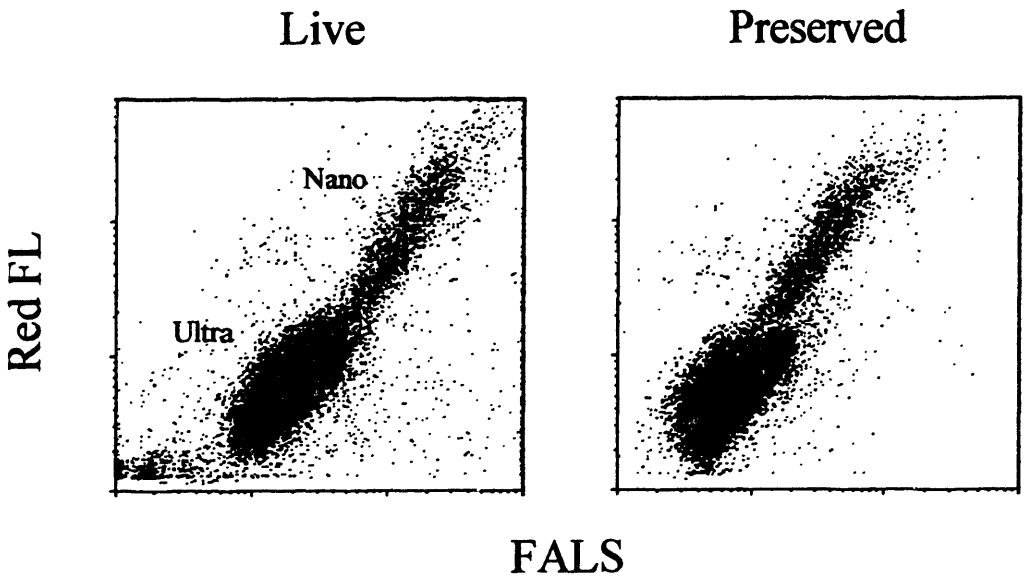
Live
Preserved
Red FL
Nano
Ultra
FALS

Figure 7:

Data from Fig. 3 adjusted to account for possible changes in forward angle light scatter (FALS) which were decoupled from changes in cell volume. The line is that based on Mie theory with a refractive index of 1.06 assumed for cells (Fig. 5). Axes in B are switched from A to aid in comparison of these data to those from other investigations (Fig. 8).

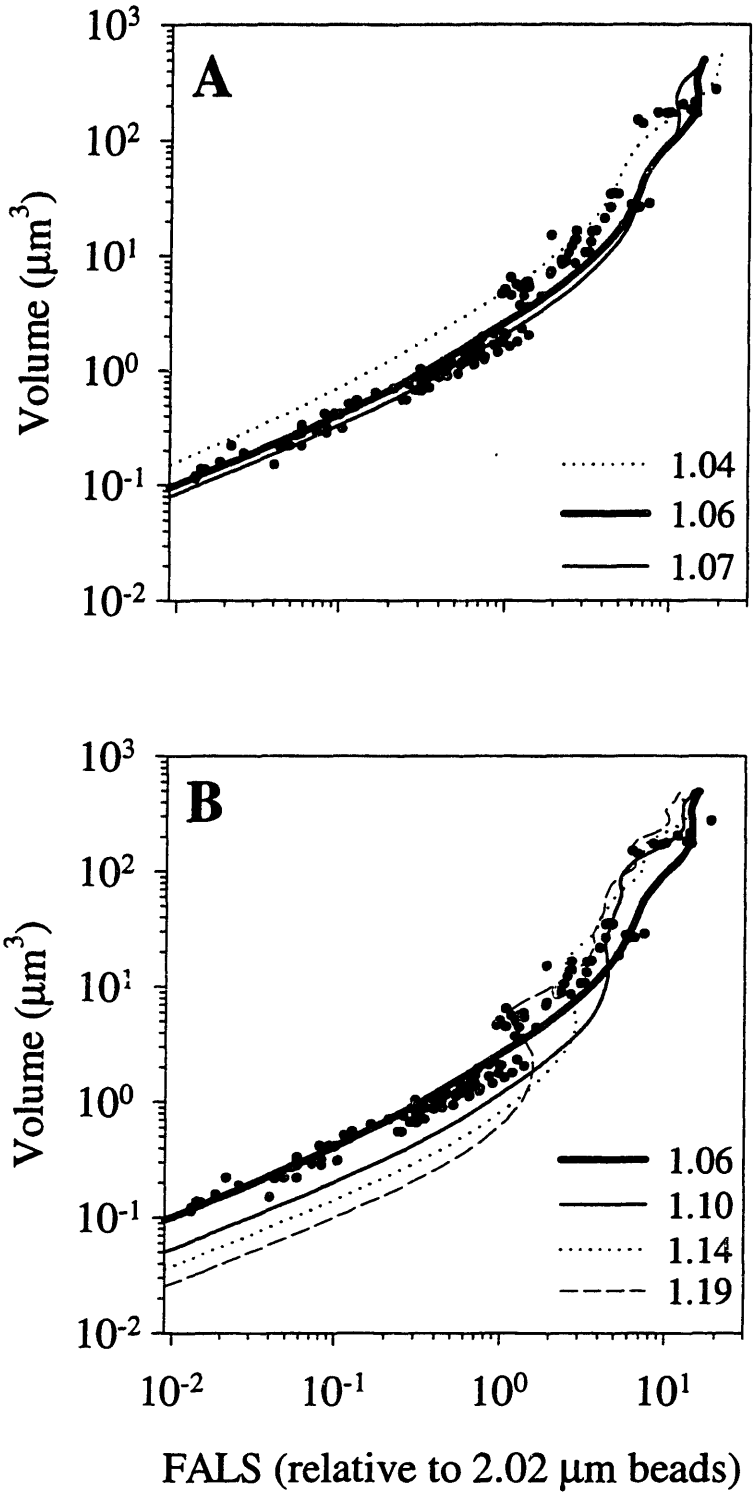
A
B
Volume (μm³)
10³
10²
10¹
10⁰
10⁻¹
10⁻²
1.04
1.06
1.07
1.10
1.14
1.19
FALS (relative to 2.02 μm beads)

Figure 8:

Compilation of calibrations of forward angle light scatter (FALS) in terms of cell volume from several other investigations. In both panels, the computed line based on Mie theory (Fig. 6) represents this study. Data shown are from: Olson et al. (1989), unpublished studies of Shalapyonok and Olson, unpublished studies used for the Coastal Mixing and Optics program (M. DuRand personal communication), and Gin (1996). Note that FALS values were normalized to the value of a $10\mu m^3$ cell in order to compare calibrations from different instruments, and that Olson et al. (1989) data was just for cells larger than $10\ \mu m^3$.

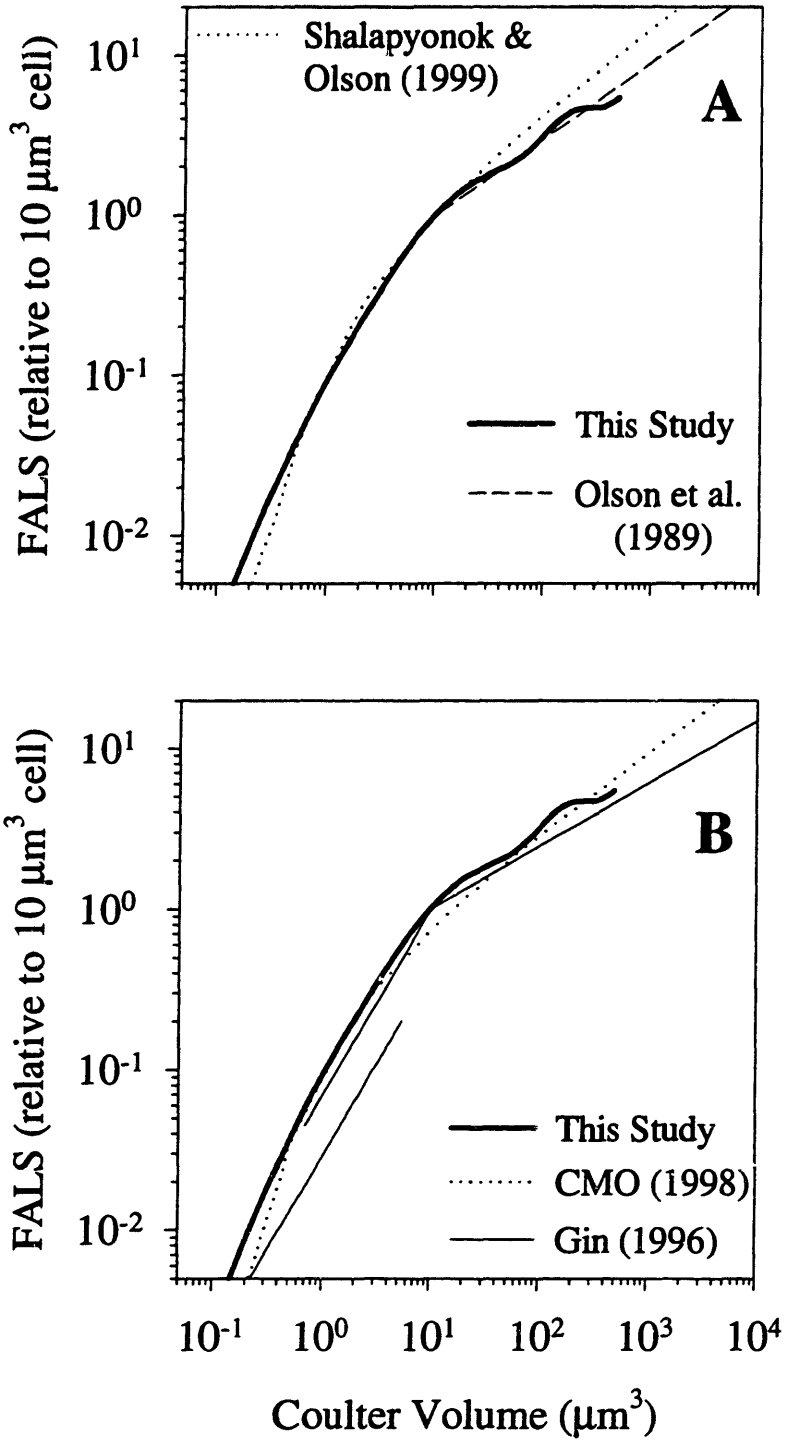
Shalapyonok &
Olson (1999)
A
This Study
Olson et al.
(1989)
FALS (relative to 10 μm³ cell)
10¹
10⁰
10⁻¹
10⁻²
B
This Study
CMO (1998)
Gin (1996)
10⁻¹
10⁰
10¹
10²
10³
10⁴
Coulter Volume (μm³)

Figure 9:

Compilation of calibration data resulting from the sorting (filled circles) and the filter-based (open squares and circles) protocols.

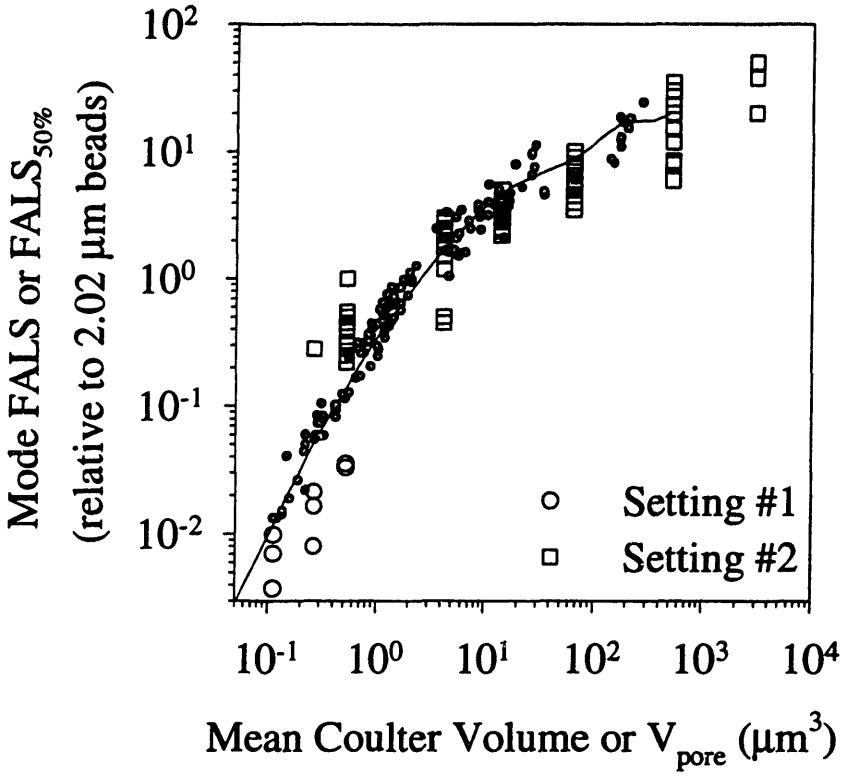
Mode FALS or FALS50%
(relative to 2.02 µm beads)
10^2
10^1
10^0
10^-1
10^-2
Setting #1
Setting #2
10^-1
10^0
10^1
10^2
10^3
10^4
Mean Coulter Volume or V_pore (µm^3)

protocol used (Vaulot *et al.* 1989; Lepesteur *et al.* 1993). It is expected that all cells would undergo some amount of shrinkage following preservation (Verity *et al.* 1992; Montagnes *et al.* 1994), which should lead to a concentration of the solid materials in the cell, thereby increasing the cell's refractive index (Stramski 1999). It is possible that $m$ could have increased beyond the relevant range for the nanoplankton. Using the same preservation protocol as was used here, Vaulot *et al.* (1989) observed an increase in the refractive index of the cell wall of a marine dinoflagellate, indicating that changes in $m$ might be decoupled from changes in cell volume following preservation. Thus, it is plausible that $m$ increased upon preservation for all cells and may have increased due to effects which were decoupled from changes in cell volume for the nanoplankton. If this could explain the discontinuity, we should be able to see relative changes in FALS between the ultra- and nanoplankton groups before and after preservation. In fact, we regularly saw a relative shift in the FALS values of these populations following preservation (Fig. 6). When compared to the FALS of the calibration microspheres added to each sample, the shift was usually explained by changes in FALS of the nanoplankton, and not the ultraplankton.

Two possible scenarios, which are not mutually exclusive, remain: (i) $m$ increased as a result of cell shrinkage, and (ii) either $m$ or cell volume changed independently of the other. We have no measures of cell volume before preservation, thus we cannot rule out the first scenario. However, the shift in nanoplankton populations observed (Fig. 6) suggests a role for the second scenario. We explored a way to apply a correction to our data assuming that increases in refractive index, and therefore decreases in FALS, were not matched by equivalent decreases in cell volume for the nanoplankton.

To do so, we compared the FALS distribution for each sample which had also been analyzed at sea prior to preservation. This comparison revealed that in many cases the FALS distribution of the nanoplankton had shifted markedly towards smaller values in the preserved samples, contrasting with the distributions of the ultraplankton which changed little or not at all (*see* Appendix C) . We estimated a factor representing this shift for the entire group and applied this correction to the data in Fig. 3A in an attempt to correct for changes in FALS due to preservation. We made these adjustments to the ultraplankton and to both the small and large nanoplankton, but found that little adjustment was warranted for *Prochlorococcus* or

*Synechococcus* (*see* Appendix C), resulting in a calibration data set which lacked a discontinuity (Fig. 7). Added to the adjusted data is a curve based on Mie theory ($m$ = 1.06 from Fig. 5), which could be used as a calibration curve to represent our data.

Our adjusted calibration data agree with those found by other investigators (Fig. 8), suggesting that our adjustment, which took into account only changes in FALS due to preservation, is reasonable. Aside from Gin's (1996) calibration, all the others resulted from simultaneous measurements of FALS and Coulter volume for laboratory cultures. In addition, Koch *et al.* (1996) estimated that the FALS of bacterial cells in the range of 0.01 to 1 $\mu m^3$ should increase as a 1.33 power of volume, which is in very close agreement with that region of our calibration data (FALS $\propto$ (volume)$^{1.4}$). Gin (1996) used culture-based data from DuRand (1995) for her relationship at large FALS combined with a preliminary calibration based on the same filter fractionation method used in our study for small FALS values. Gin used an intermediary line having the same slope as the lower line as a way to deal with the discontinuity between the two calibration methods (Fig. 8B). Comparing Fig. 8B with Fig. 2B, we see that a discontinuity is apparent in our calibration data based on filter fractionation. From further comparison of either of these with the discontinuous data seen in Fig. 3A, it is clear that the location of the discontinuities arising from the two methods are not similar.

If we re-cast the filter fractionation data from this study with that collected via the sorting protocol (Fig. 9), the fact that Gin's lowest line in Fig. 8 does not agree with the other calibrations is understandable. That is, for those filters analyzed on the high-sensitivity settings (#1), there appears to be a considerable over-estimate of volume for a given FALS. The reverse is true for the 1 µm pore size filter ($V_{pore}$ = 0.52 $\mu m^3$) analyzed on the lower-sensitivity setting (#2); the explanation for these discrepancies is unknown. For the larger filters, however, the data consistently fall near or on the predicted Mie theory line.

Given the apparent site-to-site variability and the under- and over-estimation of volume based on certain filter sizes, we do not recommend the filter-based method as a means for future calibrations of FALS. We found a strong relationship between FALS and cell volume for *Prochlorococcus*, *Synechococcus*, and the ultraphytoplankton using our sorting-based calibration

method. After applying a preservation correction to the nanophytoplankton, Mie theory explained the FALS-volume relationship for our entire data set. Comparison of our overall relationship to those from other studies suggests that our preservation correction was justified. Furthermore, good agreement between the theoretical model based on Mie theory, which represented our data, with the calibration curves from other studies, supports future use of theoretical relationships between FALS and volume.

## REFERENCES


Ackelson, S. G. and R. W. Spinrad 1988. Size and refractive index of individual marine particulates: a flow cytometric approach. *Applied Optics* **27**: 1270-1277.

Ahrens, M. A. and R. H. Peters 1991. Patterns and limitations in limnoplankton size spectra. *Canadian Bulletin of Fisheries and Aquatic Sciences* **48**: 1967-1978.

Binder, B. J., S. W. Chisholm, R. J. Olson, S. L. Frankel and A. Z. Worden 1996. Dynamics of picophytoplankton, ultraphytoplankton and bacteria in the central equatorial Pacific. *Deep-Sea Research* **43**: 907-931.

Bohren, C. F. and D. R. Huffman (1983). Absorption and scattering of light by small particles John Wiley and Sons.

Campbell, L., D. Vaulot and H. A. Nolla 1994. The importance of *Prochlorococcus* to community structure in the central North Pacific Ocean. *Limnology and Oceanography* **39**: 954-961.

Cavender-Bares, K. K., S. L. Frankel and S. W. Chisholm 1998. A dual sheath flow cytometer for shipboard analyses of phytoplankton communities from the oligotrophic oceans. *Limnology and Oceanography* **43**: 1383-1388.

Cavender-Bares, K. K., E. L. Mann, S. W. Chisholm, M. E. Ondrusek and R. R. Bididgare 1999. Differential response of equatorial Pacific phytoplankton to iron fertilization. *Limnology and Oceanography* **44**: 237-246.

Chisholm, S. W. (1992). Phytoplankton size. Primary Productivity and Biogeochemical Cycles in the Sea. P. G. Falkowski and A. D. Woodhead, Eds. New York, Plenum Press.

Chisholm, S. W., R. J. Olson, E. R. Zettler, R. Goericke, J. B. Waterbury and N. A. Welschmeyer 1988. A novel free-living prochlorophyte abundant in the oceanic euphotic zone. *Nature* **334**: 340-343.

DuRand, M. D. Phytoplankton growth and diel variations in beam attenuation through individual cell analysis. Ph.D. Thesis, M.I.T. and W.H.O.I., 1995. pp. 263.

Gin, K. Microbial size spectra from diverse marine ecosystems. Ph.D. Thesis, M.I.T./W.H.O.I. Joint Program, 1996. pp. 359.

Graziano, L. M., R. J. Geider, W. W. W. Li and M. Olaizola 1996. Nitrogen limitation of North Atlantic phytoplankton: analysis of physiological condition in nutrient enrichment experiments. *Aquatic Microbial Ecology* **11**: 53-64.

Koch, A., B. R. Robertson and D. K. Button 1996. Deduction of cell volume and mass from forward scatter intensity of bacteria analyzed by flow cytometry. *Journal of Microbiological Methods* **27**: 49-61.

Lepesteur, M., J. M. Martin and A. Fleury 1993. A comparative study of different preservation methods for phytoplankton cell analysis by flow cytometry. *Marine Ecology Progress Series* **93**: 55-63.

Li, W. K. W. 1994. Phytoplankton biomass and chlorophyll concentration across the North Atlantic. *Scientia Marina* **58**: 67-79.

Li, W. K. W. 1995. Composition of ultraphytoplankton in the central North Atlantic. *Marine Ecology Progress Series* **122**: 1-8.

Li, W. K. W., T. Zohary, Y. Z. Yacobi and A. M. Wood 1993. Ultraphytoplankton in the eastern Mediterranean Sea: towards deriving phytoplankton biomass from flow cytometric

measurements of abundance, fluorescence and light scatter. *Marine Ecology Progress Series* **102**: 79-87.

Lide, D. R., Ed. 1992. CRC handbook of chemistry and physics. CRC Press.

Montagnes, D. J. S., J. A. Berges, P. J. Harrison and F. J. R. Taylor 1994. Estimating carbon, nitrogen, protein, and chlorophyll *a* from volume in marine phytoplankton. *Limnology and Oceanography* **39**: 1044-1060.

Moore, L. R., G. Rocap and S. W. Chisholm 1998. Physiology and molecular phylogeny of coexisting *Prochlorococcus* ecotypes. *Nature* **393**: 464.

Neale, P. J., J. J. Cullen and C. M. Yentsch 1989. Bio-optical inferences from chlorophyll *a* fluorescence: What kind of fluorescence is measured by flow cytometry? *Limnology and Oceanography* **34**: 1739-1748.

Olson, R. J., A. M. Chekalyuk, H. M. Sosik and M. Y. Gorbunov (1995). Pump-during-probe technique for measuring photosynthetic characteristics of individual algal cells using flow cytometry and microfluorometry. Photosynthesis: from light to biosphere. P. Mathis, Ed. Netherlands, Kluwer Academic Publishers. **5:** 743-748.

Olson, R. J., S. W. Chisholm, S. L. Frankel and H. M. Shapiro 1983. An inexpensive flow cytometer for the analysis of fluorescence signals in phytoplankton: Chlorophyll and DNA distributions. *Journal of Experimental Marine Biology and Ecology* **68**: 129-144.

Olson, R. J., S. W. Chisholm, E. R. Zettler, M. A. Altabet and J. A. Dusenberry 1990a. Spatial and temporal distributions of prochlorophyte picoplankton in the North Atlantic Ocean. *Deep-Sea Research* **37**: 1033-1051.

Olson, R. J., S. W. Chisholm, E. R. Zettler and E. V. Armbrust 1990b. Pigments, size, and distribution of *Synechococcus* in the North Atlantic and Pacific Oceans. *Limnology and Oceanography* **35**: 45-58.

Olson, R. J., E. R. Zettler and O. K. Anderson 1989. Discrimination of eukaryotic phytoplankton cell types from light scatter and autofluorescence properties measured by flow cytometry. *Cytometry* **10**: 636-643.

Perry, M. J. and S. M. Porter 1989. Determination of the cross-section absorption coefficient of individual phytoplankton cells by analytical flow cytometry. *Limnology and Oceanography* **34**: 1727-1738.

Platt, T. and K. L. Denman 1978. The structure of pelagic marine ecosystems. *Rapports et Proces-Verbaux des Reunions-Conseil International pur l'Exploration de la Mer* **173**: 60-65.

Price, N. M., B. A. Ahner and F. M. M. Morel 1994. The equatorial Pacific Ocean: Grazer-controlled phytoplankton populations in an iron-limited ecosystem. *Limnology and Oceanography* **39**: 520-534.

Quiñones-Bergeret, R. A. Size-distribution of planktonic biomass and metabolic activity in the pelagic system. Ph.D. Thesis, Dalhousie University, 1992. pp. 225.

Reckermann, M. and M. J. W. Veldhuis 1997. Trophic interactions between picophytoplankton and micro- and nanozooplankton in the western Arabian Sea during the NE monsoon 1993. *Aquatic Microbial Ecology* **12**: 263.

Robertson, B. R. and D. K. Button 1989. Characterizing aquatic bacteria according to population, cell size, and apparent DNA content by flow cytometry. *Cytometry* **10**: 70-76.

Robertson, B. R., D. K. Button and A. L. Koch 1998. Determination of the biomasses of small bacteria at low concentrations in a mixture of species with forward light scatter measurements by flow cytometry. *Applied and Environmental Microbiology* **64**: 3900-3909.

Rodriguez, J. and M. M. Mullin 1986. Relation between biomass and body weight of plankton in a steady-state oceanic ecosystem. *Limnology and Oceanography* **31**: 316-370.

Ruiz, J., F. Guerrero, V. Rodríguez and J. Rodríguez (1992). Chlorophyll and the size-biomass spectrum of phytoplankton: analysis of fluctuations in eutrophic coastal waters. Marine eutrophication and population dynamics. G. e. a. Colombo, Ed. Denmark, Olsen and Olsen: 59-62.

Sheldon, R. W. 1972. Size separation of marine seston by membrane and glass-fiber filters. *Limnology and Oceanography* **17**: 494-499.

Sheldon, R. W., T. P. T. Evelyn and T. R. Parsons 1967. On the occurrence and formation of small particles in seawater. *Limnology and Oceanography* **12**: 367-375.

Sheldon, R. W. and W. H. J. Sutcliffe 1969. Retention of marine particles by screens and filters. *Limnology and Oceanography* **14**: 441-444.

Sosik, H. M., S. W. Chisholm and R. J. Olson 1989. Chlorophyll fluorescence from single cells: Interpretation of flow cytometric signals. *Limnology and Oceanography* **34**: 1749-1761.

Steen, H. B. (1991). Flow cytometry instrumentation. NATO ASI Series. S. Demers, Ed. Berlin, Springer-Verlag. **G27:** 3-29.

Stramski, D. 1999. Refractive index of planktonic cells as a measure of cellular carbon and chlorophyll a content. *Deep-Sea Research Part I-Oceanographic Research Papers* **46**: 335.

Stramski, D. and C. D. Mobley 1997. Effects of microbial particles on oceanic optics: A database of single-particle optical properties. *Limnology and Oceanography* **42**: 538.

Timmermans, K. R., M. Gledhill, R. F. Nolting, M. J. W. Veldhuis, H. J. W. de Baar and C. M. G. van den Berg 1998. Responses of marine phytoplankton in iron enrichment experiments in the northern North Sea and northeast Atlantic Ocean. *Marine Chemistry* **61**: 229.

Tittel, J., B. Zippel, W. Geller and J. Seeger 1998. Relationships between plankton community structure and plankton size distribution in lakes of northern Germany. *Limnology and Oceanography* **43**: 1119.

Van de Hulst, H. C. (1957). Light Scattering by Small Particles Wiley.

Vaulot, D., C. Courties and F. Partensky 1989. A simple method to preserve oceanic phytoplankton for flow cytometric analyses. *Cytometry* **10**: 629-635.

Vaulot, D., D. Marie, R. J. Olson and S. W. Chisholm 1995. Growth of *Prochlorococcus*, a photosynthetic prokaryote, in the equatorial Pacific Ocean. *Science* **268**: 1480-1482.

Vaulot, D., F. Partensky, J. Neveux, R. F. C. Mantoura and C. A. Llewellyn 1990. Winter Presence Of Prochlorophytes In Surface Waters Of the Northwestern Mediterranean-Sea. *Limnology and Oceanography* **35**: 1156-1164.

Verity, P. G., C. Y. Robertson, C. R. Tronzo, M. G. Andrews, J. R. Nelson and M. E. Sieracki 1992. Relationships between cell volume and the carbon and nitrogen content of marine photosynthetic nanoplankton. *Limnology and Oceanography* **37**: 1434-1446.

Vidondo, B., Y. T. Prairie, J. M. Blanco and C. M. Duarte 1997. Some aspects of the analysis of size spectra in aquatic ecology. *Limnology and Oceanography* **42**: 184-192.

Yentsch, C. M., *et al.* 1983. Flow cytometry and sorting: A technique for analysis and sorting of aquatic particles. *Limnology and Oceanography* **28**: 1275-1280.

Yentsch, C. S. and D. A. Phinney 1989. A bridge between ocean optics and microbial ecology. *Limnology and Oceanography* **34**: 1694-1705.

Zettler, E. R., R. J. Olson, B. J. Binder, S. W. Chisholm, S. E. Fitzwater and M. R. Gordon 1996. Iron-enrichment bottle experiments in the equatorial Pacific: responses of individual phytoplankton cells. *Deep-Sea Research* **43**: 1017-1029.

# Chapter 4

## Differential response of equatorial Pacific phytoplankton to iron fertilization

Reprinted with permission from *Limnology and Oceanography*.

Cavender-Bares, K. K., E. L. Mann, S. W. Chisholm, M. E. Ondrusek and R. R. Bididgare 1999. Differential response of equatorial Pacific phytoplankton to iron fertilization. *Limnology and Oceanography* **44**: 237-246.

Limnol. Oceanogr., 44(2), 1999, 237–246


# Differential response of equatorial Pacific phytoplankton to iron fertilization

*Kent K. Cavender-Bares*
Department of Civil and Environmental Engineering, 48-425, Massachusetts Institute of Technology, Cambridge, Massachusetts 02139

*Elizabeth L. Mann*
MIT/Woods Hole Joint Program in Biological Oceanography, 48-425 MIT, Cambridge, Massachusetts 02139

*Sallie W. Chisholm*[1]
Department of Civil and Environmental Engineering and Department of Biology, 48-425, Massachusetts Institute of Technology,
Cambridge, Massachusetts 02139

*Michael E. Ondrusek and Robert R. Bidigare*
Department of Oceanography, University of Hawaii, 1000 Pope Road, Honolulu, Hawaii 96822

*Abstract*

Recent unenclosed iron-fertilization experiments in the equatorial Pacific Ocean have shown that phytoplankton biomass can be increased substantially by the addition of iron. Analyses of size-fractionated chlorophyll indicate that much of the increase during the most recent fertilization experiment, IronEx II, occurred in the >10-$\mu$m size fraction. We used flow cytometry, combined with taxon-specific pigment measurements by high-performance liquid chromatography (HPLC), to analyze the responses of five different groups of phytoplankton: *Prochlorococcus, Synechococcus,* ultraplankton, nanoplankton, and pennate diatoms. These results are unique in the suite of measurements from the IronEx studies in that they simultaneously examine individual cell properties, which are grazer independent, and population dynamics, which reflect the net result of growth and grazing. Our results show that
the overall increase of chlorophyll *a* (Chl *a*) in the patch was due in part to increases in chlorophyll content per cell and in part to increases in cell numbers of specific groups. Cellular fluorescence was stimulated by iron addition in all five groups to a qualitatively similar degree and was correlated with taxon-specific changes in cellular pigments. In terms of net cell growth, however, these groups responded very differently. The groups that dominated the community before the addition of iron increased at most twofold in cell number; *Prochlorococcus* actually decreased. In contrast, the initially rare pennate diatoms increased 15-fold in number by the peak of the iron-induced bloom. Within 1 week, this differential response led to a dramatic change in the phytoplankton community structure, from one dominated by picoplankton to one dominated by large diatoms. It is not known whether this shift would be sustained over extended periods of fertilization, a response that would ultimately change the structure of the food web.

Oceanographers have long been puzzled by the simultaneous abundance of macronutrients, such as nitrate and phosphate, and the paucity of phytoplankton biomass in the three high-nutrient, low-chlorophyll (HNLC) regions of the world ocean: the equatorial Pacific, the subarctic Pacific, and the Southern Ocean. Early oceanographers noted these anomalies (Gran 1931; Hart 1934), and many hypotheses have been offered and debated over the years (*see* Chisholm and Morel 1991), the most compelling of which are the "iron hypothesis" (Martin 1990), the "grazing hypothesis" (Walsh 1976; Frost 1991), and the unifying "ecumenical hypothesis" (Morel et al. 1991*a;* Price et al. 1994). The debate on the iron hypothesis, based largely on iron-enriched "grow out" experiments (e.g., Martin and Fitzwater 1988; Buma et al. 1991; Coale 1991; Takeda and Obata 1995; Boyd et al.

[1] Corresponding author; chisholm@mit.edu

*Acknowledgments*

We thank the captain and crew of the R/V *Mellville,* Kenneth Coale, and the Moss Landing IronEx Group for generating and monitoring the iron-enriched patch. We also thank two anonymous reviewers for many helpful suggestions to this manuscript. This work was supported in part by the U.S. National Science Foundation (OCE 9302529), National Aeronautics and Space Administration, Environmental Protection Agency, MIT/TEPCO funds, and the MIT Joint Program in the Science and Policy of Global Change.

1996; Coale et al. 1996*a*; Zettler et al. 1996), culminated with two open-ocean in situ iron-fertilization experiments (IronEx I and II; Martin et al. 1994; Coale et al. 1996*b*).

The biological response to added iron during IronEx II, as indicated by changes in Chl *a*, exceeded the observed increase in IronEx I by nearly one order of magnitude (Martin et al. 1994; Coale et al. 1996*b*). A large portion of the response to iron fertilization was due to a bloom of initially rare diatoms, whose biomass increased 85-fold inside the iron-fertilized patch (Coale et al. 1996*b*). Concomitant with this massive increase in phytoplankton biomass was a drawdown of roughly 5 $\mu$M nitrate, attributed almost completely to cells >5 $\mu$m (Coale et al. 1996*b*). Other changes of biogeochemical significance included a decrease in $CO_2$ fugacity of nearly 100 $\mu$atm (Cooper et al. 1996), a 3.5-fold increase in dimethyl sulfide production (DMS; Turner et al. 1996), and a 7‰ enrichment in the $\delta$ $^{13}C$ of phytoplankton (Bidigare et al. submitted).

There is evidence that the smaller, initially dominant phytoplankton were also stimulated by the iron addition. Using epifluorescence microscopy, Coale et al. (1996*b*) found modest increases in cell biomass for the smaller, nondiatom taxonomic groups. This analysis did not include the ubiquitous picoplankter *Prochlorococcus*, which cannot be resolved easily using this method. Photochemical quantum efficiency, the ratio of the quantum yield of variable fluorescence ($F_v$) to that of the light-saturated fluorescence yield ($F_m$), increased dramatically in both experiments hours after the addition of iron (Kolber et al. 1994; Behrenfeld et al. 1996). Behrenfeld et al. (1996) contend that since $F_v/F_m$ increased prior to a shift in species composition, all phytoplankton taxa were physiologically limited by iron—reinforcing the finding of significant increases in $F_v/F_m$ for all size fractions during IronEx I (Kolber et al. 1994). In addition, results from bottle dilution experiments (Landry and Hassett 1982) indicate that the net autotrophic growth rate of the phytoplankton community <5 $\mu$m in size more than doubled inside the enriched patch while the microzooplankton grazing rates increased threefold (Coale et al. 1996*b*). Higher grazing rates inside the patch and only a modest increase in small phytoplankton biomass suggest that all phytoplankton were stimulated by the addition of iron, but only the initially rare diatoms escaped grazing pressure and bloomed.

Most of the reports to date use bulk measurements, which do not distinguish between subgroups, to investigate phytoplankton dynamics inside the iron-fertilized patch. We used analyses of size-fractionated chlorophyll to monitor changes between large (>10 $\mu$m) and small (<10 $\mu$m) size classes following enrichment. To follow the response of specific groups of phytoplankton to iron enrichment, we used flow cytometry, combined with taxon-specific pigment measurements. This allowed us to distinguish between changes in cell number and cellular chlorophyll since a change in either would affect bulk chlorophyll measurements. Moreover, flow cytometric analyses provide a measure of cell-specific responses to iron enrichment, independent of any changes, or lack thereof, in population numbers. Finally, this is the first report documenting the response to in situ iron fertilization of the picophytoplankter *Prochlorococcus*, which is typically a large contributor to standing stocks in the equatorial Pacific (e.g., Binder et al. 1996).

## Methods

*Iron patch and sampling*—IronEx II was conducted between 29 May and 15 June 1995 starting at 4°S, 105°W in a region with high (ca. 10 $\mu$M) nitrate concentrations (Coale et al. 1996*b*). Iron, added as Fe(II) in seawater at pH 2, was injected into surface waters three times over a 7-d period, initially forming a 72-km$^2$ patch. The target iron concentration for the initial fertilization was 2 nM—a 40-fold increase from the 0.05-nM ambient concentration; the second and third injections were designed to add another 1 nM Fe each (Coale et al. 1996*b*). A 1,000-km$^2$ survey of the general study site was conducted prior to the first iron infusion to ensure against possible patch subduction, as occurred in IronEx I (Martin et al. 1994), and to verify that a representative site was chosen. Stations were occupied daily inside and outside the patch, although in some cases, only one of these was possible. All data presented here are from stations sampled at local dawn to eliminate complications arising from diel patterns.

*Pigments*—We used size-fractionated Chl *a* concentrations to compare broad changes in phytoplankton community structure in and out of the patch. The fractions were analyzed in duplicate by parallel filter fractionation, using polycarbonate 10-$\mu$m pore-size filters (Poretics) and Whatman GF/F filters for the total. After extraction in 90% acetone for 24 h, Chl *a* was assayed fluorometrically (Parsons et al. 1984) on a 10-AU fluorometer (Turner Designs), which was calibrated using extracts of spinach Chl *a* (Sigma-Aldrich). Chl *a* in the >10-$\mu$m fraction equaled the material retained on the 10-$\mu$m filter, whereas the <10-$\mu$m fraction was the difference between the total and that retained on the 10-$\mu$m filter.

Taxon-specific pigments were monitored in whole-water (bulk) samples to complement the flow cytometry data (*see below*). Seawater samples were filtered onto Whatman GF/F filters, and acetone extracts were then analyzed by HPLC for chlorophyll and carotenoid quantification (Goericke and Repeta 1993). Divinyl chlorophyll *a* (Chl $a_2$) and fucoxanthin were used as chemotaxonomic markers for *Prochlorococcus* spp. and diatoms, respectively. The sum of 19′-hexanoyloxyfucoxanthin, 19′-butanoyloxyfucoxanthin, and peridinin (HBP) was used as a marker for the group consisting of pelagophytes, prymnesiophytes, and dinoflagellates (Vesk and Jeffrey 1987; Wright and Jeffrey 1987; Simon et al. 1994; Andersen et al. 1996). It has been shown that prymnesiophytes and dinoflagellates contribute significantly to the nanophytoplankton (2–20 $\mu$m) biomass of the equatorial Pacific (Chavez et al. 1990; Coale et al. 1996*b*), and it is likely that the pelagophytes are in the group of eukaryotic picoplankton (<2 $\mu$m) termed the "red fluorescing picoplankton" (Chavez et al. 1990; Coale et al. 1996*b*). Thus, for the sake of comparison, we have used the HBP sum to represent the pigment biomass of the ultra- and nanophytoplankton groups combined (*see below*). Note that chemotaxonomic markers for *Synechococcus* were not measured.

*Flow cytometry*—A modified Coulter EPICS V flow cytometer (Cavender-Bares et al. 1998) was used to characterize the phytoplankton community in terms of autofluorescence per cell, which is related to pigment concentration (Sosik et al. 1989; Li et al. 1993; Jonker et al. 1995), and forward angle light scatter (FALS) per cell, which is correlated with cell size (Van de Hulst 1957; Ackelson and Spinrad 1988). A 40.5-mm spherical lens was used to focus the 488-nm laser beam (Innova 90 at 800 mW; Coherent), either alone for picoplankton analyses or in combination with a 150-mm cylindrical lens, which was focused on the back focal plane of the spherical lens, for analyses of larger cells. These configurations produced a 17-$\mu$m circular and a 17- × 400-$\mu$m elliptical laser spot, respectively, for sample illumination within the quartz flow cell. Chlorophyll or red fluorescence (Red FL) signals passed first through a 488-nm long-pass filter, then were reflected by a 630-nm short-pass dichroic filter, and finally passed through a 680-nm bandpass filter (40-nm bandwidth; Omega Optical). Phycoerythrin or orange fluorescence (Orange FL) signals passed through the 630-nm short-pass dichroic and also through a 515-nm long-pass filter. FALS signals, which passed beyond a wide obscuration bar and then through a vertical polarization filter, were measured using a PMT (photo multiplier tube) detector. Log-integrated values were collected for all three signals. When the range of fluorescence values exceeded the nominal three-decade range of the instrument, we employed an extra electronic circuit to expand the Red FL scale. A subtraction module can be used to subtract electronically one signal from a second and is typically used to separate spillover of one signal into a second. Only partial subtraction of one signal from the other is possible with a maximum of 50% for those modules associated with the flow cytometer. Two modules were used in series, and the Red FL signal from the PMT was split and input as two separate signals, resulting in a new signal that equaled 25% of the original Red FL signal. This "reduced" Red FL signal was used to characterize those cells that were offscale on the standard Red FL scale.

We are able to differentiate five separate groups of photosynthetic cells based on their distinct fluorescence and light scatter signals as represented in Fig. 1. The two cyanobacteria *Prochlorococcus* and *Synechococcus* are easily differentiated from each other since only *Synechococcus* exhibits Orange FL (Chisholm et al. 1988; Olson et al. 1990). Both cyanobacteria have relatively low FALS signals, which separates them from the ultra- and nanoplankton. The smallest ultraplankton are also distinguishable from *Synechococcus* because of their lack of Orange FL. The ultra- and nanophytoplankton are identified based on their size and fluorescence characteristics (Zettler et al. 1996), and pennate diatoms can be identified because they scatter less light than would be expected for their size because of their long, slender shape (Olson et al. 1989; Zettler et al. 1996). Fluorescence and light scatter values are reported relative to the value of calibration microspheres added to each sample (Polysciences; 0.474 and 2.02 $\mu$m [Fig. 1A,B and C, respectively]). Note that although red fluorescence values are shown in Fig. 1 for *Synechococcus*, they are not reported in our

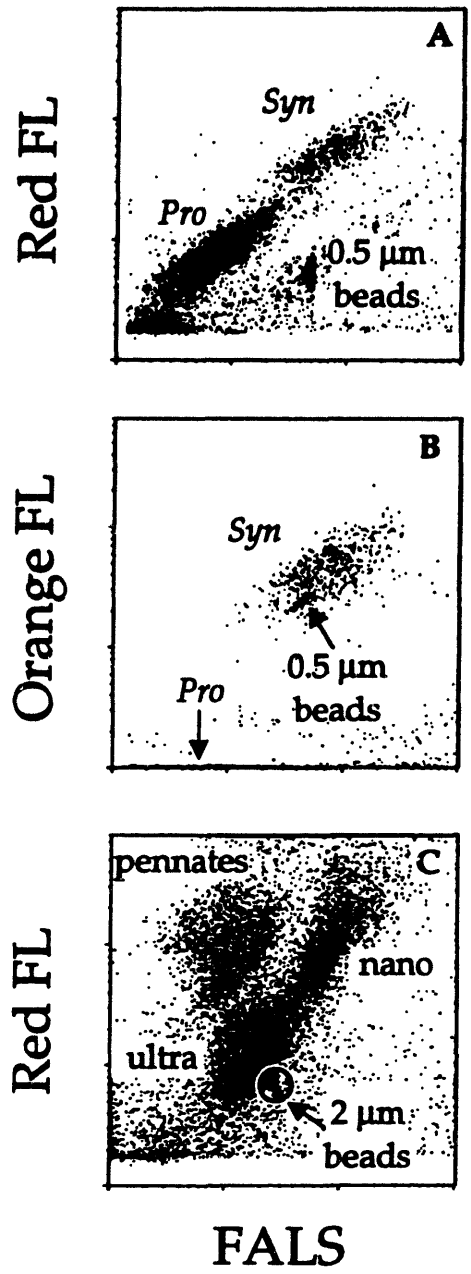


Fig. 1. (A) Flow cytometric scattergram of *Prochlorococcus* and *Synechococcus*, with Red FL plotted against FALS. (B) Orange FL vs. FALS scattergram showing how *Synechococcus* are separated from *Prochlorococcus*, since the latter do not exhibit Orange FL. (C) Scattergram showing the larger cells in the ultra- and nanoplankton and pennate diatom groups. Each dot denotes an individual cell for a 10-m sample taken on day 7 inside the iron patch. Calibration microspheres (beads) of different sizes were added to each sample as internal standards: 0.47 $\mu$m for A,B; and 2.02 $\mu$m circled in C.

results since a portion of the orange fluorescence from phycoerythrin may also have been detected as red fluorescence.

To put bounds on the sizes of the flow cytometrically determined ultra- and nanoplankton groups, we analyzed material that passed through differently sized Poretics polycarbonate membrane filters. On day 5 inside the patch, 75% of the ultraplankton passed through a 2-$\mu$m filter, while 95% passed through a 5-$\mu$m filter. On the same day, 50% of the nanoplankton passed through a 2-$\mu$m filter, and >95% passed through a 10-$\mu$m filter. These flow cytometric populations do not conform well to the "pico" (<2 $\mu$m) and "nano" (2–20 $\mu$m) size ranges as originally defined (Sieburth et al. 1978); therefore, our use of "ultra" and "nano" modifiers in this paper is operational. Determining that 60% of the pennates passed through a 10-$\mu$m filter reveals little about their dimensions because of their long slender shape and uncertainty as to how they would pass through a filter. However, Zettler et al. (1996) found that this flow cytometric group consisted mainly of cells up to 50 $\mu$m in length, in agreement with microscopic observations during IronEx II, which found this group included cells up to roughly 60 $\mu$m in length (Tanner pers. comm.).

There is good evidence that flow cytometrically derived fluorescence per cell is related to pigment per cell for individual species (e.g., Sosik et al. 1989; Li et al. 1993; Jonker et al. 1995; Moore et al. 1995; Moore and Chisholm in press), and we demonstrate this directly for *Prochlorococcus* in this study (*see below*). This relationship need not be linear, however, and can be confounded by variations in accessory pigments and the "package effect" (Sosik et al. 1989). Thus, particularly for larger cells, equivalent increases in pigment per cell may not result in proportional increases in Red FL per cell, thereby limiting quantitative interspecific comparisons of cellular fluorescence. The relationship between cellular fluorescence and absolute pigment concentration may also be influenced by changes in fluorescence yield (Falkowski and Kiefer 1985; Falkowski and Kolber 1995). Since the addition of DCMU [3-(3, 4-dichlorophenyl)−1,1-dimethylurea] does not affect flow cytometrically derived fluorescence signals except at excitation intensities well below those used in this study (Xu et al. 1990; Furuya and Li 1992), we do not consider variable fluorescence yield to be an issue in interpreting our data.

## Results and discussion

*Size-fractionated Chl* a—Total Chl *a*, a proxy for phytoplankton biomass, averaged 0.2 $\mu$g liter$^{-1}$ in surface waters outside the iron-enriched patch (Fig. 2A), a typical value for the equatorial Pacific (Chavez et al. 1990). After 2 d of iron enrichment, total Chl *a* had doubled, and by day 6, it had increased 12-fold to 2.6 $\mu$g liter$^{-1}$ (Fig. 2A,B). Initially, the phytoplankton community was dominated by cells <10 $\mu$m, which accounted for 90% of the total. By day 6, total chlorophyll in the <10- and >10-$\mu$m fractions was roughly equal inside the patch and had increased 7- and 60-fold, respectively (Fig. 2A,B). The >10-$\mu$m fraction rose from 10 to 60% of the total, representing a major shift in community composition from small to large cells (Fig. 2C). This shift

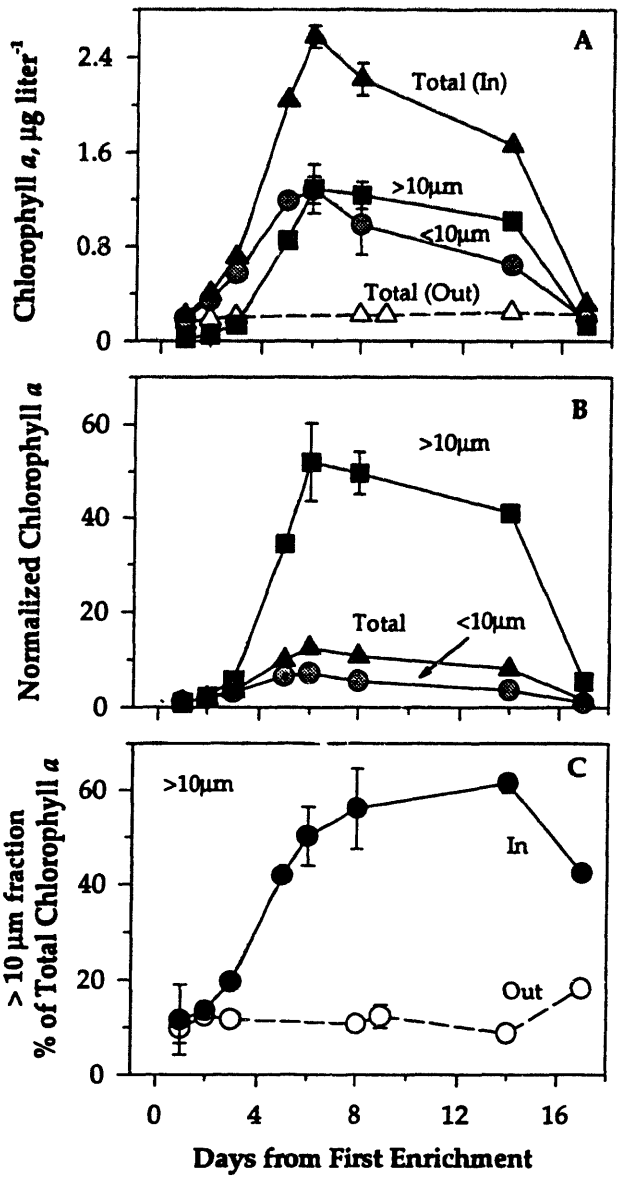


Fig. 2. Size-fractionated Chl *a* ± 1 SD at 15 m as a function of time over the course of the iron-enrichment experiment. (A) Concentrations inside the iron-enriched patch (solid symbols and lines) and outside the patch (open symbols, dashed line). (B) Concentrations measured inside the patch normalized to the average for each fraction outside the patch. (C) The >10-$\mu$m fraction is shown as a percentage of the total Chl *a* inside and outside the patch (symbols and lines as in A). Days of iron addition are marked with vertical bands.

is consistent with observations that high total Chl *a* is accompanied by an abundance of large cells (Raimbault et al. 1988; Chavez et al. 1996). Judging from the analysis of material passing through filters (discussed in Methods), all of the flow cytometrically defined groups contributed to the

<10-μm fraction, while a significant portion of the pennate diatoms were caught on 10-μm filters, thereby contributing to the >10-μm fraction.

*Flow cytometric pigments*—Chlorophyll fluorescence (or in the case of *Synechococcus*, phycoerythrin fluorescence) per cell increased in all groups over the first 7 d of the experiment (Fig. 3A). The simplest interpretation of these increases, supported reasonably well by the taxon-specific pigment data presented below, is that they reflect an increase in cellular pigment concentration for all groups in response to iron enrichment, which indicates that all of these groups were iron limited at the start of the experiment. Such an interpretation is consistent with what is known about the physiological responses of phytoplankton when released from nutrient limitation, since increased cellular Chl *a* concentration is a standard response when phytoplankton are shifted from nutrient-limited to nutrient-replete conditions (e.g., Eppley and Renger 1974; Perry 1976). This pattern has held true in a range of iron-limited phytoplankton cultures (Geider et al. 1993; Trick et al. 1995; Wilhelm and Trick 1995; Kudo and Harrison 1997; McKay et al. 1997; Sunda and Huntsman 1997) and can be indicative of the degree of iron limitation. However, because of the potentially complex relationship between flow cytometrically derived cellular fluorescence and pigment per cell, we cannot interpret the relative magnitude of the fluorescence response between the groups as a measure of the degree of iron limitation. Further, a change in species composition within a group over time might influence its mean cellular fluorescence—a nuance that would be missed by the process of averaging. That is, it is impossible to distinguish between either an entire group, or just a subset of that group responding to iron, if there is no change in shape of the flow cytometric signature.

*Taxonomic marker pigments by HPLC*—Pigments that are indicative of different classes of phytoplankton were measured over the course of the experiment using HPLC. By normalizing these pigment concentrations to the cell numbers in the different groups defined flow cytometrically, we used these data to interpret Red FL cell$^{-1}$ values and to help judge how well the pennate diatoms detected by flow cytometry represented the larger diatom community as a whole. Cellular Red FL values are expected to covary with xanthophyll concentrations for the ultra- and nanoplankton and pennate diatom groups, since they absorb light at the excitation wavelength used in the flow cytometer (488 nm) and pass energy on to Chl *a* (Bidigare et al. 1990). In contrast, Chl $a_2$ was directly compared to cellular Red FL for *Prochlorococcus*, as it is unique to this group. When plotted on a relative scale, we found that variations in cell-specific pigment concentrations determined for *Prochlorococcus* and the ultra- and nanophytoplankton combined (*see Methods*) followed the same patterns as those observed for the corresponding cellular Red FL values (Fig. 4A,B). Calculated cellular Chl $a_2$ cell$^{-1}$ for *Prochlorococcus* ranged from 0.2 to 0.9 fg cell$^{-1}$, which is consistent with values measured in laboratory cultures (Moore et al. 1995; Moore and Chisholm in press). Because *Prochlorococcus* uniquely contains Chl $a_2$, the significant correlation shown in Fig. 4D indicates that when Chl $a_2$ cell$^{-1}$ doubled, so did cellular Red FL (model II regression; Sokal and Rohlf 1995). For the ultra- and nanoplankton, when HBP cell$^{-1}$ doubled, so did Red FL cell$^{-1}$ (Fig. 4E). Yet, without knowing the relationship between cellular HBP and Chl *a*, a strong conclusion about the relationship between Red FL cell$^{-1}$ and Chl *a* cell$^{-1}$ cannot be made for this group. A varying cellular HBP:Chl *a* ratio would, for instance, likely cause variation in the relationship between cellular Red FL and Chl *a* (Sosik et al. 1989).

To estimate the degree to which the total diatom community can be represented by our flow cytometric pennate diatom group, we compared the relative changes in the bulk concentration of the diatom-specific pigment fucoxanthin with the relative changes in total pennate fluorescence measured per liter (Fig. 4C,F). Diatoms as a group were represented by more than the pennates over the course of the experiment (Coale et al. 1996*b*). The largest diatoms, particularly the chain-forming types, would have been poorly sampled by flow cytometry. In addition, a second pennate diatom population, common to iron-enrichment studies (Zettler et al. 1996), was detected on days 6–8 only. This population was offscale on the y-axis above the pennate population depicted in Fig. 1C and had a low cell abundance (maximum = 450 cells ml$^{-1}$), but it had a 10-fold higher mean Red FL cell$^{-1}$ than the more numerous pennate population. This ephemeral population was not represented in Fig. 3 because the cells were undetectable outside the patch, but we do include it in the bulk Red FL data for Fig. 4. The difference between the dashed and solid half-tone lines in Fig. 4C indicates the importance of this population to the total Red FL per milliliter. By day 8, this second pennate population had waned, and our subsequent flow cytometric analyses clearly missed a large component of the diatom community, as is evidenced by the disparity between the bulk concentrations of Red FL and fucoxanthin (Fig. 4C). For this reason, data from day 8 were excluded from the regression in Fig. 4F. However, the agreement between pigment and fluorescence concentrations prior to day 8 (Fig. 4C) confirms that the pennate diatoms we identified by flow cytometry were the major contributors to the total diatom assemblage up to that point.

*Individual cell size*—Mean FALS per cell, an indicator of cell size (Van de Hulst 1957; Ackelson and Spinrad 1988), increased over the first 7 d of the experiment for all groups, roughly paralleling changes in fluorescence per cell (Fig. 3B). Mean FALS per cell increased more than twofold for *Prochlorococcus* and *Synechococcus*, which corresponds approximately to a 1.5-fold increase in cell volume for these species. Similar increases for the ultra- and nanophytoplankton over this same period reflect roughly a twofold increase in mean cell volume (data not shown; *see* DuRand 1995; Dusenberry 1995). The mean FALS per cell for the pennate diatoms, which could not be calibrated because of the geometry of the cells (Olson et al. 1989), showed an increase similar to that of the other populations, but not as pronounced.

Given the simultaneous increase in cellular FALS and FL in all populations, it is unclear if the response to iron en-

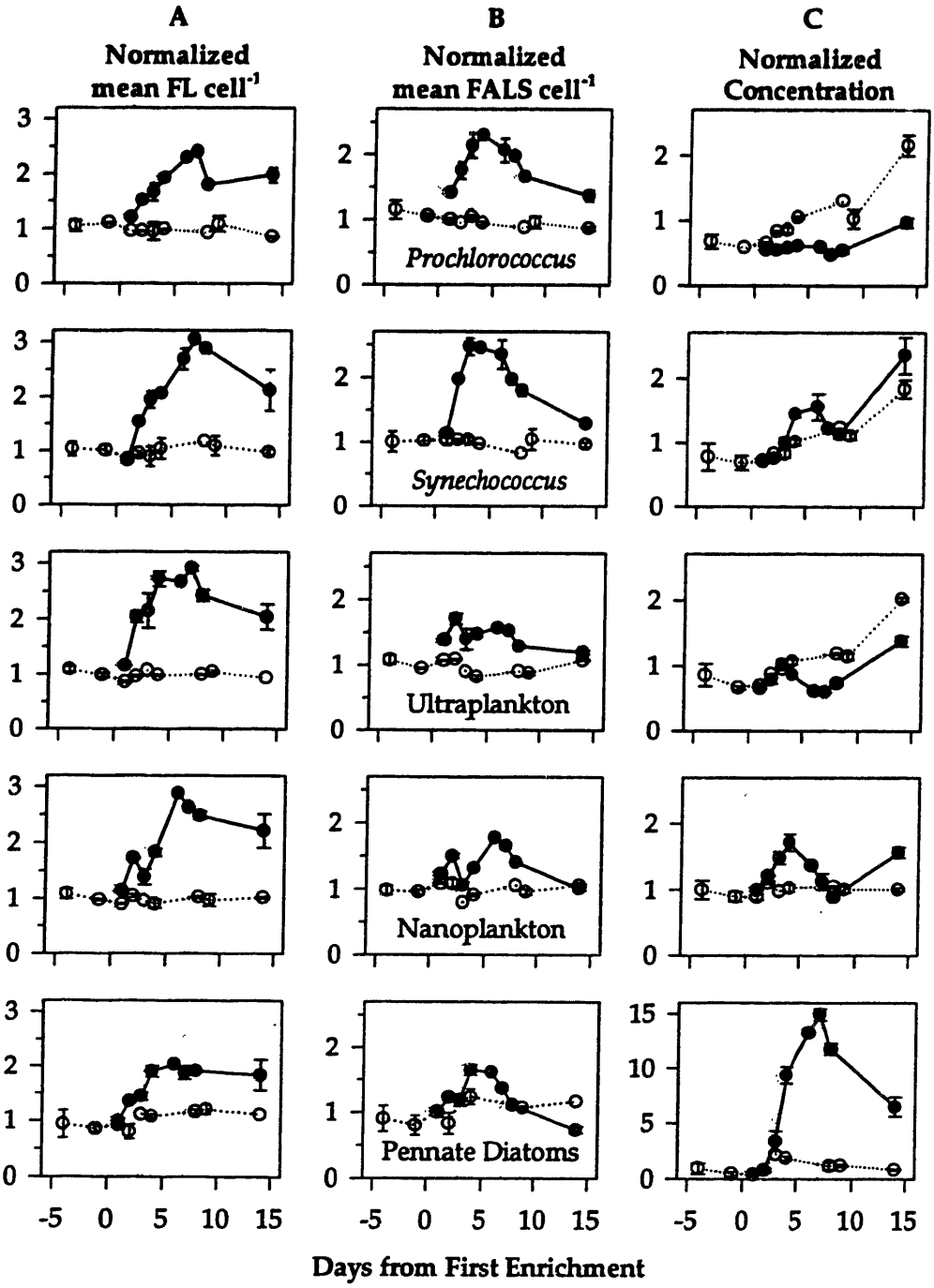


Fig. 3 Response of different phytoplankton groups to iron enrichment in the patch (solid symbols and lines) relative to outside the patch (open symbols, dashed lines) as measured by flow cytometric analysis of individual cells. (A) Normalized mean pigment fluorescence per cell: Orange FL for *Synechococcus* and Red FL for the other groups; (B) normalized mean FALS per cell; and (C) normalized cell concentration. All values reported normalized to the average values outside the patch; data points typically represent average mixed-layer values (3, 10, and 15 m ± 1 SD). Average cell concentrations outside the patch were $1.4 \times 10^5$, $7.6 \times 10^3$, $1.1 \times 10^4$, $2.0 \times 10^3$, and $1.4 \times 10^2$ cells $ml^{-1}$ for *Prochlorococcus, Synechococcus,* ultraplankton, nanoplankton, and pennate diatoms, respectively. Note change of scale in normalized concentration for the pennate diatoms. Days of iron addition are marked by vertical bands.

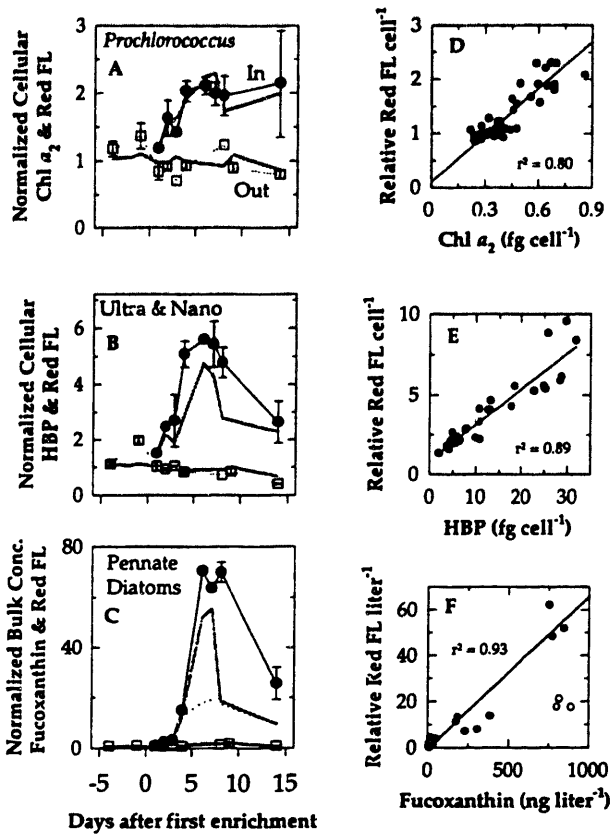


Fig. 4 (A–C) Phytoplankton pigments in the patch (solid circles and lines) and outside the patch (open squares, dashed lines) as measured by HPLC, with corresponding flow cytometry data from Fig. 3 shown for reference (half-tone lines). (A) Normalized cell-specific Chl $a_2$ concentration and Red FL for *Prochlorococcus*. (B) Normalized cell-specific HBP concentration and Red FL for the ultra- and nanoplankton combined. In A and B, bulk pigment concentrations representative of each of the groups of phytoplankton were divided by the flow cytometrically derived cell abundances to yield pigment per cell; they were then normalized to the average value of 3-, 10-, and 15-m samples outside of the patch (±1 SD), as in Fig. 3. (C) Normalized bulk concentrations of fucoxanthin and red fluorescence (Red FL cell$^{-1}$ × cells liter$^{-1}$); a second dashed half-tone line added to show the contribution of the numerically dominant pennate population, whereas the solid half-tone line combines red fluorescence values from this and the far less abundant, but highly pigmented, pennate population that appeared on days 6–8 (*see text*). (D–F) Relationship between HPLC and flow cytometry data using all of the non-normalized data from (A–C), respectively, including Model II regression lines (reduced major axis; Sokal and Rohlf 1995). Note that the data from day 8 (open circles) were excluded from the regression in F.

richment involved an increase in the volumetric concentration of pigment or whether pigment simply increased in proportion to increases in cellular volume. For all the groups except *Prochlorococcus*, the uncertainties involved in converting FL to Chl *a* and FALS to volume are too large to distinguish between these two possibilities. Based on culture studies (Moore et al. 1995; Moore and Chisholm in press) and the data reported here, we know that the 2.5-fold increase in cellular Red FL for *Prochlorococcus* over the first 4 d of the experiment (Fig. 3A) corresponded to a 2.5-fold increase in Chl $a_2$ cell$^{-1}$ (Fig. 4D). Using an empirical calibration of FALS to volume for this species (data not shown) and evidence from synchronized populations in cultures and in the field, where the drop in the FALS signal as cells divide reflects a halving of the cell volume (DuRand 1995; Dusenberry 1995; Binder et al. 1996), we find that over the first 4 d, the 2.3-fold increase in mean FALS per cell for *Prochlorococcus* (Fig. 3B) was associated with a 1.6-fold increase in mean cell volume. Thus, these data suggest that Chl $a_2$: volume for *Prochlorococcus* increased approximately 1.5-fold inside the patch. That is, *Prochlorococcus* increased Chl $a_2$ beyond that which would have been necessary simply to match increases in cell volume. An elevated Chl $a_2$: volume is consistent with a positive correlation between Chl *a*: C and iron concentration observed in iron-limited cultures of coastal eukaryotic phytoplankton (Sunda and Huntsman 1997) since cell volume and cell C are positively correlated (Strathman 1967; Lee and Fuhrman 1987; Simon and Azam 1989; Verity et al. 1992). We are currently working to constrain the uncertainty in estimates of Chl *a*: volume for the other phytoplankton groups based on these flow cytometric data.

*Cell number response*—In terms of cellular Red FL and FALS, all of the groups responded to iron enrichment in a qualitatively similar manner. However, when changes in cell numbers are considered, dramatic differences between the groups are apparent (Fig. 3C). The pennate diatoms, which averaged 140 cells ml$^{-1}$ outside the patch, reached 2,100 cells ml$^{-1}$ inside the patch. Over the first 4 d, their net growth (reflecting $\mu$, the rate of cell division, minus cell losses) was exponential, and they had a net growth rate ($\mu_{net}$) of 1.0 d$^{-1}$. There was a distinct increase in ultraplankton cell numbers inside the patch, but a similar increase was observed outside the patch; thus, the former cannot necessarily be attributed to iron addition. The nanoplankton, however, displayed increases in cell number inside the patch by day 3, more than doubled in number by day 4, and then returned to out-of-patch levels. In contrast, the increase in cell numbers of the smaller phytoplankton inside the enriched patch was modest at best. Relative to unfertilized waters, *Prochlorococcus* cell numbers actually decreased inside the patch. Using cell cycle analysis, Mann and Chisholm (submitted) found that $\mu$ for *Prochlorococcus* increased approximately 60% inside the patch, which suggests that the decrease in *Prochlorococcus* cells inside the patch was due to increased grazing rates.

*Synechococcus* cell numbers increased twofold inside the patch by day 7, but they then quickly receded to match out-of-patch populations. The majority of this increase occurred between days 3 and 4, suggesting a rapid decrease in grazing pressure, an increase in $\mu$, or both. Rue and Bruland (1997) found increased production of an organic ligand capable of binding iron shortly following iron enrichment. *Synechococcus* is known to produce such ligands in culture, apparently to maintain high growth rates at very low iron concentrations

(Wilhelm et al. 1996). Production of siderophores by *Synechococcus* would increase their access to the iron pool and could therefore be viewed as a signal that *Synechococcus* responded to the iron addition much as if it were an aeolian deposition event. Speculating one step further, if the growth rate of *Synechococcus* were limited by iron, sequestration of added iron by newly produced siderophores would enhance the availability of iron to *Synechococcus*, leading to an increase in $\mu$.

These data indicate that even though some of the smaller phytoplankton groups increased twofold in concentration, only the initially rare pennate diatoms broke free from grazer control. This is in agreement with evidence that microzooplankton exert strong control over the typically dominant phytoplankton of the equatorial Pacific (Price et al. 1994; Landry et al. 1995, 1997) and with evidence suggesting that an increased $\mu$ of the phytoplankton community was matched by heightened microzooplankton grazing pressure during IronEx II (Coale et al. 1996*b*). Assuming that cell losses were dominated by the rate of grazing (g) during the early stages of the iron-enriched patch (i.e., $\mu_{net} \approx \mu - g$), then a simple explanation for the bloom of pennates is that iron fertilization caused a substantial elevation in $\mu$ relative to g for these populations (Cullen 1995), resulting in the measured $\mu_{net}$ of 1.0 $d^{-1}$. This is in accord with the limited grazing impact of the mesozooplankton measured inside the patch (Coale et al. 1996*b*). After this growth burst, cell numbers declined, even though there had been a third addition of iron on day 7 and mean fluorescence per cell remained elevated over out-of-patch levels (Fig. 3A).

The decline in pennate cell numbers could have resulted from a combination of events, including increased removal rates, such as grazing and or sinking (Bidigare et al. submitted), or reduction in growth rate because of limitation by another factor. $^{234}$Th inventories measured during IronEx II indicate that the particulate organic carbon (POC) flux increased sevenfold between days 7 and 14 following initial enrichment (Bidigare et al. submitted). Kudela and Chavez (1996) suggest that the decreased transparency of patch waters may have induced light limitation of phytoplankton growth. As argued by Erdner (1997), incomplete relief from iron limitation was also a possibility. She showed that there was no detectable switch from flavodoxin to ferredoxin in the phytoplankton community throughout IronEx II, as would be expected upon the relief of iron limitation. In addition, silica, which is essential for diatom growth, has recently been argued as the ultimate factor producing HNLC conditions in the equatorial Pacific (Dugdale et al. 1995; Dugdale and Wilkerson 1998). As nitrate dropped from ca. 10 $\mu$M outside the patch to 7 $\mu$M inside on day 7 (Coale et al. 1996*b*), silicate dropped from ca. 4 $\mu$M to 1 $\mu$M (Coale pers. comm.). Dugdale and Wilkerson (1998) argue that at silicate concentrations below roughly 2 $\mu$M, nitrate uptake by diatoms is curtailed, which could help explain the decrease in net growth seen for the pennate diatoms after day 7 (Fig. 3C).

## Conclusions

These results document clear differential changes within the phytoplankton community over the course of the iron-enriched bloom during IronEx II. Using fractionated Chl *a*, we measured a dramatic size-based shift as biomass in the >10-$\mu$m fraction increased 60-fold. The overall increase in Chl *a* resulted in part from increases in cellular pigment concentration, which were amplified to varying extents by increases in cell numbers across the groups studied. The pennate diatoms, which increased >10-fold, were the only cells identified in this study that bloomed following iron enrichment. These findings are consistent with the recent equatorial Pacific synopsis (Landry et al. 1997), as well with as the "ecumenical iron hypothesis" (Morel et al. 1991*b*; Price et al. 1994; Cullen 1995), which allows for the coregulation of phytoplankton in this region by iron limitation and grazing, the latter playing a particularly significant role in regulating the small, dominant cells.

In our view, the most significant conclusion from the IronEx experiments and related work (e.g., Martin and Fitzwater 1988; Coale 1991; Takeda and Obata 1995; Boyd et al. 1996; Coale et al. 1996*a*; Zettler et al. 1996) is that phytoplankton community structure changes dramatically when productivity is stimulated by nutrient enrichment. As pointed out by Howarth (1988), the concept of "nutrient limitation" must include both the limitation of extant dominant species and the limitation of the potential rate of net primary production, which can only be realized upon the supply of the limiting nutrient together with an accompanying shift in community structure. It is important to keep in mind that the response of the phytoplankton community seen in IronEx II was transient. We do not know what the structure of the food web would look like if iron were supplied continuously over time scales much longer than the generation times of the relevant organisms. Modeling studies (e.g., Sarmiento and Orr 1991; Frost and Franzen 1992; Armstrong 1994), which take into account the potential for changes in community structure, will be important for projecting hypothetical outcomes to fertilization scenarios. Only through carefully designed long-term experiments, however, will we be able to predict the ecological consequences of, and changes in export carbon resulting from, ocean fertilization. These will be important for developing policies to regulate commercial ocean fertilization (Markels 1995; Sørensen 1995; Jones 1996; Jones and Young 1997).

## References

ACKELSON, S. G., AND R. W. SPINRAD. 1988. Size and refractive index of individual marine particulates: A flow cytometric approach. Appl. Opt. **27**: 1270–1277.

Andersen, R. A., R. R. Bidigare, M. D. Keller, and M. Latasa. 1996. A comparison of HPLC pigment signatures and electron microscopic observations for oligotrophic waters of the North Atlantic and Pacific Oceans. Deep-Sea Res. **43**: 517–537.

ARMSTRONG, R. A. 1994. Grazing limitation and nutrient limitation in marine ecosystems: Steady state solutions of an ecosystem model with multiple food chains. Limnol. Oceanogr. **39**: 597–608.

BEHRENFELD, M. J., A. J. BALE, A. S. KOLBER, J. AIKEN, AND P. G. FALKOWSKI. 1996. Confirmation of iron limitation of phytoplankton photosynthesis in the equatorial Pacific Ocean. Nature **383**: 508–511.

BIDIGARE, R. R., M. E. ONDRUSEK, J. H. MORROW, AND D. A.

KIEFER. 1990. *In vivo* absorption properties of algal pigments. Proc. SPIE Ocean Opt. X **1302:** 290–302.

BINDER, B. J., S. W. CHISHOLM, R. J. OLSON, S. L. FRANKEL, AND A. Z. WORDEN. 1996. Dynamics of picophytoplankton, ultraphytoplankton and bacteria in the central equatorial Pacific. Deep-Sea Res. **43:** 907–931.

BOYD, P. W., D. L. MUGGLI, D. E. VARELA, R. H. GOLDBLATT, R. CHRETIEN, K. J. ORIANS, AND P. J. HARRISON. 1996. *In vitro* iron enrichment experiments in the NE subarctic Pacific. Mar. Ecol. Prog. Ser. **136:** 179–193.

BUMA, A. G. J., H. J. W. DE BAAR, R. F. NOLTING, AND A. J. VAN BENNEKOM. 1991. Metal enrichment experiments in the Weddell-Scotia Seas: Effects of iron and manganese on various plankton communities. Limnol. Oceanogr. **36:** 1865–1878.

CAVENDER-BARES, K. K., S. L. FRANKEL, AND S. W. CHISHOLM. 1998. A dual sheath flow cytometer for shipboard analyses of phytoplankton communities from the oligotrophic oceans. Limnol. Oceanogr. **43:** 1383–1388.

CHAVEZ, F. P., K. R. BUCK, AND R. T. BARBER. 1990. Phytoplankton taxa in relation to primary production in the equatorial Pacific. Deep-Sea Res. **37:** 1733–1752.

———, ———, S. K. SERVICE, J. NEWTON, AND R. T. BARBER. 1996. Phytoplankton variability in the central and eastern tropical Pacific. Deep-Sea Res. **43:** 835–870.

CHISHOLM, S. W., AND F. M. M. MOREL [EDS.]. 1991. What controls phytoplankton production in nutrient-rich areas of the open sea? Limnol. Oceanogr. **36:** 1507–1965.

———, R. J. OLSON, E. R. ZETTLER, R. GOERICKE, J. B. WATERBURY, AND N. A. WELSCHMEYER. 1988. A novel free-living prochlorophyte abundant in the oceanic euphotic zone. Nature **334:** 340–343.

COALE, K. H. 1991. Effects of iron, manganese, copper, and zinc enrichments on productivity and biomass in the subarctic Pacific. Limnol. Oceanogr. **36:** 1851–1864.

———, S. E. FITZWATER, R. M. GORDON, K. S. JOHNSON, AND R. T. BARBER. 1996*a*. Control of community growth and export production by upwelled iron in the equatorial Pacific Ocean. Nature **379:** 621–624.

———, AND OTHERS. 1996*b*. A massive phytoplankton bloom induced by an ecosystem-scale iron fertilization experiment in the equatorial Pacific Ocean. Nature **383:** 495–501.

COOPER, D. J., A. J. WATSON, AND P. D. NIGHTINGALE. 1996. Large decrease in ocean-surface $CO_2$ fugacity in response to *in situ* iron fertilization. Nature **383:** 511–513.

CULLEN, J. J. 1995. Status of the iron hypothesis after the Open-Ocean Enrichment Experiment. Limnol. Oceanogr. **40:** 1336–1343.

DUGDALE, R. C., AND F. P. WILKERSON. 1998. Silicate regulation of new production in the equatorial Pacific upwelling. Nature **391:** 270–273.

———, ———, AND H. J. MINAS. 1995. The role of a silicate pump in driving new production. Deep-Sea Res. **42:** 697–719.

DURAND, M. D. 1995. Phytoplankton growth and diel variations in beam attenuation through individual cell analysis. Ph.D. thesis, M.I.T. and W.H.O.I.

DUSENBERRY, J. A. 1995. Picophytoplankton photoacclimation and mixing in the surface oceans. Ph.D. thesis, M.I.T. and W.H.O.I.

EPPLEY, R. W., AND E. H. RENGER. 1974. Nitrogen assimilation of an oceanic diatom in nitrogen-limited continuous culture. J. Phycol. **10:** 15–23.

ERDNER, D. L. 1997. Characterization of ferredoxin and flavodoxin as molecular indicators of iron limitation in marine eukaryotic phytoplankton. Ph.D. thesis, M.I.T. and W.H.O.I.

FALKOWSKI, P., AND D. A. KIEFER. 1985. Chlorophyll *a* fluorescence in phytoplankton: Relationship to photosynthesis and biomass. J. Plankton Res. **7:** 715–731.

FALKOWSKI, P. G., AND Z. KOLBER. 1995. Variations in chlorophyll fluorescence yields in phytoplankton in the world oceans. Aust. J. Plant Physiol. **22:** 341–355.

FROST, B. W. 1991. The role of grazing in nutrient-rich areas of the open sea. Limnol. Oceanogr. **36:** 1616–1630.

———, AND N. C. FRANZEN. 1992. Grazing and iron limitation in the control of phytoplankton stock and nutrient concentration: A chemostat analogue of the Pacific equatorial upwelling zone. Mar. Ecol. Prog. Ser. **83:** 291–303.

FURUYA, K., AND W. K. W. LI. 1992. Evaluation of photosynthetic capacity in phytoplankton by flow cytometric analysis of DCMU-enhanced chlorophyll fluorescence. Mar. Ecol. Prog. Ser. **88:** 279–287.

GEIDER, R. J., J. LA ROCHE, R. M. GREENE, AND M. OLAIZOLA. 1993. Response of the photosynthetic apparatus of *Phaeodactylum tricornutum* (Bacillariophyceae) to nitrate, phosphate, or iron starvation. J. Phycol. **29:** 755–766.

GOERICKE, R., AND D. J. REPETA. 1993. Chlorophylls *a* and *b* and divinyl chlorophylls *a* and *b* in the open subtropical North Atlantic Ocean. Mar. Ecol. Prog. Ser. **101:** 307–313.

GRAN, H. H. 1931. On the conditions for the production of plankton in the sea. Rapp. P-V. Reun. Cons. Int. Explor. Mer. **75:** 37–46.

HART, T. J. 1934. On the phytoplankton of the south-west Atlantic and the Bellingshausen Sea, 1929–31. Discovery Rep. **8:** 1–268.

HOWARTH, R. W. 1988. Nutrient limitation of net primary production in marine ecosystems. Annu. Rev. Ecol. **19:** 89–110.

JONES, I. S. F. 1996. Enhanced carbon dioxide uptake by the world's oceans. Energy Convers. Manage. **37:** 1049–1052.

———, AND H. E. YOUNG. 1997. Engineering a large sustainable world fishery. Environ. Conserv. **24:** 99–104.

JONKER, R. R., J. T. MEULEMANS, G. B. J. DUBELAAR, M. F. WILKINS, AND J. RINGELBERG. 1995. Flow cytometry: A powerful tool in analysis of biomass distributions in phytoplankton. Water Sci. Technol. **32:** 177–182.

KOLBER, Z. S., AND OTHERS. 1994. Iron limitation of phytoplankton photosynthesis in the equatorial Pacific Ocean. Nature **371:** 145–149.

KUDELA, R. M., AND F. P. CHAVEZ. 1996. Bio-optical properties in relation to an algal bloom caused by iron enrichment in the equatorial Pacific. Geophys. Res. Lett. **23:** 3751–3754.

KUDO, I., AND P. J. HARRISON. 1997. Effect of iron nutrition on the marine cyanobacterium *Synechococcus* grown on different N sources and irradiances. J. Phycol. **33:** 232–240.

LANDRY, M. R., AND OTHERS. 1997. Iron and grazing constraints on primary production in the central equatorial Pacific: An EqPac synthesis. Limnol. Oceanogr. **42:** 405–418.

———, J. CONSTANTINOU, AND J. KIRSHTEIN. 1995. Microzooplankton grazing in the central equatorial Pacific during February and August, 1992. Deep-Sea Res. **42:** 657–671.

———, AND R. P. HASSETT. 1982. Estimating the grazing impact of marine micro-zooplankton. Mar. Biol. **67:** 283–288.

LEE, S., AND J. A. FUHRMAN. 1987. Relationships between biovolume and biomass of naturally derived marine bacterioplankton. Appl. Environ. Microbiol. **53:** 1298–1303.

LI, W. K. W., T. ZOHARY, Y. Z. YACOBI, AND A. M. WOOD. 1993. Ultraphytoplankton in the eastern Mediterranean Sea: Towards deriving phytoplankton biomass from flow cytometric measurements of abundance, fluorescence and light scatter. Mar. Ecol. Prog. Ser. **102:** 79–87.

MARKELS, M. 1995. Fishing for markets. Regulation **3:** 73–79.

MARTIN, J. H. 1990. Glacial–interglacial $CO_2$ change: The iron hypothesis. Paleoceanography **5:** 1–13.

———, AND OTHERS. 1994. Testing the iron hypothesis in ecosystems of the equatorial Pacific Ocean. Nature **371:** 123–129.

———, AND S. E. FITZWATER. 1988. Iron deficiency limits phytoplankton growth in the north-east Pacific subarctic. Nature **331:** 341–343.

MCKAY, R. M. L., R. J. GEIDER, AND J. LAROCHE. 1997. Physiological and biochemical response of the photosynthetic apparatus of two marine diatoms to Fe stress. Plant Physiol. **114:** 615–622.

MOORE, L. R., AND S. W. CHISHOLM. Photophysiology of the marine cyanobacterium *Prochlorococcus*: Ecotypic differences among cultured isolates. Limnol. Oceanogr. In press.

———, R. GOERICKE, AND S. W. CHISHOLM. 1995. Comparative physiology of *Synechococcus* and *Prochlorococcus*: Influence of light and temperature on growth, pigments, fluorescence and absorptive properties. Mar. Ecol. Prog. Ser. **116:** 259–275.

MOREL, F. M. M., R. J. HUDSON, AND N. M. PRICE. 1991*a*. Limitation of productivity by trace metals in the sea. Limnol. Oceanogr. **36:** 1742–1755.

———, J. G. RUETER, AND N. M. PRICE. 1991*b*. Iron nutrition of phytoplankton and its possible importance in the ecology of ocean regions with high nutrient and low biomass. Oceanography **4:** 56–61.

OLSON, R. J., S. W. CHISHOLM, E. R. ZETTLER, M. A. ALTABET, AND J. A. DUSENBERRY. 1990. Spatial and temporal distributions of prochlorophyte picoplankton in the North Atlantic Ocean. Deep-Sea Res. **37:** 1033–1051.

———, E. R. ZETTLER, AND O. K. ANDERSON. 1989. Discrimination of eukaryotic phytoplankton cell types from light scatter and autofluorescence properties measured by flow cytometry. Cytometry **10:** 636–643.

PARSONS, T. R., Y. MAITA, AND C. M. LALLI. 1984. A manual of chemical and biological methods for seawater analysis. Pergamon.

PERRY, M. J. 1976. Phosphate utilization by an oceanic diatom in phosphorus-limited chemostat culture and in oligotrophic waters of the central North Pacific. Limnol. Oceanogr. **21:** 88–107.

PRICE, N. M., B. A. AHNER, AND F. M. M. MOREL. 1994. The equatorial Pacific Ocean: Grazer-controlled phytoplankton populations in an iron-limited ecosystem. Limnol. Oceanogr. **39:** 520–534.

RAIMBAULT, P., M. RODIER, AND I. TAUPIER-LETAGE. 1988. Size fraction of phytoplankton in the Ligurian Sea and the Algerian Basin (Mediterranean Sea): Size distribution versus total concentration. Mar. Microb. Food Webs **3:** 1–7.

RUE, E. L., AND K. W. BRULAND. 1997. The role of organic complexation on ambient iron chemistry in the equatorial Pacific Ocean and the response of a mesoscale iron addition experiment. Limnol. Oceanogr. **42:** 901–910.

SARMIENTO, J. L., AND J. C. ORR. 1991. Three-dimensional simulations of the impact of Southern Ocean nutrient depletion on atmospheric $CO_2$ and ocean chemistry. Limnol. Oceanogr. **36:** 1928–1950.

SIEBURTH, J. MCN., V. SMETACEK, AND J. LENZ. 1978. Pelagic ecosystem structure: Heterotrophic compartments of the plankton and their relationship to plankton size fractions. Limnol. Oceanogr. **23:** 1256–1263.

SIMON, M., AND F. AZAM. 1989. Protein content and protein synthesis rates of planktonic marine bacteria. Mar. Ecol. Prog. Ser. **51:** 201–213.

SIMON, N., R. G. BARLOW, D. MARIE, F. PARTENSKY, AND D. VAULOT. 1994. Characterization of oceanic photosynthetic picoeukaryotes by flow cytometry. J. Phycol. **30:** 922–935.

SOKAL, R. R., AND F. J. ROHLF. 1995. Biometry, 3rd ed. W. H. Freeman.

SØRENSEN, R. 1995. Maricult-planting the seeds of a blue revolution. Tellus **2:** 4–7.

SOSIK, H. M., S. W. CHISHOLM, AND R. J. OLSON. 1989. Chlorophyll fluorescence from single cells: Interpretation of flow cytometric signals. Limnol. Oceanogr. **34:** 1749–1761.

STRATHMAN, R. R 1967. Estimating the organic carbon content of phytoplankton from cell volume or plasma volume. Limnol. Oceanogr. **12:** 411–418.

SUNDA, W. G., AND S. A. HUNTSMAN. 1997. Interrelated influence of iron, light and cell size on marine phytoplankton growth. Nature **390:** 389–392.

TAKEDA, S., AND H. OBATA. 1995. Response of equatorial Pacific phytoplankton to subnanomolar Fe enrichment. Mar. Chem. **50:** 219–227.

TRICK, C. G., S. W. WILHELM, AND C. M. BROWN 1995. Alterations in cell pigmentation, protein expression, and photosynthetic capacity of the cyanobacterium *Oscillatoria tenuis* grown under low iron conditions. Can. J. Microbiol. **41:** 1117–1123.

TURNER, S. M., P. D. NIGHTINGALE, L. J. SPOKES, M. I. LIDDICOAT, AND P. S. LISS. 1996. Increased dimethyl sulphide concentrations in sea water from *in situ* iron enrichment. Nature **383:** 513–517.

VAN DE HULST, H. C. 1957. Light scattering by small particles. Wiley.

VERITY, P. G., C. Y. ROBERTSON, C. R. TRONZO, M. G. ANDREWS, J. R. NELSON, AND M. E. SIERACKI. 1992. Relationships between cell volume and the carbon and nitrogen content of marine photosynthetic nanoplankton. Limnol. Oceanogr. **37:** 1434–1446.

VESK, M., AND S. W. JEFFREY. 1987. Ultrastructure and pigments of two strains of the picoplanktonic alga *Pelagococcus subviridis* (Chrysophyceae). J. Phycol. **23:** 322–336.

WALSH, J. J. 1976. Herbivory as a factor in patterns of nutrient utilization in the sea. Limnol. Oceanogr. **21:** 1–13.

WILHELM, S. W., D. P. MAXWELL, AND C. G. TRICK. 1996. Growth, iron requirements, and siderophore production in iron-limited *Synechococcus* PCC 7 )2. Limnol. Oceanogr. **41:** 89–97.

———, AND C. G. TRICK. 1995. Physiological profiles of *Synechococcus* (Cyanophyceae) in iron-limiting continuous cultures. J. Phycol. **31:** 79–85.

WRIGHT, S. W., AND S. W. JEFFREY. 1987. Fucoxanthin pigment markers of marine phytoplankton analysed by HPLC and HPTLC. Mar. Ecol. Prog. Ser. **38:** 259–266.

XU, C., J. AUGER, AND GOVINDJEE. 1990. Chlorophyll *a* fluorescence measurements of isolated spinach thylakoids obtained by using single-laser-based flow cytometry. Cytometry **11:** 349–358.

ZETTLER, E. R., R. J. OLSON, B. J. BINDER, S. W. CHISHOLM, S. E. FITZWATER, AND M. R. GORDON. 1996. Iron-enrichment bottle experiments in the equatorial Pacific: Responses of individual phytoplankton cells. Deep-Sea Res. **43:** 1017–1029.

*Received: 24 July 1997*
*Accepted: 28 August 1998*
*Amended: 3 November 1998*

Note:

Bidigare et al. (submitted) which was cited in this paper has been accepted and is in press in *Paleoceanography*

Chapter 5

# Relationships between bacterio- and phytoplankton community structure and nutrient concentrations along a transect in the western Atlantic Ocean

Kent K. Cavender-Bares[1]
David M. Karl[2]
Sallie W. Chisholm[1]

[1] Ralph M. Parsons' Laboratory, MIT

[2] School of Ocean and Earth Science and Technology (SOEST), University of Hawaii, Honolulu, HI 96822

ABSTRACT

High sensitivity measurements of nitrate plus nitrite (N+N) and soluble reactive phosphorus (SRP) were made in conjunction with analysis of the microbial community structure along a transect in the Atlantic Ocean. In the past, comparisons of microbial abundance with nutrient concentrations in this ocean basin have been possible only at depth or during periods of deep mixing. This is the first study for the Atlantic which combines detailed analysis of the microbial community by flow cytometry with determinations of N+N by chemiluminescence and SRP by the magnesium induced co-precipitation (MAGIC) protocol. We enumerated six groups of microorganisms: bacteria, *Prochlorococcus*, *Synechococcus*, ultra- and nanophytoplankton, cryptophytes, and coccolithophores. We found that the abundance of bacteria was well correlated with the concentration of SRP, and that the abundance of ultra- and nanophytoplankton was well correlated with the concentration of N+N. The abundance of *Prochlorococcus* was best explained by a positive relationship with temperature, while none of our measured parameters explained changes in abundance for *Synechococcus*. Our nutrient measurements support the hypothesis that elevated ratios of N+N to SRP in the upper thermocline of the Sargasso Sea result from remineralization of nitrogen-fixing cells.

## INTRODUCTION

Historically, efforts to understand the relationships between microorganisms and nutrient availability in the Sargasso Sea have been hampered because of the exceedingly low levels of inorganic nitrogen and phosphorus present (Garside 1985; Glover *et al.* 1988; Ormaza-González and Statham 1991; Michaels *et al.* 1994; Michaels and Knap 1996; Cotner *et al.* 1997). In fact, the concentration of nitrate plus nitrite (N+N) and soluble reactive phosphorus (SRP) have remained below the detection limit of standard colorometric methods over much of the last decade at the Bermuda Atlantic Time-series Study (BATS) site (BATS web site available at: http://www.bbsr.edu/bats/; Michaels *et al.* 1994; Michaels and Knap 1996). We have been involved in a project which was designed to study changes in the size structure of marine microorganisms across a range of nutrient environments (*see* Chapter 6). To enable this study, it was necessary to apply high-sensitivity methods to the measurement of inorganic nutrients in the oligotrophic waters of the Atlantic Ocean. Overall, these nutrient analyses not only serve as a necessary backdrop for our ecological studies of size structure, but also shed light on current hypotheses of the regulation of global N and P cycles.

There has been a recent effort to explain elevated ratios of inorganic N:P which have been observed in the west central North Atlantic (Fanning 1989; Fanning 1992; Michaels *et al.* 1994; Michaels and Knap 1996; Gruber and Sarmiento 1997). Historical compilations (e.g., GEOSECS) and the Bermuda Atlantic Time-series Study (BATS) have provided evidence that inorganic N:P ratios exceed 16:1 and can reach as high as 40:1 in the approximate depth range of 200 to 600 m. Several hypotheses as to the cause of these elevated N:P ratios have been put forth, including links to atmospheric deposition of nitrogen (Fanning 1989) and dinitrogen fixation ($N_2$-fixation) by phytoplankton (Michaels *et al.* 1996). The latter requires that cells which carry out $N_2$-fixation (i.e., diazotrophs) are rich in nitrogen, compared to the Redfield ratio (16:1; Redfield 1934), and are remineralized within the depth range of 200-600 m with comparable rates of remineralization for both nitrogen and phosphorus. A little emphasized corollary of this hypothesis is that inorganic N should be depleted with respect to inorganic P in surface waters for periods of the annual cycle in order to stimulate $N_2$-fixation. For this reason, it is useful to consider the ratio of new nitrogen (i.e., N+N; Dugdale and Goering 1967) to

inorganic phosphorus (SRP) in the euphotic zone, which should be less than 16:1 during stratified periods for the corollary to hold.

For selected surface samples during oligotrophic periods in the Sargasso Sea, nitrate values have been reported to range from below 2 nM to 20 nM (Garside 1982; Glover *et al.* 1988); SRP has been shown to range from below 1 to 10 nM during February near BATS (Ormaza-González and Statham 1991) and has been estimated to range from 5 to 10 nM during March and August at BATS, respectively (Cotner *et al.* 1997). However, there are no reports in which nanomolar levels of inorganic nitrogen and phosphorus have been measured simultaneously for the North Atlantic.

We made high sensitivity measurements of N+N and SRP along a transect from the southern Sargasso Sea, to the BATS site, and then across the Gulf Stream into coastal waters off New York. The cruise captured oligotrophic regions as well as the spring bloom in-progress at BATS. From these analyses and those from several other cruises in the region, we are now able to provide added insight to the N and P data from the BATS program. We found elevated N:P ratios during the deeply mixed periods, as would be expected because deep waters with elevated ratios (Michaels *et al.* 1994) ventilate the surface layer. Perhaps more importantly, we found sub-Redfield N:P ratios in the mixed layer of the Sargasso Sea during stratified periods. This is indicative of N-limitation of new production during these periods, and it is in agreement with our corollary to the hypothesis of Michaels *et al.* (1994).

As stated earlier, our overall goal was to study the relationship between nutrients and the size structure of microorganisms in the western Atlantic Ocean, to determine whether plankton distributions could be convincingly explained by nutrient concentrations. Along the transect, we measured the abundance of six microbial groups: bacteria (i.e., prokaryotes which lacked pigment autofluorescence), *Prochlorococcus*, *Synechococcus*, a loosely defined group of ultra- and nanoplankton, cryptophytes, and coccolithophores. Aside from N+N and SRP, we measured dissolved organic nitrogen (DON) and phosphorus (DOP) along the transect. Abundance patterns of two out of six plankton groups studied could be explained well by nutrients. Reinforcing the findings of Cotner *et al.* (1997), we found a strong correlation between the

abundance of bacteria and SRP concentrations. Abundances of the ultra- and nanoplankton were well correlated with N+N values, which is consistent with their peak in numbers at BATS during the spring bloom (DuRand *et al.* submitted). We found no other meaningful correlations with nutrients, however, *Prochlorococcus* concentrations were strongly correlated with temperature along the transect, in agreement with laboratory (Moore *et al.* 1995) and field data (Partensky *et al.* in press).

## METHODS

*Sampling and plankton analyses*—Samples were collected either from Niskin bottles attached to a rosette frame equipped with a CTD, or from the ship's flow-through seawater system (~ 3 m) on a series of four cruises aboard the R/V *Oceanus* in the Atlantic Ocean (Fig. 1). The most extensive sampling occurred during March 1998 on a transect from 26°N, 70°W to the Bermuda Atlantic Time-series Study (BATS) site; the cruise continued northwest to the Gulf Stream and then north towards New England. The other three cruises comprised of two during June and one during February.

Samples were collected for nutrient, chlorophyll, and flow cytometric analyses. Nutrient samples (~ 200 ml) were collected in 250 ml low density polyethylene (LDPE) bottles which had previously been washed with Micro detergent, rinsed repeatedly, washed in 1 N HCl, and rinsed three times with the seawater to be sampled. Sample bottles were frozen (-20°C) promptly (Dore *et al.* 1996) until analysis within 3 months to 2 years. Total chlorophyll *a* (Chl *a*) samples consisted of ~50 ml of seawater filtered onto GF/F (Whatman) filters, which were stored in liquid nitrogen and analyzed following the method of Welschmeyer (1994). Some samples for flow cytometry were preserved in 0.1 % glutaraldehyde and frozen in liquid nitrogen (Vaulot *et al.* 1989), while others were analyzed onboard ship. A modified Epic V flow cytometer (Beckman Coulter; Cavender-Bares *et al.* 1998) was configured on land for high-sensitivity to analyze *Prochlorococcus* and *Synechococcus* (Fig. 2A and B) and lower-sensitivity to analyze the larger ultra- and nanoplankton (Fig. 2D-F) at sea, as has previously been described (Cavender-Bares *et al.* 1999). Within the ultra- and nanoplankton group, we were able to

Figure 1:

Map of sampling stations in the western Atlantic Ocean. Different symbols represent different cruises. The approximate location of the Gulf Stream is shown by a dotted line and the Bermuda Atlantic Time-series (BATS) site is denoted.

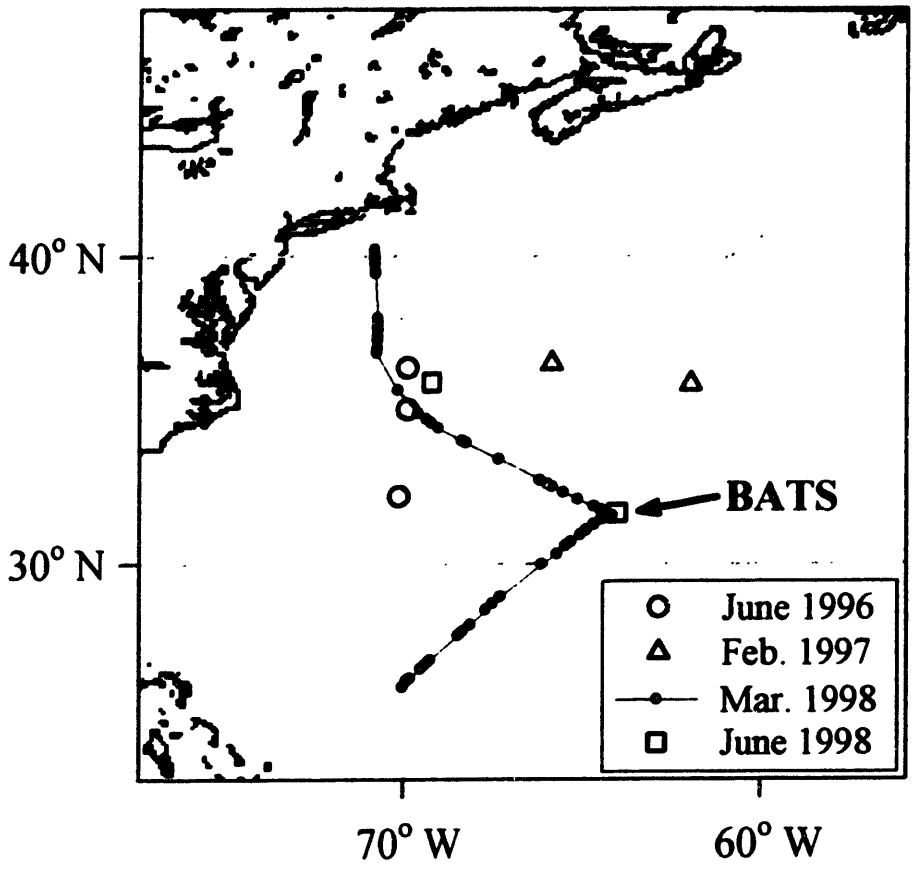
40° N
30° N
70° W
60° W
BATS
June 1996
Feb. 1997
Mar. 1998
June 1998

Figure 2:

Description of microbial groups enumerated using flow cytometry. (A,B) *Prochlorococcus* and *Synechococcus*. (C) bacteria visible because of their orange fluorescence after staining with SYBR Green I. (D) The ultra- and nanoplankton, shown here as individual groups, but considered as one since they were not always distinct from each other. (E) Coccolithophores distinguishable because they depolarize the laser beam. (F) Cryptophytes, which display orange fluorescence and can be separated from the remainder of the ultra- and nanoplankton. Notation: red fluorescence (Red FL), orange fluorescence (Orange FL), forward angle light scatter (FALS), horizontally-polarized forward angle light scatter (HFALS). Calibration beads shown in each panel, except E.

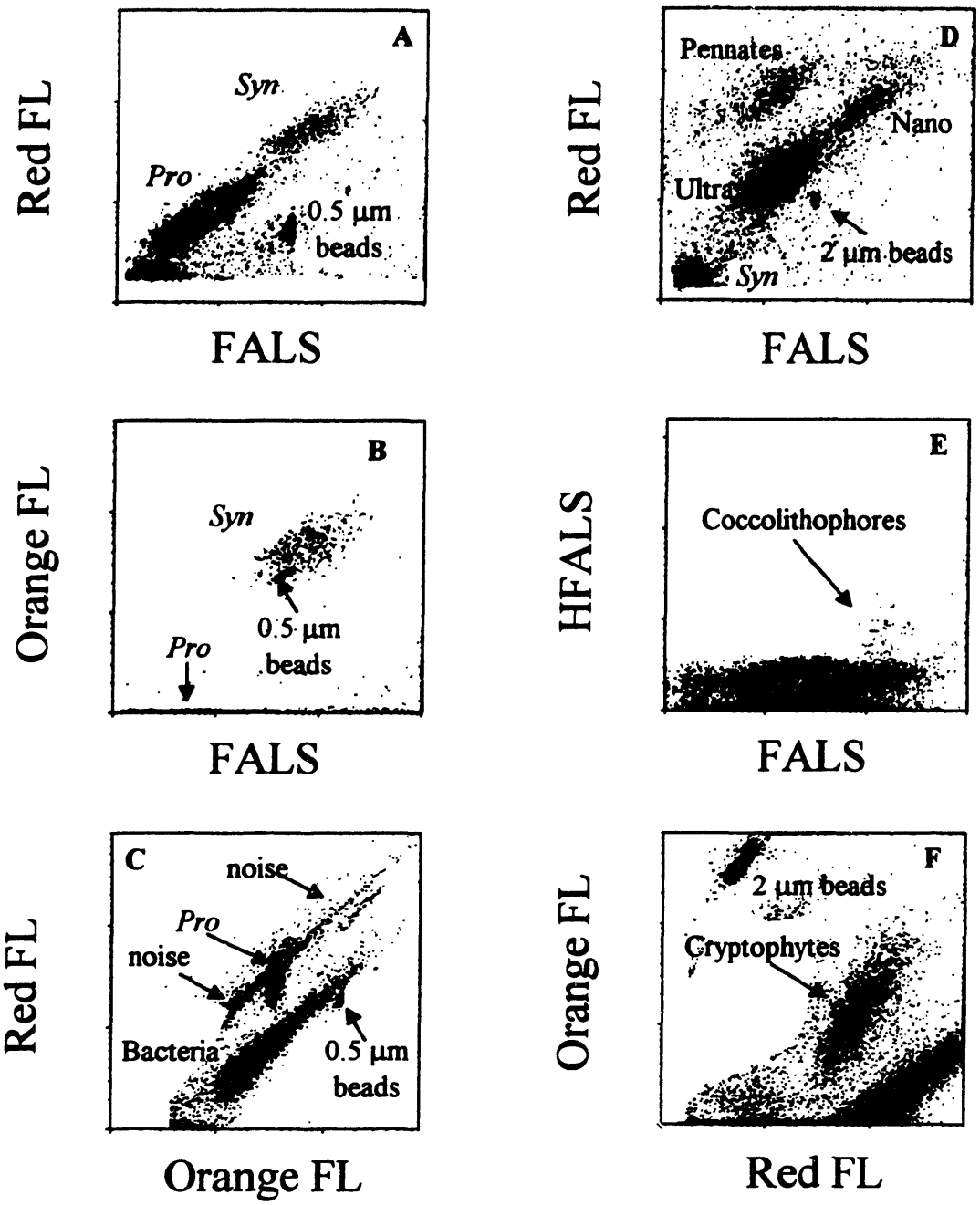
A
Syn
Pro
0.5 µm beads
Red FL
FALS
D
Pennates
Nano
Ultra
2 µm beads
Syn
Red FL
FALS
B
Syn
0.5 µm beads
Pro
Orange FL
FALS
E
Coccolithophores
HFALS
FALS
C
noise
Pro
noise
Bacteria
0.5 µm beads
Red FL
Orange FL
F
2 µm beads
Cryptophytes
Orange FL
Red FL

distinguish coccolithophores, because they depolarize the laser light, and cryptophytes because they display orange fluorescence from phycoerythrin (Olson *et al.* 1989). Bacteria (Fig. 2C) were enumerated following the method of Marie *et al.* (1997) using the nucleic acid stain SYBR Green-I (Molecular Probes). In most cases, there was clear separation between bacterial and *Prochlorococcus* flow cytometric signatures. When there was an overlap, abundances of bacteria were affected only slightly because only a small portion of the *Prochlorococcus* was included in the bacterial counts, and because *Prochlorococcus* abundances were an order of magnitude less than those for the bacteria. Note that we use the term bacteria operationally to represent all prokaryotes which lack pigment autofluorescence on our instrument.

*Nutrient analyses*—Because of the limitation standard colorometric methods, the bulk of measurements made in the upper 100 m at the Bermuda Atlantic Time-series Study (BATS) site have captured only the periods of deep mixing when there are high nutrients (Michaels *et al.* 1994; Michaels and Knap 1996). Garside (1982) brought the chemiluminescent method to oceanography and has reported depth profiles during oligotrophic periods in the Sargasso Sea (Garside 1985; Glover *et al.* 1988). N+N was analyzed following the method of Garside (1982). Briefly, nitrate and nitrite are reduced to nitric oxide, which reacts with ozone to form an excited nitrogen dioxide. A photon is released as nitrogen dioxide returns to the ground state, and the sum of these light pulses for a given sample is related to its N+N concentration.

Several issues arise concerning the measurement of SRP. Much like in the case of N+N, low concentrations of SRP in surface waters of the oligotrophic ocean have, in some cases, prevented SRP measurement by standard colorometric methods (detection limit 20-50 nM). It is clear from the BATS data set that SRP has been nearly undetectable in the upper 100 m over the past decade (Michaels *et al.* 1994; Michaels and Knap 1996). Several approaches have been taken to measure or estimate low SRP values. Ormaza-González and Statham (1991) used a 60-cm pathlength cuvette to measure the first complete depth profile of SRP for the Sargasso Sea at Station S (32° 09'N, 64° 34'W). This profile was made during February 1990 and had values ranging from their 1-nM detection limit up to about 10 nM in the upper 160 m. Ormaza-González and Statham (1991) found values of about 80 nM at 200 m, which agree with the

contour plots published for the BATS site (Michaels and Knap 1996), however, SRP was not actually reported near 200 m for February 1990 (BATS web site).

Another approach that has been taken to improve the sensitivity of SRP analysis is the magnesium-induced coprecipitation (MAGIC) procedure (Karl and Tien 1992). The advantage of this method is that SRP is concentrated without concentrating the elements which contribute to the blank. In other words, an improved signal to noise ratio is possible. There are no published data indicating that MAGIC has been successfully implemented in the Sargasso Sea, although others have recently produced results which are consistent with ours (J. Wu, personal communication).

We used the MAGIC procedure for analyses of SRP. The standard MAGIC protocol requires a 2.5% v/v addition of 1 N NaOH to initiate the precipitation of brucite ($MgO(OH)_2$), which is subsequently pelletized by centrifugation. SRP is co-precipitated and concentrated in this process and then re-solublized when the pellet is dissolved in weak acid (0.1 N HCl) prior to measurement by standard molybdate color reactions (see Appendix A; Parsons *et al.* 1984). The magnitude of the SRP concentration effect is governed by the ratio of initial sample volume to that of the volume of the pellet dissolved in HCl; typical values range from 5- to 10-fold when starting with a 50-ml sample. Due to the exceedingly low levels of SRP (< 10 nM) expected in the Sargasso Sea we anticipated the need for further concentration beyond that which is adequate for year-round samples from Station Aloha at the Hawaii Ocean Time-series (HOT) site (Karl and Tien 1997). In general, the SRP from a total sample volume of 250 ml was concentrated to approximately 5 ml. In addition, we applied the recently modified MAGIC procedure (Bulldis-Thomson and Karl 1998), which was designed to approximate more closely the dissolved inorganic phosphorus pool (P*i*) by using only 0.25% v/v of 1 M NaOH (rather than 2.5%) to initiate brucite precipitation. This latter procedure is referred to as "modified MAGIC" (Bulldis-Thomson and Karl 1998).

Sub-samples (40 ml) of the supernatant solution from the initial centrifugation step were removed for the analyses of total N and P by uv-oxidation ($N_{uv-ox}$, $P_{uv-ox}$). The interpretation of our $N_{uv-ox}$ and $P_{uv-ox}$ measurements is complicated because we used the MAGIC supernatant and

because we did not filter the seawater samples prior to nutrient analyses. As a first approximation, $N_{uv\text{-}ox}$ and $P_{uv\text{-}ox}$ should include both dissolved and particulate organic N (DON, PON) and P (DOP, POP) fractions. Also, dissolved inorganic nitrogen (DIN) should be present in the MAGIC supernatant and should, therefore, be included in $N_{uv\text{-}ox}$. As a way to constrain our interpretations, we performed modified MAGIC precipitations on three field samples, one from the equatorial Pacific and two from separate cruises in the Sargasso Sea, which had been preserved for flow cytometry following the method of Vaulot *et al.* (1989). Starting with 20-ml samples in each 50-ml centrifuge tube, only 6 ml were removed following centrifugation as an analog to an aliquot removed from a 50-ml sample for uv-oxidation. This disproportionately small volume was chosen to prevent contamination by any cells which would be on the surface of the brucite pellet and which might have been included had 80% of the supernatant been removed. We found that <10 % of the bacteria and < 2% of *Prochlorococcus*, *Synechococcus*, and the ultra- and nanophytoplankton were included in this supernatant (*see* Appendix A). Assuming that detrital particles and any large heterotrophic organisms would also be largely removed from the supernatant, this suggests that $N_{uv\text{-}ox}$ would consist primarily of DIN and DON, and $P_{uv\text{-}ox}$ would include only DOP. Following this assumption, we represent total dissolved N (TDN) by $N_{uv\text{-}ox}$ directly expecting that this excludes PON; total dissolved P (TDP) is equated to $P_{uv\text{-}ox}$ plus the estimation of P*i* (SRP) made by the modified MAGIC analysis and should exclude POP.

## RESULTS AND DISCUSSION

The principal field study for this work was designed to detail cha. ges in the size structure of marine microorganisms along a gradient in nutrients. This transect (Fig. 1) during March 1998 in the Atlantic Ocean, began in stratified waters of the southern Sargasso Sea (26°N, 70°W), passed through waters—extending from just south of the Bermuda Atlantic Time-series Study (BATS) site north across the Gulf Stream—which were deeply mixed and presumably high in nutrients and phytoplankton biomass, and ended in coastal waters off the coast of New York.

*Temperature and chlorophyll*—Surface temperature declined gradually from a high of 25°C at the southern extent of the transect until deeply mixed waters were reached just south of BATS, at which point water temperatures remained at about 19°C northward until the warm (23°C) waters of the Gulf Stream were transected (Fig. 3A). The northern edge of the Gulf stream was well defined by an abrupt drop in temperature from 20°C to about 10°C followed by 5°C temperatures further northward. Total chlorophyll *a* (Chl *a*) values ranged from 0.06 to 0.1 $\mu g\ l^{-1}$ in the southern portion of the transect and then increased to values ranging from 0.3 to 0.6 $\mu g\ l^{-1}$ just south of BATS (Fig. 3A). These values are consistent with those reported by Michaels *et al.* (1994) for the spring bloom at BATS. Chl *a* remained at these levels on the north-west transect across the Gulf Stream, beyond which values in excess of 1 $\mu g\ l^{-1}$ were seen in coastal waters. The last data point suggests a decrease from these high Chl *a* levels further to the north.

*Inorganic N*—N+N ranged from 2.5 to 7 nM in the southern region of the transect; values increased steadily at the face of the spring bloom, eventually reaching a mean value of 600 nM in the waters north of BATS (Fig. 3B). N+N dropped somewhat in the Gulf Stream to a mean of about 400 nM, with a steady increase at the northern edge of the Gulf Stream. This latter increase, which began at a water temperature of 23°C, persisted until leveling off at values ranging from 3 to 5 µM in the low-temperature coastal waters.

N+N values at the surface resembled those throughout the mixed layer at two points along the transect (26°N and BATS; Fig. 4A,B). In addition, these two profiles of N+N were similar to several other depth profiles taken at various locations and times in the Sargasso Sea. Specifically, the profile from 26°N compares well with other profiles taken during stratified periods at and near BATS (Fig. 4A), while that at BATS during March 1998 compares well with two profiles taken during another deeply mixed period (Fig. 4B). Thus, surface measurements of N+N were representative of the mixed layer for the transect as well as for similar mixing regimes during other cruises. Our values of N+N (Fig. 4A) are consistent with Garside's measurements of nitrate, which ranged from the detection limit (2 nM) to about 20 nM for the mixed layer during summer in the Sargasso Sea (Garside 1985; Glover *et al.* 1988).

Figure 3:

Transect across Sargasso Sea, Gulf Stream, and coastal waters during March 1998. Vertical shaded bars indicate the approximate location of the Bermuda Atlantic Time-series (BATS) site and the Gulf Stream. (A) Temperature and total chlorophyll (Chl *a*) as a function of latitude (*see* Fig. 1 for cruise track). (B) Concentration of nitrate + nitrite (N+N) and soluble reactive phosphorus (SRP) as a function of latitude. (C) Ratio of N+N to SRP as a function of latitude, with a dotted line at a ratio of 16:1. All samples nominally from 3 m.

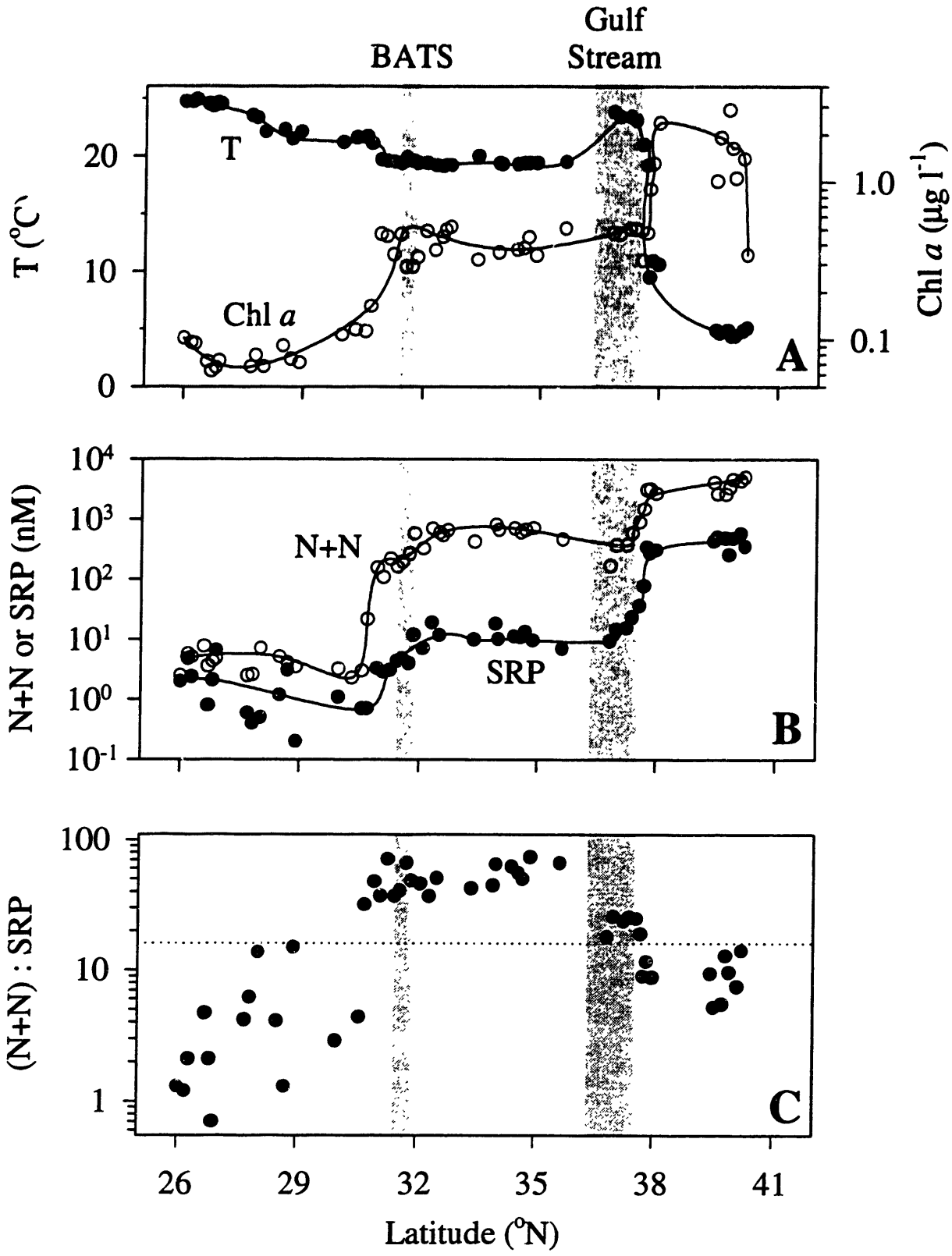
BATS
Gulf Stream
T
Chl a
A
T (°C)
Chl a (µg l-1)
20
10
0
1.0
0.1
B
N+N
SRP
N+N or SRP (nM)
10^4
10^3
10^2
10^1
10^0
10^-1
C
(N+N) : SRP
100
10
1
26
29
32
35
38
41
Latitude (°N)

Figure 4:

Representative depth profiles of nitrate + nitrite (N+N), soluble reactive phosphorus (SRP), and their ratio for the Sargasso Sea. (A,C,E) Oligotrophic profiles, with large filled circles for profile from 26°N station from the 1998 transect (B,D,F) Deeply mixed profiles, with large filled circles for profile from the Bermuda Atlantic Time-series Study (BATS) site from the 1998 transect. Symbols correspond to those in Fig. 1 and represent the different cruises. Note that the size of the symbols for the March 1998 transect are enlarged for clarity.

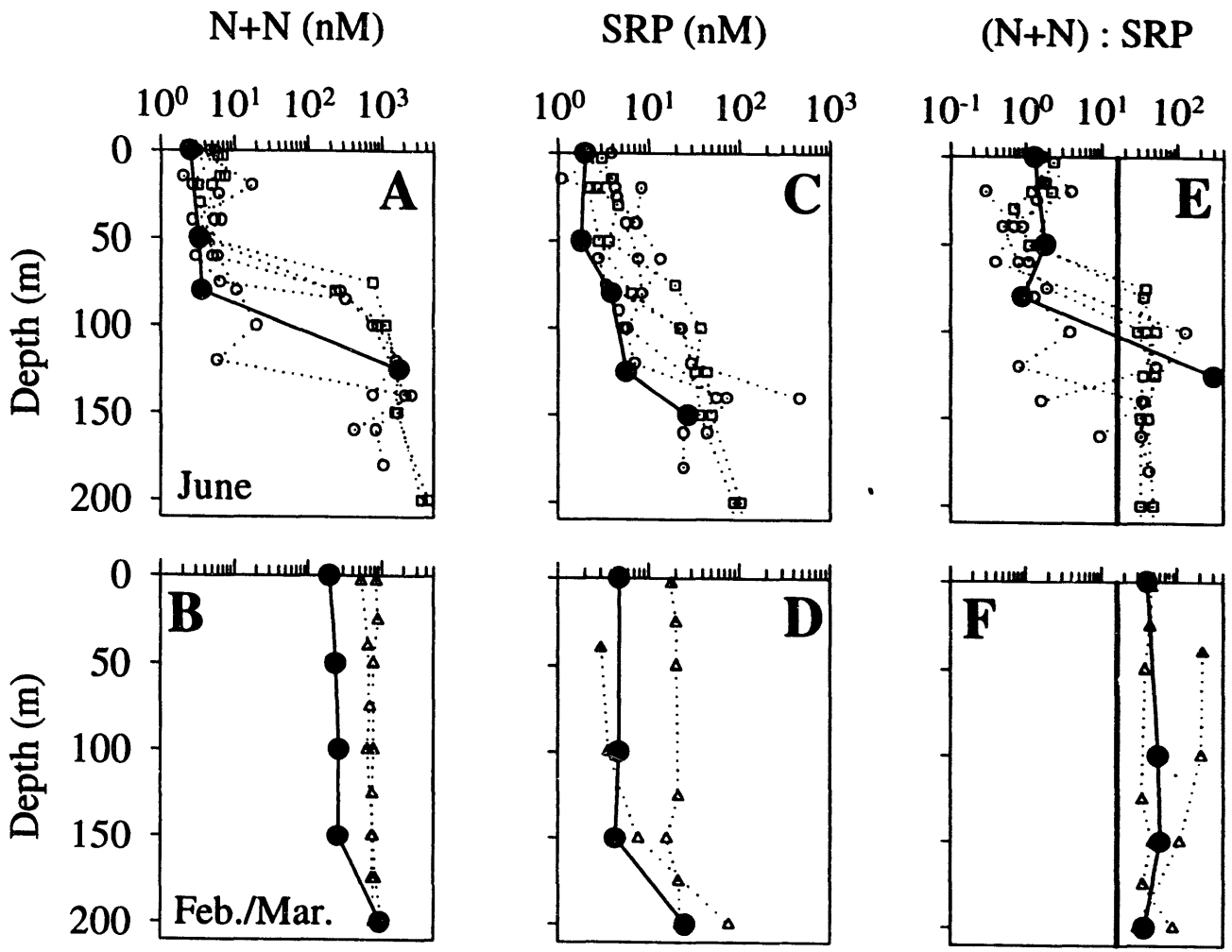
N+N (nM)
SRP (nM)
(N+N) : SRP
10⁰ 10¹ 10² 10³
10⁰ 10¹ 10² 10³
10⁻¹ 10⁰ 10¹ 10²
Depth (m)
0
50
100
150
200
A
B
C
D
E
F
June
Feb./Mar.

Figure 5:

Comparison of data from the Bermuda Atlantic Time-series (BATS) site with those from this study. Small filled circles for BATS data, open circles for data shown in Figs. 3B (southern portion of transect) and 4A,C; open squares for data shown in Figs. 3B (northern portion of Sargasso Sea) and 4B,D. (A) Depth profile of nitrate + nitrite (N+N). (B) Depth profile of soluble reactive phosphorus (SRP). Inset is temperature data plotted against depth. (C) Depth profile of the ratio of (N+N) to SRP, with a solid line added for a ratio of 16:1. In all cases, upper panels represent the full extent of available data, whereas lower panels represent the upper 200 m, consistent with Fig. 4. Data represent BATS cruises 17-100 (Feb. 1990 to Jan. 1997).

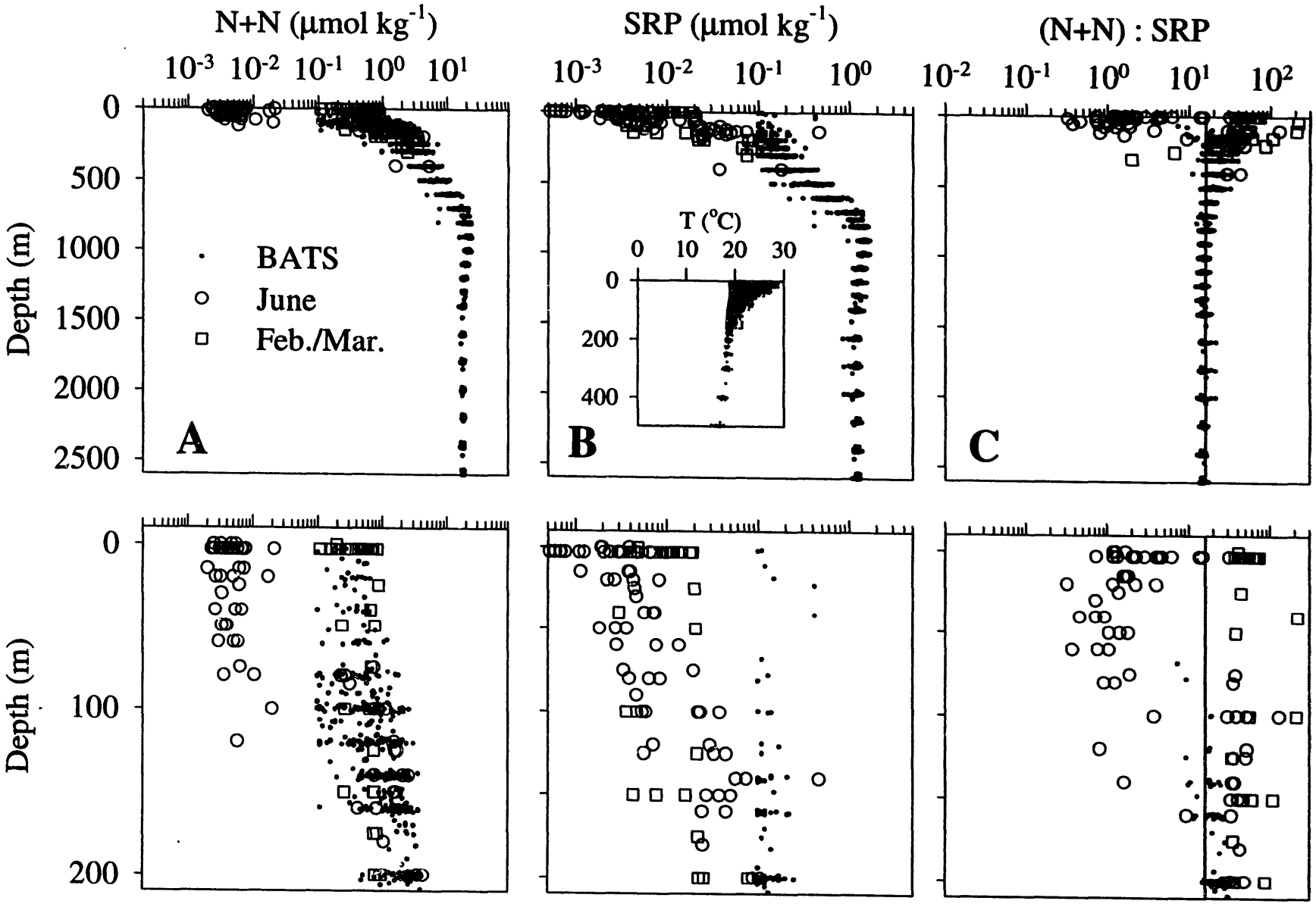
N+N (µmol kg-1)
SRP (µmol kg-1)
(N+N) : SRP
10-3 10-2 10-1 100 101
10-3 10-2 10-1 100
10-2 10-1 100 101 102
Depth (m)
0
500
1000
1500
2000
2500
BATS
June
Feb./Mar.
A
B
C
T (°C)
0 10 20 30
0
200
400
Depth (m)
0
100
200

Figure 6:

Summary of nutrient data from the Hawaiian Ocean Time-series (HOT) site in the Pacific Ocean, for comparison to Fig. 5. (A) Depth profile of nitrate + nitrite (N+N). (B) Depth profile of soluble reactive phosphorous (SRP). Inset is temperature plotted against depth. (C) Depth profile of the ratio of (N+N) to SRP. Data from HOT cruises 1-88 (Oct. 1988 to Dec. 1997).

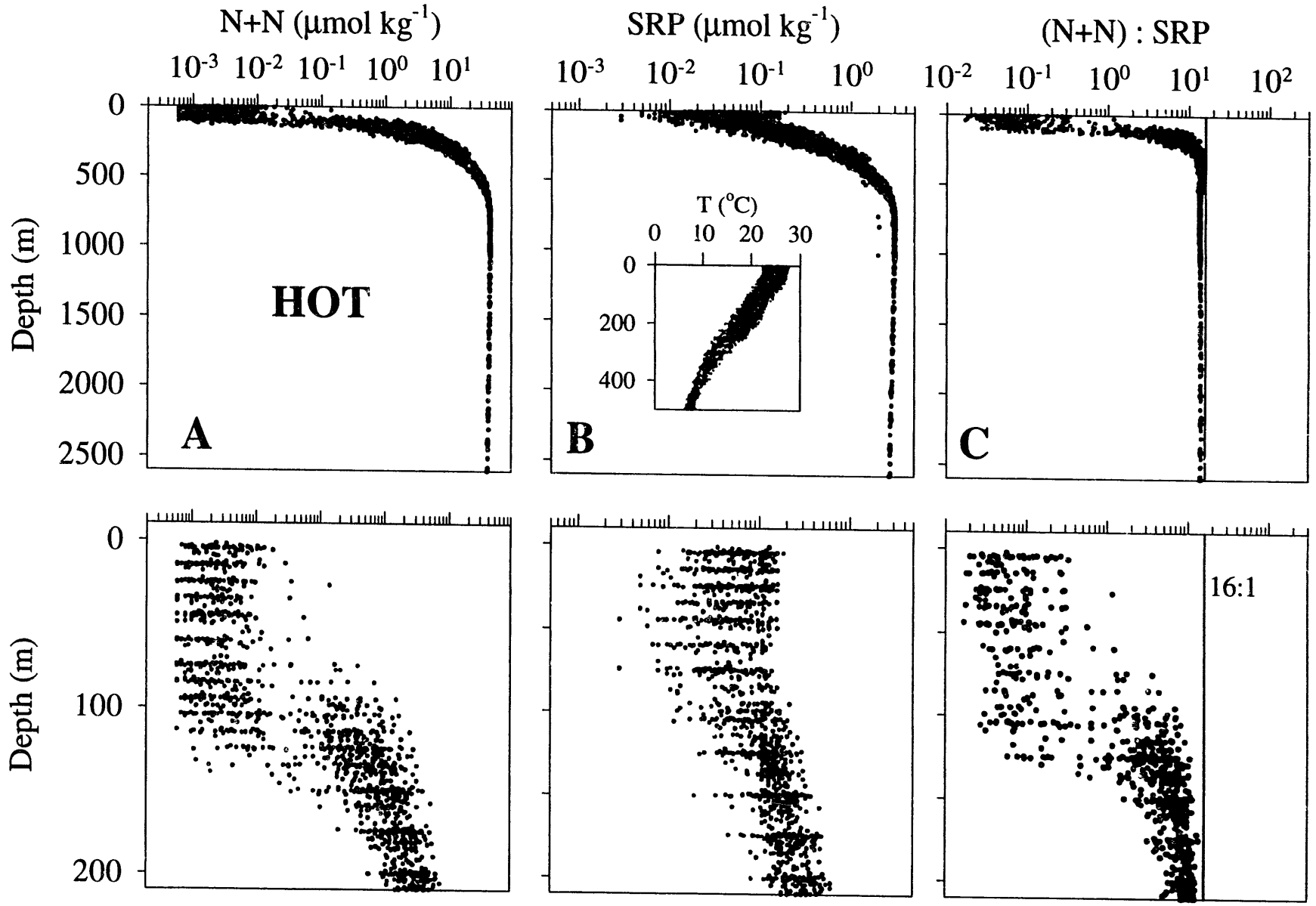
N+N (µmol kg-1)
10-3 10-2 10-1 100 101
SRP (µmol kg-1)
10-3 10-2 10-1 100
(N+N) : SRP
10-2 10-1 100 101 102
Depth (m)
0
500
1000
1500
2000
2500
HOT
A
T (°C)
0 10 20 30
0
200
400
B
C
Depth (m)
0
100
200
16:1

In an attempt to complete the image of how N+N is distributed at the BATS site year-round, we have merged our data from this study with those produced through the ongoing monitoring program at BATS (data available at: http://www.bbsr.edu/bats/; Fig. 5A). We contrast these data with those from the Hawaiian Ocean Time-series site (HOT) in the Pacific Ocean (data available at: http://hahana.soest.hawaii.edu/hot/hot_jgofs.html), where low levels of N and P are measured routinely (Fig. 6A). While waters at BATS undergo seasonal stratification, those at HOT are stratified year-round (insets, Fig. 5B and 6B). At BATS, there are seasonal differences in the distribution of N+N in the upper 200 m, which lead to a wide range of N+N values: the lowest during stratified periods, the highest during periods of deep mixing. Such a pattern is absent at the HOT site, where N+N varies much less in the continually stratified waters.

*Inorganic P*—Changes in SRP paralleled those of N+N, however, SRP increased at the face of the spring bloom by only a factor of 10 instead of the 100-fold increase for N+N (Fig. 3B). Values in the southern portion of the transect ranged from 0.5 to nearly 5 nM, with one point below our 0.5-nM detection limit. These values are in general agreement with SRP measurements made by Ormaza-González and Statham (1991) and the estimates, based on a bioassay technique, made by Cotner *et al.* (1997). In the northern portion of the Sargasso Sea delineated by the face of the spring bloom, the mean SRP value was 12-nM and ranged from 7 to 18-nM. SRP values ranged from 9 to 23 nM in the Gulf Stream, before steadily rising to a mean of 400 nM in coastal waters. As in the case of N+N, these surface measurements of SRP were representative of both the mixed layer during the transect, as well as similar mixing regimes during other cruises (Fig. 4C,D).

SRP is typically drawn down to considerably lower levels at BATS as compared to the HOT site (Figs. 5B and 6B), although on occasion SRP has been below the limit of detection (< 1 nM) at the HOT site (Karl and Tien 1997). Fanning (1989) explained low levels of SRP in the Sargasso Sea, in relation to other regions of the world ocean, as a product of enhanced deposition of nitrogen in this region due to industrial activity in North America. He rationalized that this enhanced deposition would drive plankton to reduce already low levels of SRP to the vanishingly

low, or undetectable levels observed. It is also possible that diazotrophs draw down SRP relative to N+N because their N-requirement is met with dinitrogen.

*Ratio of N to P*—A clear transition in the ratio of N+N to SRP occurred at the face of the spring bloom (Fig. 3C). The ratio in the southern portion of the transect was less than 16:1, the Redfield ratio (Redfield 1934), but increased within the spring bloom waters ranging from 30:1 to 70:1. These elevated ratios persisted (mean 52:1) northward to the Gulf Stream, at which point the ratio dropped somewhat to a mean of 24:1; ratios fell below 16:1 in coastal waters. Similar N+N and SRP values for the mixed layer during the transect led to rather constant ratios of N+N to SRP (Fig. 4C,F). More generally, ratios remained less than 16:1 in the mixed layers of oligotrophic waters (Fig. 4C), and exceeded 16:1 in deeply mixed water columns (Fig. 4F).

As was discussed in general for the central Atlantic by Fanning (1989; 1992) and shown in detail at the BATS site by Michaels *et al.* (1994), the ratio of N+N to SRP is typically in excess of 16:1 in the upper thermocline. Michaels *et al.* (1994) found values up to 40:1 at BATS over the range of 200-600 m (Fig. 5C). Because it is a ratio, either low SRP or elevated N+N, or both, would lead to increased ratios of N+N to SRP. Michaels *et al.* (1996) argued that the elevated ratios result ultimately from nitrogen fixation. It has been observed that *Trichodesmium*, a globally significant daizatroph (Capone *et al.* 1997), maintains elevated proportions of N relative to P (Karl *et al.* 1992), compared to the Redfield ratio. Michaels *et al.* (1996) postulated that these N-rich cells sink and undergo remineralization, causing N+N to be elevated relative to SRP.

It is of little surprise that ratios of N+N to SRP during the deeply mixed periods (Fig. 4F) are consistent with the elevated ratios reported by Michaels *et al.* (1994) for deep (200- 600 m) at BATS, because surface waters should resemble deeper waters from which they originated. We believe, however, that surface waters should be deplete in N+N relative to SRP (i.e., N:P < 16:1) in order warrant the high energy expense required for diazotrophs to fix nitrogen. We have found low ratios of N+N to SRP for oligotrophic periods in the Sargasso Sea (Fig. 4C). An image which supports the hypothesis of Michaels *et al.* (1996) is clearly apparent when samples originating from stratified periods (open circles) are compared in the lower panels of Fig. 5: N+N

Figure 7:

Soluble and total nitrogen and phosphorus, and their ratio. Vertical shaded bars indicate the approximate location of the Bermuda Atlantic Time-series Study (BATS) site and the Gulf Stream. (A) Concentrations of total nitrogen (TN) and phosphorus (TP), and dissolved organic nitrogen (DON) and phosphorus (DOP) during March 1998 surface transect. (B) Their ratios as a function of latitude, with a dotted lines added at a N:P ratio of 16:1.

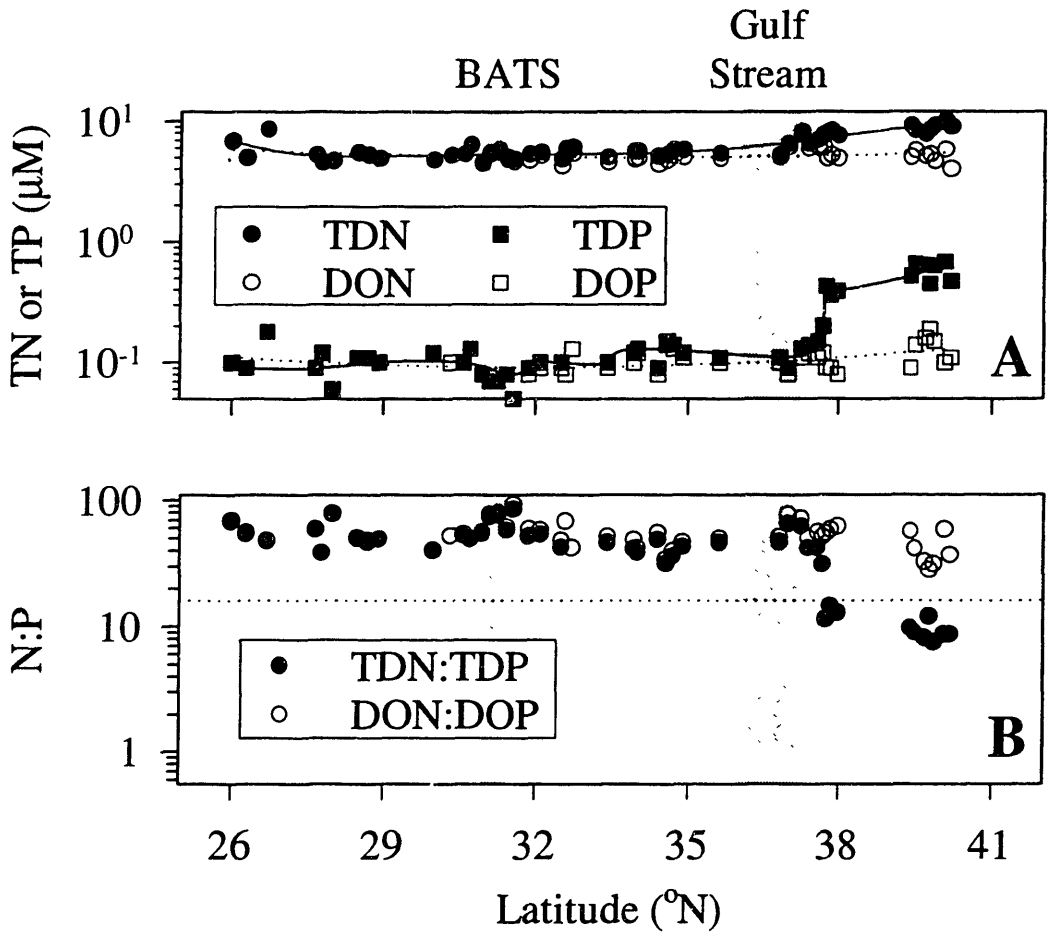
BATS
Gulf Stream
TN or TP (μM)
$10^1$
$10^0$
$10^{-1}$
TDN
TDP
DON
DOP
A
N:P
100
10
1
TDN:TDP
DON:DOP
B
26
29
32
35
38
41
Latitude (°N)

and SRP are both low, yet of comparable concentrations, leading to sub-Redfield N:P ratios in the upper 200 m.

*Total and dissolved organic N & P*—There was no prominent trend along the transect for total dissolved nitrogen (TDN), which had a mean of 6.3 μM (range 4.6 to 10.2 μM) at a depth of 3 m (Fig. 3C). Total dissolved phosphorus (TDP) had two noticeable features, a slight depression from a mean of 0.1 μM at the face of the spring bloom, and elevated values in coastal waters with a maximum of 0.7 μM (Fig. 3C). Dissolved organic nitrogen (DON) and phosphorus (DOP) showed similar patterns to TDN and TDP, respectively (Fig. 3C). There is virtually no difference in the trends between dissolved and total fractions along the transect in the Sargasso Sea and the Gulf Stream. We do see, however, a clear decrease in the dissolved organic N and P pools relative to the pools of total dissolved N and P in coastal waters.

*Community structure along the transect*—Patterns of the abundance of microorganisms in surface samples along the transect (Fig. 8) aligned with prominent features in N+N and SRP (Fig. 3). Concentrations of bacteria, the smallest plankton studied, increased gradually along the entire transect in the Sargasso Sea and Gulf Stream (range 2.6 to 5.6 x $10^5$ cells $ml^{-1}$). An apparent 25% drop in concentration occurred near the face of the spring bloom. There was an abrupt peak in bacterial numbers (9 x $10^5$ cells $ml^{-1}$) just beyond the north edge of the Gulf Stream; concentrations receded further north.

The smallest phytoplankter, *Prochlorococcus*, reached maximal abundance (7 x $10^4$ cells $ml^{-1}$) at the southern extent of the transect and declined somewhat before declining substantially in spring bloom waters. *Prochlorococcus* concentrations remained low (mean of 9 x $10^3$ cells $ml^{-1}$) north of BATS, but increased markedly in the Gulf Stream to levels close to those at 26°N, and then disappeared in coastal waters. The concentration of the other picophytoplankter, *Synechococcus*, increased steadily from 26°N to the face of the spring bloom (maximum of 2.9 x $10^4$ cells $ml^{-1}$ ). Beyond BATS, concentrations dropped off only to rise again in the Gulf Stream

to match the highest concentrations seen at BATS. In the coastal waters, concentrations were low, but still detectable.

The larger phytoplankton have been characterized by three groups (*see* Fig. 2): the ultra- and nanoplankton, cryptophytes, and coccolithophores. The former group excludes concentrations of the latter two. Ultra- and nanoplankton numbers were low (mean of $1.4 \times 10^3$ cells $ml^{-1}$) south of the spring bloom waters and then increased nearly 10-fold to a mean of $1.1 \times 10^4$ cells $ml^{-1}$ in the northern portion of the Sargasso Sea (maximum of $1.7 \times 10^4$ cells $ml^{-1}$). Concentrations receded in the Gulf stream, and then increased again to maximal levels in coastal waters. Cryptophytes were not detected in the southern extent of the transect, but were found at concentrations ranging from 100 to 270 cells $ml^{-1}$ from the bloom waters northward across the Gulf Stream. There was a sharp peak in concentration (370 cells $ml^{-1}$) just past the north edge of the Gulf Stream, coincident with the sharp peak in bacterial cell numbers. Coccolithophores had the same general pattern as the cryptophytes, however they were detectable in the southern region of the transect (mean of 4 cells $ml^{-1}$), and then increased in concentration slightly sooner than the cryptophytes appeared. Following this burst in cell number, coccolithophores maintained low numbers north across the Gulf Stream (mean 2.6 cells $ml^{-1}$). There was a doubling of cell numbers coincident with the peaks for bacteria and cryptophytes in coastal waters.

We cannot characterize all phytoplankton by flow cytometry, yet it is possible to estimate the percentage of biomass associated with the groups measured based on size-fractionated chlorophyll. Most of the cells analyzed on our instrument would have been less than about 10 μm in diameter (*see* Chapter 3). The percentage of total Chl *a* which was in the fraction >10 μm remained fairly constant at about 10-25% in all but the coastal waters, in which the contribution from cells larger than 10 μm increased to be >50% of the total Chl *a* (Fig. 9A). Thus, for the Sargasso Sea and the Gulf Stream, cells from our analysis by flow cytometry probably contributed >75% to the total phytoplankton biomass. Furthermore, the drop in *Prochlorococcus* and the increase in ultra- and nanoplankton abundances in spring bloom waters (Fig. 8) resulted in a redistribution of Chl *a* within the <10 μm fraction. Specifically, Chl *a* in the 1-10 μm

Figure 8:

Plankton abundances along March 1998 surface transect (Fig. 3). Vertical shaded bars indicate the approximate location of Bermuda Atlantic Time-series (BATS) site and the Gulf Stream.

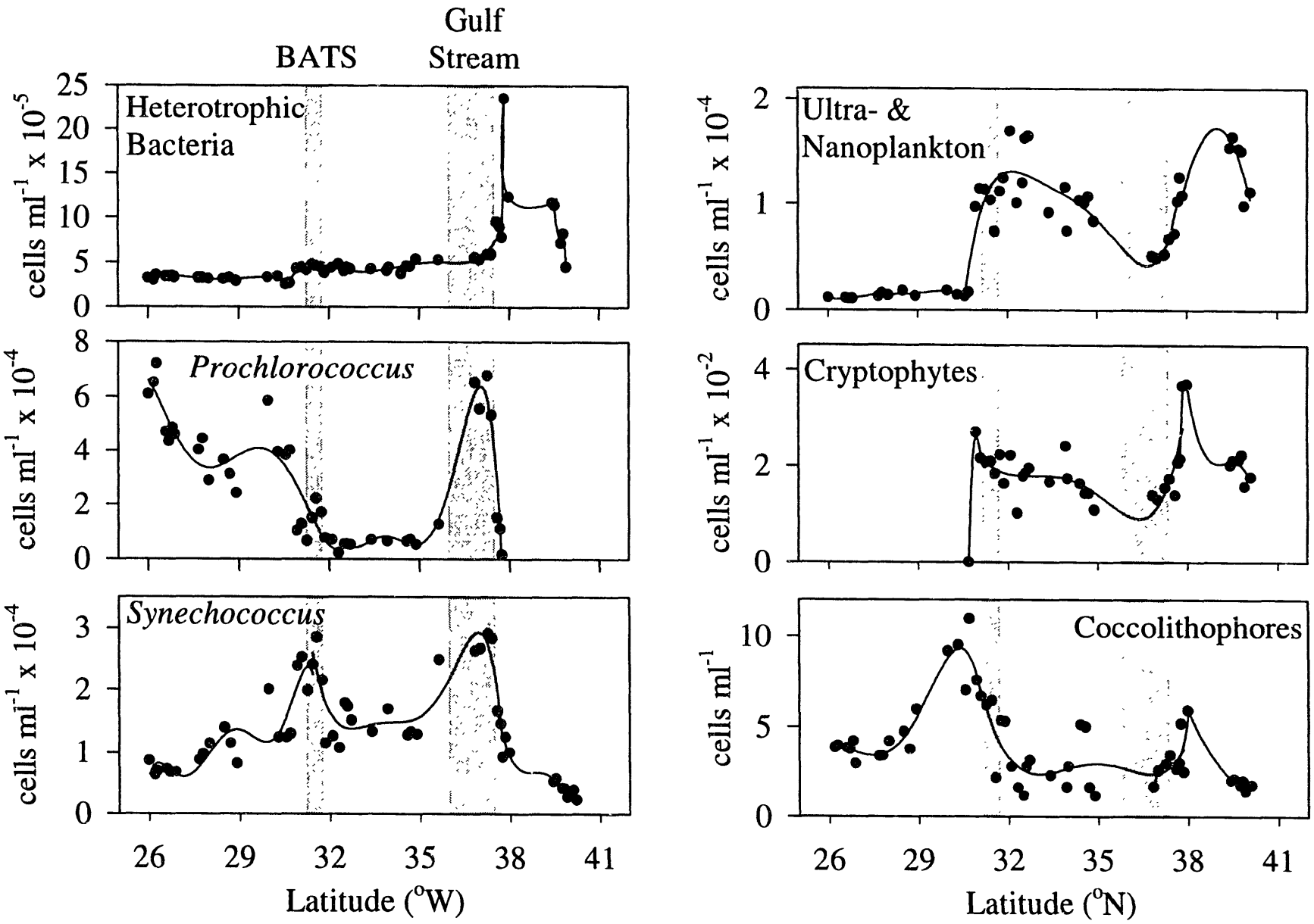
BATS
Gulf Stream
Heterotrophic Bacteria
cells ml-1 x 10-5
Prochlorococcus
cells ml-1 x 10-4
Synechococcus
cells ml-1 x 10-4
Ultra- & Nanoplankton
cells ml-1 x 10-4
Cryptophytes
cells ml-1 x 10-2
Coccolithophores
cells ml-1
26 29 32 35 38 41
Latitude (°W)
Latitude (°N)

fraction increased from about 50% to 70% of the total in spring bloom waters (Fig. 9B), while that in the <1 μm fraction dropped from about 30% to 20% of the total (Fig. 9C).

Overall, changes in the abundance of bacterio- and phytoplankton corresponded with fluctuations in nutrients along the transect suggesting that nutrients played an important role in controlling these populations, or vice versa. The bacteria have two interesting features: a decline at the face of the spring bloom, and an overall maximum at the northern edge of the Gulf Stream. Correlating their abundance with both nutrient concentrations (Fig. 10A) suggests a somewhat more important role for SRP than N+N in controlling bacterial numbers. This is especially apparent because N+N values fall into two groups (high and low) whereas SRP has intermediate values. This apparent dependence on SRP is consistent with the findings of Cotner *et al.* (1997) which showed that bacterioplankton at BATS experience P-limitation.

Like the bacteria, *Prochlorococcus* ranged over nearly an order of magnitude in cell number (Fig. 8). Unlike the bacteria, however, the abundance of *Prochlorococcus* can be divided into four regimes: high in the southern waters, low from the bloom northward in the Sargasso Sea, high in the Gulf Stream, and absent in coastal waters. Olson *et al.* (1990) found that depth of the median concentration of *Prochlorococcus* occurred at depths close to the nitricline in the Sargasso Sea, and they suggested that nitrate, or another nutrient which co-varied with it, controlled the growth of *Prochlorococcus*. In a recent analysis of BATS data, DuRand *et al.* (submitted) also found a significant correlation between *Prochlorococcus* median cell concentration and depth of the nitricline. The data along the transect run counter to this finding, because the abundance of *Prochlorococcus* is negatively correlated with N+N (Fig. 10B). DuRand *et al.* (submitted) found that *Prochlorococcus* bloomed atypically at BATS during the spring of 1990, a year with less entrainment of nutrients into surface waters via deep mixing. This also does not support a strong need for N+N, as we see that stratified waters quickly become depleted of N+N. This conflict can be resolved because low levels of light would be associated with the nitricline, and, as was pointed out by DuRand *et al.* (submitted), the apparent relationship between *Prochlorococcus* abundance and the depth of the nitricline may well be a manifestation of the ability of *Prochlorococcus* to prosper at low light levels (Moore *et al.* 1995; Moore *et al.* 1998; Moore and Chisholm 1999).

There are several "outliers" in the relationship between *Prochlorococcus* abundance and N+N (Fig. 10B). It turns out that these are the high values seen in Fig. 8 for the Gulf Stream. These points provide an indication that temperature may actually be the main controlling factor of *Prochlorococcus*. The strong positive correlation between *Prochlorococcus* abundance and temperature (Fig. 11A) is interesting for two reasons. It makes sense physiologically, where a negative correlation with N+N does not. Also, when the abundance data for *Prochlorococcus* are plotted against temperature, rather than N+N, the Gulf Stream points fall in-line with the overall relationship. *Prochlorococcus* was alone in its strong dependence on warm water temperatures (Fig. 11B).

The distribution of *Synechococcus* along the transect cannot be readily explained by either nutrients or temperature, as *Synechococcus* abundance lacks a correlation with N+N or SRP (Fig. 10C) or temperature (Fig. 11B). Maxima in cell number occurred at and around BATS and in the Gulf Stream—similar in nutrient concentrations but disparate in terms of temperature. The high cell numbers at the face of the spring bloom are consistent with the observation of DuRand *et al* (submitted) that *Synechococcus* blooms during spring (March-May, depending on year) at BATS.

The abundance of the ultra- and nanophytoplankton (Fig. 8), in general, was a good surrogate for changes in nutrients along the transect (Fig. 3B); there was a strong positive correlation between their concentration and N+N and a weaker one with SRP (Fig. 10D). Abundances were somewhat higher than those measured by DuRand *et al.* (submitted), which ranged from 4 to 6 x $10^3$ cells $ml^{-1}$ at peak periods during February and March (1992 and 1993, respectively). It is possible that differences resulted because we analyzed fresh samples, whereas they analyzed preserved samples; cell losses can occur as a result of preservation (Vaulot *et al.* 1989; Lepesteur *et al.* 1993; Gin 1996).

The appearance of cryptophytes at the face of the spring bloom and further peak in cell numbers just north of the Gulf Stream is a strong indicator that their populations are also controlled by nutrients. However, correlations (not shown) with nutrients were limited because

Figure 9:

Size-fractionated chlorophyll *a* (Chl *a*) along March 1998 transect (Fig. 3). Vertical shaded bars indicate the approximate location of Bermuda Atlantic Time-series (BATS) site and the Gulf Stream. Percent of total Chl *a* in (A) >10 μm fraction, (B) 1 to 10 μm fraction, and (C) <1 μm fraction.

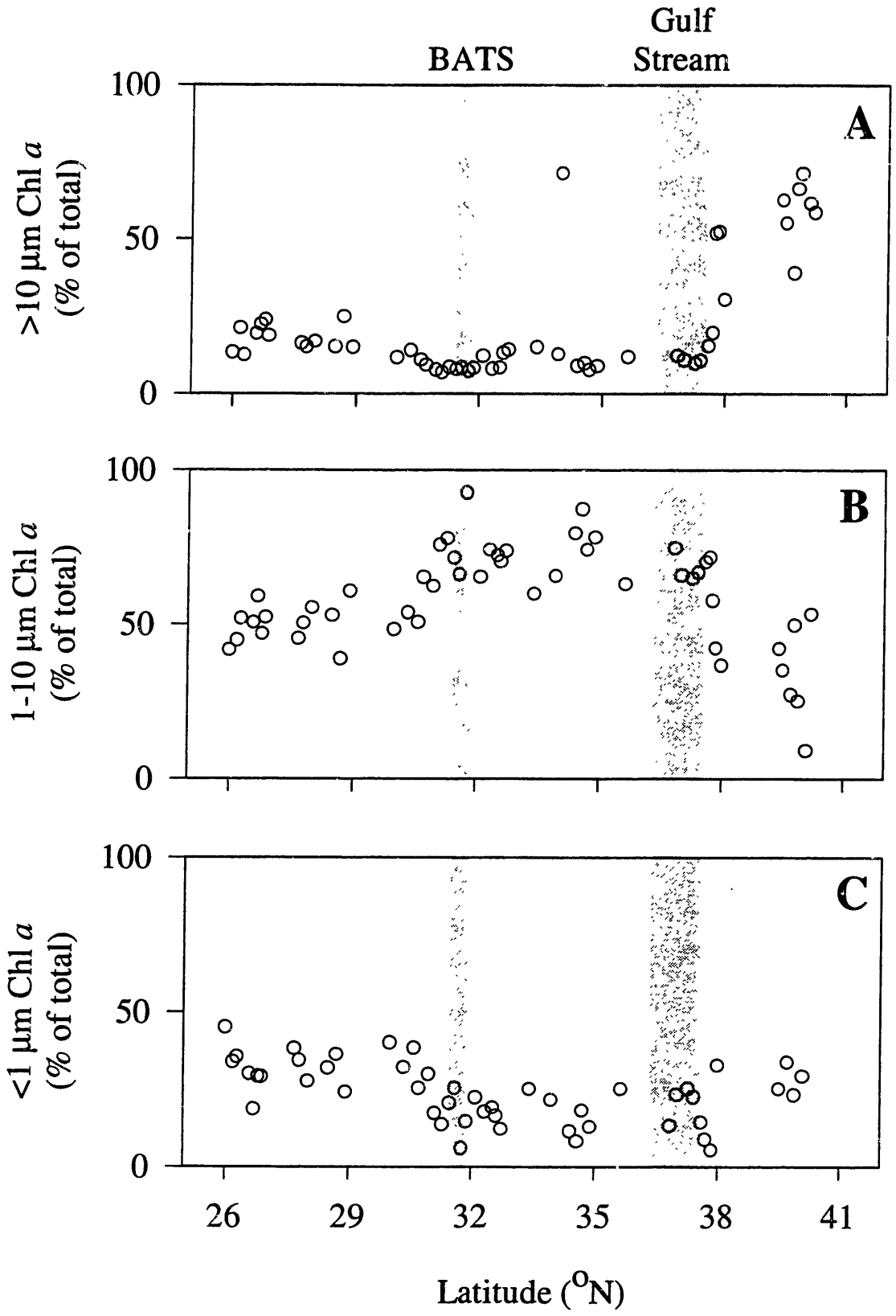
BATS
Gulf Stream
A
B
C
>10 µm Chl a (% of total)
1-10 µm Chl a (% of total)
<1 µm Chl a (% of total)
100
50
0
26
29
32
35
38
41
Latitude (°N)

Figure 10:

Correlations between plankton groups and nutrients along March 1998 surface transect (Fig. 3). Left panels for nitrate + nitrite (N+N) and right panels for soluble reactive phosphorus (SRP). In some cases correlation coefficients ($R^2$) are indicated. In B, open circles are used to denote samples from the Gulf Stream.

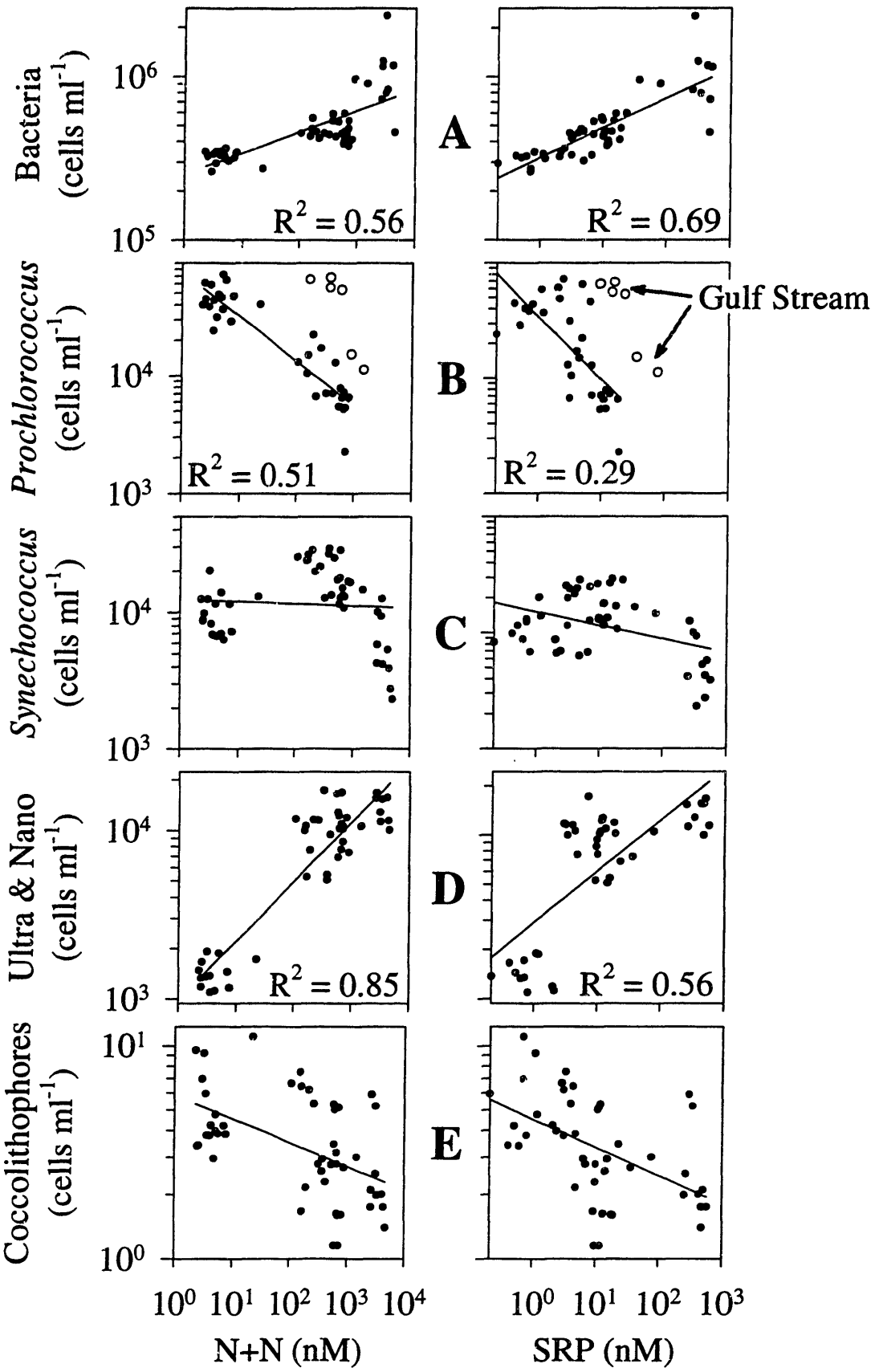
Bacteria (cells ml-1)
Prochlorococcus (cells ml-1)
Synechococcus (cells ml-1)
Ultra & Nano (cells ml-1)
Coccolithophores (cells ml-1)
A
B
C
D
E
R2 = 0.56
R2 = 0.69
R2 = 0.51
R2 = 0.29
R2 = 0.85
R2 = 0.56
Gulf Stream
10^6
10^5
10^4
10^3
10^1
10^0
10^0 10^1 10^2 10^3 10^4
N+N (nM)
10^0 10^1 10^2 10^3
SRP (nM)

Figure 11:

Relationships between plankton abundance and temperature along transect. (A) for *Prochlorococcus* with open circles representing Gulf Stream samples; and (B) for all other groups.

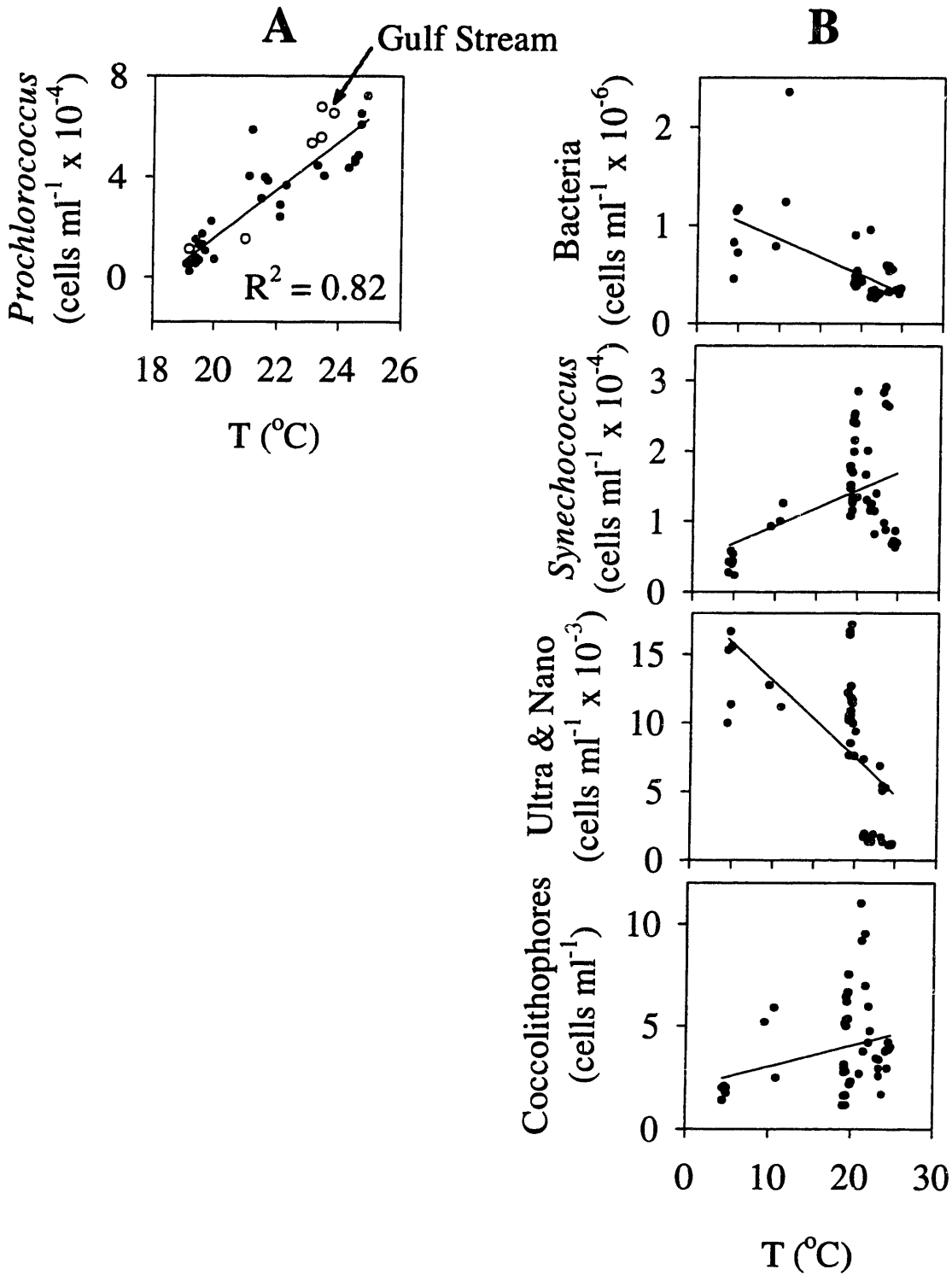
A
Gulf Stream
Prochlorococcus (cells ml-1 x 10-4)
8
4
0
R2 = 0.82
18 20 22 24 26
T (°C)
B
Bacteria (cells ml-1 x 10-6)
2
1
0
Synechococcus (cells ml-1 x 10-4)
3
2
1
0
Ultra & Nano (cells ml-1 x 10-3)
15
10
5
0
Coccolithophores (cells ml-1)
10
5
0
0 10 20 30
T (°C)

cryptophyte cells were not detected at low nutrient concentrations in the southern portion of the transect. This apparent absence could be explainable if the cryptophytes in the southern portion of the transect lacked phycoerythrin, which has been observed in N-limiting conditions (R. Olson, personal communication); if they lacked phycoerythrin we would not have been able to detect their presence. Even though coccolithophores had peaks in cell numbers at the edge of the spring bloom and at the north edge of the Gulf Stream, overall their numbers decreased along the transect from south to north. Their concentration, therefore, had a weak negative correlation with nutrients (Fig. 10E). The cell concentrations measured are close to those measured by DuRand *et al.* (submitted) at the BATS site, although we did not observe concentrations as high as the maximum they measured (50 cells $ml^{-1}$).

## CONCLUSIONS

This transect in the western Atlantic Ocean provides an unique glimpse into the relationships between microorganism abundance and macronutrient concentration. The transect spanned diverse ecosystems encompassing the oligotrophic waters of the Sargasso Sea, the spring bloom waters near the BATS site, high nutrient conditions in the Gulf Stream, and high nutrient coastal waters. This may be the first data set to combine low-level measurements of N+N and SRP in the Sargasso Sea, both during high and low nutrient conditions. Our nutrient measurements are consistent with the hypothesis of Michaels *et al.* (1996) that the mid-depths (200-600 m) at BATS are enriched in N+N relative to SRP. The ratios of N+N to SRP in stratified waters were less than the Redfield ratio, suggesting that new production was N-limited.

Plankton abundances varied along the transect, but not following the same pattern for the six individual groups. We found that the abundance of bacteria was well correlated with levels of SRP. The most compelling factor controlling the abundance of *Prochlorococcus* appeared to be temperature; no factor that we measured explained the distribution of *Synechococcus*. Abundances of the larger, ultra- and nanophytoplankton were well correlated with N+N concentrations, although no relationships were seen for the other two eukaryotic groups.

## REFERENCES


Bulldis-Thomson, A. and D. Karl 1998. Application of a novel method for phosphorus determination in the oligotrophic North Pacific Ocean. Limnology and Oceanography 43: 156-1577.

Capone, D. G., J. P. Zehr, H. W. Paerl, B. Bergman and E. J. Carpenter 1997. Trichodesmium, a globally significant marine cyanobacterium. Science 276: 1221-1229.

Cavender-Bares, K. K., S. L. Frankel and S. W. Chisholm 1998. A dual sheath flow cytometer for shipboard analyses of phytoplankton communities from the oligotrophic oceans. Limnology and Oceanography 43: 1383-1388.

Cavender-Bares, K. K., E. L. Mann, S. W. Chisholm, M. E. Ondrusek and R. R. Bididgare 1999. Differential response of equatorial Pacific phytoplankton to iron fertilization. Limnology and Oceanography 44: 237-246.

Cotner, J. B., J. W. Ammerman, E. R. Peele and E. Bentzen 1997. Phosphorus-limited bacterioplankton growth in the Sargasso Sea. Aquatic Microbial Ecology 13: 141-149.

Dore, J. E., T. Houlihan, D. V. Hebel, G. Tien, L. Tupas and D. M. Karl 1996. Freezing as a method of sample preservation for the analysis of dissolved inorganic nutrients in seawater. Marine Chemistry 53: 173-185.

Dugdale, R. C. and J. J. Goering 1967. Uptake of new and regenerated nitrogen in primary productivity. Limnology and Oceanography 12: 196-206.

DuRand, M. D., R. J. Olson and S. W. Chisholm submitted. Phytoplankton population dynamics at the Bermuda Atlantic Time-series Station in the Sargasso Sea. Deep Sea Research.

Fanning, K. A. 1989. Influence of atmospheric pollution on nutrient limitation in the ocean. Nature 339: 460-463.

Fanning, K. A. 1992. Nutrient provinces in the sea: concentration ratios, reaction rate ratios, and ideal conversions. Journal of Geophysical Research 97: 5693-5712.

Garside, C. 1982. A chemiluminescent technique for the determination of nanomolar concentrations of nitrate and nitrate in seawater. Marine Chemistry 11: 159-167.

Garside, C. 1985. The vertical distribution of nitrate in open ocean surface water. Deep-Sea Research 32: 723-732.

Gin, K. Microbial size spectra from diverse marine ecosystems. Ph.D. Thesis, M.I.T./W.H.O.I. Joint Program, 1996. pp. 359.

Glover, H. E., B. B. Prézelin, L. Campell, M. Wyman and C. Garside 1988. A nitrate-dependent Synechococcus bloom in surface Sargasso Sea water. Nature 331: 161-163.

Gruber, N. and J. L. Sarmiento 1997. Global patterns of marine nitrogen fixation and denitrification. Global Biogeochemical Cycles 11: 235-266.

Karl, D. M., R. Letelier, D. V. Hebel, D. F. Bird and C. D. Winn (1992). Trichodesmium blooms and new nitrogen in the north Pacific gyre. Marine Pelagic Cyanobacteria: Trichodesmium and other Diazatrophs. E. J. Carpenter and e. al., Eds. Netherlands, Kluwer Academic Publishers: 219-237.

Karl, D. M. and G. Tien 1992. MAGIC: A sensitive and precise method for measuring dissolved phosphorous in aquatic environments. Limnology and Oceanography 37: 105-116.

Karl, D. M. and G. Tien 1997. Temporal variability in dissolved phosphorus concentrations in the subtropical North Pacific Ocean. Marine Chemistry 56: 77.

Lepesteur, M., J. M. Martin and A. Fleury 1993. A comparative study of different preservation methods for phytoplankton cell analysis by flow cytometry. Marine Ecology Progress Series 93: 55-63.

Marie, D., F. Partensky, S. Jacquet and D. Vaulot 1997. Enumeration and cell cycle analysis of natural populations of marine picoplankton by flow cytometry using the nucleic acid stain SYBR Green I. Applied and Environmental Microbiology 63: 186-193.

Michaels, A. F. and A. H. Knap 1996. Overview of the U.S. JGOFS Bermuda Atlantic Time-series Study and the Hydrostation S program. Deep-Sea Research 42: 157-198.

Michaels, A. F., et al. 1994. Seasonal patterns of ocean biogeochemistry at the U.S. JGOFS Bermuda Atlantic Time-series Study site. Deep-Sea Research 41: 1013-1038.

Michaels, A. F., D. Olson, J. L. Sarmiento, J. W. Ammerman, K. Fanning, R. Jahnke, A. H. Knap, F. Lipschultz and J. M. Prospero 1996. Inputs, losses and transformations of nitrogen and phosphorus in the pelagic North Atlantic Ocean. Biogeochemistry 35: 181-226.

Moore, L. R. and S. W. Chisholm 1999. Photophysiology of the marine cyanobacterium Prochlorococcus: Ecotypic differences among cultured isolates. Limnology and Oceanography 44: 628-638.

Moore, L. R., R. Goericke and S. W. Chisholm 1995. Comparative physiology of Synechococcus and Prochlorococcus: influence of light and temperature on growth, pigments, fluorescence and absorptive properties. Marine Ecology Progress Series 116: 259-275.

Moore, L. R., G. Rocap and S. W. Chisholm 1998. Physiology and molecular phylogeny of coexisting Prochlorococcus ecotypes. Nature 393: 464.

Olson, R. J., S. W. Chisholm, E. R. Zettler, M. A. Altabet and J. A. Dusenberry 1990. Spatial and temporal distributions of prochlorophyte picoplankton in the North Atlantic Ocean. Deep-Sea Research 37: 1033-1051.

Olson, R. J., E. R. Zettler and O. K. Anderson 1989. Discrimination of eukaryotic phytoplankton cell types from light scatter and autofluorescence properties measured by flow cytometry. Cytometry 10: 636-643.

Ormaza-González, F. I. and P. J. Statham 1991. Determination of dissolved inorganic phosphorus in natural waters at nanomolar concentrations using a long capillary cell detector. Analytica Chimica Acta 244: 63-70.

Parsons, T. R., Y. Maita and C. M. Lalli (1984). A manual of chemical and biological methods for seawater analysis Pergamon Press.

Partensky, F., W. R. Hess and D. Vaulot in press. Prochlorococcus, a key marine photosynthetic prokaryote. .

Redfield, A. C. (1934). On the proportions of organic derivatives in sea water and their relation to the composition of plankton. James Johnstone Memorial Volume, University Press of Liverpool: 176-192.

Vaulot, D., C. Courties and F. Partensky 1989. A simple method to preserve oceanic phytoplankton for flow cytometric analyses. Cytometry 10: 629-635.

Welschmeyer, N. A. 1994. Fluorometric analysis of chlorophyll a in the presence of chlorophyll *b* and pheopigments. Limnology and Oceanography 39: 1985-1992.

Chapter 6

# Size spectra of microbial plankton in the Atlantic and Pacific Oceans

Kent K. Cavender-Bares[1]
Andrea Rinaldo[1,2]
Sallie W. Chisholm[1]

[1] Ralph M. Parsons Laboratory, MIT
[2] University of Padua, Italy

Abstract

Microbial size spectra, including bacteria and phytoplankton up to 5 μm in size, were studied across both seasonal and spatial nutrient gradients in the Atlantic Ocean. Cruises were designed to transect the oligotrophic Sargasso Sea, the Gulf Stream, and coastal waters, providing a range of ecosystem conditions. Nutrient gradients (nitrate and phosphate) were measured with techniques capable of resolving concentrations below 10 nM. Microbial abundance was measured using flow cytometry, and estimates of size were made using an experimental calibration relating light scatter to cell volume. The relative contribution of large- or small-sized cells to total biomass can be inferred from size spectra, typically by their decay, which is best described by their slope in a double logarithmic plot. We found consistent trends in slopes for the various regions of the transects, and with depth. A simple, global relationship between slopes and nutrient concentrations, however, was not found, indicating that the ecosystem dynamics are complex. Spectral shape, or the relative conformity to a function described by a power law, ranged from smooth and linear during the spring bloom in the Sargasso Sea to distinctly non-linear in coastal waters. We hypothesize that smooth shapes which conform to power laws occur only during extended periods of nutrient enrichment, such as the spring bloom, when the growth of phytoplankton out-paces the ability of zooplankton to crop their growth. Analyses of size spectra from two enrichment studies, including the *in situ* iron-fertilization experiment (IronEx II) in the equatorial Pacific Ocean, show that such transient enrichments cannot replicate the effects of enrichments extended over longer periods, such as the spring bloom. We conclude that size spectra are important and distinctive indicators of the status of the microbial ecosystem, and may possibly enable us to single out stressing factors or to issue predictions about population dynamics of marine organisms on a global scale.

## INTRODUCTION

Interest in size spectra of pelagic systems has grown out of the first observations of particle distributions across the world ocean made by Sheldon and co-workers thirty years ago (Sheldon and Parsons 1967; Sheldon *et al.* 1972). Regardless of their mathematical form, size spectra convey a synoptic image of the size structure of a system which is taxon-independent. From the outset, the predictive powers of size spectra were recognized. Sheldon *et al.* (1972; 1977) suggested that fish stocks, for example, could be predicted if the planktonic size spectrum were known. They hypothesized that roughly equivalent amounts of biomass existed in logarithmic size classes of equal width—from bacteria to whales—which became known as the linear biomass hypothesis. Since then, numerous attempts have been made to test this hypothesis in freshwater and marine ecosystems.

Considerable attention has been paid to the theoretical aspects of size spectra (see: Platt 1985; Thiebaux and Dickie 1992; Vidondo *et al.* 1997). Platt and Denman's (1977) normalized biomass spectrum, with refinements by Blanco *et al.*(1994), has been the model for representing size spectra of planktonic organisms. Such a spectrum, in idealized form, fits a linear model on a double logarithmic plot (i.e., a power law), and the relative contribution of small- and large-sized cells to total biomass can be inferred from its slope. Countless investigations have shown that a linear model appropriately characterizes planktonic spectra (e.g., Rodriguez and Mullin 1986; Ahrens and Peters 1991; Quiñones-Bergeret 1992) , although not equally well in all situations (e.g., Sprules *et al.* 1983; Tittel *et al.* 1998). Rodriguez and Mullin (1986) recognized the value of being able to describe size spectra with a simple function like a power law and that determining the exact slope, or agreement of slopes between studies, was of secondary interest. If a constant relationship over a wide range in size can be demonstrated, then it may be appropriate to use size spectra as a predictive tool (Sheldon *et al.* 1977), to integrate them into models used to simulate ocean biogeochemistry (Armstrong 1994; Hurtt and Armstrong 1996) or to interpret ocean color measurements from satellites based on properties which scale with cell size (Stramski and Kiefer 1991).

A central focus of our work has been to explore how well size spectra conform to a power law. A power law structure of the probability distribution characterizing cell number as a function of cell size would be indicative of spatially scale-free, or critical behavior (e.g., Mandelbrot 1983). Such criticality essentially implies some form of scale invariance of the process. In other words, this means that the part (any part, in fact) is similar to the whole in the statistical description of an object, or process, and that such similarity holds over orders of magnitude. Furthermore, power laws are signatures of self-organization on the dynamics of open, dissipative systems with many degrees of freedom, where the features of the system tend to be attracted in states without a preferential scale regardless of initial conditions or parameter tuning (Bak 1996). Power laws in the probability distribution characterizing spatial or temporal features of natural processes are ubiquitous in nature. They have been demonstrated in coastlines, mountain ranges, and clouds (Mandelbrot 1983), particle fragmentation and earthquake frequency (Turcotte 1992), river networks (Rodriguez-Iturbe and Rinaldo 1997), to name a few. Systems exhibiting power laws in their statistical descriptions are considered fractal, implying that by whatever means they are characterized on one scale, they will retain this characteristic on a finer or coarser scale.

Criticality in planktonic size spectra, for example, would require that the mean particle size scales with the volume of sample measured. This is intuitively obvious because one would expect that 1 ml of seawater would contain proportionally fewer large cells than would a 1-liter sample, because large cells are present at lower concentrations (Chisholm 1992; Kiørboe 1993), and the 1-ml sample would have a lower mean particle size than would the 1-liter sample. Of course, at some upper limit, plankton of all sizes would be adequately represented, and the mean size of particles in still larger samples would not change. This highlights the fact that power law relationships have cut-offs, both upper and lower. In the plankton example, lower cut-offs (i.e., deviations from linearity on a double logarithmic plot in the smallest size classes) are most likely due to methodological limitations. For example, the smallest organisms enumerated in our study were bacteria. A deviation from linearity in the smallest size classes would be indicative of the fact that viruses were not enumerated in this study, *not* that the power law relationship breaks down at small size. Upper cut-offs would probably reflect under sampling of the largest organisms, and would not be characteristic of the actual size spectrum *in situ*. To use a power

law for predictive purposes, one would need to ascertain the specific nature of an upper cut-off and whether it was a characteristic of the sampling method or the actual planktonic system. If planktonic systems could be demonstrated to have fractal behavior, it would then be appropriate to evaluate whether these systems share traits, such as self-organization (Bak 1996), which are common to other systems which display critical behavior.

Historically, several approaches have been taken to construct planktonic size spectra. Sheldon and co-workers (Sheldon and Parsons 1967; Sheldon *et al.* 1967; Sheldon *et al.* 1972; Sheldon *et al.* 1973) used the Coulter Counter, which cannot distinguish between intact cells and detritus. Subsequent studies have relied on microscopy to characterize microorganisms in order to eliminate the bias which would result from the inclusion of detrital particles (e.g., Rodriguez and Mullin 1986; Sprules *et al.* 1991; Ahrens and Peters 1991; Gaedke 1992; Quiñones-Bergeret 1992; Ruiz *et al.* 1996; Tittel *et al.* 1998). Li (1994) used flow cytometry in a detailed analysis of microbial spectra in the North Atlantic, although his spectra differed from others in the literature because he used a particle's forward angle light scatter (FALS) as a proxy for volume, based on the strong correlation between these two parameters found by Olson *et al.*(1989). More recent studies that utilized flow cytometry have attempted to take into account the fact that FALS is not a constant function of cell size (Gin 1996; Gin *et al.* in press). Specifically, Gin *et al.*(in press) used a calibration relating FALS to cell volume which was a hybrid between calibrations based on microbial populations from the laboratory and the field. We build on the methodology of Gin *et al.* (in press) in this work by using a refined relationship between FALS and cell size which was derived from field populations of marine phytoplankton, and we use the latest method for representing size spectra (Vidondo *et al.* 1997).

Our goal of this study was understand the variability of the size spectra of marine microorganisms across ocean regions which varied temporally and spatially and in terms of nutrient availability. Here we present microbial size spectra from three systematic survey cruises within the Atlantic Ocean. These cruises transected nutrient gradients within and across the Sargasso Sea, the Gulf Stream, and coastal waters. Seasonal variability was captured by cruises during the spring, summer, and winter, and nutrient gradients were characterized with methods capable of resolving nitrate and phosphate at concentrations below 10 nM. Consistent patterns

of the shape (i.e., relative conformity to a power law) and slope of the spectra were observed. We hypothesize that smooth spectra conforming to power laws occur only during nutrient rich periods in which microbes may grow under reduced grazing pressure, and which persist on time scales substantially greater than the relevant time scales of the microbes involved (i.e., generation time). The spring bloom in the Sargasso Sea appeared to be an example of such a case. However, spectral analyses from an enrichment experiment in the Sargasso Sea and an iron-fertilization experiment conducted *in situ* (IronEx II; Coale *et al.* 1996) show that spectra after transient fertilization do not conform to these smooth power laws. We attribute this lack of conformity to an imbalance between growth and grazing rates that cause dramatic changes in species abundance on time scales equal to or shorter than the duration of the experiments.

## METHODS

We made measurements of biological and chemical features along three transects in the Atlantic (Fig. 1). The most extensive, both spatially and in sampling resolution, was during March 1998. We made two shorter transects during June 1996 and February 1997.

*Measurement of chlorophyll and nutrients*—Chlorophyll *a* (Chl *a*) was analyzed following the acid-correction method (Parsons *et al.* 1984) or Welschmeyer (1994) method, which eliminates the need for a pheophytin correction. Analyses were done at sea or on GF/F filters (Whatman) which had been frozen in liquid nitrogen. Detailed methods for the analysis of nitrate + nitrite (N+N) and soluble reactive phosphorus (SRP) have been reported elsewhere (*see* Chapter 5). The measurements of SRP are of particular interest since the method used approximates the actual inorganic P concentration in the sample (Bulldis-Thomson and Karl 1998), and we were able to measure nanomolar levels which have been reported only once before for a single depth profile in the Sargasso Sea (Ormaza-González and Statham 1991). Detection limits for N+N were approximately 2-nM, while those for SRP were about 0.5-nM.

*Collection of size-structured data*—A modified Epics V flow cytometer was used both at sea and in the laboratory for all plankton analyses. The particular details of the instrument configuration have been reported elsewhere (see Chapters 2 and 4; Cavender-Bares *et al.* 1998; Cavender-Bares *et al.* 1999). Four groups of plankton were distinguished by these analyses. Bacteria were enumerated by staining samples with a nucleic acid-specific stain (SYBR-Green I, Molecular Probes) following the protocol of Marie *et al.* (1997). Samples which had been preserved using 0.1 % glutaraldehyde and frozen in liquid nitrogen (Vaulot *et al.* 1989) were used for these analyses. *Prochlorococcus* and *Synechococcus* were analyzed either at sea or on similarly preserved, but unstained samples. The group of larger phytoplankton, which have been classified as ultra- and nanoplankton (Zettler *et al.* 1996; Cavender-Bares *et al.* 1999), were in all cases analyzed in unpreserved samples at sea.

We have applied a calibration curve (Fig. 2) to the raw flow cytometry data in order to convert from forward angle light scatter (FALS) to volume. The development of this calibration curve has been described elsewhere (*see* Chapter 3). In brief, each data point resulted from sorting (via flow cytometry) a subset of a preserved sample away from the other cells and then sizing those cells using a Coulter Counter. A fit to the data using Mie theory (Bohren and Huffman 1983) is shown in Fig. 2, along with dotted lines representing our estimate of 95% confidence intervals on predicting volume from FALS. The points at low FALS correspond to populations of *Prochlorococcus*, but instrument limitations did not permit bacteria from being sorted or sized. However, the Mie fit to the data in this region agrees with work relating FALS to volume of marine bacteria (Robertson and Button 1989; Koch *et al.* 1996; Robertson *et al.* 1998). Note that because the smooth relationship between FALS and volume breaks down above a FALS of approximately 10 units, we did not include cells of this FALS or greater in our size spectra.

*Background on representing size spectra*—Over the past thirty years there has been considerable attention given to measuring planktonic size spectra. Sheldon and Parsons (1967), who collected their data using a Coulter Counter, argued that the most appropriate way to present size structured data was to plot concentration of particles (by volume) against the logarithm (base 2) of diameter. We have plotted two samples from our data set in Fig. 3A using this method.

Figure 1:

Map of sampling stations in the western Atlantic Ocean. Different symbols are used to represent different cruises (*see* Key). The approximate location of the Gulf Stream is shown by a dotted line and the Bermuda Atlantic Time-series (BATS) site is denoted.

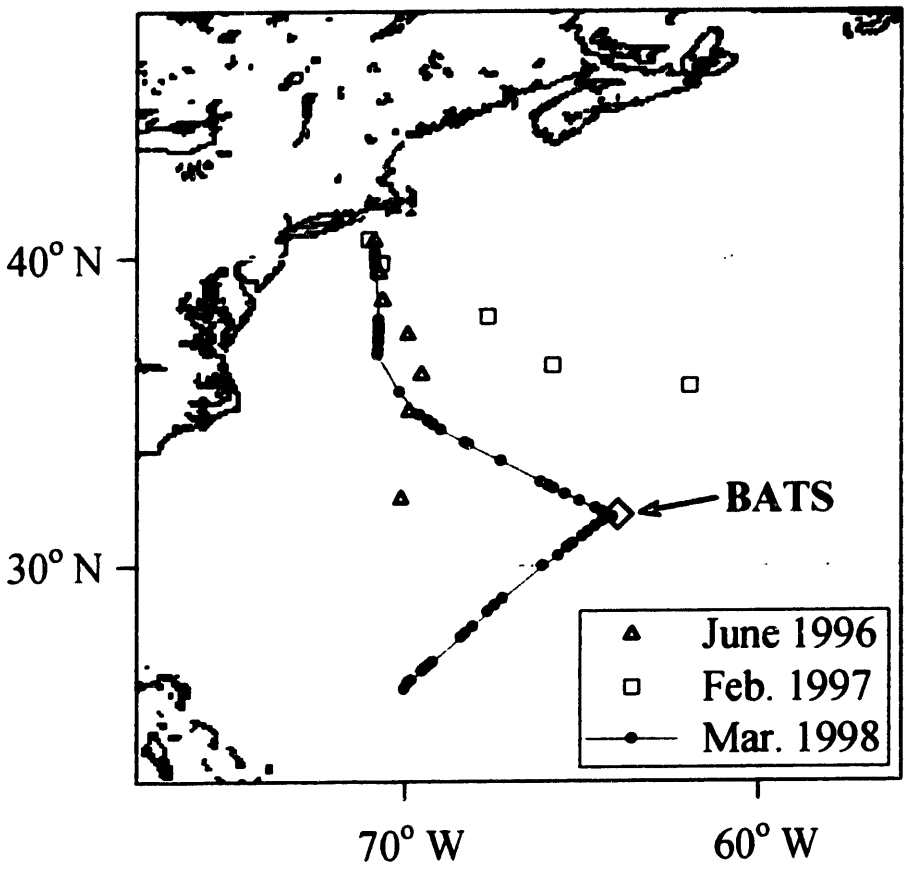
40° N
30° N
70° W
60° W
BATS
June 1996
Feb. 1997
Mar. 1998

Figure 2:

Calibration curve used to convert forward angle light scatter (FALS) to equivalent spherical volume as measured by a Coulter Counter. Two groups of phytoplankton are shown: filled circles for *Prochlorococcus*, *Synechococcus*, and the ultraphytoplankton; open circles for the nanophytoplankton. Solid line calculated from Mie theory and dotted lines represent estimated confidence limits for predicting volume from FALS.

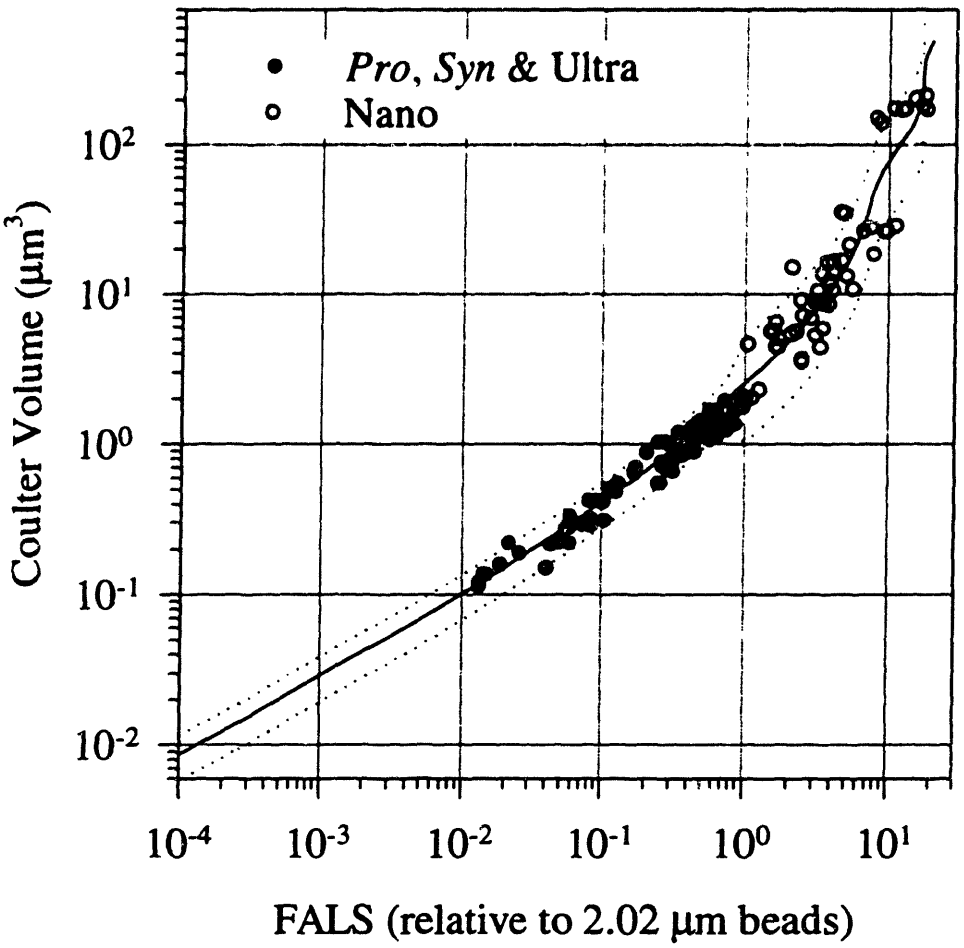
*Pro*, *Syn* & Ultra
Nano
Coulter Volume (μm³)
10²
10¹
10⁰
10⁻¹
10⁻²
10⁻⁴
10⁻³
10⁻²
10⁻¹
10⁰
10¹
FALS (relative to 2.02 μm beads)

Plotted on the y-axis is simply the total particulate biovolume for a given diameter divided by overall sample volume. Sheldon and co-workers went on to employ this method in far-reaching studies of the Atlantic and Pacific Oceans (Sheldon *et al.* 1972; Sheldon *et al.* 1973; Sheldon *et al.* 1977). In another early use of the Coulter Counter, Bader (1970) took a very different approach: he used cumulative number distributions (i.e., $N_1 = k\ v^{-m}$, where $N_1$ is the number of particles of volume greater than a certain volume, $v$; k and m are constants for a given sample) and a truncated version of this to address the tailing off of some distributions at large size. Bader discussed the use—and some shortcomings—of the number distribution (i.e., $\Delta N/\Delta v$ plotted against volume on a double logarithmic plot, where $\Delta v$ is the width of the volume bin for which the $\Delta N$ particles have been grouped), which is essentially what has become known as the normalized concentration spectrum (Fig. 3B; Blanco *et al.* 1994). Specifically, Bader commented that certain irregularities in distributions are more clearly visualized in cumulative number distributions than in ordinary number distributions, which are the numerical derivative of the former.

Platt and Denman (1978) presented a framework for constructing the normalized biomass spectrum [$\beta(w) = b(w)/\Delta w$, where $b(w)$ is the biomass in a certain weight class, $w$, and , $\Delta w$ is the width of the weight class], which has been implemented over the years since by many investigators (e.g., Rodriguez and Mullin 1986; Ahrens and Peters 1991; Quiñones-Bergeret 1992; Gin *et al.* in press; Ruiz *et al.* 1996; Tittel *et al.* 1998). Platt and Denman proposed this method in part to overcome difficulties which would arise from comparison of Sheldon-type spectra (concentration by volume) between investigators who choose to use different width size bins to collect data. When particle density, in terms of carbon or whatever measure of biomass used, is equal across size classes, then the normalized biomass spectrum is equivalent to the normalized biovolume spectrum (Fig. 3C). As first pointed out by Prothero (1986), and later discussed in relation to size spectra by Blanco *et al.* (1994), this process of normalization can produce misleading results. That is, it can be shown that a set of random numbers representing biomass (or, biovolume) arranged in size classes will produce a normalized spectrum that has a slope very similar to actual biomass spectra (i.e., close to –1). This happens when a variable which ranges over only a couple orders of magnitude (e.g., biomass in log (base 2) bins) is normalized by numbers spanning many orders of magnitude (e.g., size); the fluctuations of

biomass can be wiped out. Blanco *et al.*(1994) recommended the use of the normalized concentration spectrum as a way to avoid the problems inherent with the original normalized biomass spectrum.

Vidondo *et al.* (1997) proposed representing plankton spectra as probabilities of exceedence, which are, in cases for which one has an abundance of data points, the cumulative distribution used by Bader (1970) divided by the total number of particles ($N_t$). Normalizing by $N_t$ has the advantage of facilitating comparison of spectra since they all have the value of unity for the smallest size particle. As discussed by Vidondo *et al.* (1997), the greatest advantage of the probability of exceedence method is that data need not be binned into size classes. Two samples are presented in the form of probability of exceedence plots in Fig. 3D, where we use the notation Prob ($V \geq v$) to represent the probability of having particles greater or equal to a given volume, v. Vidondo *et al.* (1997) propose fitting such spectra with either the Pareto type I or II model. The type I Pareto is simply a linear fit on a log-log plot. The Type II model would be ideal for spectra which have very few particles in the lower size range, and therefore a relatively flat initial portion of the spectrum. Such a model is inappropriate in this study as any such behavior in our data is most probably a result of the exclusion of a smaller size class of particles (e.g., smaller bacteria or viruses), and would not represent an actual feature of the size spectrum, but rather an artifact of data collection. Due to the fact that cumulative probability plots have historically been used both in oceanography (e.g., Bader 1970; Kitchen *et al.* 1982; Stramski and Kiefer 1991) and in other disciplines (see references in Vidondo *et al.* 1997), it is the method that we have chosen to represent size spectra here. It should be noted that this is not an exhaustive discussion of the possible methods for representing size spectra. For example, Risovic (1993) proposed using gamma distributions to model size distributions, and Jonasz and Fournier (1996) suggested that a series of normal distributions could be used to represent complex size distributions.

The slope of the spectra shown in Fig. 3 are of great interest, as much of the interpretation of spectra has historically focused on the slope. A slope ($\beta$) of $-1$ on a Prob ($V \geq v$) plot indicates that particle abundance is inversely proportional to particle size, and that total biovolume is constant across size classes. As $\beta$ becomes more negative (e.g., -1.2),

Figure 3:

Comparison of four methods for constructing size spectra: (A) Sheldon et al. style spectra, (B) normalized concentration, (C) normalized biovolume, and (D) probability of exceedence [Prob ($V \geq v$)]. For the two normalized spectra, binning of the data is required and Log (base 2) bins were chosen. Two different natural samples of marine phytoplankton and heterotrophic bacteria are shown in the upper (oligotrophic station in Sargasso Sea) and lower (spring bloom in Sargasso Sea) panels. Slopes of the regression lines are shown panels B-D.

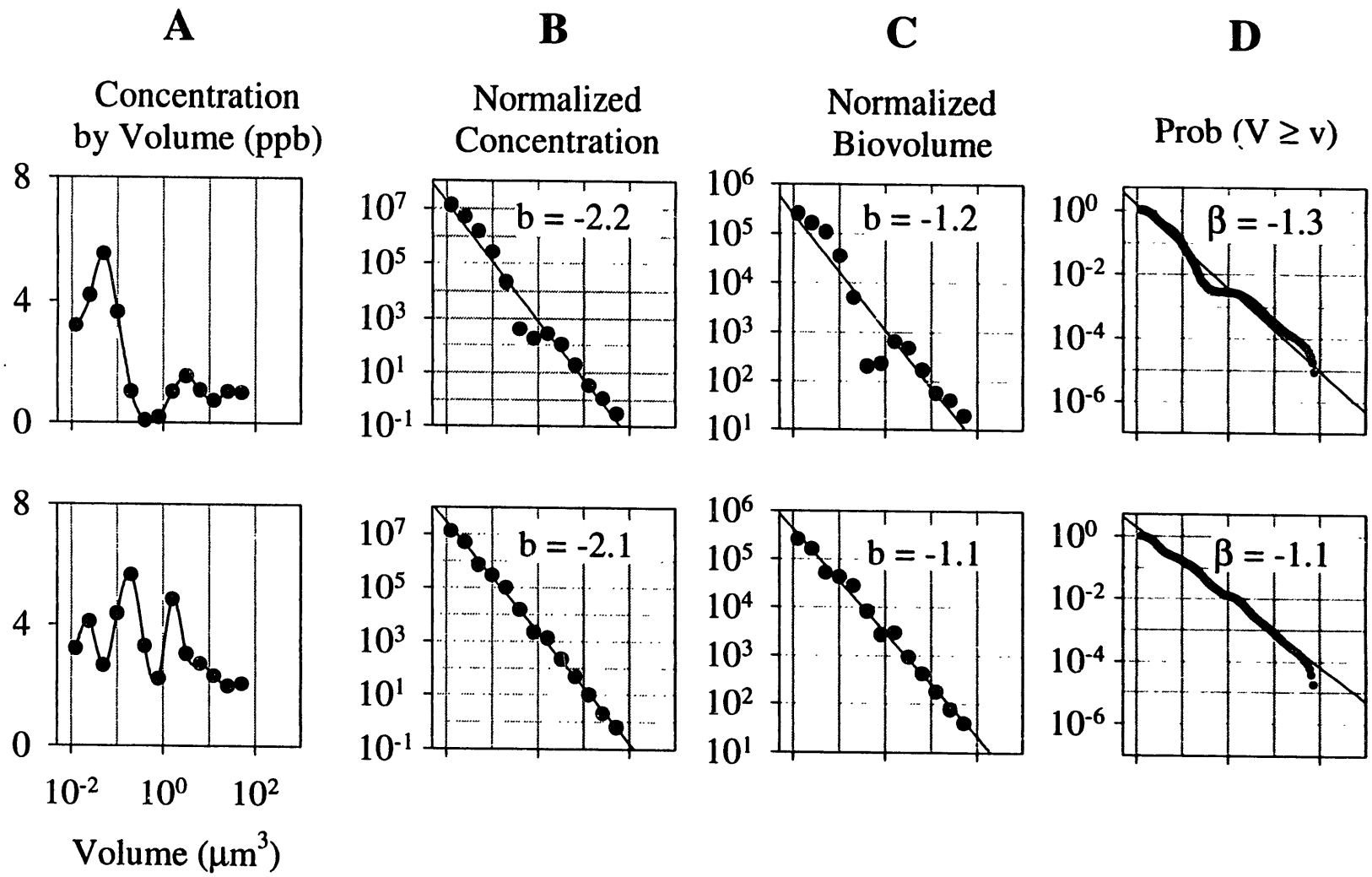
A
B
C
D
Concentration by Volume (ppb)
Normalized Concentration
Normalized Biovolume
Prob (V ≥ v)
8
4
0
$10^{7}$
$10^{5}$
$10^{3}$
$10^{1}$
$10^{-1}$
b = -2.2
$10^{6}$
$10^{5}$
$10^{4}$
$10^{3}$
$10^{2}$
$10^{1}$
b = -1.2
$10^{0}$
$10^{-2}$
$10^{-4}$
$10^{-6}$
β = -1.3
b = -2.1
b = -1.1
β = -1.1
$10^{-2}$
$10^{0}$
$10^{2}$
Volume (μm$^3$)

proportionally more biovolume is distributed in small size classes; the opposite is true as $\beta$ becomes more positive. Because the normalized concentration spectrum is essentially the derivative of the cumulative probability distribution (see Bader 1970; Blanco *et al.* 1994), it is expected to have a slope more negative by 1, as is seen by comparing Fig. 3B and D. Note that there is some discrepancy. However, this is to be expected because the normalized spectrum is an approximate derivative of the probability of exceedence. Note also that $\beta$ values are reported with more significant figures in cases where multiple spectra are averaged together (e.g., Figs. 7).

As discussed in the previous section, the largest cells were in some cases omitted from our spectra due to the nature of the calibration curve in that region. Cells larger than a given FALS (the same for all samples) were simply omitted from the size spectrum for a given sample. However, it was confirmed that this truncation did not impact the features of the Prob ($V \geq v$) curves.

## RESULTS AND DISCUSSION

Size spectra were measured on three transects in the Atlantic Ocean (Fig. 1). The March 1998 transect was the most extensively sampled, and it extended from oligotrophic waters in the Sargasso Sea, through spring bloom waters in the vicinity of the Bermuda Atlantic Time-series Study (BATS) site, across the Gulf Stream, and into coastal waters off New York. The other two transects, during June 1996 and February 1997, consisted of sampling stations in the Sargasso Sea, the Gulf Stream, continental slope, and continental shelf regions. We show that features of the spectra vary consistently during different seasons across waters ranging from the oligotrophic Sargasso Sea to nutrient rich coastal waters. In the final section, results from nutrient enrichment experiments suggest that transient enrichments add instability, rather than stability to community structure

*Chemical and biological features of the transects*

*March 1998 transect*— Chlorophyll *a* (Chl *a*) increased about 4-fold just south of BATS to reach a mean of 0.4 $\mu g\ l^{-1}$ (Fig. 4A). These high chlorophyll levels are consistent with values reported by Michaels *et al.* for the spring bloom at BATS (Michaels *et al.* 1994; Michaels and Knap 1996).Both nitrate + nitrite (N+N) and soluble reactive phosphorus (SRP) were less than 10 nM in the southern portion of the transect (Fig. 4B). Moving northward, N+N increased nearly 100-fold just before reaching the Bermuda Atlantic Time-series Study (BATS) site, but SRP increased only about of 10-fold. The disparity between the increases of the two nutrients caused their ratio (N:P), which was less than 16:1 in the southern region of the transect, to increase to a mean of 50:1 in the northern section of the Sargasso Sea (Fig. 4C). Slight changes in their absolute concentrations caused the N:P ratio to drop to 25:1 in the Gulf Stream. Both N+N and SRP increased substantially in coastal waters and the N:P ratio dropped further to less than 16:1. In a general sense, the ratio of N:P can be used to infer whether new production is N-limited (Dugdale and Goering 1967). N:P ratios less than 16:1, the Redfield ratio (1934), suggest N-limitation. N:P ratios along the transect (Fig. 4C) suggested that new production in the southern region of the Sargasso Sea was N-limited.

*Summer 1996 transect*—Nutrient concentrations ranged from nanomolar to micromolar levels at seven stations (Fig. 1) along a transect during June 1996 (Fig. 8). N+N and SRP were generally below 10 nM in the mixed layer of three stations in the Sargasso Sea and one in the Gulf Stream (Fig. 8A-D). Surface Chl *a* concentrations ranged from 0.05 to 0.1 $\mu g\ l^{-1}$ for these four stations, while maximum values at depth ranged from 0.3 to 0.5 $\mu g\ l^{-1}$. Coastal stations had nearly 100-fold more SRP in the mixed layer, yet N+N was typically drawn down below 10 nM (Fig. 8E-G). In general, N+N to SRP ratios in the mixed layers were less than 16:1 and the ratio in deeper waters was much greater than 16:1. Surface Chl *a* values in coastal waters ranged from 0.1 to 0.2 $\mu g\ l^{-1}$, and deep Chl *a* maxima were generally a factor of two larger in concentration—except for the transitional station (Fig. 8F) for which Chl *a* reached 2 $\mu g\ l^{-1}$ at 40 m. The depth of the Chl *a* maximum ($D_{cm}$) shoaled substantially in coastal waters (Fig. 8).

Figure 4:

Chemical and biological features along a transect during March 1998 from south of Bermuda in the Sargasso Sea across the Gulf Stream and into coastal waters (Fig. 1). (A) Chlorophyll *a* (Chl *a*), (B) Nitrate + Nitrite (N+N) and soluble reactive phosphate (SRP), and (C) Ratio of N+N to SRP along the transect. (D) Slope ($\beta$) of probability of exceedence spectra as a function of latitude. Lower case letters (above panel D) indicate the statistical difference between $\beta$ values for the different regions which can be summarized by: Gulf Stream < southern Sargasso Sea < northern Sargasso Sea; $\beta$ values for the Coastal waters were not different from either the southern Sargasso Sea or the Gulf Stream.

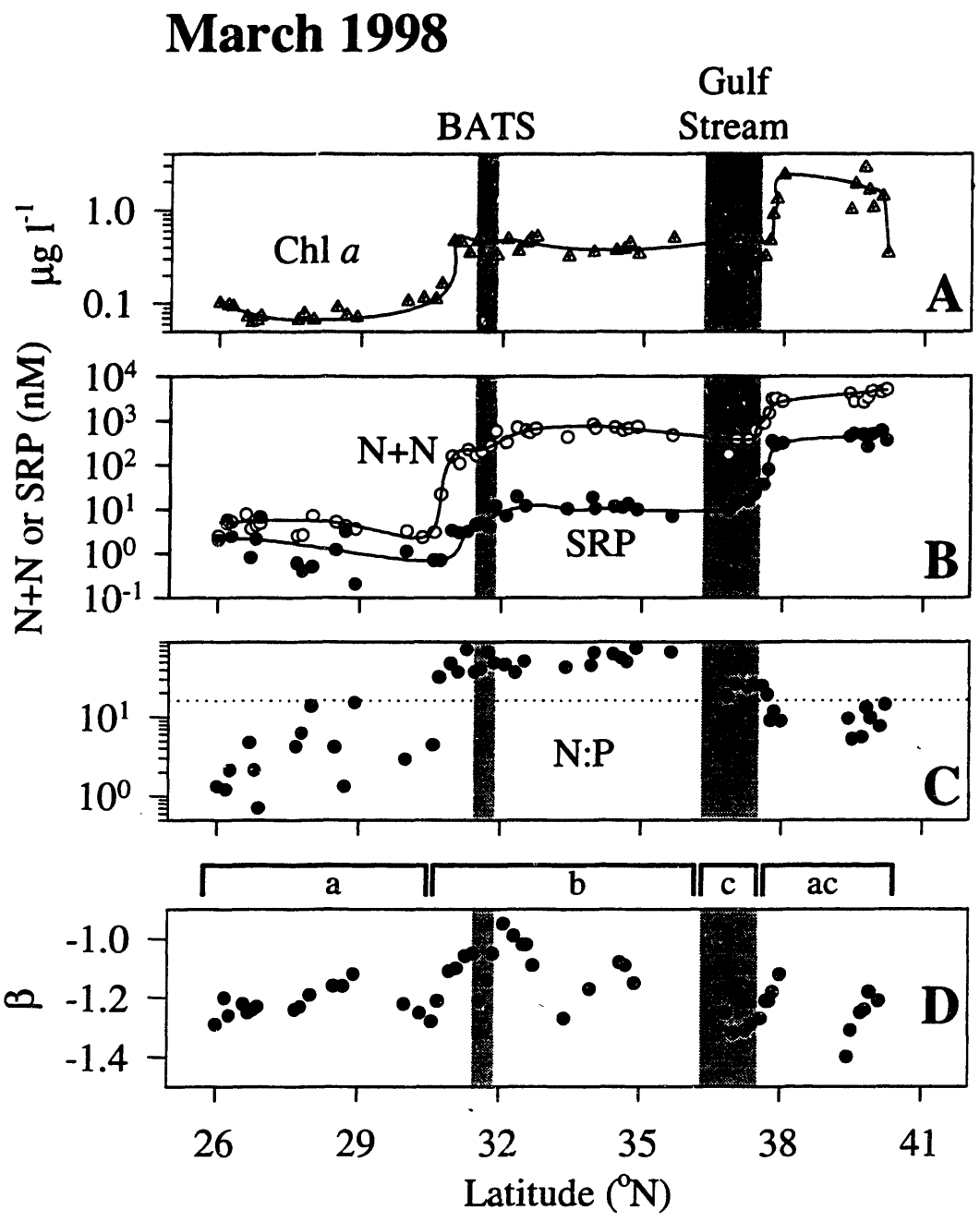
March 1998
Gulf
Stream
BATS
1.0
0.1
μg l-1
Chl a
A
N+N or SRP (nM)
10^4
10^3
10^2
10^1
10^0
10^-1
N+N
SRP
B
10^1
10^0
N:P
C
a
b
c
ac
-1.0
-1.2
-1.4
β
D
26
29
32
35
38
41
Latitude (°N)

*Winter 1997 transect*—Nutrient concentrations were markedly elevated for this transect (Fig. 9) compared to the summer cruise (Fig. 8), but were similar to those found in the same regions of the 1998 transect (Fig. 4B). Only the northern Sargasso Sea station (Fig. 9B) had SRP values in the mixed layer less than 10 nM. In all cases, N+N was higher than SRP, at least by an order of magnitude (Fig. 9). N+N to SRP ratios were greater than 16:1 in the Sargasso Sea and the Gulf Stream and coastal waters had ratios close to 16:1, as was seen during March 1998 (Fig. 4C). Chl *a* was fairly constant in the mixed layers, and at the surface it increased from south to north along the transect, from 0.3 to 1 $\mu g\ l^{-1}$.

*Patterns of size spectral features*

*Spectral slope*—Slopes ($\beta$) of individual spectra (Fig. 5) from the March 1998 transect varied between –1.4 and –1.0 (Fig. 4D). The most negative $\beta$ (-1.4) was measured in coastal waters, while the most positive (-1.0) was measured near BATS in spring bloom waters. We divided the entire transect into four regions on the basis of relative N and P concentrations and their ratio (Fig. 4B,C): the low-nutrient southern Sargasso Sea, the high-nutrient northern Sargasso Sea, the Gulf Stream, and coastal waters. As has been done previously to test the statistical difference between groups of spectra in terms of their slopes (Rodriguez and Mullin 1986; Tittel *et al.* 1998), we applied a non-parametric rank-sum test (two-tailed Mann-Whiney U-test; Sokal and Rohlf 1995) to the groups of individual spectra. All differences are at the $P < 0.05$ level and are indicated by lowercase letters above Fig. 4D.

The spectra from the southern Sargasso Sea were more negative than those of the northern Sargasso Sea, but less negative than those of the Gulf Stream; the slope of coastal waters differed (more negative) only from those of the northern Sargasso Sea. In addition to these overall trends, it is clear that slopes are least negative near the face of the spring bloom in the vicinity of BATS. This is because of a 10-fold increase in relatively large ultra- and nanoplankton that was observed in spring bloom waters (*see* Chapter 5), which is consistently seen during spring at the BATS site (Gin *et al.* in press; DuRand *et al.* submitted). Also evident from the trends in $\beta$, is a local minimum centered at the BATS site. This may be explained by the fact that this station and the one immediately to the south were separated temporally by a two

day period, during which convective mixing broke down early signs of stratification. Also, the fluctuation in slopes further north in the Sargasso Sea coincided with a winter storm. The increasingly positive β values at the northern extent of the Gulf Stream coincide with large increases in nutrients (Fig. 4B), however, the similar trend observed further to the north in coastal waters is not readily explained by any of the parameters measured.

Cell cycles present another possible explanation for the trends observed in β over narrow spatial scales. *Prochlorococcus*, for example, displays a tightly synchronized cell cycle: cells increase in size during the day until reaching a maximum just prior to cell division in the late afternoon (e.g., Vaulot and Chisholm 1987; Vaulot *et al.* 1995). Not all species divide synchronously, yet we explored whether this effect could be seen in our data because samples were taken throughout the day and night. Values of β for the two regions of the transect in the Sargasso Sea appear to vary across the day (Fig. 6). These variations, especially in the southern region of the Sargasso Sea, provide evidence suggesting diurnal fluctuations in β. *Prochlorococcus* which approached their maximal size in the afternoon would cause β to become less negative, as is seen for the several samples taken in the afternoon of March 4$^{th}$. Thus, it is possible that differences in slope between the different regions of the transect would have been more pronounced had all samples been taken at the same time of day.

Even though we found differences in β that were statistically significant along the transect, it is important to understand the biological significance of these differences in the context of the methodology used to construct the spectra. Consider two samples of equal volume, both of which contain the same total number of cells. The distribution of cells across the volume axis is different in each sample, although these distributions have common minimum and maximum cell sizes similar to those in our samples. β can be used to calculate the number of cells of the maximum size, which is directly proportional to the biovolume of cells of that size. Using these hypothetical samples, we can vary β in order to see the difference in biovolume for cells of the maximum size. If β values were –1.17 and –1.13, the difference in biovolume for cells of the largest size would be 30%; if they were –1.28 and –1.00, the biovolumes would differ by a factor of two. Variation in β does reflect a significant difference in

Figure 5:

Individual size spectra for March 1998 transect. Spacing between spectra is constant in the figure, but was not constant spatially (*see* Fig. 4 for approximate spacing). Each panel represents a portion of the transect, with beginning and ending latitudes shown. Approximate locations of the Bermuda Atlantic Time-series Study (BATS) site and the Gulf Stream are indicated.

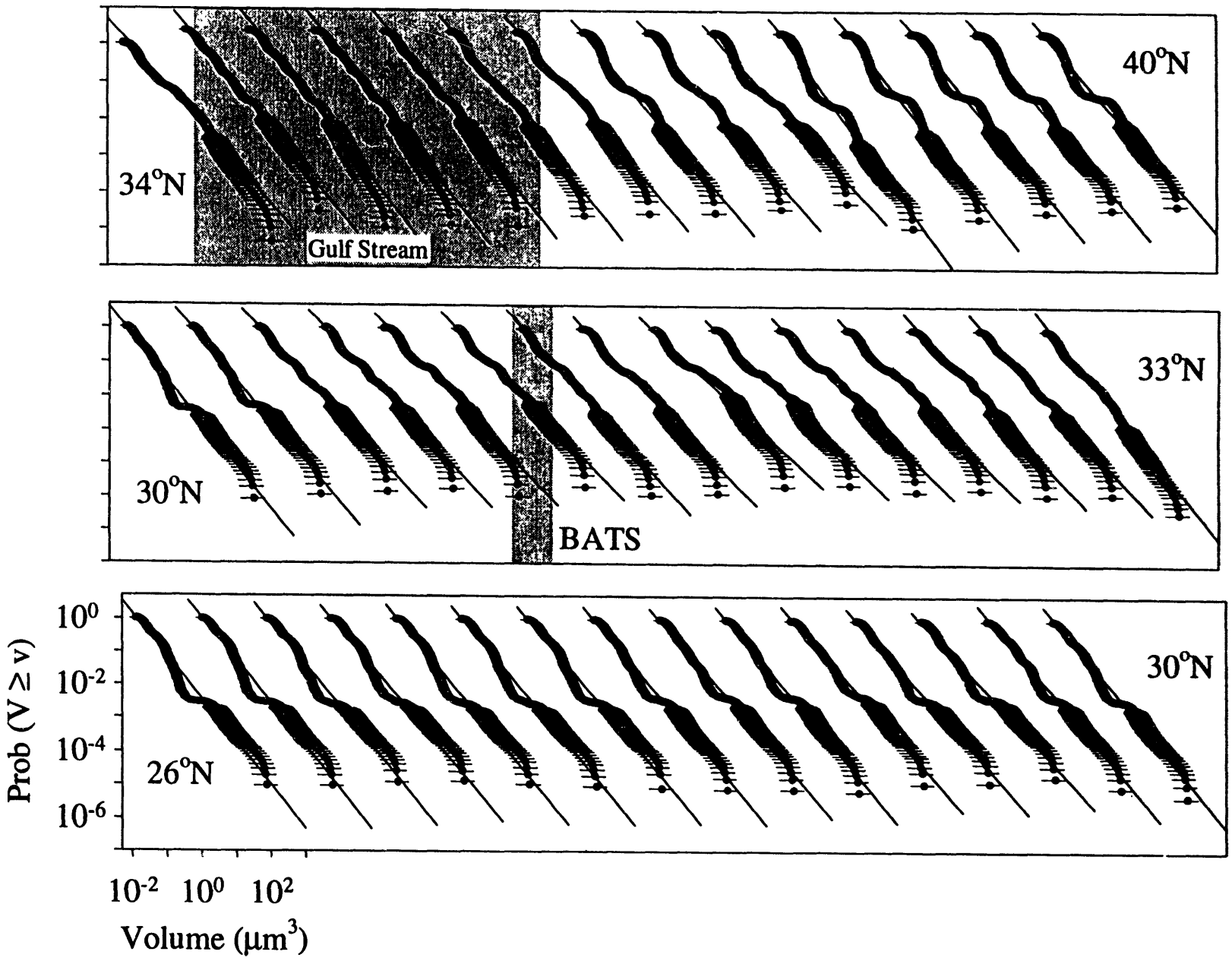
40°N
34°N
Gulf Stream
33°N
30°N
BATS
30°N
26°N
Prob (V ≥ v)
10^0
10^-2
10^-4
10^-6
10^-2 10^0 10^2
Volume (μm^3)

Figure 6:

Slopes of the size spectra from Fig. 4D plotted against time of day for the two regions of the Sargasso Sea for March 1998 transect. Dark bars in each panel represent approximate periods of darkness, with dates shown at local midnight.

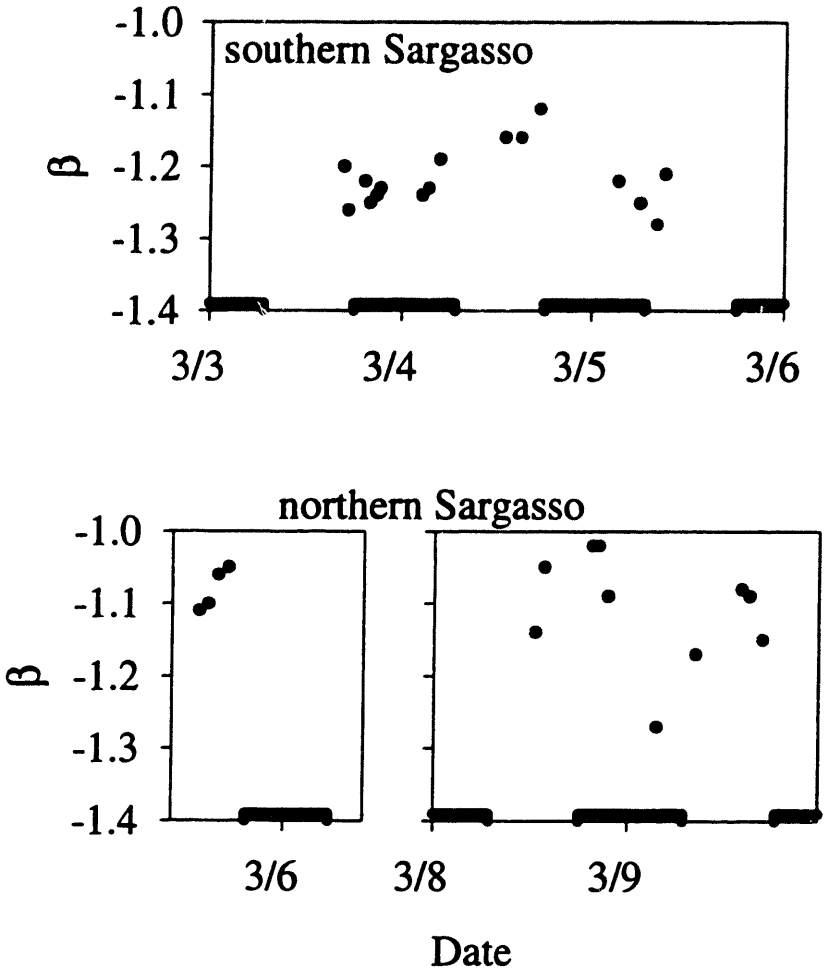
southern Sargasso
northern Sargasso
β
-1.0
-1.1
-1.2
-1.3
-1.4
3/3
3/4
3/5
3/6
3/8
3/9
Date

the biovolume in this maximum size class. Of course, for field samples we measure size distributions and estimate values of β, and there is some uncertainty in our measurement of these distributions (Fig. 2). In fact, if we were simply to measure the total biovolume in the maximum size class in the hypothetical samples, our estimate would be bounded by a confidence interval of at least ± 30%, or an upper and lower volume limit differing by nearly a factor of two. Thus, while we believe that trends in β are real, further methodological refinement would be necessary before the absolute value of β can be fully interpreted.

Slopes ranged from −1.0 to −1.4 for all stations during the June 1996 transect, both at the surface and at the $D_{cm}$ (Fig. 8). At the surface, the Gulf Stream slope was the most negative (Fig. 8D), which agrees with the rank-order of slopes from the March 1998 cruise. The Sargasso Sea spectra were similar at the surface, in terms of slope (Fig. 8A-C). From data on the individual populations, we can say that the presence of *Prochlorococcus* only at the northern station (Fig. 8C) and a high abundance of bacteria at the middle station (Fig. 8B) impacted β for these three stations. A large relative increase in the abundance of *Prochlorococcus* or bacteria would cause β to become more negative. For the coastal stations (Fig. 8E-G), β was variable, much as it was in the coastal region of the March 1998 cruise (Fig. 4D). In all cases β values at the chlorophyll maximum ($D_{cm}$) were at least as negative as at the surface, and usually more so (Fig. 8).

Consistent with the shallow slopes in the northern region of the Sargasso Sea during March 1998 (Fig. 4D), β was the least negative in the Sargasso Sea during winter (Feb. 1997; Fig. 9A,B). Relative to the Sargasso Sea, β in the Gulf Stream (Fig. 9C) was slightly more negative, and was not clearly different than the coastal regions (Fig. 9D,E); the same rank-order of β that was found during March 1998 (Fig. 4D). As found during June 1996 (Fig. 8), deeper samples all had slopes at least as negative as their surface counterparts (Fig. 9).

There were significant changes in β across regions of the March 1998 transect (Fig. 4D). The rank-order of the β values suggests that overall there is no relationship between β and nutrient concentration. This was especially apparent in the case of the southern Sargasso Sea and the Gulf Stream (Fig. 4D): the latter had much higher nutrient concentrations, yet had steeper

slopes than the former. Formalizing this observation, we found no correlation between the β and either N+N or SRP (Fig. 10A,B) for surface samples. Note that only points for the March 1998 transect are shown in Fig. 10, however, all of the relationships were maintained after the inclusion of data points from surface samples for the other two cruises. Nevertheless, we did find isolated correlation between β and nutrients, such as in the vicinity of BATS (Fig. 4D) where slopes became less negative as nutrients increased. It is generally believed that large cells, especially diatoms, predominate in nutrient rich conditions (e.g., Chisholm 1992; Kiørboe 1993), which would give rise to less negative β values with increasing nutrients. Our composite data set, however, does not support a shift in the size distribution associated with increasing nutrients (Fig. 10A,B). This is in agreement with Gin *et al.*(in press) who found little change in slope between periods of deep mixing (high-nutrient) and stratification (low-nutrient) at BATS. It is likely that the large cells, which supposedly respond to higher nutrients, were simply outside of the upper limit of our analyses (diameter of about 5 μm), and would, therefore, not impact our measurement of β. Ruiz *et al.*(1996) found trends of increasingly negative slopes in more productive waters and attributed this to a larger proportion of biomass in small cells. Ruiz *et al.* had a complicating factor, however, because more productive waters often were found at depth. Using filter-fractionated chlorophyll measurements, Raimbault *et al.*(1988) showed that with increasing total Chl *a*, the relative amount of Chl *a* in larger size classes increased. Using Chl *a* as a proxy for cell biovolume, one would expect that as Chl *a* increased, the slope of spectra would become less negative. Our data did not support this idea because there was no correlation between β and total Chl *a* for the surface samples (Fig. 10C).

A consistent, albeit sometimes weak trend of increasingly negative β values with depth has emerged from the depth comparisons from the 1996 and 1997 cruises (Figs. 8 and 9). This trend is supported by more complete depth profiles for three stratified (Fig. 11A,C,D) water columns and one which was deeply mixed (Fig. 11B). By comparing the slope variations with depth profiles of N+N and SRP, it is clear that in many cases changes in β occurred independently from changes in nutrients. The literature on the subject of spectra slopes as a function of depth is not coherent, as was discussed by Ruiz *et al.*(1996). Rodriguez and Mullin (1986) found less negative slopes with depth in the Pacific, which is consistent with Revelante and Gilmartin's (1995) observation of an increased contribution of large cells to total biomass at

Figure 7:

Size spectra along a transect during March 1998 from south of Bermuda in the Sargasso Sea across the Gulf Stream and into coastal waters (Fig. 1). (A) Changes in the slope ($\beta$) of the Prob($V \geq v$) spectra along the transect, with lower case letters representing significantly different regions of the transect (*see* Fig. 4). (B-E) Probability of exceedence spectra. (B) Ensemble average for the southern Sargasso Sea, and (C) the northern Sargasso Sea, and (D) the Gulf Stream, and (E) coastal waters. Axes on the spectra plots, Prob ($V \geq v$) and volume, are scaled the same for all panels and slopes of the regression lines ($\beta$) are shown. Confidence intervals on the estimation of cell size are shown by horizontal lines for each point. In all cases, a 1-to-1 dotted line ($\beta = -1$) is included which begins at the volume of the smallest cell measured. (F-I) Cell concentration against volume for the regions in (B-E). Four groups are shown, from small to large: heterotrophic bacteria, *Prochlorococcus*, *Synechococcus*, and the ultra- and nanoplankton. Arrows are added to F and G to denote the absence of cells in these size classes for F, and how this gap was filled by a sub-population of the ultra- and nanoplankton which appeared in spring bloom waters (see text).

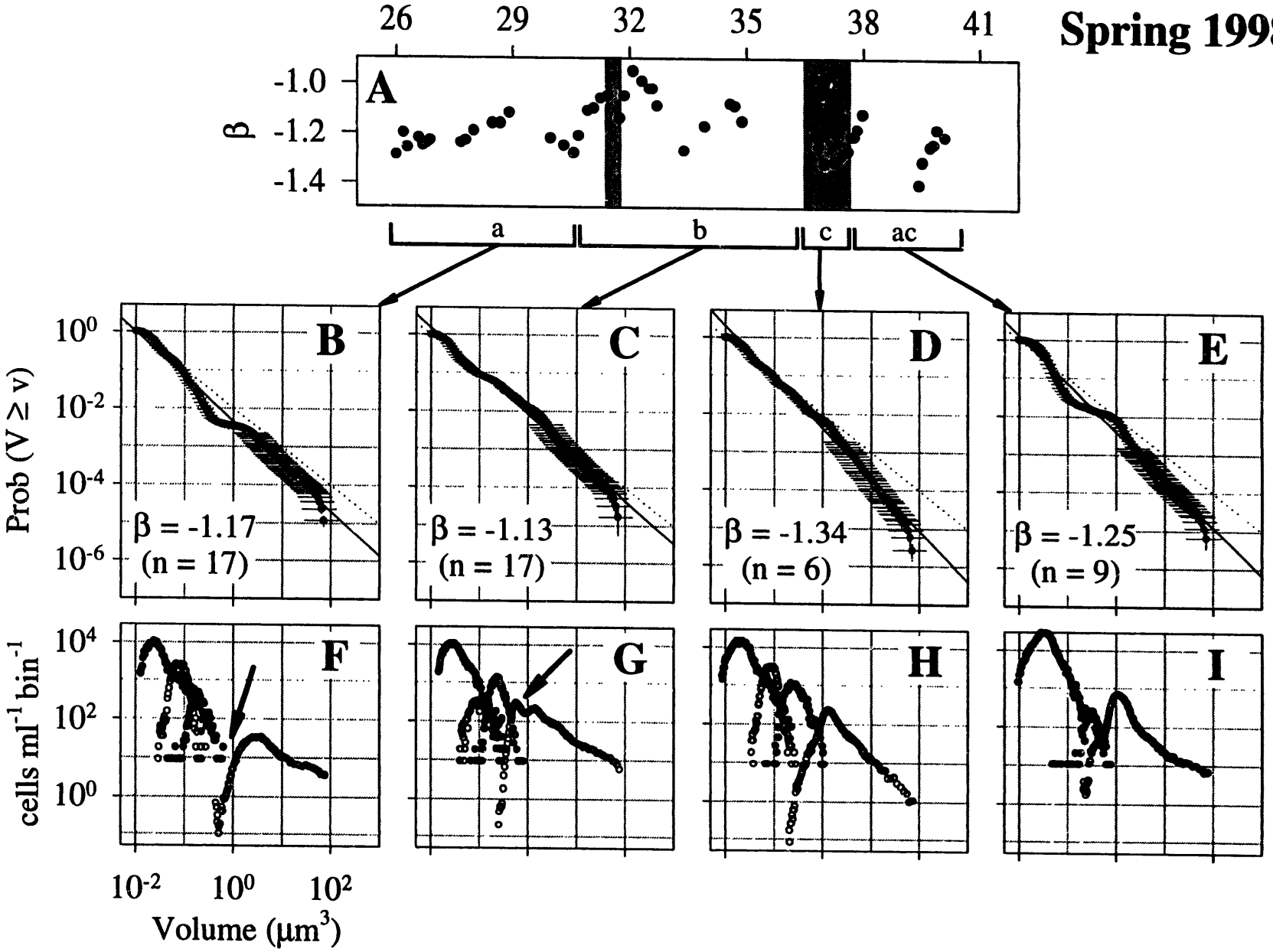
Spring 1998
A
β
-1.0
-1.2
-1.4
26
29
32
35
38
41
a
b
c
ac
B
C
D
E
F
G
H
I
Prob (V ≥ v)
10^0
10^-2
10^-4
10^-6
β = -1.17
(n = 17)
β = -1.13
(n = 17)
β = -1.34
(n = 6)
β = -1.25
(n = 9)
cells ml^-1 bin^-1
10^4
10^2
10^0
10^-2
10^0
10^2
Volume (μm^3)

subsurface maxima in the Adriatic Sea. Quiñones-Bergeret (1992) found no change in slopes with depth in the Sargasso Sea, nor did Delgado *et al.*(1992) in the Mediterranean. Gin *et al.*(in press), however, found increasingly negative slopes with increasing depth at BATS, both during periods of deep mixing and during stratification, which agrees with the findings of this study and of Ruiz *et al.*(1996) for the Mediterranean. In marine environments where *Prochlorococcus* is abundant, it is logical that the slopes should become more negative with depth, because *Prochlorococcus* it is often found to have maxima at depth (e.g., Olson *et al.* 1990). Such maxima are consistent with the ability of lab cultures of *Prochlorococcus* to grow at very low light levels (Moore *et al.* 1995; Moore *et al.* 1998; Moore and Chisholm 1999).

*Size spectra within a region*—We found that $\beta$ values within a region for the March 1998 transect were similar and, in most cases, different than those from other regions (Fig. 4D), and the spectral shapes were also similar within a given region (Fig. 5). In order to understand how well conserved spectra were for a given region of the transect, we took ensemble averages of the individual spectra for each region (Fig. 7B-E). In a spectrum of the ensemble average, variability between spectra would manifest as large vertical error bars, which are small in all cases (Fig. 7B-E). The ensemble average of the 17 spectra from the southern region of the transect demonstrated that all of these spectra were very similar (Fig. 7B), and that they shared a common departure from linearity centered at a volume of 0.4 $\mu m^3$ (diameter of 0.9 $\mu m$). The ensemble average representing the northern portion of the Sargasso Sea (Fig. 7C) was much more linear, indicating a constant rate of decrease in cell number with increasing cell size. Equally consistent spectra were found for the Gulf Stream (Fig.7D) and coastal (Fig. 7E) portions of the transect.

An important finding from these ensemble averages (Fig. 7B-E) is that size spectra from a given region were conserved. Many individual spectra from a given region collapsed into a single spectrum with small vertical error bars, indicating very little variation between spectra. This has important implications for the use of flow cytometry in characterizing the size spectra of distinct regions of the ocean, as labor is reduced if minimal replication is required.

*Spectral shape*—Throughout the samples examined, several prominent spectral shapes were seen. These ranged from smooth linear functions (Fig. 7C,D) to spectra with several different deviations from linearity (e.g., Fig. 7E). In between, was a spectral shape characterized by a deviation from linearity located at the overlap between *Synechococcus* and the ultra- and nanoplankton (e.g., Fig. 7B). The deviations from linearity in coastal waters seen over the various cruises agree with the observations of others (Sheldon *et al.* 1972; Witek and Krajewskasoltys 1989; Rodriguez *et al.* 1987). These spectra can be considered to represent non-steady state systems, perhaps undergoing a species succession. In some cases this shape, with multiple deviations from linearity, was seen in open ocean samples, which would suggest that these systems were also far removed from a steady state.

Visual inspection of the individual spectra from the March 1998 transect (Fig. 5) indicates that the spectra from a given region have similar shapes. There is some small variation among spectral shapes from the northern Sargasso Sea, which may reflect the winter storm encountered in that region. By comparing the spectra (Fig. 7B-E) with the raw data used in their construction (Fig. 7F-I), their shapes can be readily explained. The nearly flat region of the Prob($V \geq v$) spectrum for the southern Sargasso Sea (Fig. 7B) coincided with a lack of overlap between *Synechococcus* populations and the ultra- and nanoplankton (arrow in Fig. 7F). Such overlap of these populations was clearly evident in the northern Sargasso Sea (Fig. 7G) and the Gulf Stream (Fig. 7H). The individual components of the plankton community contrasted sharply between the northern Sargasso Sea and the Gulf Stream. This demonstrates that more than a single combination of plankton groups can yield a uniform spectrum. A small-sized, yet numerous sub-population within the ultra- and nanoplankton appeared in spring bloom waters of the Sargasso Sea (arrow in Fig. 7G), which in large part closed the 'gap' between *Synechococcus* and the ultra- and nanoplankton. In the Gulf Stream, however, both the *Synechococcus* and the ultra- and nanoplankton groups were distributed over wider ranges in volume, thereby eliminating this gap and resulting in a smooth decrease in Prob($V \geq v$) as cell volume increased (Fig. 7D).

Spectra from the June 1996 transect (Fig. 8) had shapes similar to some of those from the March 1998 transect (Fig. 7B-E), however, these shapes were not well distinguished among

Figure 8:

Size spectra along a transect beginning in the Sargasso Sea and ending in coastal waters off New England during June of 1996 (Fig. 1). (A-G, upper) Depth profiles of nitrate + nitrite (N+N), soluble reactive phosphorus (SRP), chlorophyll *a* (Chl *a*), and temperature. Horizontal dotted lines indicate depths from which the size spectra samples were taken. (A-G, lower) Probability of exceedence (Prob($V \geq v$)) spectra along the transect, for two depths: surface and depth of the Chl *a* maxima, as shown by dotted lines in upper panels. Axes on the spectra plots, Prob ($V \geq v$) and volume, are scaled the same for all panels and slopes of the regression lines are shown. Confidence intervals on the estimation of cell size are shown by horizontal lines for each point. In all cases, a 1-to-1 dotted line ($\beta = -1$) is included which begins at the volume of the smallest cell measured. Coastal stations (E-G) included continental slope, shelf, and transition point in between. Spectra for a given depth profile have been offset vertically so that they are easily compared. The offset is equivalent to three orders of magnitude between depths.

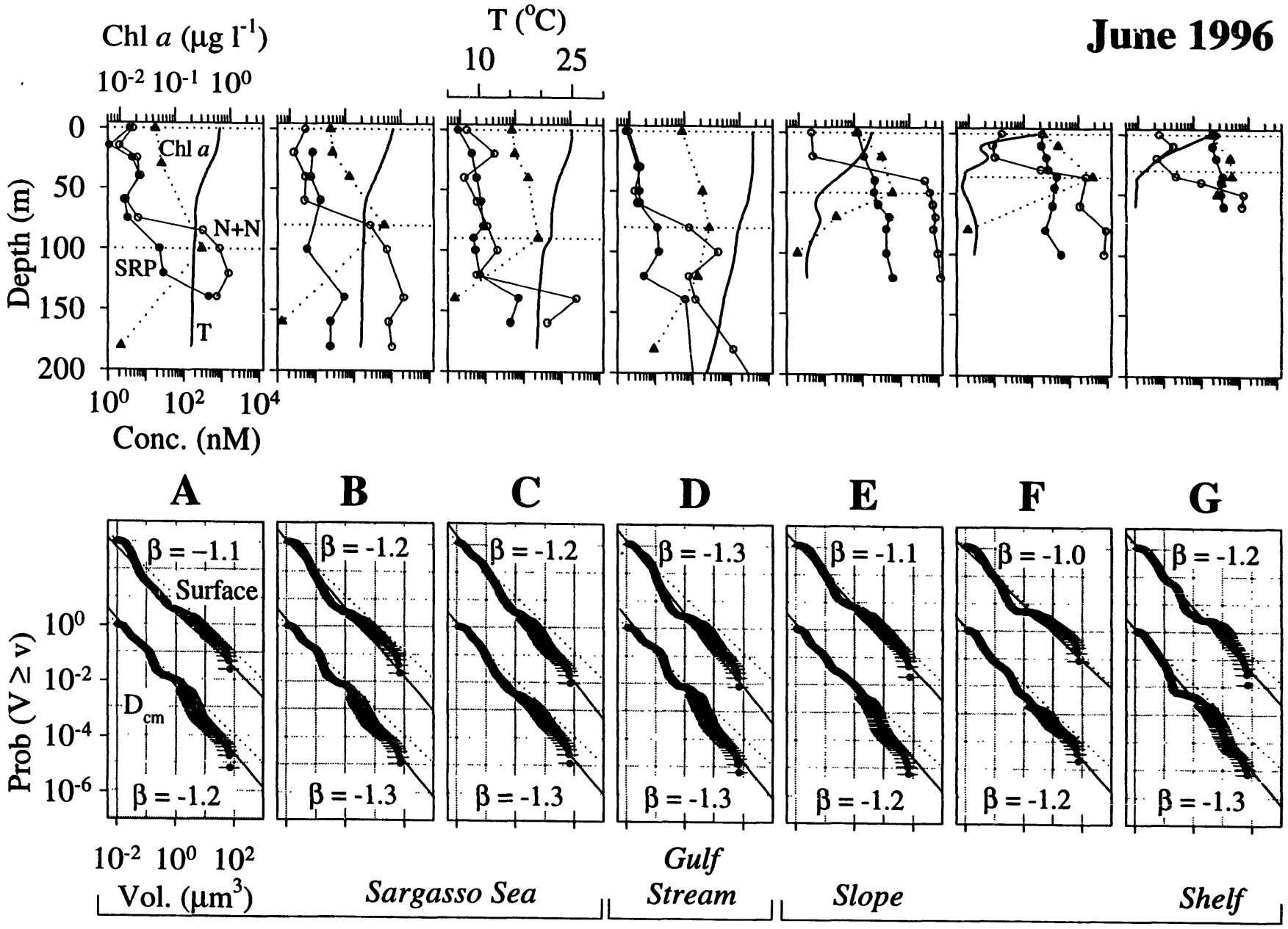
June 1996
Chl a (µg l-1)
10-2 10-1 10^0
T (°C)
10 25
Depth (m)
0
50
100
150
200
Chl a
N+N
SRP
T
10^0 10^2 10^4
Conc. (nM)
A
B
C
D
E
F
G
Prob (V ≥ v)
10^0
10-2
10-4
10-6
Surface
Dcm
β = -1.1
β = -1.2
β = -1.2
β = -1.3
β = -1.1
β = -1.0
β = -1.2
β = -1.2
β = -1.3
β = -1.3
β = -1.3
β = -1.2
β = -1.2
β = -1.3
10-2 10^0 10^2
Vol. (µm3)
Sargasso Sea
Gulf Stream
Slope
Shelf

Figure 9:

Size spectra along a transect from the Sargasso Sea into New England coastal waters during February 1997 (Fig. 1). (A-E, upper) Depth profiles of nutrients and chlorophyll along transect. See Fig. 8 legend for details. (A-E, lower) Two Sargasso Sea stations (A,B) were followed by one in the Gulf Stream (C), one on the continental slope (D), and one in shelf waters (E). Spectra from two depths are shown at each station, however a clear chlorophyll maximum was typically not present. Axes on the spectra plots, Prob ($V \geq v$) and volume, are scaled the same for all panels and slopes of the regression lines ($\beta$) are shown. Confidence intervals on the estimation of cell size are shown by horizontal lines for each point. In all cases, a 1-to-1 dotted line ($\beta = -1$) is included which begins at the volume of the smallest cell measured. Spectra for a given depth profile have been offset vertically so that they are easily compared. The offset is equivalent to three orders of magnitude between depths.

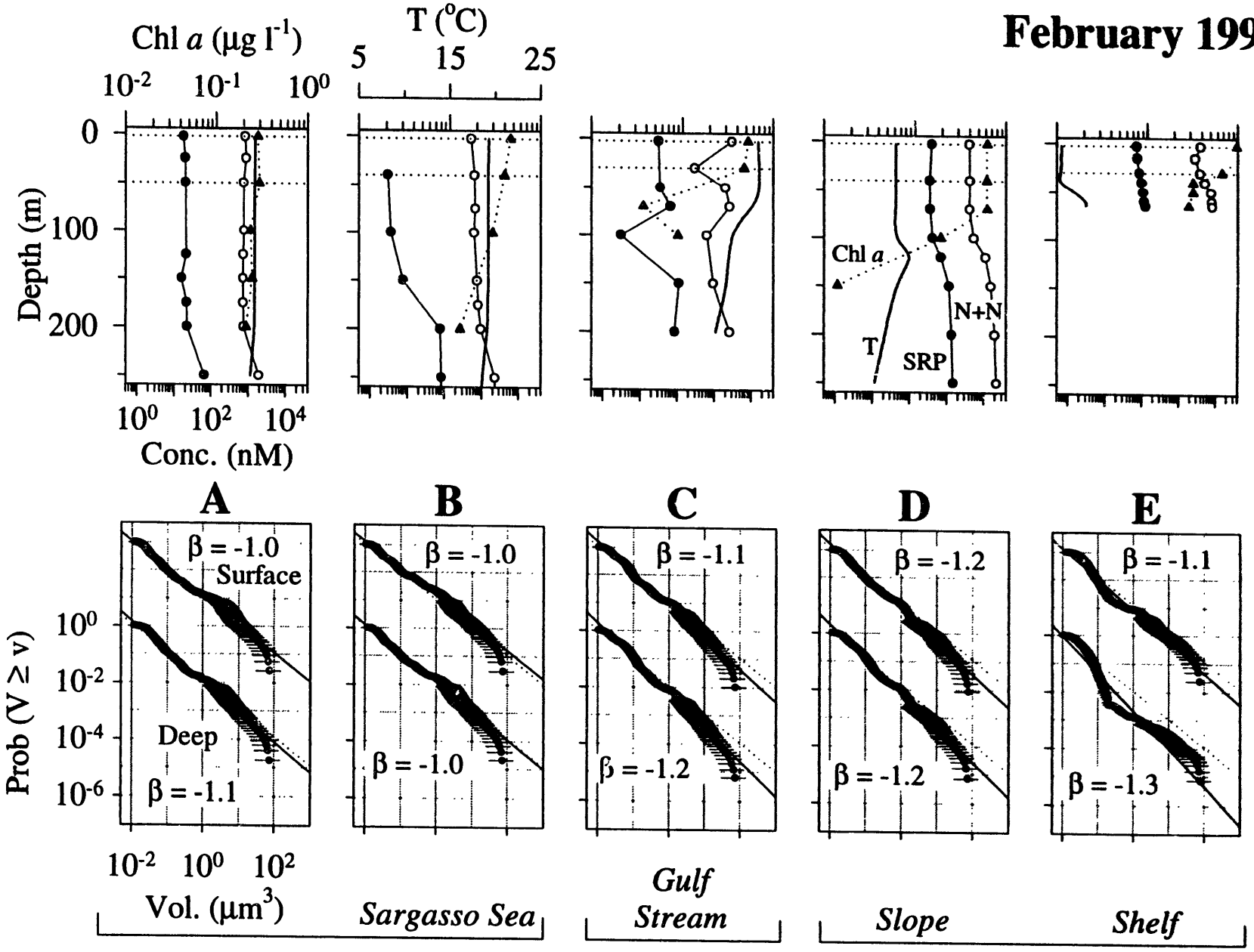
February 1997
Chl a (µg l-1)
10-2 10-1 100
T (°C)
5 15 25
Depth (m)
0
100
200
Chl a
N+N
T
SRP
100 102 104
Conc. (nM)
A
B
C
D
E
β = -1.0
Surface
Deep
β = -1.1
β = -1.0
β = -1.0
β = -1.1
β = -1.2
β = -1.2
β = -1.1
β = -1.3
Prob (V ≥ v)
10-2 100 102
Vol. (µm3)
Sargasso Sea
Gulf Stream
Slope
Shelf

Figure 10:

Relationships between slope of the Prob($V \geq v$) plots ($\beta$) and (A) Nitrate + nitrite (N+N), (B) Soluble reactive phosphorus (SRP), and (C) Total chlorophyll *a* (Chl *a*). Data are from March 1998 transect, with the four regions shown by different symbols (refer to Fig. 4).

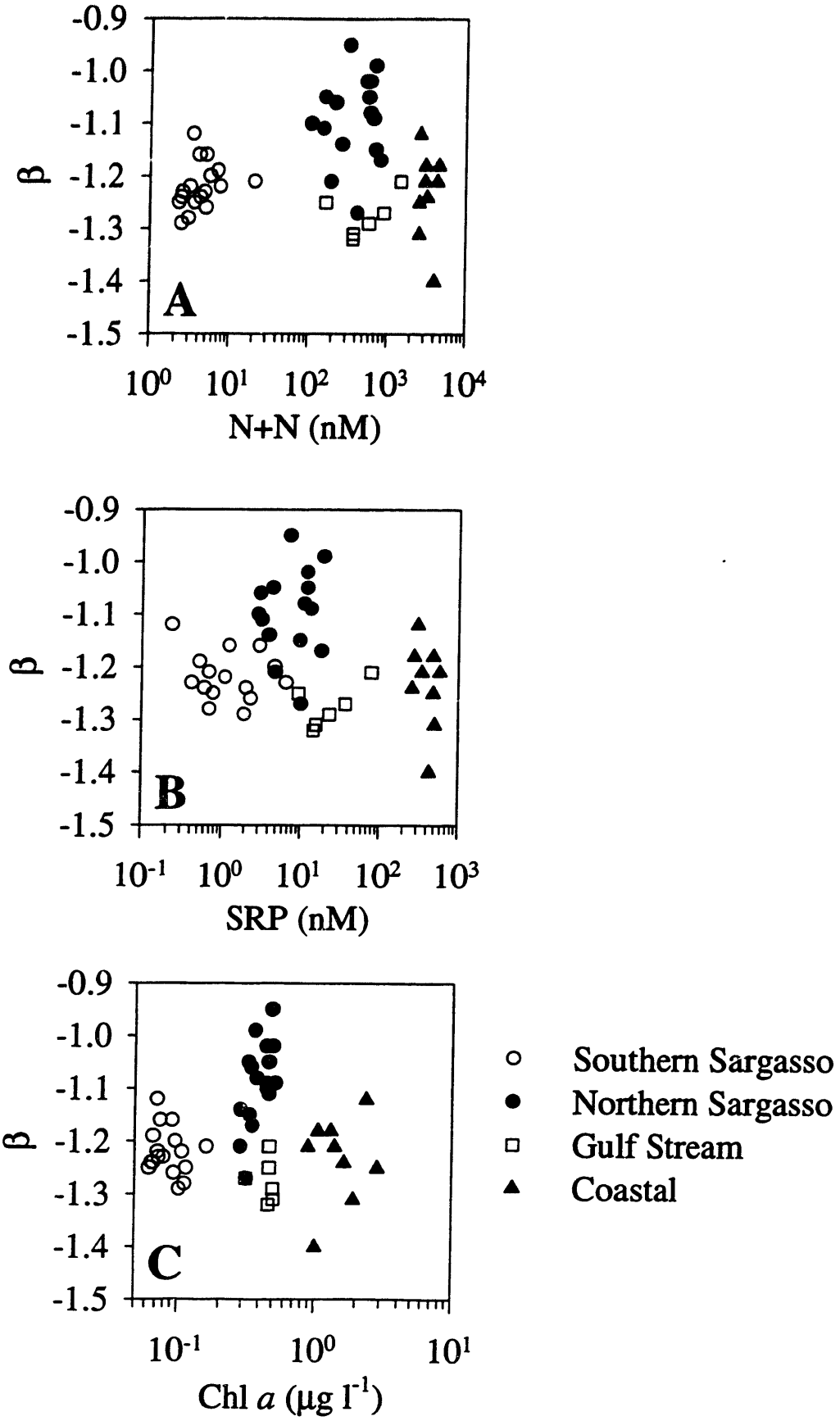
-0.9
-1.0
-1.1
-1.2
-1.3
-1.4
-1.5
β
A
$10^0$ $10^1$ $10^2$ $10^3$ $10^4$
N+N (nM)
B
$10^{-1}$ $10^0$ $10^1$ $10^2$ $10^3$
SRP (nM)
C
$10^{-1}$ $10^0$ $10^1$
Chl *a* (μg $l^{-1}$)
Southern Sargasso
Northern Sargasso
Gulf Stream
Coastal

Figure 11:

Depth profiles for four stations in the Sargasso Sea. (A-D, upper) Depth profiles of nutrients and chlorophyll. (A-D, lower) Depth profiles of size spectra from (*see* Fig. 1) (A) 26°N station during March 1998, (B) Bermuda Atlantic Time-series Study (BATS) site during March 1998, (C) southern station in Sargasso Sea during June 1996 (Fig. 8A), and (D) northern Sargasso Sea station during June 1996 (Fig. 8C). Axes on the spectra plots, Prob ($V \geq v$) and volume, are scaled the same for all panels and slopes of the regression lines ($\beta$) are shown. Confidence intervals on the estimation of cell size are shown by horizontal lines for each point. In all cases, a 1-to-1 dotted line ($\beta = -1$) is included which begins at the volume of the smallest cell measured. Spectra for a given depth profile have been offset vertically so that they are easily compared. The offset is equivalent to three orders of magnitude between each successive depth.

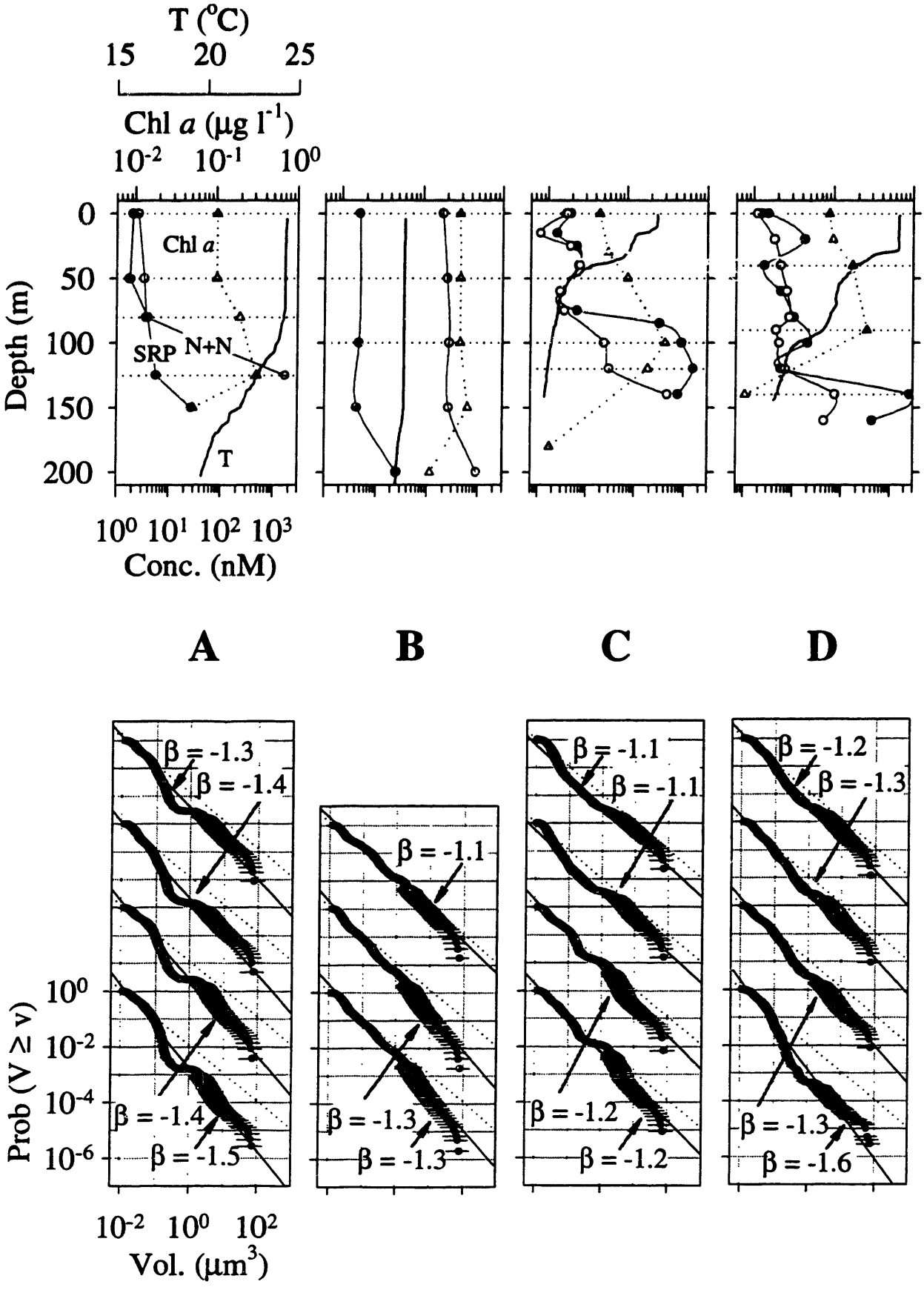
T (°C)
15 20 25
Chl a (µg l-1)
10-2 10-1 100
Depth (m)
0
50
100
150
200
Chl a
SRP
N+N
T
100 101 102 103
Conc. (nM)
A
B
C
D
Prob (V ≥ v)
100
10-2
10-4
10-6
β = -1.3
β = -1.4
β = -1.4
β = -1.5
β = -1.1
β = -1.3
β = -1.3
β = -1.1
β = -1.1
β = -1.2
β = -1.2
β = -1.2
β = -1.3
β = -1.3
β = -1.6
10-2 100 102
Vol. (µm3)

different regions of the transect. None of the spectra shared the smooth linear shape of the ones from the northern Sargasso Sea and the Gulf Stream in March 1998 (Fig. 7C,D). However, the spectrum at the $D_{cm}$ for the coastal station at the transition between the continental slope and shelf (Fig. 8F) was fairly linear. Otherwise, spectra from the Sargasso Sea and the Gulf Stream resembled the spectra from the southern portion of the March 1998 cruise (Fig. 7B), although the deviations from linearity were in some cases more subtle or occurred at multiple points on the spectra yielding a wavy shape. While a few of the coastal stations resembled these spectra (Fig. 7 E,F surface) others had more pronounced waviness (Fig. 8G) characteristic of the coastal stations during March 1998 (Fig. 7E).

Spectra shapes for the Sargasso Sea and the Gulf Stream during February 1997 (Fig. 9A-C) are reminiscent of those from the northern Sargasso Sea and the Gulf Stream during March 1998 (Fig. 7C,D). The continental slope station's spectrum (Fig. 9D) was also relatively smooth, but the shelf station's deviated from a smooth linear shape—especially for the deeper sample.

It is apparent from the literature that deviations from a uniform spectral shape occur in high latitude and coastal marine waters (Sheldon *et al.* 1972; Witek and Krajewskasoltys 1989), as compared to the relatively uniform shapes seen in the central gyres (Sheldon *et al.* 1972; Rodriguez and Mullin 1986). Theoretical models of size spectra (Kerr 1974; Platt and Denman 1977; Sheldon *et al.* 1977) have assumed steady-state conditions for linear spectra. Deviations from a regression line through size spectra data has been equated with deviations from steady-state conditions (Sprules and Munawar 1986; Tittel *et al.* 1998). Specifically, Tittel *et al.*(1998) found a relationship between the scatter around the regression line and the biomass of the zooplankter *Daphnia*, suggesting that grazing activity disrupted the smooth shape of their spectra. Following this interpretation, we would infer that the southern waters of the Sargasso Sea (Fig. 5D) were further from steady-state conditions than were the northern waters (Fig. 5F). Intuition might suggest just the opposite because one would expect spring bloom waters to be in a greater state of flux than the nutrient deplete southern waters, a point to which we will return.

The characteristic shape with the deviation in small size classes (Fig. 7B) is particularly interesting because this pattern is consistent with the concept of preferential grazing. This

flattening of the spectrum in a size range <1 μm in diameter results when few cells are counted over a small range of sizes. Sherr *et al.* (1992) found that phagotrophic protists selectively grazed larger bacterioplankton in estuarine enclosure experiments, and others have found size-selective grazing of larger bacterial cells in culture studies (Turley *et al.* 1986; Andersson *et al.* 1986). Monger and Landry (1990) provided a conceptual model which suggested that smaller bacteria would be less intensively grazed, and they later supported their model with experimental data (Monger and Landry 1991). Sherr *et al.*(1992) rationalized that such size-selective grazing could explain low standing stocks of bacteria in marine environments because grazers might selectively target dividing cells thereby limiting the accumulation of bacterial cells Preferential grazing could certainly explain the apparent decline in standing stock over a narrow range of cell sizes as we found for some samples (e.g., Fig 7B).

In order for preferential grazing to explain this pattern, it is necessary to rule out other possible explanations. Our methods do not include heterotrophic protists less than 5 μm in size. While we cannot prove directly that the reduced cell numbers in the flat region of the Prob($V \geq v$) plot (Fig. 7B) occurred because we missed protists, indirectly we can show that this is unlikely. Caron *et al.*(1999) found that grazing pressure was eliminated by passing seawater through a 1-μm pore size filter near BATS. Of course, grazers may have been damaged through filtration, but Caron *et al.* provide convincing evidence that this was not the case because grazing pressure was normal in seawater which had passed through a 2-μm pore size filter.

In addition, Sheldon *et al.*(1977) contrasted spectra from two regions of the Sargasso Sea using a Coulter Counter, which would have included all particles. These regions were similar spatially and temporally to those represented by the southern and northern regions of the Sargasso Sea during the March 1998 transect (Fig. 7B,C), and their spectra would presumably have included all particles. Replotting their data as Prob($V \geq v$) plots suggests that they found shapes consistent with ours for these regions (*see* Appendix D). Thus, we are confident that this characteristic shape is real, and conclude that preferential grazing is the most likely cause.

SIZE SPECTRA FOLLOWING NUTRIENT ENRICHMENT

From our observations thus far, we hypothesize that smooth, linear microbial spectra in the form of a power law, occur only during extended periods of high nutrients, perhaps with low grazing pressure. While we might expect surface waters of the oligotrophic ocean to approximate a steady-state, resulting in the smooth spectra, deviations of these spectra from a power law do occur (Fig. 7B). We reason that preferential grazing best explains these deviations, and we expect that such grazing effects would be reduced during a phytoplankton bloom.

An idealized nutrient enrichment experiment would simulate the high nutrient conditions characteristic of those during a spring bloom. However, starting points for enrichment studies are typically waters in which the phytoplankton are accustomed to very low nutrient concentrations, and grazing rates closely balance growth rates (Landry *et al.* 1997; Caron *et al.* 1999), unlike the conditions during the spring bloom. Observations from the IronEx II study (Coale *et al.* 1996; Cavender-Bares *et al.* 1999) have shown that changes in the abundance of populations occur on time scales of several days following enrichment. Rodriguez and Mullin (1987) saw community structure changes also on time scales of days during a natural injection of nutrients into coastal waters of the Mediterranean, and they argued that dynamics between size classes led to the oscillations observed in the spectra over time. From this we would infer that during a transient enrichment with nutrients, such as IronEx II, size spectra would tend toward a shape which would be decidedly non-uniform. We expect that species succession during such an experiment would be evident as multiple departures from a power law in the size spectrum, as was seen in coastal waters (Fig. 7E). As we show below, enrichment experiments in the Sargasso Sea and the equatorial Pacific meet this expectation.

*Sargasso Sea enrichment experiment*—An enrichment study was conducted at the southern-most station of the June 1996 transect (Figs. 1 and 8A). Water was collected from 20 m and dispensed into triplicate bottles for both control and treatments; 80 μM $NO_3$ and 5 μM $PO_4$ were added to treated bottles. Initial nutrient concentrations were well below 10 nM for both N+N and SRP (Fig. 7A). Chl *a* increases of more than 30-fold in bottles with added N and

P (Fig. 12A), were driven by a dramatic bloom of *Synechococcus* and a lesser—but significant—bloom of ultra- and nanoplankton (Fig. 12B). Bacteria doubled in abundance over the course of the incubation (Fig.12B). *Prochlorococcus* were undetectable *in situ* at 20 m, consistent with the observations of Olson *et al.* (1990): *Prochlorococcus* are of low abundance in this region during summer, and they remained undetectable at the end of the experiment. The spectra shown represent ensemble averages (± range) for triplicate bottles, except for the day 0 sample.

Spectra over the course of the experiment showed that with time—and presumably exhaustion of nutrients—the slope in the control bottles became more negative (Fig. 12C). This is a result of slight increases in the concentration of the two smallest groups: bacteria and *Synechococcus*. In clear contrast, the slope of the spectra from the enriched bottles became less negative with time, reflecting the bloom of *Synechococcus* and the ultra- and nanoplankton (Fig. 12D). When the spectra for the control and enriched bottles are plotted together for day 5 (Fig. 12E), clear differences are apparent. Slopes differed by 0.2 units, indicating that relatively more of the total biovolume was contained within cells of large size in the bottles amended with N and P.

The shapes of the spectra can also be used to describe the relative changes between treatment and control. The *Synechococcus* cells which bloomed also got larger. This can be seen by the plateau centered at about $10^{-1}$ $\mu m^3$ (i.e., *Synechococcus* moved out of those size classes resulting in a size gap which apparently was not filled by other groups). The huge numbers of *Synechococcus* translated into a rapidly declining probability of exceedence curve (steeper slope) which was seen between the plateau and slightly beyond 1 $\mu m^3$. The bloom of the ultra- and nanoplankton resulted in a similar feature between 1 and 10 $\mu m^3$. As expected, the shape of the spectra from this enrichment resembled those of coastal waters (Fig. 7E) which are probably in a state of disequilibrium, more than the nutrient rich waters of a spring bloom (Fig. 7C).

*IronEx II study in the equatorial Pacific*—In an iron-enrichment experiment conducted *in situ* in the equatorial Pacific Ocean (IronEx II; Coale *et al.* 1996), we showed that phytoplankton in all size classes responded on a single-cell level soon after enrichment (Cavender-Bares *et al.*

Figure 12:

Size spectra from a nutrient enrichment experiment in the Sargasso Sea (southern-most station on Fig. 1 for June 1996 (Fig. 6A). (A) Endpoint chlorophyll *a* (Chl *a*) from duplicate bottles. (B) Changes in cell concentration for three microbial groups ordered from small to large cell-size: heterotrophic bacteria, *Synechococcus*, and the ultra- and nanophytoplankton (see text for further descriptions). (C,D) Size spectra from three sampling times (days 0, 3, and 5) for control bottles (C) and bottles with added $NO_3$ and $PO_4$ (+N&P; D). Note that the spectrum for day 0 is repeated in both panels. Each spectrum represents the average for triplicate bottles, with vertical error bars indicating the range between replicates. (E) Day 5 spectra on expanded scale. Axes on the spectra plots, Prob ($V \geq v$) and volume, are scaled the same for all panels and slopes of the regression lines ($\beta$) are shown. Confidence intervals on the estimation of cell size are shown by horizontal lines for each point. In all cases, a 1-to-1 dotted line is included which begins at the volume of the smallest cell measured. Spectra for a given day have been offset vertically so that they are easily compared. The offset is equivalent to three orders of magnitude between each successive days.

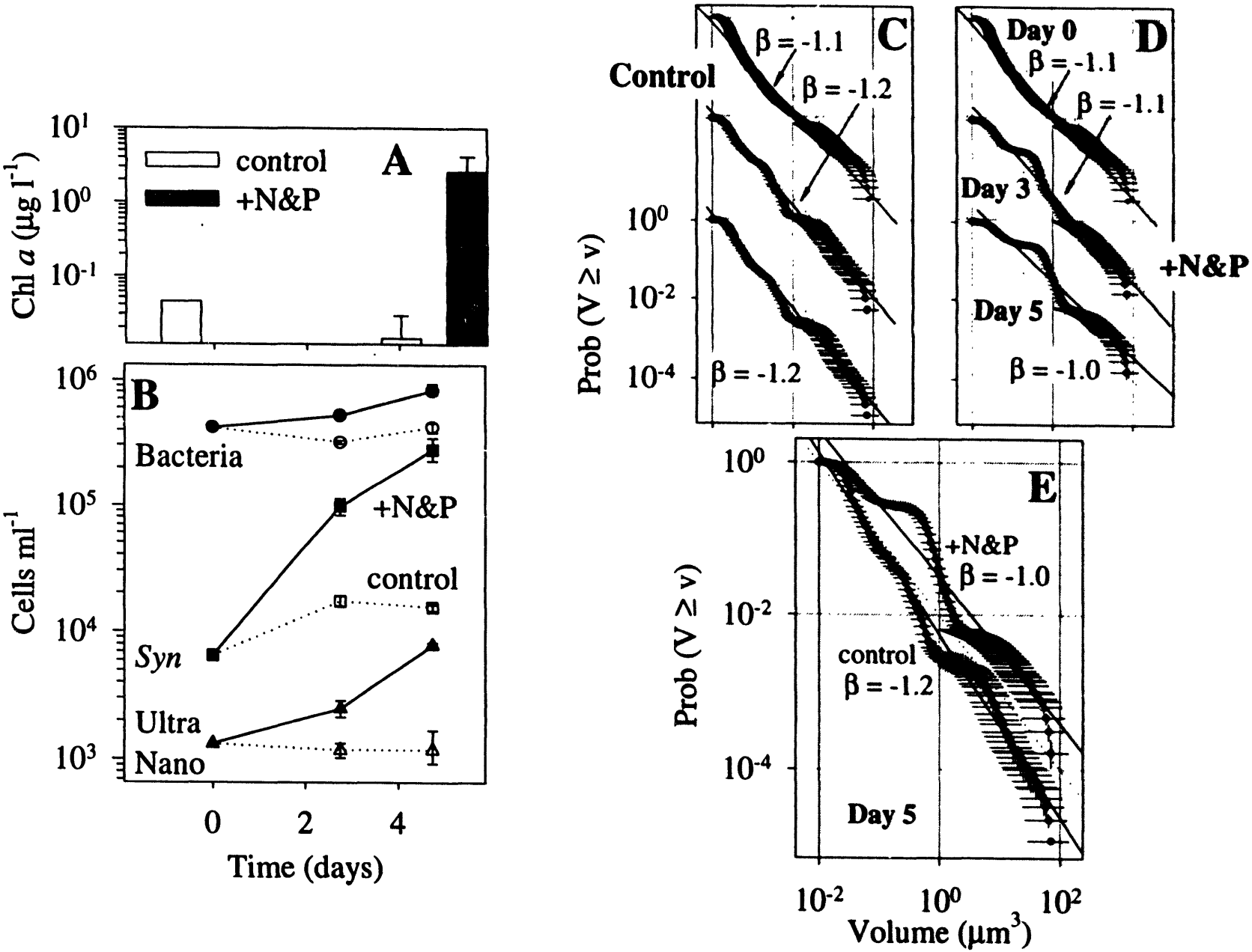
A
control
+N&P
Chl a (μg l-1)
B
Bacteria
+N&P
control
Syn
Ultra
Nano
Cells ml-1
Time (days)
C
Control
β = -1.1
β = -1.2
β = -1.2
D
Day 0
β = -1.1
β = -1.1
Day 3
+N&P
Day 5
β = -1.0
Prob (V ≥ v)
E
+N&P
β = -1.0
control
β = -1.2
Day 5
Volume (μm3)

Figure 13:

Size spectra from the IronEx II study in the equatorial Pacific Ocean during May/June 1995. (A) Map of the general area. The dotted line on the map indicates the cruise track, with the stations of interest shown by filled circles. The location of the Galápagos Islands are shown for reference, and arrows denote stations for days 1 and 8. (B) Changes in total chlorophyll *a* (Chl *a*) with time outside and inside the iron-enriched patch. (C,D) Two spectra are shown for each day representing stations outside (C) and inside (D) iron-enriched waters, except for day 6 on which only an inside station was occupied. Axes on the spectra plots, Prob ($V \geq v$) and volume, are scaled the same for all panels and slopes of the regression lines ($\beta$) are shown. Confidence intervals on the estimation of cell size are shown by horizontal lines for each point. In all cases, a 1-to-1 dotted line ($\beta = -1$) is included which begins at the volume of the smallest cell measured. Spectra for a given day have been offset vertically so that they are easily compared. The offset is equivalent to three orders of magnitude between each successive days.

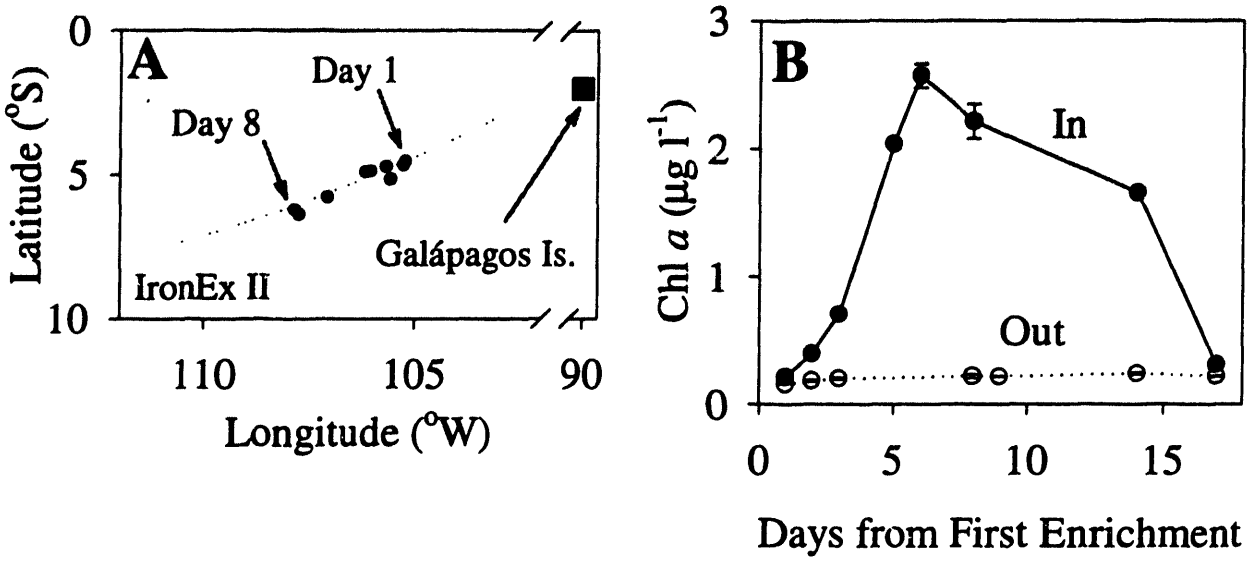
A
Day 1
Day 8
Galápagos Is.
IronEx II
Latitude (°S)
Longitude (°W)
0
5
10
110
105
90
B
In
Out
Chl a (µg l-1)
Days from First Enrichment
0
1
2
3
0
5
10
15

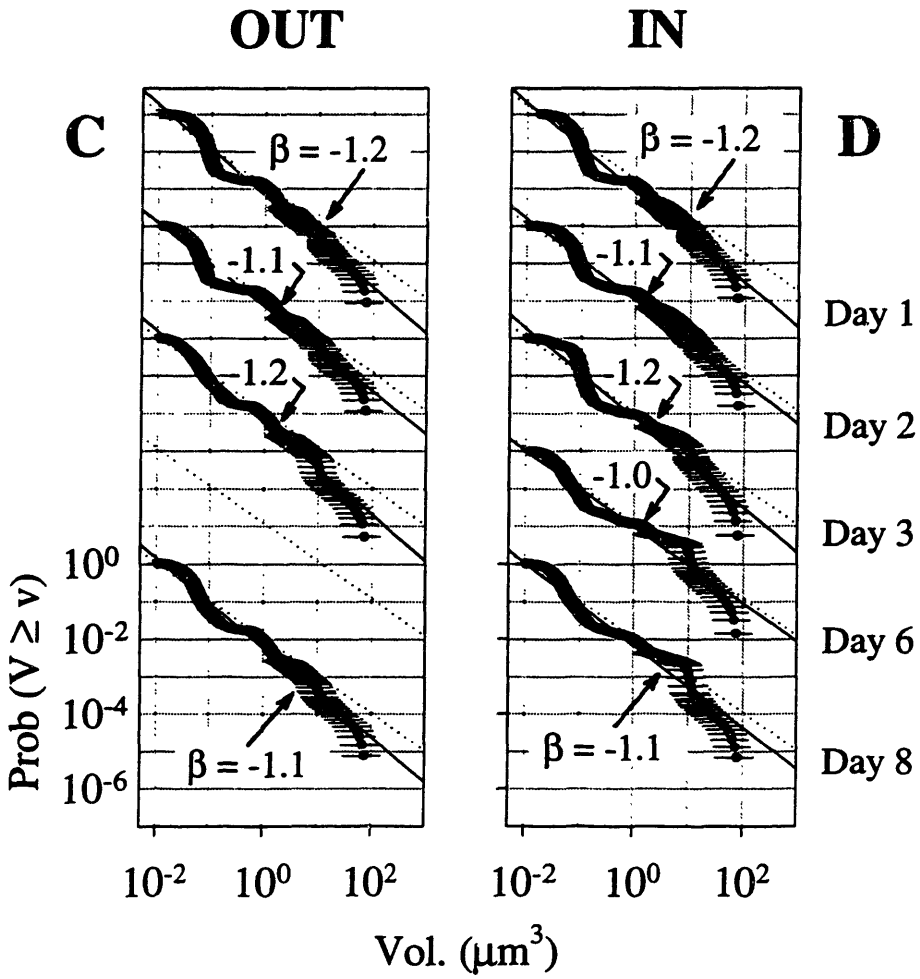
OUT
IN
C
D
β = -1.2
-1.1
-1.2
-1.0
β = -1.1
Day 1
Day 2
Day 3
Day 6
Day 8
Prob (V ≥ v)
10^0
10^-2
10^-4
10^-6
10^-2
10^0
10^2
Vol. (µm^3)

1999). Nevertheless, dramatic changes in phytoplankton abundance did not occur until about day 4 when pennate diatoms had increased substantially in concentration; their numbers dropped off somewhat by day 8. This response is summarized by the greater than 10-fold increase in Chl *a* over the first six days of the experiment (Fig. 13B)

Values of β differed little for samples taken from outside or inside fertilized waters over the course of the experiment (Fig. 13C,D). A trend in slopes, with them becoming less negative inside enriched waters (Fig. 13D), was disrupted on day 3. An extra population on bacteria in fertilized waters, equal in size and abundance to *Prochlorococcus*, were present on this day, causing β to become more negative. The shape of all the spectra, in- and outside enriched waters, were distinctly non-linear and did not conform to the shape characteristic of a power law. The bloom of pennate diatoms can be seen in the shape of spectra on days 6 and 8 (Fig. 13D), although the deviations from linearity caused by enrichment are less pronounced than in the Sargasso Sea bottle experiment (Fig. 12). This may be due to a more active, and fully represented, grazing community being present in the IronEx study in comparison to the bottle incubations.

## Conclusions

Size spectra were shown to follow consistent patterns seasonally and spatially across several regions of the Atlantic Ocean. Changes in slope of the spectra were statistically different between an oligotrophic region of the Sargasso Sea, spring bloom waters to the north, and the Gulf Stream during a transect in March 1998. Slopes were found to have the same relative ranking for these regions for all three transects, which spanned several seasons. We observed spectral shapes which conformed to power laws over nearly four orders of magnitude in cell volume. We hypothesize that these spectra are constrained to high nutrient systems in which phytoplankton grow with, perhaps, fewer controls imposed by grazers, such as would occur during a phytoplankton bloom. We have shown also that transient enrichment experiments, either in bottles or *in situ*, do not produce spectra resembling those from a spring bloom. We

attribute this to the fact that changes in microbial abundance occur on the same time scales as the experiments.

As methods are refined and sampling schemes are broadened, we may be able to understand fully if size spectra display behavior which is fractal. Such a spectrum would conform to a power law, regardless of the size range of study. Does this mean that a spectrum which deviates from a power law is not fractal? Because fractal systems display critical behavior, it is possible that deviations from a power law represent a fractal system undergoing self-organization. In such a system, the least stable component can trigger a reaction of any size, that is communicated across the size spectrum. Elucidating such behavior in planktonic size spectra, we believe, should be studied as intensely over the next thirty years as was the linear biomass hypothesis of Sheldon *et al.* (1972) over the past thirty years.

## REFERENCES


Ahrens, M. A. and R. H. Peters 1991. Patterns and limitations in limnoplankton size spectra. *Canadian Bulletin of Fisheries and Aquatic Sciences* **48**: 1967-1978.

Andersson, A., U. Larsson and A. Hagstrom 1986. Size-selective grazing by a microflagellate on pelagic bacteria. *Marine Ecology Progress Series* **33**: 51-57.

Armstrong, R. A. 1994. Grazing limitation and nutrient limitation in marine ecosystems: Steady state solutions of an ecosystem model with multiple food chains. *Limnology and Oceanography* **39**: 597-608.

Bader, H. 1970. The hyperbolic distribution of particle sizes. *Journal of Geophysical Research* **75**: 2822-2830.

Bak, P. (1996). How nature works: the science of self-organized criticality Copernicus-Springer.

Blanco, J. M., F. Echevarría and C. M. García 1994. Dealing with size-spectra: some conceptual and mathematical problems. *Scientia Marina* **58**: 17-29.

Bohren, C. F. and D. R. Huffman (1983). Absorption and scattering of light by small particles John Wiley and Sons.

Bulldis-Thomson, A. and D. Karl 1998. Application of a novel method for phosphorus determination in the oligotrophic North Pacific Ocean. *Limnology and Oceanography* **43**: 156-1577.

Caron, D. A., E. R. Peele, E. L. Lim and M. R. Dennet 1999. Picoplankton and nanoplankton and their trophic coupling in surface waters of the Sargasso Sea south of Bermuda. *Limnology and Oceanography* **44**: 259-272.

Cavender-Bares, K. K., S. L. Frankel and S. W. Chisholm 1998. A dual sheath flow cytometer for shipboard analyses of phytoplankton communities from the oligotrophic oceans. *Limnology and Oceanography* **43**: 1383-1388.

Cavender-Bares, K. K., E. L. Mann, S. W. Chisholm, M. E. Ondrusek and R. R. Bididgare 1999. Differential response of equatorial Pacific phytoplankton to iron fertilization. *Limnology and Oceanography* **44**: 237-246.

Chisholm, S. W. (1992). Phytoplankton size. Primary Productivity and Biogeochemical Cycles in the Sea. P. G. Falkowski and A. D. Woodhead, Eds. New York, Plenum Press.

Coale, K. H., *et al.* 1996. A massive phytoplankton bloom induced by an ecosystem-scale iron fertilization experiment in the equatorial Pacific Ocean. *Nature* **383**: 495-501.

Delgado, M., M. Latasa and M. Estrada 1992. Variability in the size-fractionated distributions of the phytoplankton across the Catalan front of the north-west Mediterranean. *Journal of Plankton Research* **14**: 753-771.

Dugdale, R. C. and J. J. Goering 1967. Uptake of new and regenerated nitrogen in primary productivity. *Limnology and Oceanography* **12**: 196-206.

DuRand, M. D., R. J. Olson and S. W. Chisholm submitted. Phytoplankton population dynamics at the Bermuda Atlantic Time-series Station in the Sargasso Sea. *Deep Sea Research.*

Gaedke, U. 1992. The size distribution of plankton biomass in a large lake and its seasonal variability. *Limnology and Oceanography* **37**: 1202-1220.

Gin, K. Microbial size spectra from diverse marine ecosystems. Ph.D. Thesis, M.I.T./W.H.O.I. Joint Program, 1996. pp. 359.

Gin, K. Y. H., S. W. Chisholm and R. J. Olson in press. Seasonal and depth variation in microbial size spectra at the Bermuda Atlantic Time Series Station. *Deep-Sea Research.*

Hurtt, G. C. and R. A. Armstrong 1996. A pelagic ecosystem model calibrated with BATS Data. *Deep-Sea Research* **43**: 653-683.

Jonasz, M. and G. Fournier 1996. Approximation of the size distribution of marine particles by a sum of log-normal functions. *Limnology and Oceanography* **41**: 744-754.

Kerr, S. R. 1974. Theory of size distribution in ecological communities. *Journal of the Fisheries Research Board Canada* **31**: 1895-1862.

Kiørboe, T. (1993). Turbulence, phytoplankton cell size, and the structure of pelagic food webs. Advances in Marine Biology. J. H. S. Blaxter and A. J. Southward, Eds. Boston, Academic Press. **29**: 1-72.

Kitchen, J. C., J. R. V. Zaneveld and H. Pak 1982. Effect of particle size distribution and chlorophyll content on beam attenuation. *Applied Optics* **21**: 3913-3918.

Koch, A., B. R. Robertson and D. K. Button 1996. Deduction of cell volume and mass from forward scatter intensity of bacteria analyzed by flow cytometry. *Journal of Microbiological Methods* **27**: 49-61.

Landry, M. R., *et al.* 1997. Iron and grazing constraints on primary production in the central equatorial Pacific: an EqPac synthesis. *Limnology and Oceanography* **42**: 405-418.

Li, W. K. W. 1994. Phytoplankton biomass and chlorophyll concentration across the North Atlantic. *Scientia Marina* **58**: 67-79.

Mandelbrot, B. B. (1983,. The fractal geometry of nature Freeman.

Marie, D., F. Partensky, S. Jacquet and D. Vaulot 1997. Enumeration and cell cycle analysis of natural populations of marine picoplankton by flow cytometry using the nucleic acid stain SYBR Green I. *Applied and Environmental Microbiology* **63**: 186-193.

Michaels, A. F. and A. H. Knap 1996. Overview of the U.S. JGOFS Bermuda Atlantic Time-series Study and the Hydrostation S program. *Deep-Sea Research* **42**: 157-198.

Michaels, A. F., *et al.* 1994. Seasonal patterns of ocean biogeochemistry at the U.S. JGOFS Bermuda Atlantic Time-series Study site. *Deep-Sea Research* **41**: 1013-1038.

Monger, B. C. and M. R. Landry 1990. Direct-interception feeding by marine zooflagellates: the importance of surface and hydrodynamic forces. *Marine Ecology Progress Series* **65**: 123-140.

Monger, B. C. and M. R. Landry 1991. Prey-size dependency of grazing by free-living marine flagellates. *Marine Ecology Progress Series* **74**: 239-248.

Moore, L. R. and S. W. Chisholm 1999. Photophysiology of the marine cyanobacterium *Prochlorococcus*: Ecotypic differences among cultured isolates. *Limnology and Oceanography* **44**: 628-638.

Moore, L. R., R. Goericke and S. W. Chisholm 1995. Comparative physiology of *Synechococcus* and *Prochlorococcus*: influence of light and temperature on growth, pigments, fluorescence and absorptive properties. *Marine Ecology Progress Series* **116**: 259-275.

Moore, L. R., G. Rocap and S. W. Chisholm 1998. Physiology and molecular phylogeny of coexisting *Prochlorococcus* ecotypes. *Nature* **393**: 464.

Olson, R. J., S. W. Chisholm, E. R. Zettler, M. A. Altabet and J. A. Dusenberry 1990. Spatial and temporal distributions of prochlorophyte picoplankton in the North Atlantic Ocean. *Deep-Sea Research* **37**: 1033-1051.

Olson, R. J., E. R. Zettler and O. K. Anderson 1989. Discrimination of eukaryotic phytoplankton cell types from light scatter and autofluorescence properties measured by flow cytometry. *Cytometry* **10**: 636-643.

Ormaza-González, F. I. and P. J. Statham 1991. Determination of dissolved inorganic phosphorus in natural waters at nanomolar concentrations using a long capillary cell detector. *Analytica Chimica Acta* **244**: 63-70.

Parsons, T. R., Y. Maita and C. M. Lalli (1984). A manual of chemical and biological methods for seawater analysis Pergamon Press.

Platt, T. 1985. Structure of the marine ecosystem: its allometric basis. *Canadian Bulletin of Fisheries and Aquatic Sciences* **213**: 55-64.

Platt, T. and K. L. Denman 1977. Organisation in the pelagic ecosystem. *Helgolaender wiss. Meeresunters* **30**: 575-581.

Platt, T. and K. L. Denman 1978. The structure of pelagic marine ecosystems. *Rapports et Proces-Verbaux des Reunions-Conseil International pur l'Exploration de la Mer* **173**: 60-65.

Prothero, J. 1986. Methodological aspects of scaling in biology. *Journal of Theoretical Biology* **118**: 259-286.

Quiñones-Bergeret, R. A. Size-distribution of planktonic biomass and metabolic activity in the pelagic system. Ph.D. Thesis, Dalhousie University, 1992. pp. 225.

Raimbault, P., M. Rodier and I. Taupier-Letage 1988. Size fraction of phytoplankton in the Ligurian Sea and the Algerian Basin (Mediterranean Sea): Size distribution versus total concentration. *Marine Microbial Food Webs* **3**: 1-7.

Redfield, A. C. (1934). On the proportions of organic derivatives in sea water and their relation to the composition of plankton. James Johnstone Memorial Volume, University Press of Liverpool: 176-192.

Revelante, N. and M. Gilmartin 1995. The relative increase of larger phytoplankton in a subsurface chlorophyll maximum of the northern Adriatic Sea. *Journal of Plankton Research* **17**: 1535-1562.

Risovic, D. 1993. Two component model of sea particle size distribution. *Deep-Sea Research* **40**: 1459.

Robertson, B. R. and D. K. Button 1989. Characterizing aquatic bacteria according to population, cell size, and apparent DNA content by flow cytometry. *Cytometry* **10**: 70-76.

Robertson, B. R., D. K. Button and A. L. Koch 1998. Determination of the biomasses of small bacteria at low concentrations in a mixture of species with forward light scatter measurements by flow cytometry. *Applied and Environmental Microbiology* **64**: 3900-3909.

Rodriguez, J., F. Jiménez, B. Bautista and V. Rodriguez 1987. Planktonic biomass spectra dynamics during a winter production pulse in Mediterranean coastal waters. *Journal of Plankton Research* **9**: 1183-1194.

Rodriguez, J. and M. M. Mullin 1986. Relation between biomass and body weight of plankton in a steady-state oceanic ecosystem. *Limnology and Oceanography* **31**: 316-370.

Rodriguez-Iturbe, I. and A. Rinaldo (1997). Fractal river basins: chance and self-organization Cambridge Univ. Press.

Ruiz, J., C. M. García and J. Rodríguez 1996. Vertical patterns of phytoplankton size distribution in the Cantabric and Balearic Seas. *Journal of Marine Systems* **9**: 269-282.

Sheldon, R. W., T. P. T. Evelyn and T. R. Parsons 1967. On the occurrence and formation of small particles in seawater. *Limnology and Oceanography* **12**: 367-375.

Sheldon, R. W. and T. R. Parsons 1967. A continuous size spectrum for particulate matter in the sea. *Journal of the Fisheries Research Board Canada* **24**: 909-915.

Sheldon, R. W., A. Prakash and W. H. Sutcliffe 1972. The size distribution of particles in the ocean. *Limnology and Oceanography* **17**: 327-340.

Sheldon, R. W., W. H. Sutcliffe Jr. and M. A. Paranjae 1977. Structure of pelagic food chain and relationship between plankton and fish production. *Journal of the Fisheries Research Board Canada* **34**: 2344-2353.

Sheldon, R. W., W. H. Sutcliffe and A. Prakash 1973. The production of particles in the surface waters of the ocean with particular reference to the Sargasso Sea. *Limnology and Oceanography* **18**: 719-733.

Sherr, B. F., E. B. Sherr and J. McDaniel 1992. Effect of protistan grazing on the frequency of dividing cells in bacterioplankton assemblages. *Applied and Environmental Microbiology* **58**: 2381-2385.

Sokal, R. R. and F. J. Rohlf (1995). Biometry. Third Ed. W.H. Freeman and Company.

Sprules, W. G., S. B. Brandt, D. J. Stewart, M. Munawar, E. H. Jin and J. Love 1991. Biomass Size Spectrum of the Lake-Michigan Pelagic Food Web. *Canadian Journal of Fisheries and Aquatic Sciences* **48**: 105.

Sprules, W. G., J. M. Casselman and B. J. Shuter 1983. Size distribution of pelagic particles in lakes. *Canadian Journal of Fisheries and Aquatic Sciences* **40**: 1761-1769.

Sprules, W. G. and M. Munawar 1986. Plankton size spectra in relation to ecosystem productivity, size, and perturbation. *Canadian Journal of Fisheries and Aquatic Sciences* **43**: 1789-1794.

Stramski, D. and D. A. Kiefer 1991. Light scattering by microorganisms in the open ocean. *Progress in Oceanography* **28**: 343-383.

Thiebaux, M. L. and L. M. Dickie 1992. Models of aquatic biomass size spectra and the common structure of their solutions. *Journal of Theoretical Biology* **159**: 147-161.

Tittel, J., B. Zippel, W. Geller and J. Seeger 1998. Relationships between plankton community structure and plankton size distribution in lakes of northern Germany. *Limnology and Oceanography* **43**: 1119.

Turcotte, D. L. (1992). Fractals and chaos in geology and geopyhsics Cambridge Univ. Press.

Turley, C. M., R. C. Newell and D. B. Robins 1986. Survival strategies of two small marine ciliates and their role in regulating bacterial community structure under experimental conditions. *Marine Ecology Progress Series* **33**: 59-70.

Vaulot, D. and S. W. Chisholm 1987. A simple model of growth of phytoplankton populations in light/dark cycles. *Journal of Plankton Research* **9**: 345-366.

Vaulot, D., C. Courties and F. Partensky 1989. A simple method to preserve oceanic phytoplankton for flow cytometric analyses. *Cytometry* **10**: 629-635.

Vaulot, D., D. Marie, R. J. Olson and S. W. Chisholm 1995. Growth of *Prochlorococcus*, a photosynthetic prokaryote, in the equatorial Pacific Ocean. *Science* **268**: 1480-1482.

Vidondo, B., Y. T. Prairie, J. M. Blanco and C. M. Duarte 1997. Some aspects of the analysis of size spectra in aquatic ecology. *Limnology and Oceanography* **42**: 184-192.

Welschmeyer, N. A. 1994. Fluorometric analysis of chlorophyll *a* in the presence of chlorophyll *b* and pheopigments. *Limnology and Oceanography* **39**: 1985-1992.

Witek, Z. and A. Krajewskasoltys 1989. Some Examples of the Epipelagic Plankton Size Structure in High-Latitude Oceans. *Journal of Plankton Research* **11**: 1143.

Zettler, E. R., R. J. Olson, B. J. Binder, S. W. Chisholm, S. E. Fitzwater and M. R. Gordon 1996. Iron-enrichment bottle experiments in the equatorial Pacific: responses of individual phytoplankton cells. *Deep-Sea Research* **43**: 1017-1029.

# FUTURE DIRECTIONS

Size spectra of marine microorganisms were compared spatially and seasonally over a variety of ecosystems in this thesis. Interest in size spectra has persisted over the last thirty years for several reasons. Spectra provide a synoptic, taxon-independent picture of planktonic communities. Thus, instead of comparing the abundance of an array of groups of different size within the plankton, spectra offer a means for simple comparisons between samples. They also hold promise as a means for predicting biomass in one size class given the biomass in one or more other size classes (Sheldon *et al.* 1977; Platt and Denman 1977). The analysis of spectra in this thesis has focused on how well their shapes conform to power laws (e.g., $Y \propto X^{\beta}$). Ultimately, it would be of great value if the size distributions of plankton—and larger organisms—could be shown to have critical, or scale-free behavior (e.g., Mandelbrot 1983). This would mean that regardless of the range of sizes measured, the size spectrum for a given region would be a function described by a single power law. If so, such a size spectrum could be considered to be fractal. Not only would such a finding facilitate prediction of biomass in one size class from that in another, but it would then be prudent to explore whether the communities represented by the spectra exhibit properties, such as self-organization (Bak 1996), common to other systems which exhibit critical behavior. Such findings would advance our ability to model planktonic communities and would be play a large role in future biogeochemical models of the world ocean. For these reasons, future work should focus on exploring the behavior of size spectra to ascertain if, in fact, they display critical behavior. Specific areas of study might include representing all planktonic organisms over a given size range by flow cytometry, expanding the size range studied—both smaller and larger—and improving current methods for characterizing individual plankton.

This thesis builds from the work of Gin (1996) by using a more-refined calibration of forward angle light scatter (FALS) to volume and an improved method for presenting size spectra (Vidondo *et al.* 1997). Nevertheless, there is still room for improvement in the application of flow cytometry to the collection of size-structured data.

Even though flow cytometry can be used to enumerate bacteria, which are of similar size as the picophytoplankton, other heterotrophs (e.g., microzooplankton) cannot yet be characterized. It may be possible to expand analyses to include these organisms, although it will require overcoming several obstacles. The first concerns the fragility of small protists. It has been found that extremely gentle techniques are necessary in order to protect these micrograzers from damage during conventional sampling from Niskin or Go-Flo bottles (e.g., Landry and Hassett 1982; Landry *et al.* 1995). Therefore, it would be necessary to integrate gentle sampling methods; sampling from a ship's flow-thru seawater system, for example, would probably be found to misrepresent these fragile cells. (Of course, little has been done to verify that similarly fragile phytoplankton escape damage during our sampling methods, making this another topic worthy of future investigation.) Second, staining protocols will need to be developed such that they can be used at sea, because the fragile zooplankton will likely be damaged during preservation protocols. Hence, it would be ideal if staining protocols required only single-wavelength excitation to enable the simplest flow cytometers to be used at sea. Third, if FALS is used to estimate cell size, a calibration specific to these heterotrophic cells would be necessary.

It would be of considerable value to repeat at sea the protocol used in Chapter 3, which combined sorting by flow cytometry with sizing by a Coulter Counter. In so doing, the potential for preservation effects, which were accounted for in Chapter 3, would be eliminated. A systematic series of measurements on several cruises might establish a more robust relationship between FALS and cell volume over a wider size range. Such an improved calibration would permit stronger conclusions to be drawn about differences, or similarities, in spectra.

The analyses used in this thesis included bacterioplankton and phytoplankton ranging from *Prochlorococcus* (~0.7 μm in diameter) to nanoplankton in the size range of 5-10 μm. In order to extend the size range of these analyses given the low abundance of larger cells, sampling schemes would have to be expanded to permit the processing of much larger sample volumes. Once larger cells can be sampled adequately, further work will be necessary to estimate their size. With increasing size, the relationship between FALS and volume is less sensitive to changes in cell volume. That is, a small change in FALS corresponds to a large change in

volume (*see* Fig. 5, Chapter 3). Therefore, it would be worth pursuing alternative methods to size these larger cells.

One avenue that, to my knowledge, has not been pursued in oceanography, is pulse length as a way to measure particle size. Some twenty years ago, Eisert and co-workers explored using flow cytometers with multiple beams to make accurate measurements of cell size (Eisert *et al.* 1975; Eisert 1979; Eisert and Dennenloehr 1981; Eisert 1981). They suggested that measurements "well below" 2 μm were possible, however, there would likely be limitations at sizes approaching the wavelength of the laser beam, because it is difficult to focus a laser to a point having dimensions similar to the laser's wavelength. However, this should not prevent further consideration of this method, because our calibration work (Chapter 3) suggests that the correlation between FALS and volume for the smaller cells is strong; it is the larger cells for which the method of Eisert and co-workers' would be useful.

In addition, this protocol could readily be applied to other aspects of phytoplankton ecology. For example, cells could be sorted from field samples on the basis of their cellular fluorescence, rather than their FALS, and then the chlorophyll in these cells could be measured. This could help our understanding between pigment fluorescence and content. Alternatively, single cells could be sorted and examined by electron microscopy. I began work in this direction in case the calibration in Chapter 3 did not materialize. Specifically, I was interested in measuring the cellular carbon content using X-ray microanalysis (Norland *et al.* 1995) and relating it to FALS. I believe this method is very promising and could be applied to other elements besides carbon.

## REFERENCES


Bak, P. (1996). How nature works: the science of self-organized criticality Copernicus-Springer.

Eisert, W. G. 1979. Cell differentiation based on absorption and scattering. *The Journal of Histochemistry and Cytochemistry* **27**: 404-409.

Eisert, W. G. 1981. High resolution optics combined with high spatial reproducibility in flow. *Cytometry* **1**: 254-259.

Eisert, W. G. and M. Dennenloehr 1981. Nozzle design for the generation of plane liquid surfaces. *Cytometry* **1**: 249-253.

Eisert, W. G., R. Ostertag and E.-G. Niemann 1975. Simple flow microphotometer for rapid cell population analysis. *Revue of Scientific Instruments* **46**: 1021-1024.

Gin, K. Microbial size spectra from diverse marine ecosystems. Ph.D. Thesis, M.I.T./W.H.O.I. Joint Program, 1996. pp. 359.

Landry, M. R. and R. P. Hassett 1982. Estimating the grazing impact of marine micro-zooplankton. *Marine Biology* **67**: 283-288.

Landry, M. R., J. Kirshtein and J. Constantinou 1995. A refined dilution technique for measuring the community grazing impact of microzooplankton, with experimental tests in the central equatorial Pacific. *Marine Ecology Progress Series* **120**: 53-63.

Mandelbrot, B. B. (1983). The fractal geometry of nature Freeman.

Norland, S., K. M. Fagerbakke and M. Heldal 1995. Light element analysis of individual bacteria by X-ray microanalysis. *Applied and Environmental Microbiology* **61**: 1357-1362.

Platt, T. and K. L. Denman 1977. Organisation in the pelagic ecosystem. *Helgolaender wiss. Meeresunters* **30**: 575-581.

Sheldon, R. W., W. H. Sutcliffe Jr. and M. A. Paranjae 1977. Structure of pelagic food chain and relationship between plankton and fish production. *Journal of the Fisheries Research Board Canada* **34**: 2344-2353.

Vidondo, B., Y. T. Prairie, J. M. Blanco and C. M. Duarte 1997. Some aspects of the analysis of size spectra in aquatic ecology. *Limnology and Oceanography* **42**: 184-192.

# Appendix A

## Application of the magnesium-induced co-precipitation (MAGIC) method for the analysis of phosphate in the western Sargasso Sea

A modification (Bulldis-Thomson and Karl 1998) of the standard magnesium-induced co-precipitation (MAGIC) method (Karl and Tien 1992) was used. The following is a description of the protocol used:

1) to increase sensitivity above the normal modified-MAGIC (about 5-fold), I repeated the procedure for either 3 or 5 replicate sample tubes and at the very end combined the solution just before reading on the spectrophotometer. I recommend doing it this way even though it means carrying more tubes through the whole process as I was convinced that the addition of the reducing agent and/or molybdate mix helped to dissolve the pellet. (i.e., the combination of tubes prior to this step yielded messy results).

2) 50 ml of sample pipetted into 50-ml orange-cap centrifuge tubes (polypropylene)

3) to induce precipitation, 150 microliters of 1N NaOH (Fluka Chemical) was added to each tube

4) tubes were mixed by hand twice (by inverting) with a 5-minute space in between; after another 5-min. they were centrifuged at 1000xg for 1-hr. (not sure all of this mixing and waiting was necessary, but it worked well for me).

5) supernatant was vacuum aspirated; there is usually one way to rotate the tube so that the bulk of the transparent pellet is facing up while aspirating, which will help prevent aspirating the pellet.

6) 0.1 N HCl was added to the pellet and vortexed immediately. The quantity of HCl depended on the number of tubes (50-ml) being combined (i.e., the level of concentration beyond the normal modified-MAGIC). Note that I did not save any sample for As analyses, so right from the beginning I was getting about twice the concentration effect as the normal modified-MAGIC. This is what I used:

| # of tubes to be combined | volume of HCl added per tube |
|---|---|
| 1 (normal) | 4-ml |
| 3 (150-ml total) | 1.25-ml per tube |
| 5 (250-ml total) | 0.75-ml per tube |

7) reducing and molybdate reagent mixes were added such that 15 minutes elapsed between these additions; tubes were vortexed after each addition.

8) I used the standard ratios of reagents for the two mixes, but used varying amounts of each mix per tube, again depending on how many tubes I was going to combine. Here's what I used:

| # of tubes to be combined | volume of each reagent mix added per tube |
|---|---|
| 1 (normal) | 0.75-ml |
| 3 (150-ml total) | 0.25-ml per tube |
| 5 (250-ml total) | 0.15-ml per tube |

Reducing mix (keep ratios of volumes constant):
5.6 ml of 5N $H_2SO_4$
2.4 ml of DI water
16 ml of Na-metabisulfite
16 ml Na-thiosulfate

Molybdate mix (keep ratios of volumes constant):
8 ml ammonium molybdate
20 ml of 5 N $H_2SO_4$
8 ml of ascorbic acid
4 ml antimony potassium tartarate

Reagents:
14% (w/w) Na-metabisulfite (2.24 g per 16 ml DI water)
Na-thiosulfate (4.43 g into 500 ml DI water)
ammonium molybdate (6 g into 200 ml DI water)
ascorbic acid (5.4 g into 100 ml DI water)
antimony potassium tartarate (0.3407 g into 250 ml DI water)

9) I waited a full 15 minutes before starting to combine the tubes together—I used disposable transfer pipets (new ones for each sample set unless I was sure that the last sample was less concentrated) to combine samples as pouring from tube to tube seemed to produce messy results.

10) I used analytical grade $KH_2PO_4$ (Wako Chemicals) to make up standards

References

Bulldis-Thomson, A. and D. Karl 1998. Application of a novel method for phosphorus determination in the oligotrophic North Pacific Ocean. *Limnology and Oceanography* **43**: 156-1577.

Karl, D. M. and G. Tien 1992. MAGIC: A sensitive and precise method for measuring dissolved phosphorous in aquatic environments. *Limnology and Oceanography* **37**: 105-116.

# Appendix B

## Sorting verification for an EPICS V flow cytometer

Figure B-1:

A series of samples were analyzed fresh (at sea) and after the standard preservation technique (0.1% glutaraldehyde, frozen in liquid nitrogen, eventually moved to -80°C). Samples were from three *Oceanus* cruises (OC 279, 297, and 318) and the IronEx II cruise (Fexii). This comparison was conducted to shown that it was reasonable to construct a calibration of forward angle light scatter (FALS) using preserved (frozen) samples. In some cases the agreement between fresh and frozen was very good, and in other cases, this agreement was not so good. In cases where agreement was poor, an adjustment was applied to the calibration (*see* Chapter 3 and Appendix I).

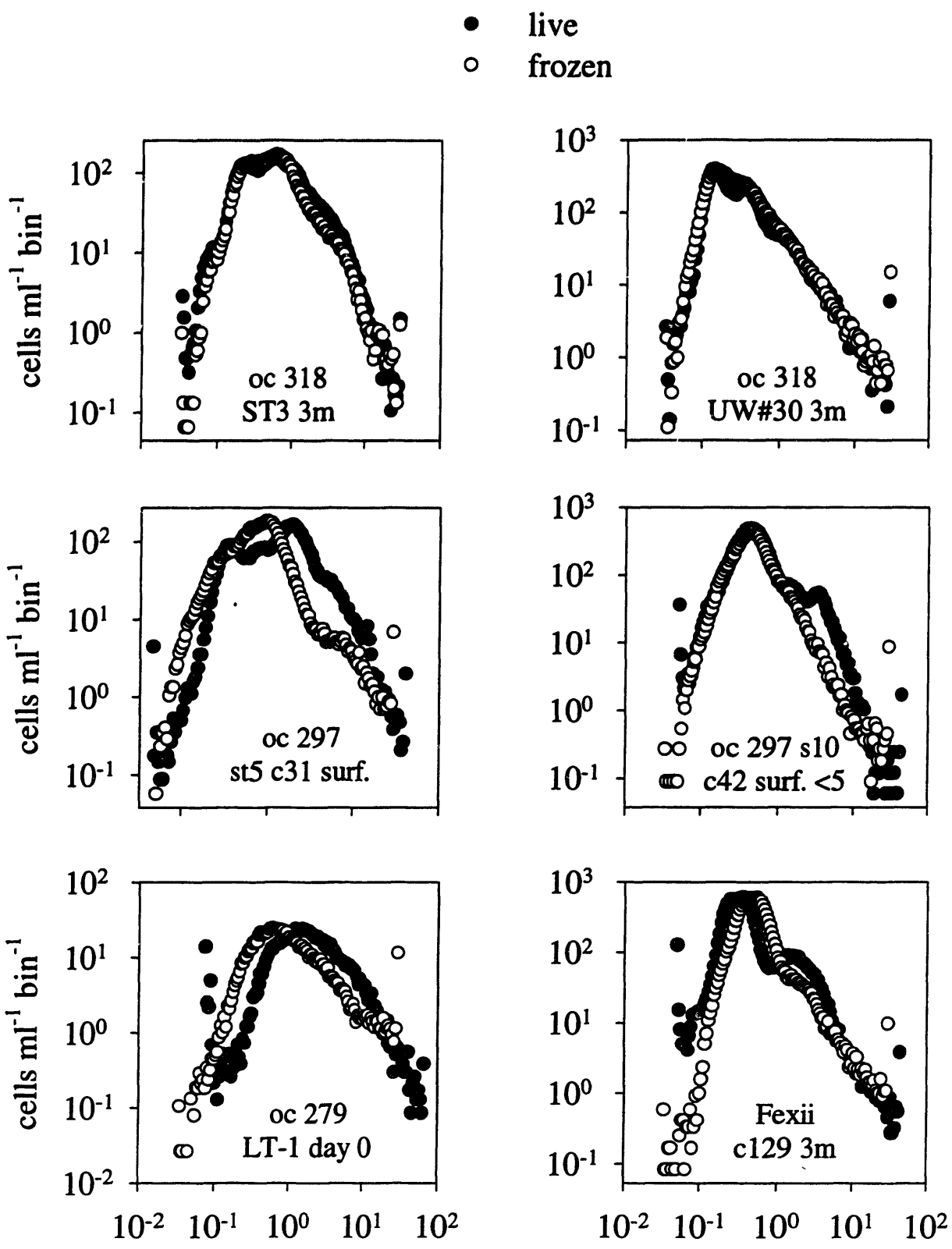
live
frozen
cells ml$^{-1}$ bin$^{-1}$
oc 318
ST3 3m
oc 318
UW#30 3m
oc 297
st5 c31 surf.
oc 297 s10
c42 surf. <5
oc 279
LT-1 day 0
Fexii
c129 3m
FALS (rel. to 2.02 µm bds)

Figure B-2:

Verification of sorting capability of EPICS V flow cytometer using a *Prochlorococcus* culture. In all panels, the dotted curve represents the un-sorted sample as it was measured on the flow cytometer. The solid curve in each panel represents the *Prochlorococcus* population that was sorted away from the remainder of the population. The sort region is denoted by two vertical dotted lines in panels B, C, and D. (A) the entire *Prochlorococcus* population was sorted. (B-D) only a narrow region of forward angle light scatter (FALS) was sorted. It was found that the mode FALS value for cells in the sort region agreed well with the mean value of the population as measured after sorting.

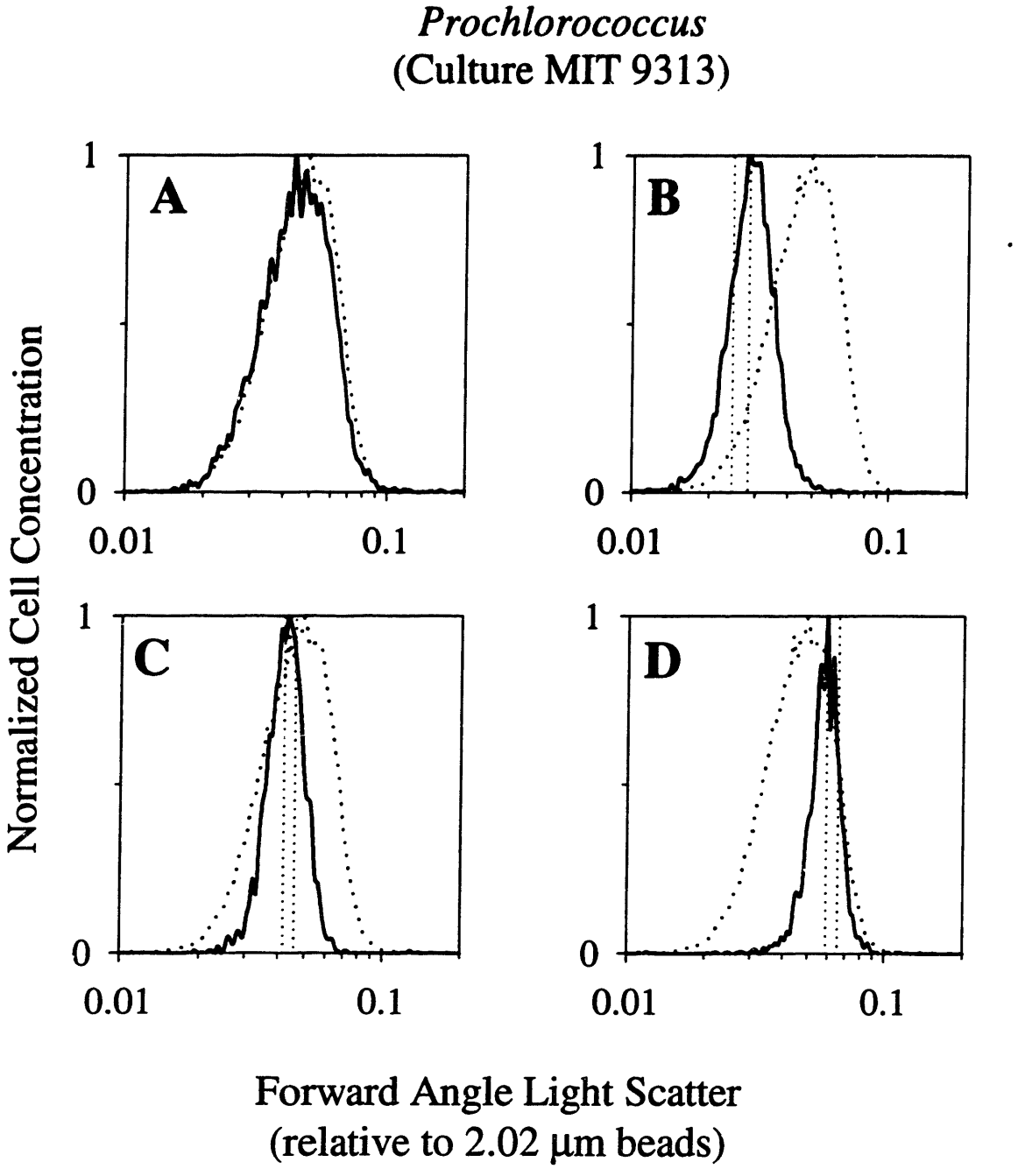
*Prochlorococcus*
(Culture MIT 9313)
Normalized Cell Concentration
A
B
C
D
1
0
0.01
0.1
Forward Angle Light Scatter
(relative to 2.02 μm beads)

Figure B-3:

Verification of sorting capability of EPICS V flow cytometer using a preserved sample from the IronEx II cruise. In all panels, the dotted curve represents the un-sorted sample as it was measured on the flow cytometer. The solid curve in each panel represents the portion of the ultraplankton population that was sorted away from the remainder of the population. The sort region is denoted by two vertical dotted lines in panels B, C, and D. (A) the entire ultraplankton population was sorted. (B-D) only a narrow region of forward angle light scatter (FALS) was sorted. It was found that the mode FALS value for cells in the sort region agreed well with the mean value of the population as measured after sorting.

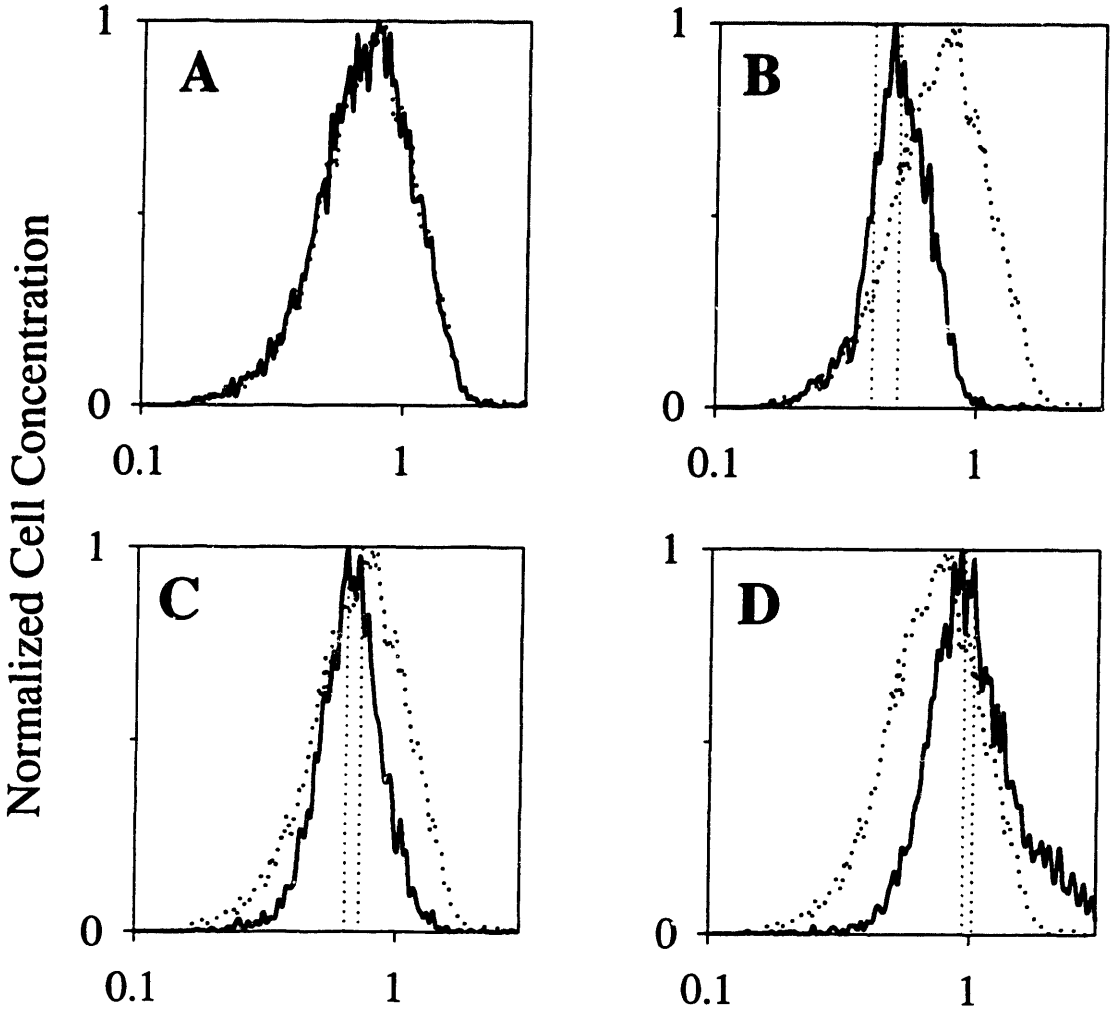
IronEx II Cast 335 40m
A
B
C
D
1
0
0.1
1
Normalized Cell Concentration
Forward Angle Light Scatter
(relative to 2.02 µm beads)

# Appendix C

Description of adjustment for calibration of forward angle light scatter (FALS) signals

Figure C-1:

Comparison of the distribution of picoplankton before and after preservation. Sample was from *Oceanus* cruise OC318. Upper panel for *Prochlorococcus* and lower panel for *Synechococcus*. Fairly good overlap was seen for both populations at higher values of forward angle light scatter (FALS). Note that small *Prochlorococcus* cells were not detectable on the flow cytometer setup, thus, their distribution from the frozen sample was truncated at low FALS values. For this sample, no adjustment to the calibration was made (refer to Chapter 3). It is possible that some adjustment would have been in order for *Synechococcus*, although it was not a convincing case.

OC 318 station 1 cast 3 surface

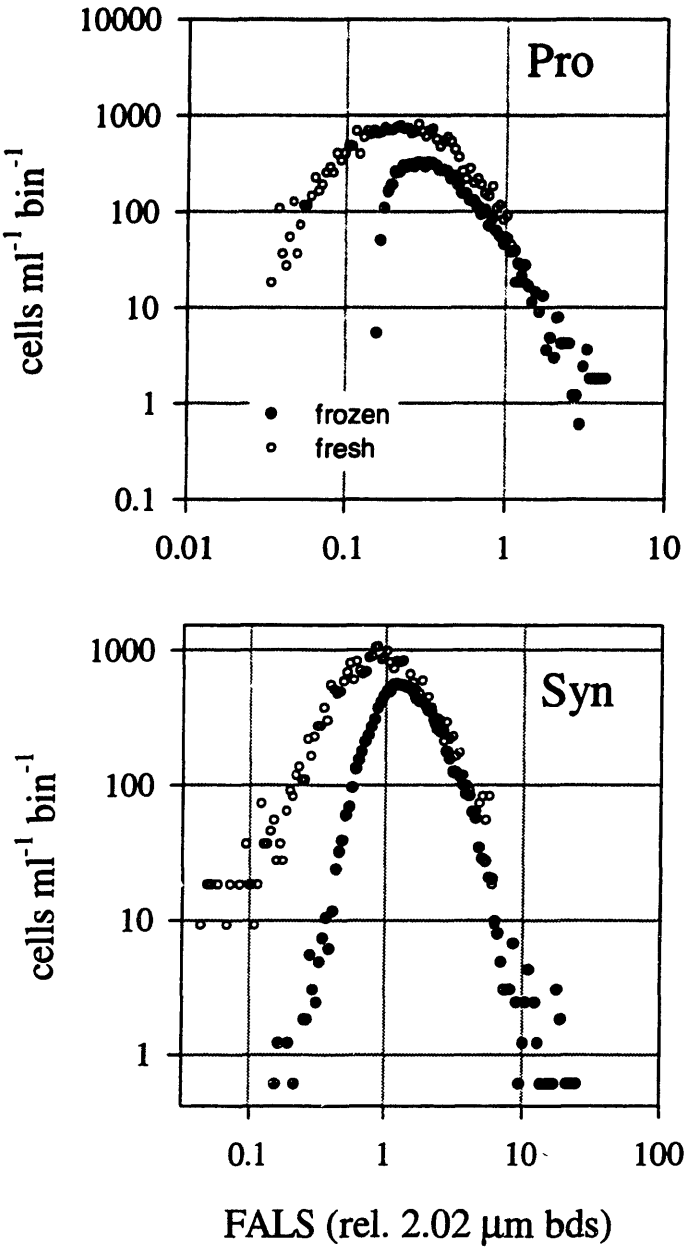

Figure C-2:

Comparison of the distribution of ultra- and nanoplankton before and after preservation. Sample was from *Oceanus* cruise OC297. Upper panel for ultraplankton and lower panel for the nanoplankton. Good overlap was seen for the ultraplankton for all values of forward angle light scatter (FALS). The nanoplankton samples did not overlap well. An adjustment was made such that the frozen distribution was moved to the right until it aligned with the curve from the fresh sample. Clearly the fresh sample was bimodal and the frozen was unimodal. This adds confusion to the adjustment process, however, study of the raw data in the form of flow cytometric signatures convinced me that the adjustment should be made.

OC 297 station 10 cast 40 surface

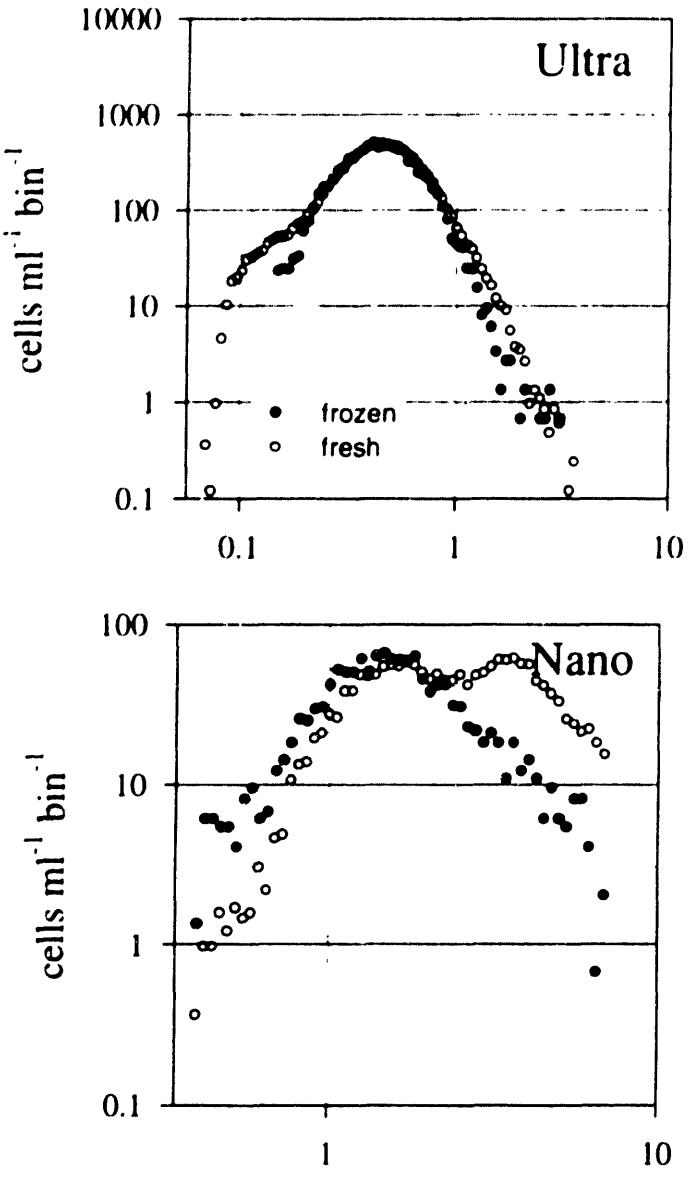

# Appendix D

## Sheldon et al. (1997) revisited

Figures replotted from:

Sheldon, R. W., W. H. Sutcliffe Jr. and M. A. Paranjae 1977. Structure of pelagic food chain and relationship between plankton and fish production. *Journal of the Fisheries Research Board Canada* **34**: 2344-2353.

Figure D-1:

Figure 1a from Sheldon et al. (1977). Upper panel is of the form they used; lower panel is the probability of exceedence method used in Chapter 6. The slope of the regression line is indicated by $\beta$.

Sheldon et al. (1977) Fig. 1a
(26N--Sargasso)

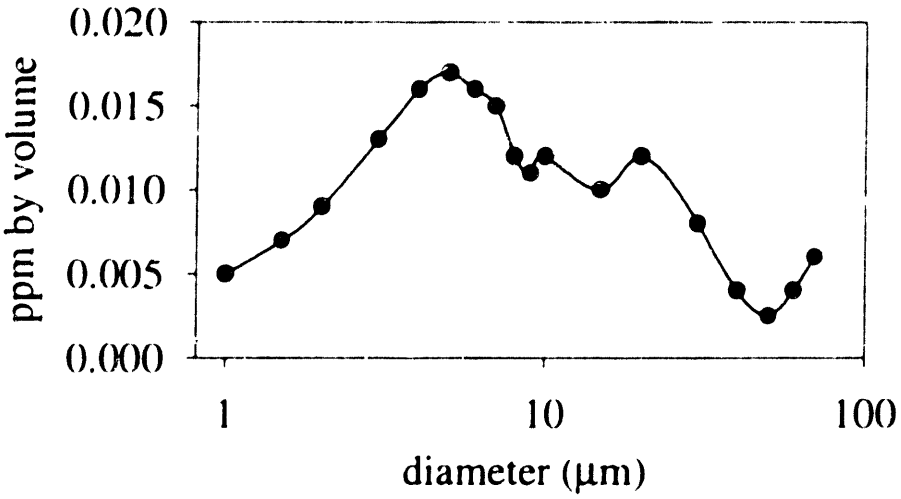


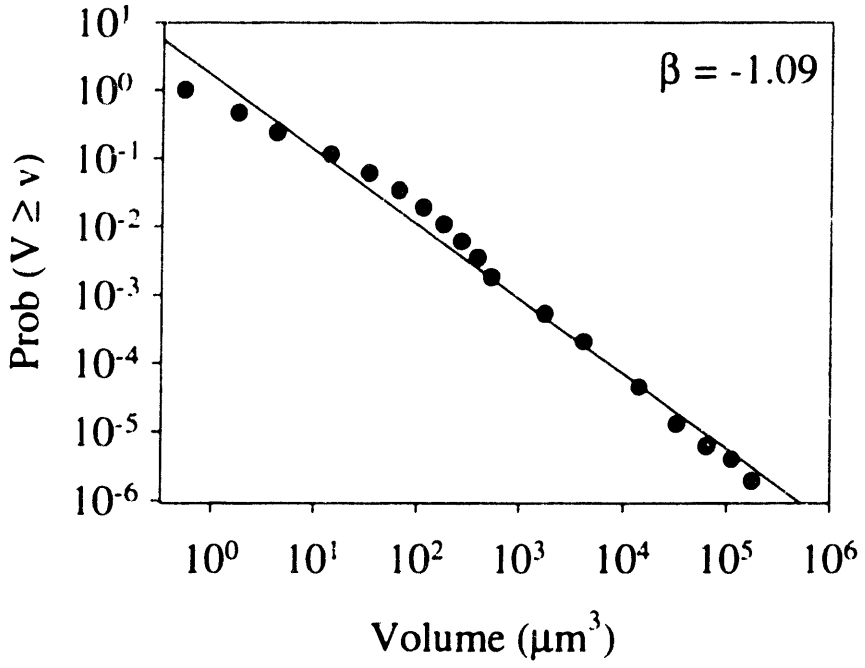

Figure D-2:

Figure 1b from Sheldon et al. (1977). Upper panel is of the form they used; lower panel is the probability of exceedence method used in Chapter 6. The slope of the regression line is indicated by $\beta$.

Sheldon et al. (1977) Fig. 1b
(26N--Sargasso)

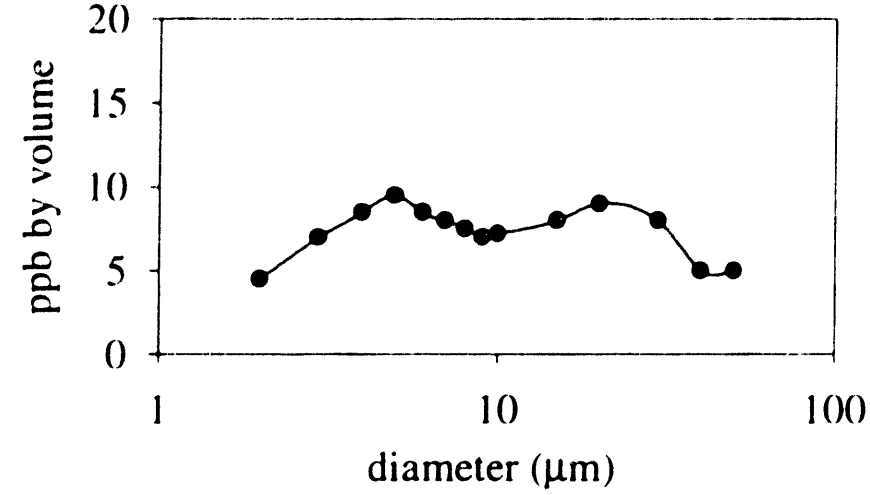


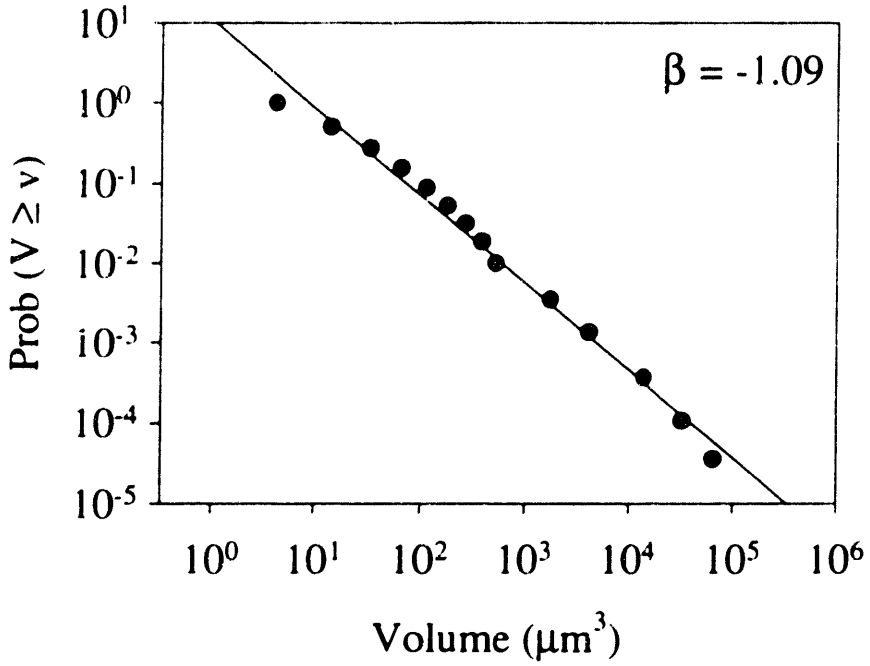

Figure D-3:

Figure 1d from Sheldon et al. (1977). Upper panel is of the form they used; lower panel is the probability of exceedence method used in Chapter 6. The slope of the regression line is indicated by $\beta$.

Sheldon et al. (1977) Fig. 1d
(32N--Sargasso)

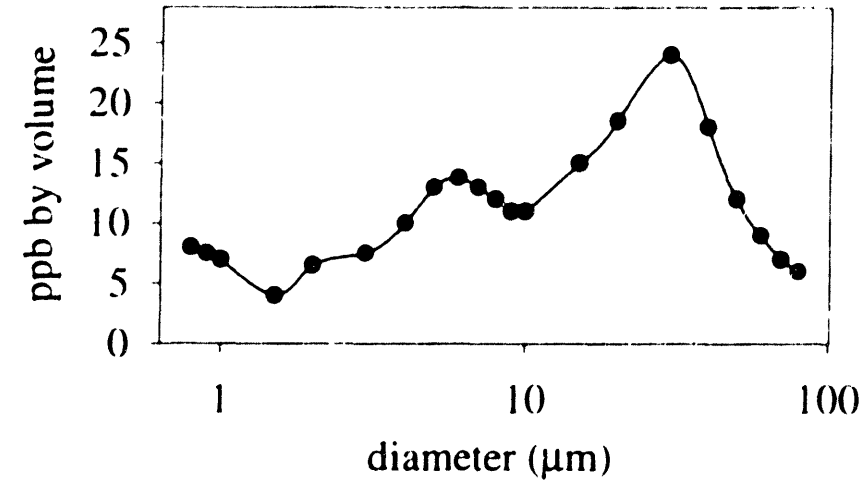


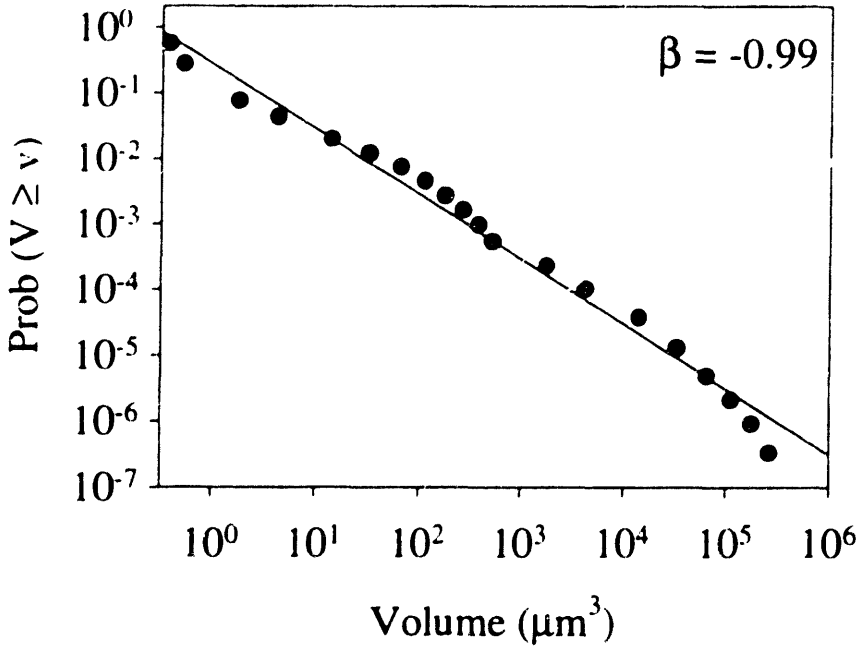

Figure D-4:

Figure 1e from Sheldon et al. (1977). Upper panel is of the form they used; lower panel is the probability of exceedence method used in Chapter 6. The slope of the regression line is indicated by $\beta$.

Sheldon et al. (1977) Fig. 1e
(32N--Sargasso)